

SYNTHESIS AND EVALUATION OF NOVEL HETEROCYCLES AS POTENTIAL HIV-1 ENZYME INHIBITORS

A thesis submitted in fulfilment of the requirements for the degree of

DOCTOR OF PHILOSOPHY

of

RHODES UNIVERSITY

by

NGNIE TUEMGNIE GAELLE TATIANA
MSc (Yaoundé)

February 2014

ABSTRACT

This project has focussed on the synthesis and the evaluation of organic compounds as potential HIV-1 enzyme inhibitors, by making use of green chemistry (microwave assisted synthesis and click chemistry), palladium catalyzed reactions (Heck and Sonogashira coupling), Baylis Hillman methodology and aldol condensation. These compounds were synthesized in good yields and fully characterised by spectroscopic techniques. Biological assay data revealed that some of the compounds possess high inhibitory activity and their effective inhibitory concentration was as good as those of drugs in clinical use. These potential drug molecules were identified by preliminary investigations carried out by molecular modelling where a trend of their inhibitory activity against different enzymes was anticipated.

Benzotriazole-AZT conjugates generated by 1,3-dipolar cycloaddition of anthranilic acid derivatives with AZT showed good inhibitory activity *in silico* against both HIV-1 protease (PR) and HIV-1 reverse transcriptase (RT) enzymes. Still in line with our dual action strategy, cinnamate ester-AZT conjugates were synthesized in three steps starting from benzaldehyde derivatives with a click reaction at the final step. These compounds also showed some inhibitory activity against HIV-1 RT enzyme (88%). In addition, the cinnamoyl fragment attached to AZT appeared to improve the activity of AZT against HIV-1 RT.

Peptide chemistry involving carbonyl diimidazole as a coupling reagent between cinnamic acid derivatives and protected amino acids was used to prepare substituted amino acid derivatives which appeared to be very active against the integrase (IN) enzyme (88%).

Commercially available coumarin was iodinated and derivatized through palladium catalyzed Heck and Sonogashira reactions with activated alkenes and a terminal alkyne respectively to afford novel coumarin derivatives in good yields. Optimization studies on the Heck reaction with regards to the phosphine ligand, the palladium catalyst and the solvent were carried out to afford novel formyl substituted cinnamate esters with nonaflyl salicylaldehyde derivatives.

ACKNOWLEDGEMENTS

I would like to acknowledge the superb contribution of the following people and organisations:

My amazing supervisor Dr. Rosalyn Klein, I really appreciate the invitation allocated to me in 2011 to work in your research team, the training and the care you gave me throughout the three years of my program. I am also grateful to the trust you had in me and that motivated me to work harder every day. As I used to tell you, “you believe in me more than I do believe in myself”.

Professor Perry Kaye, for his incessant help and guidance throughout my project.

Dr Kevin Lobb, our “amazing Dr Lobb” for never minding helping me out with molecular modelling studies and STD NMR on public holidays or even when he was away.

Dr Adrienne Edkins from the Department of Biochemistry, Microbiology and Biotechnology (Rhodes University) for training me on how to conduct the bioassays and for giving me the opportunity to work in her laboratory.

Dr Pierre Kempgens, for training me on the 600 MHz and 400 MHz NMR instruments.

Dr Derek Ndinteh, Dr Idris Olasupo, Dr Matshawe Tukulula, Dr David Khanye, Dr Anabel Lanterna for their precious advices.

My former supervisors at the University of Yaounde I, Professor Joseph Ketcha, Professor Horace Ngoma and Professor Charles Abi, for always trusting me.

My South African family (F22 lab mates), Yusuf Hassan, Christopher Rafael, Yollande Fomogne, Xavier Noundou, Melody Manyeruke, Khethobole Sekgota for providing a pleasant environment of work.

My former lab mates, Dubekile Nyoni, Tope Olomola, Lulama Mciteka, Christiana Idahosa, for providing me a very good support.

My friends from the chemistry department, Jessica Taylor, Tope Olalekan, Bridget Moronkola, Dr Samuel Chigome, for the words of encouragement in the corridors of the chemistry department.

My very close friends, Virginie Poka, Marius Talla, Charles Njine, Aline Nzeket, Aude Molha, Katia Nchimi, Sonia Nkenfack, Nokuthula Ngomane for always being there for me when I needed their support.

My friend from the pharmacy department, Maynard Chiwakata for being far too understanding and always willing to help in any situation and at any time.

Mr André Adriaan from the chemistry department workshop, for always smiling at me each and every time I brought broken glassware to him for reparation.

My parents in-law André Dedzo and family, my brother in-law Theophile Stapi and family, my uncles Abraham Kouajiep and family, Francois Tchualak and family, my Godmother Julienne Tchamaleu and family, for showing understanding and moral support while I was away doing this programme.

My siblings, Yolande, Arnaud and Christian Ngnie, for just being the best siblings ever.

My parents, Emmanuel and Pauline Ngnie, for always believing in me and never failing to care about me all the time. I will be forever grateful for having such amazing parents.

My incredible husband Gustave Kenne, for always cheering me up when I am nearly losing my mind after my countless difficult syntheses, for providing me advices and valuable resources that made my research progress less difficult and finally thank him for just being my blessing.

Radio France International (RFI) for keeping me awake, productive and well updated day and night especially during my write-up.

The Organisation of Women in Science of the Developing World (OWSDW), SIDA (Swedish International Development Agency), the Medical Research Council (MRC) of South Africa and Rhodes University for the financial support throughout my project.

DEDICATION

To my husband **KENNE DEDZO GUSTAVE**

LISTS OF ABBREVIATIONS

1,3-DC	1,3 Dipolar Cycloaddition
ADT	Autodock Tools
AZT	Azidothymidine
BSA	Bovine Serum Albumin
BOC	Di- <i>tert</i> -butyldicarbonate
COSY	Correlation Spectroscopy
DEPT	Distortionless Enhancement by Polarisation Transfer
DIG-POD	Digoxigenin Peroxidase
DMF	Dimethylformamide
DNA	Deoxyribonucleic Acid
DSV	Discovery Studio Visualizer
ELISA	Enzyme-Linked Immunosorbent Assay
FMO	Frontier Molecular Orbital
GA	Genetic Algorithms
HIV	Human Immunodeficiency Virus
HMBC	Heteronuclear Multiple-Bond Coherence
HOMO	Highest Occupied Molecular Orbital
HRMS	High Resolution Mass Spectrometry
HSQC	Heteronuclear Single-Quantum Coherence
IN	Integrase
IR	Infrared

LUMO	Lowest Unoccupied Molecular Orbital
MeOH	Methanol
MW	Microwave
MTP	Microtiter Plate
Nf	Nonaflyl (-SO ₂ C ₄ F ₉)
NMR	Nuclear Magnetic Resonance
VDW	van der Waals
PDB	Protein Data Bank
PI	Protease Inhibitor
PR	Protease
RNA	Ribonucleic Acid
RT	Reverse Transcriptase
STD	Saturation Transfer Difference
THF	Tetrahydrofuran
TLC	Thin Layer Chromatography
TOCSY	Total Correlation Spectroscopy

CONTENTS

	Page
Abstract	ii
Acknowledgements	iii
Dedication	v
List of abbreviations	vi
Contents	viii
 CHAPTER ONE.....	 1
GENERAL INTRODUCTION	1
1.1. GENETICS AND LIFE CYCLE OF HUMAN IMMUNODEFICIENCY VIRUS	1
1.1.1. HIV enzymes	4
1.1.2. HIV mutations.....	7
1.2. DRUG DESIGN AND DISCOVERY.....	8
1.2.1. Successful HIV-1 inhibitors	8
1.2.2. Anti HIV medication.....	11
1.3. BACKGROUND OF RESEARCH AND PROBLEM STATEMENT	17
 CHAPTER TWO	 19
SYNTHESIS OF POTENTIAL PROTEASE INHIBITORS.....	19
2.1. INTRODUCTION: PRIVILEGED ORGANIC SCAFFOLDS.....	19
2.1.1. Peptidomimetics.....	19
2.1.2. Indenols	20
2.1.3. Coumarins.....	22
2.2. SYNTHETIC STRATEGIES.....	25
2.2.1. 1,3-Dipolar cycloaddition	25
2.2.2. The Baylis Hillman reaction	34
2.2.3. Palladium catalyzed reactions	36

2.3. GREEN CHEMISTRY CONSIDERATIONS	41
2.4. RESULTS AND DISCUSSION	44
2.4.1. Synthesis of benzotriazoles	44
2.4.2. Synthesis of coumarins.....	68
2.4.3. Application of the Heck reaction	87
2.5. SUMMARY	107
CHAPTER THREE.....	108
SYNTHESIS OF POTENTIAL INTEGRASE INHIBITORS	108
3.1. INTRODUCTION	108
3.2. RESULTS AND DISCUSSION	111
3.2.1. Synthesis of acrylamide	111
3.2.2. Synthesis of cinnamic acid derivatives	116
3.2.3. Synthesis of benzyl cinnamate esters	118
3.2.4. Synthesis of protected amino acid cinnamate conjugates.....	120
3.2.5. Synthesis of cinnamate ester-AZT conjugates.....	130
3.3. SUMMARY	135
CHAPTER FOUR.....	136
EVALUATION OF COMPOUNDS AS HIV-1 ENZYME	
INHIBITORS	136
4.1. INTRODUCTION	136
4.1.1. Background: Molecular modelling	136
4.1.2. Docking modes	138
4.1.3. Major steps in molecular docking	140
4.1.4. Docking calculations	141
4.1.5. Limitations of molecular modelling.....	144
4.1.6. <i>In vitro</i> biological assays	145
4.1.7. Saturation Transfer Difference (STD) NMR experiments	148
4.2. BIOLOGICAL RESULTS AND DISCUSSION	149
4.2.1. Qualitative assessment of binding by STD NMR	149
4.2.2. Computer modelling and biological assay studies	153

4.3. SUMMARY	189
CHAPTER FIVE	192
SUMMARY AND GENERAL CONCLUSIONS	192
CHAPTER SIX.....	195
EXPERIMENTAL.....	195
6.1. GENERAL.....	195
6.2. PROCEDURES	196
6.2.1. Preparation of benzylalcohol derivatives.....	196
6.2.2. Preparation of benzylazide.....	198
6.2.3. Iodination/bromination of anthranilic acid	199
6.2.4. Preparation of benzotriazole derivatives	202
6.2.5. Preparation of coumarin analogs	217
6.2.6. Nonaflation of salicylaldehyde derivatives.....	224
6.2.7. Preparation of Heck adducts.....	226
6.2.8. Preparation of indenol derivatives	238
6.2.9. Preparation of acrylamide derivatives	239
6.2.10. Preparation of benzyl ether derivatives.....	240
6.2.11. Preparation of cinnamic acid derivatives	242
6.2.12. Preparation of protected amino acid cinnamate conjugates.....	247
6.2.13. Preparation of cinnamate ester derivatives.....	252
6.2.14. Preparation of cinnamate ester-AZT conjugates.....	255
6.2.15. General procedure for docking studies	257
6.2.16. Saturation Transfer Difference (STD) Assay	258
6.2.17. HIV-1 enzyme inhibition assays.....	259
REFERENCES.....	262
APPENDIX.....	278
A.1. IR OF VANADIUM CATALYST	278
A.2. CHARACTERISTICS OF COMMON DOCKING PROGRAMS	278

CHAPTER ONE

GENERAL INTRODUCTION

Human Immunodeficiency Virus (HIV) has had a devastating impact on the world's poorest countries. The human health impact of this disease is undeniably severe since it results in increased susceptibility to disease as well as general morbidity and mortality.

HIV incidence has fallen in 33 countries, 22 of them in sub-Saharan Africa, the region most affected by the Acquired Immuno Deficiency Syndrome (AIDS) epidemic. However, the epidemic continues to be more severe in southern Africa, with South Africa having the highest proportion of people living with HIV (an estimated 20%) than any other country in the world.¹

According to the 2011 UNAIDS Report, more people than ever are living longer with HIV, largely due to greater access to treatment. The number of people dying of AIDS-related causes fell to 1.8 million in 2010, down from a peak of 2.2 million in the mid-2000s.²

Almost all current methods of HIV infection treatment fall into the category of either containment or prevention. Due to problems associated with the mechanism of mutation of the HIV virus, all attempts to find a cure have so far been unsuccessful. Consequently, researcher's efforts are more and more directed towards the design of drugs used as HIV-1 enzyme inhibitors.

1.1. GENETICS AND LIFE CYCLE OF HUMAN IMMUNODEFICIENCY VIRUS

In order to fight against the HIV-1 virus, a detailed review of its structure and life cycle is necessary. The HIV virus has two strains which are HIV type 1 (HIV-1) and HIV type 2 (HIV-2). Ninety percent of the deaths related to the HIV infection are caused by HIV-1.

The HIV-1 virus possesses a glycoprotein linked to a lipid bilayer through the protein coat surrounding the core, which comprises the RNA and the enzymes (Figure 1.1). The complete set of genes of HIV-1 codes for 15 distinct proteins. Three of them, reverse transcriptase (RT), integrase (IN), and protease (PR) carry out important enzymatic functions in the viral proliferation.³

The mode of action of HIV in humans is now well known. As indicated in Figure 1.1, seven major steps are involved in the HIV virus replication. Before replication can take place, the virus must be attached to the membrane of the host cell (step 1). This is effected *via* the interaction of CD4 protein present on the cellular membrane of the target cell, with coreceptors CCR5 and CXCR4 attached to the viral envelope glycoprotein (gp 120, gp 41) of the virus A.⁴ Following the attachment, the genetic material is transferred into the cell (step 2) and the RNA is reverse transcribed to DNA by the reverse transcriptase (step 3). Subsequently, the integration of the viral DNA into the genetic material of the cell is catalyzed by the integrase enzyme (step 4). The integrated retroviral DNA is termed a provirus. The activation of the host cell is effected by the transcription of the viral DNA into the messenger RNA (step 5) which is then translated into viral polyproteins which are cleaved at specific locations by the last enzyme: the protease. It acts here as a molecular pair of scissors to give individual mature proteins. New virions are made by the fusion of the RNA and viral proteins (step 6) which bud out of the cell which is consequently destroyed (step 7). The released virions are ready to infect other cells and continue the cycle all over again. When the immune system of the host is completely compromised by HIV, the disease reaches its final stage which is AIDS. The patients develop opportunistic diseases such as cryptosporidiosis, histoplasmosis, toxoplasmosis, pneumonia and tuberculosis which often lead to death in a very short time if the infection is not controlled.

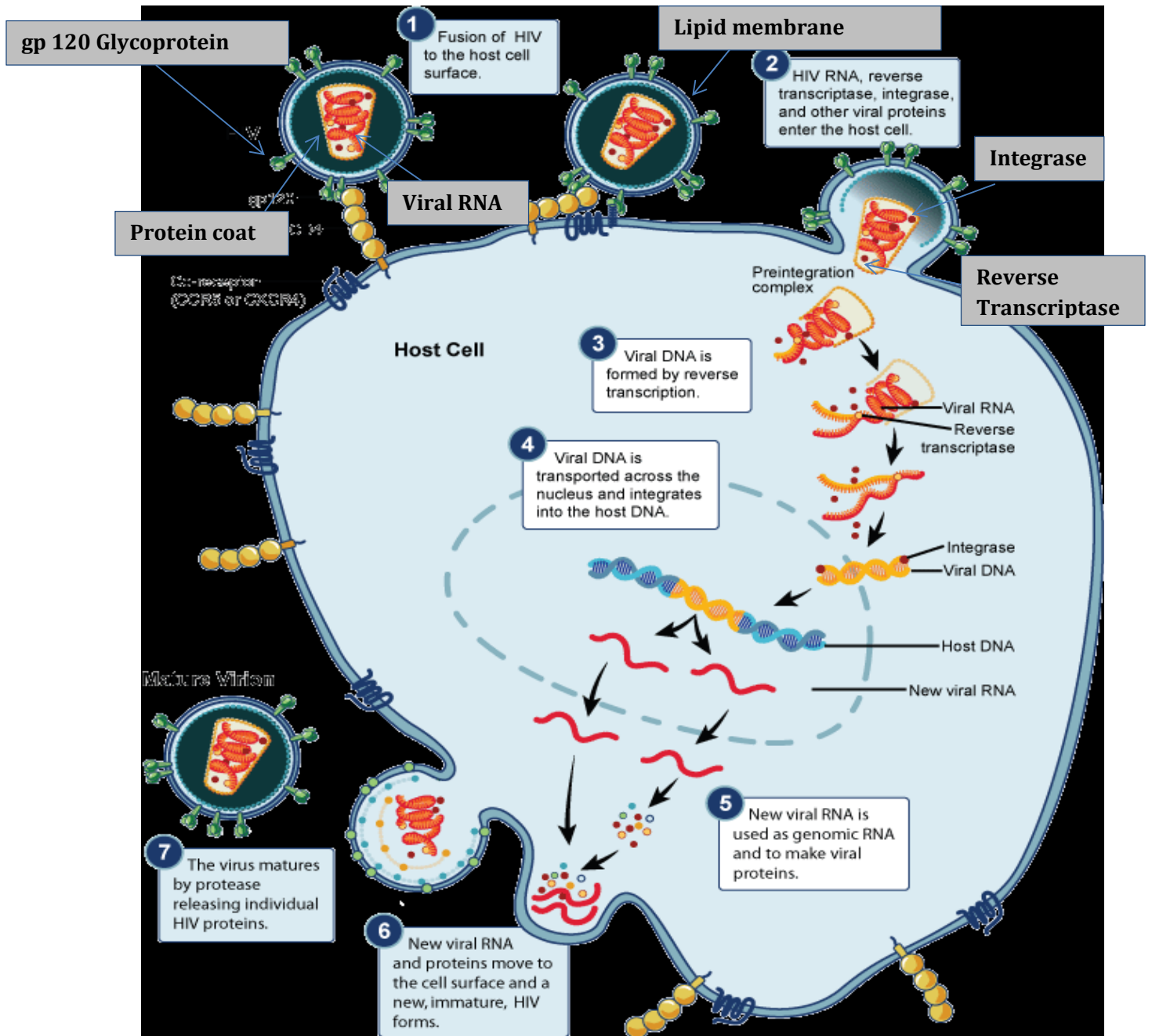


Figure 1.1. Major steps of HIV's attack on the human immune system (reproduced by permission)⁵

1.1.1. HIV enzymes

1.1.1.1. The reverse transcriptase enzyme

The HIV reverse transcriptase enzyme (RT) was discovered by Temin and Baltimore in 1972, long before AIDS was identified in 1981. For this important discovery, they received the Nobel Prize for physiology and medicine in 1975.

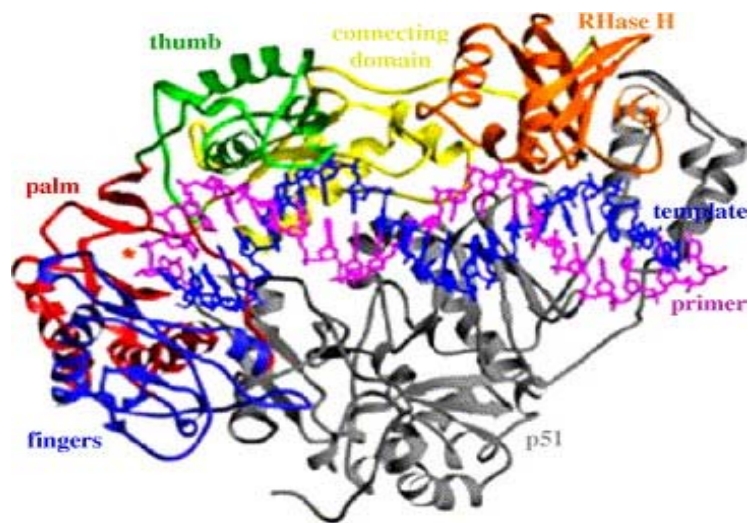


Figure 1.2. Crystal structure of the HIV-1 reverse transcriptase enzyme (reproduced by permission)^{6, 7}

From the crystal structure illustrated in Figure 1.2, it appears that the RT enzyme is a heterodimer composed of a 66 kDa subunit (p66) and a 51 kDa subunit (p51).⁸ The polymerase domains of p66 and p51 are composed of four subdomains which are the fingers, palm, thumb, and connection. Nucleic acid interactions with the protein take place on the DNA's sugar-phosphate backbone, involving amino acid residues of the palm, thumb, and fingers of p66.⁹

The RT enzyme catalyses both RNA directed DNA synthesis and DNA directed DNA synthesis in the host cell.¹⁰ During transcription in the HIV replication cycle, a single-stranded viral RNA is transcribed into a double-stranded DNA from the RNA template.^{11, 12} Generally, newly copied genomes differ from the original genome by only one nucleotide out of a total of up to 9749 nucleotides.^{13, 14}

1.1.1.2. The integrase enzyme

Proteolytic studies reported that the full-length HIV-1 integrase (IN) enzyme (288 amino acids) has three functional fragments: the catalytic core domain, the *N* terminal domain and the *C* terminal domain.¹⁵ A brief review of the structure of these domains shows that they have different functionalities.

The catalytic core domain is made of a catalytic triad of D 64 and D 116 (Aspartic acids) and E 152 (Glutamic acid) called the DDE motif.¹⁶ These residues coordinate divalent cations (Mg^{2+} or Mn^{2+}) that form a bridge with the DNA substrate and define the active site for attachment to the host DNA. The *N*-terminal domain contains a pair of HIS and CYS residues involved in chelating zinc.¹⁷

The integration process is a critical point in the replication cycle of HIV.¹⁸⁻²¹ The integration is done in a two-step coordinated process of processing and joining reactions.^{22, 23} During processing, the IN enzyme cuts the linear viral DNA between two base pairs from the 3'-end of each viral strand.²⁴ Two nucleotides are removed from each 3'-end of the viral DNA and give the terminology 3'-end processing to the reaction. Water serves as the nucleophile for cleavage at the ends of the viral DNA. The terminal 3'-hydroxyl group is then exposed and can be joined to the target DNA. Subsequently, the processed viral 3'-ends and the 5'-ends of the strand broken in the host DNA are connected in the second step.^{22, 25}

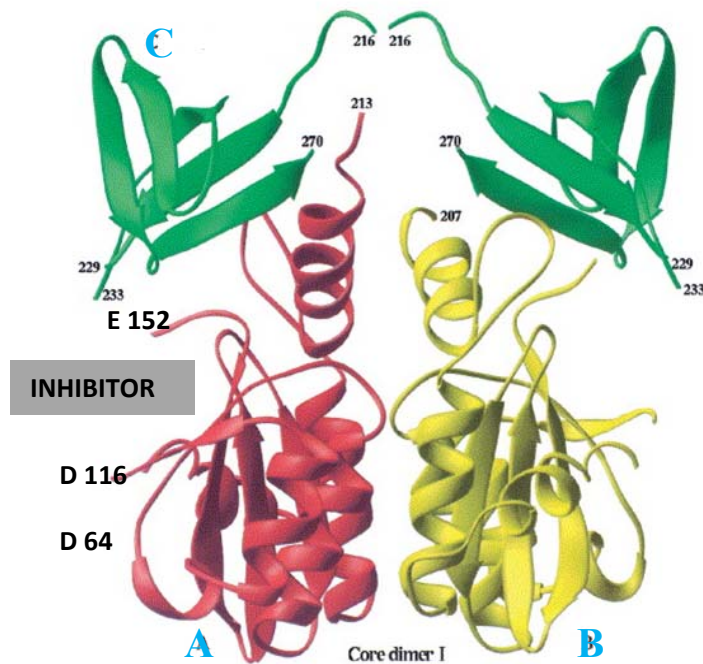


Figure 1.3. Crystal structure of the integrase enzyme, (A) catalytic core domain, (B) *N* terminal domain, (C) terminal domain (reproduced by permission)^{20, 26}

1.1.1.3. The protease enzyme

The crystallographic structure of the HIV-1 protease (PR) enzyme is well known and is the most studied of the HIV enzymes.²⁷ As depicted in Figure 1.4, it is a C_2 symmetric homodimeric enzyme having 99 amino acids in each monomer including an *N*-terminal PRO and *C*-terminal PHE, an alpha helix and 9 beta strands.^{28, 29} The tunnel formed between the two subunits is covered by two flexible protein flaps. The active site is situated at the junction between the two monomers and is composed of an ASP-THR - GLY (ASP 25, THR 26 and GLY 27) sequence common to aspartic proteases. As highlighted in Figure 1.4, ASP 25 plays a crucial role in binding the substrate (inhibitor).

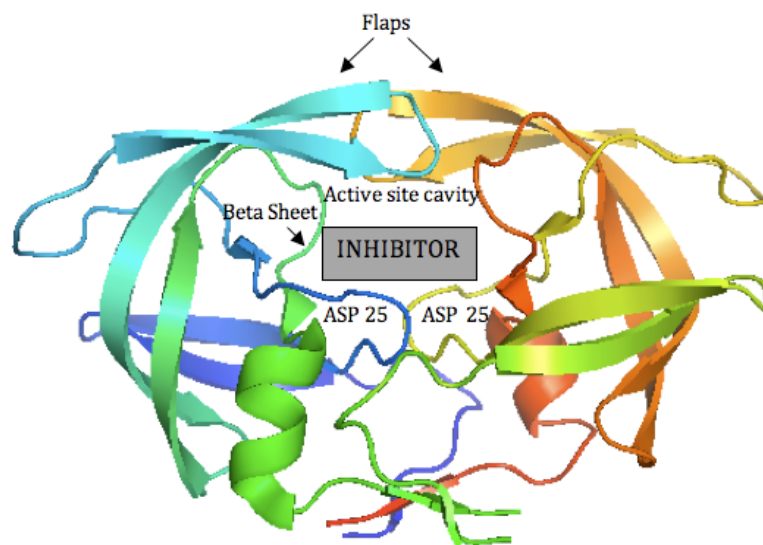


Figure 1.4. Crystal structure of HIV protease (reproduced by permission)^{30, 31}

HIV-1 PR cuts the polyprotein into the proper protein-sized pieces.³² The breaking of the proteins in the active site is performed by a water molecule acting as a nucleophile, hydrolyzing the scissile peptide bond. The individual functional HIV proteins thus obtained and two molecules of viral RNA assemble within the envelope protein to form a mature virion which buds out of the cell. The new virions then infect other healthy host cells and there repeat the viral replication cycle.

1.1.2. HIV mutations

The HIV virus is notorious for its high mutation rate. This has led to a variable viral population within and between individuals. According to Temin's discoveries, mutations in the virus take place within the replication cycle.³³ During the transcription step in the HIV-1 replication cycle, the RT enzyme makes many mistakes. It is estimated that 0.2 errors per genome during the transcription from DNA by RNA polymerase II are identified.^{34, 35} Consequently, on a daily basis nearly 10^4 to 10^5 mutations occur at each nucleotide position.³⁵

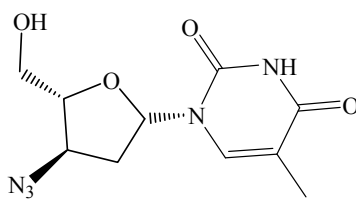
1.2. DRUG DESIGN AND DISCOVERY

A drug can be defined as a substance that can heal, cure or intoxicate a body system when it is ingested.³⁶ Due to the complexity of viruses and drug resistance, the search for new and more effective drugs against virally induced illnesses is always ongoing. Drug design and discovery have been used successfully as a tool for designing molecules to inhibit enzymes related to the development of pathologies. The strategy is the following: first select the appropriate targets; second, determine the most suitable “ hits”-small molecules which are able to bind strongly to the appropriate target; finally, design a compound which optimizes the activity and properties of interest, taking into consideration toxicity and safety concerns. In 2009, it was reported that many of the top 200 pharmaceutical products sold are enzyme inhibitors.³⁷ The impact of rational design drug discovery in the design of HIV drugs is tremendous. In a very short time, this highly lethal syndrome has been reduced to a bearable sustained infection.³⁸

1.2.1. Successful HIV-1 inhibitors

Since the discovery of HIV, the understanding of the role of each of the components involved in its life cycle has been recognized as crucial in the development of enzyme inhibitors at each step.⁴

1.2.1.1. Reverse transcriptase inhibitors Azidothymidine: the breakthrough



1 AZT

Following the first report of AIDS by the US Center for Diseases Control, after six years of intensive studies by researchers, HIV-1 was identified as the causative agent of AIDS.⁴ Reliable tests to identify infected persons not showing any apparent signs of the disease were conceived and the first rationally designed effective therapy Azidothymidine (AZT **1**) was discovered. AZT **1** was first designed to be used as an anti-cancer drug in 1960.

Due to its inefficiency against cancer cells, it was then tested as an anti HIV agent.³⁹ HIV treatment with AZT **1** considerably decreased mortality and delayed the appearance of HIV related opportunistic diseases.

Also known as Zidovudine or Retrovir, AZT **1** is a drug belonging to nucleoside analogs or nucleoside reverse transcriptase inhibitors.⁴⁰ AZT **1** seemed to have similar activity to many other antiretroviral drugs except for Stavudine. It is also active for the prevention of infection after being exposed to the virus (post-exposure prophylaxis) and prevention of mother to child transmission.⁴¹ A recent publication has established that the triphosphate metabolite of AZT **1** is responsible for the specific inhibition of HIV reverse transcriptase.⁴²

AZT **1** was a life rescuing miracle drug. Before it became available on the market, in 1987, AIDS patients had less than a year to fight the disease. The discovery of AZT **1** has fuelled the approval of other antiretroviral drugs (Table 1.1).⁴² Furthermore, these drugs (didanosine for instance) made AZT **1** cheaper.

Table 1.1. FDA approved Non-nucleoside Reverse Transcriptase Inhibitors (NNRTIs) and Nucleoside/Nucleotide Reverse Transcriptase Inhibitors (NRTIs)⁴³

Non-nucleoside Reverse Transcriptase Inhibitors (NNRTIs)		Nucleoside/Nucleotide Reverse Transcriptase Inhibitors (NRTIs)	
Generic Name (Acronym)	Brand Name	Generic Name (Acronym)	Brand Name
Delavirdine (DLV)	Rescriptor	Abacavir (ABC)	Ziagen
Efavirenz (EFV)	Sustiva	Didanosine (ddI)	Videx
Etravirine (ETR)	Intelence	Emtricitabine (FTC)	Emtriva
Nevirapine (NVP)	Viramune	Lamivudine (3TC)	Epivir
Rilpivirine (RPV)	Edurant	Stavudine (D4T)	Zerit

1.2.1.2. Integrase Inhibitors

The development of integrase inhibitors is based on tests using recombinant integrase and oligonucleotide templates acting at the extremity of the viral DNA.⁴⁴ They have a high therapeutic index because they do not hinder normal cellular processes.⁴⁵ In the presence

of these inhibitors, the integration of HIV-1 DNA into the host genome is interrupted. In this case, viral latency takes place.

1.2.1.3. Protease inhibitors

Among the several strategies involved in HIV therapy, protease inhibitors (PIs) are the most successful to date.⁴⁶ The elucidation of the mechanism of this enzyme was a great achievement in the development of effective inhibitors against HIV.⁴ PIs are designed so that they can fit into the active site of the aspartyl residue of the enzyme. Their efficacy and viability depend on their resistance to hydrolysis in the active site.⁴⁷ Accordingly, the viral load of infected patients will diminish gradually. Furthermore, they prevent the scission of host proteins and consequently diminish protease related cytotoxicity, apoptosis and necrosis of infected cells.²⁹

In Table 1.2 the names of the nine approved PIs are given. Many other HIV-1 PIs are still under clinical trial, their effectiveness being affected by the mutation of the virus.⁴⁸

Table 1.2. FDA approved PIs ⁴³

Generic Name (Acronym)	Brand Name
Atazanavir (ATV)	Reyataz
Darunavir (DRV)	Prezista
Fosamprenavir (FPV)	Lexiva
Indinavir (IDV)	Crixivan
Nelfinavir (NFV)	Viracept
Ritonavir (RTV)	Norvir
Saquinavir (SQV)	Invirase
Tipranavir (TPV)	Aptivus
Lopinavir (LPV)	Aluvia

1.2.2. Anti HIV medication

By preventing the multiplication of the HIV virus in the body system, anti-HIV drugs have significantly increased the life expectancy of infected patients. Because the HIV-1 virus develops some resistance towards mono antiviral therapy due to enzyme mutation,²⁸ recent development of daily treatment regimens combining active drugs were found to be effective in circumventing this problem. This new approach was named Anti-Retroviral Therapy (ART). An ART cocktail is made up of three or more anti-HIV medications from at least two different drug classes.

The US Food and Drug Administration (FDA), the organization in charge of food safety and pharmaceutical drug regulation in the US, has approved several enzyme inhibitors in order to satisfy the demand for anti HIV medication.⁴⁹ According to the 2012 “*Guidelines for the Use of Antiretroviral Agents in HIV-1-Infected Adults and Adolescents*” (see Table 1.1), twelve FDA approved reverse transcriptase inhibitors and the first integrase inhibitor (Raltegravir) have been accepted for clinical use.⁵⁰ Nine FDA approved PIs are also currently available (see Table 1.2).

Combinations of these drugs are administered under the name of Highly Active Anti-Retroviral Therapy (HAART).

1.2.2.1. Highly Active Anti-Retroviral Therapy

Highly Active Anti-Retroviral Therapy (HAART), also called combination anti-HIV chemotherapy,⁵¹ is a first line treatment for HIV-1 infection. In the HIV medication library, there are four main groups of inhibitors:⁵² protease inhibitors, nucleoside/nucleotide analog reverse transcriptase inhibitors (NRTIs), non-nucleoside reverse transcriptase inhibitors (NNRTIs), and cell membrane fusion inhibitors.⁵³ The strategy behind HAART is simple: by combining these classes of drugs, the CD4 level of patients is increased while the viral load in the blood is reduced and the development of opportunistic diseases is lowered.

Association of PIs with two other HIV drugs is recommended for the treatment of the HIV infection. It was demonstrated that a cocktail of NRTI's (Didanosine **3**, Lamivudine

6, Stavudine 7 and/or Zidovudine 1) and PIs (Indinavir or Saquinavir 11) have a concerted activity with Nevirapine 5 for the treatment of HIV.⁵⁴

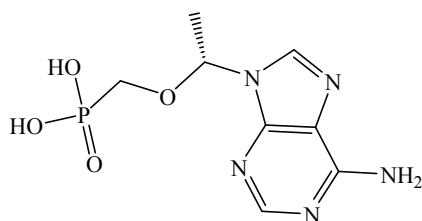
1.2.2.1.1. Examples of NRT and NNRT inhibitors

Nucleoside analogs need to go through phosphorylation before being active in the body system while nucleotide analogs are already chemically active.⁵⁵

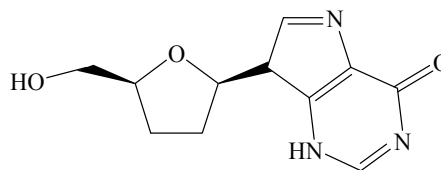
As illustrated by their chemical structure, NNRTIs have a butterfly conformation (see structures of Nevirapine and Efavirenz).⁵⁶ NNRTIs bind to a hydrophobic pocket (an allosteric ‘non-substrate binding’ site) close to the RT active site. This pocket is situated in the palm domain of the p66 subunit, at a distance of 10 Å from the polymerase active site.⁶ NNRTIs prevent the polymerization of DNA from viral RNA. Both the conformation and the mobility of the RT are altered and a non-competitive inhibition is exhibited. The activity of NNRTIs is specific to HIV-1.⁵⁷ An improvement in the activity of NNRTIs was effected by performing optimizations of hydrogen bonding with LYS 101 and hydrophobic interactions with TYR 181, TYR 188 and TRP 229 in the active site of the RT, based on data provided by their crystallographic structure.

In the 1980s, the discovery of the first two classes of NNRTIs: 1-(2,2-hydroxyethoxymethyl)-6-(phenylthio)thymine (HEPT) and tetrahydro-imidazo[4,5,1][1,4]benzodiazepin-2(1*H*)-one and thione (TIBO) compounds was an important milestone in the search for potent NNRTIs.⁵⁸ A decade later, owing to the development of technology relating to molecular biology, compound screening methods led to the identification of the first generation of FDA approved NNRTIs composed of Nevirapine 5, Delavirdine and Efavirenz 4.⁵⁹ Didanosine 3 was discovered in 1991 and is prescribed as an alternative treatment for patients resistant to AZT 1.⁶⁰

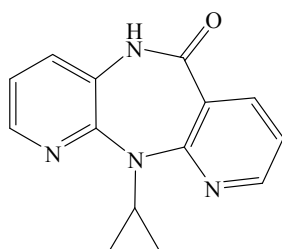
In 2010, Tenofovir 2 was the only approved nucleotide analog reverse transcriptase inhibitor used as a substitute for Stavudine 7, which presents many side effects.^{42, 61}



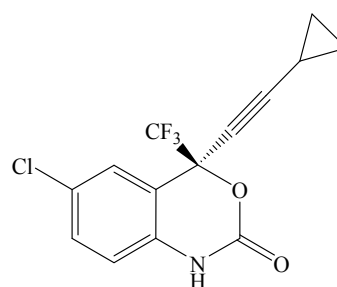
2 Tenofovir



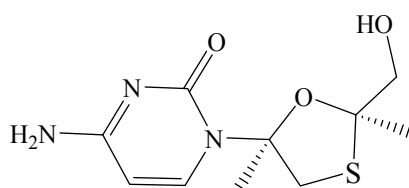
3 Didanosine



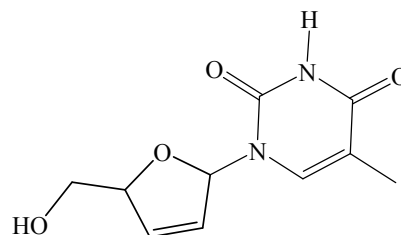
4 Efavirenz



5 Nevirapine



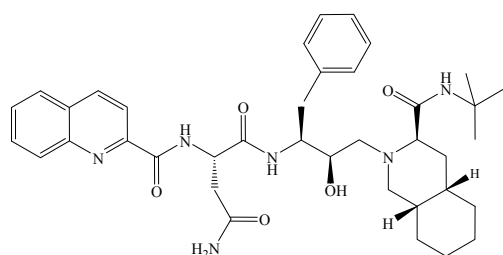
6 Lamivudine



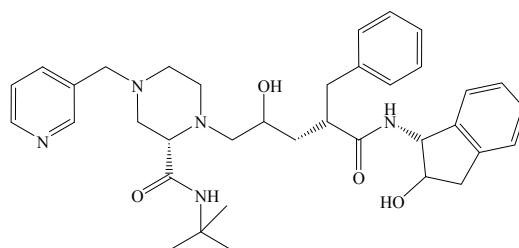
7 Stavudine

1.2.2.1.2. Examples of protease inhibitors

The time-line of PIs falls into three generations of inhibitors. The first generation included Saquinavir **8** in 1995, followed by Ritonavir and Indinavir **9** in 1996 owing to oral absorption enhancement.⁶² In 1997, the introduction of Nelfinavir and then Amprenavir in 1999 marked the end of that era. To circumvent problems associated with the development of drug resistance towards the first generation of PIs, the research community designed a second generation of inhibitors. For this purpose, in 2000 Lopinavir and Fosamprenavir were approved and three years later Atazanavir. An improvement in the genetic barrier for resistance led to the approval of a third generation of PIs consisting of Tipranavir **10** in 2005 and Darunavir **11** in 2008.⁶³

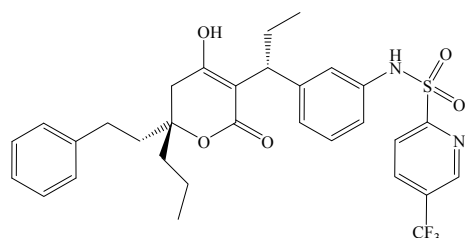


8 Saquinavir

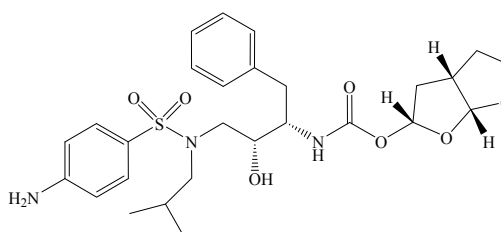


9 Indinavir

All PIs inhibit the PR enzyme, although they follow different mechanisms of action. Darunavir prevents the splitting of HIV encoded Gag-Pol polyproteins in contaminated cells and hence interrupts the formation of mature viruses. Saquinavir **8** is a peptidomimetic inhibitor which plays the same role as Darunavir **11** but whose metabolism by cytochrome P450 significantly compromises its activity.⁶³ As indicated by its structure, Tripanavir **10** is a sulfonamide functionalized hydropyrone. It is also used in combination therapy with Ritonavir. Ritonavir itself is also an inhibitor of the enzyme cytochrome P450 CYP3A4 which is involved in drug metabolism.^{64, 65} It shows a good enhancement of pharmacokinetic (PK) profiles associated with treatment with PIs.⁶⁶



10 Tripanavir

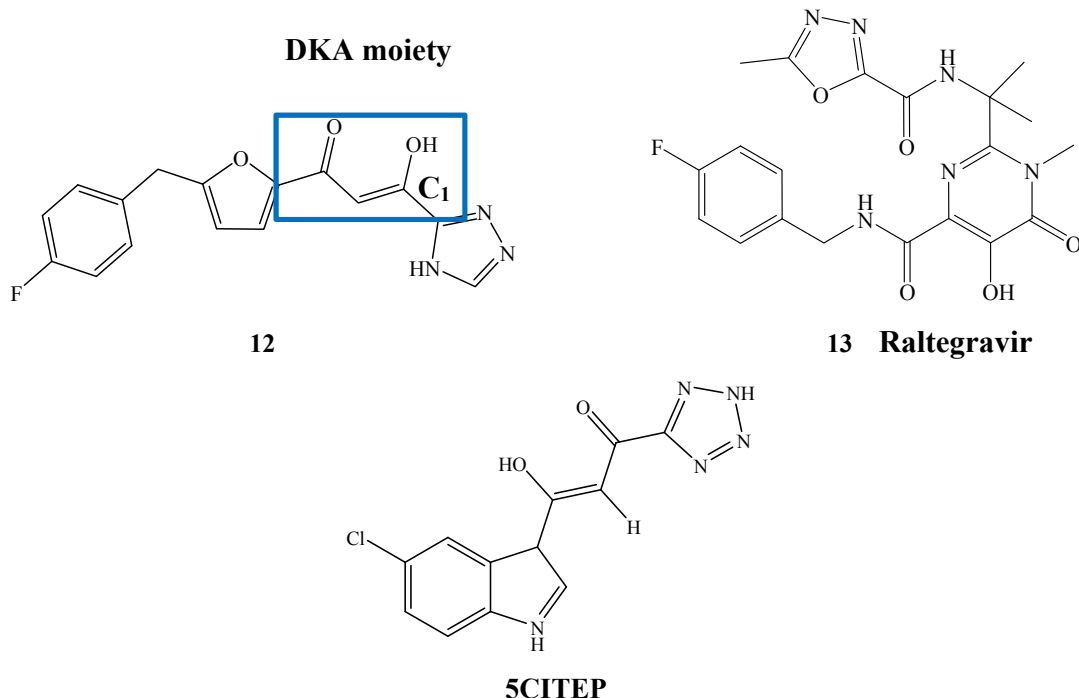


11 Darunavir

1.2.2.1.3. Examples of integrase inhibitors

It was reported that the diketo acid (DKA) functionality endows IN inhibitors with good inhibitory activity.⁶⁷ The coordination of the DKA moiety to magnesium cations in the active site of the IN enzyme, more specifically in the vicinity of ASP 64, ASP 116 and GLU 152 residues explains the importance of its presence on the backbone of the inhibitor.⁶⁸ Compound **12** was the first DKA inhibitor to undergo clinical trials. However,

the *in vivo* reduction occurring at C₁ afforded an inactive metabolite which contributed to its loss of activity.⁶⁹



Implementing changes to the DKA pharmacophore and introducing derivatisation on the skeleton of compound **12**, while maintaining its antiviral properties and reasonable toxicity and pharmacokinetic profiles yielded the discovery of Raltegravir **13** in 2007.⁷⁰ Raltegravir **13** is a pyrimidinone carboxamide derivative, first in a class of integrase inhibitors active against many HIV-1 subtypes and the *in vitro* propagation of HIV-2 as well.^{71, 72} **5CITEP** is also an integrase inhibitor which is a diketo derivative active against both 3' processing and strand transfer.

1.2.2.1.4. Examples of fixed dose combination

Fixed dose combination (FDC) treatment consists of multiple anti-retroviral (ARV) medications from one or more drug classes combined in one pill.⁷³ The introduction of FDC in HIV treatment is an important step in the reduction of the current pill burden.⁷⁴ Also, they are more affordable since they contain fewer excipients than a cocktail of individual pills.⁷⁵ Furthermore, they are easy to order, store and distribute owing to the reduced number of separate products.⁷³

Trizivir is an FDC treatment which includes three nucleoside analogs: Abacavir sulfate, Lamivudine **6** and Zidovudine **1**. Stribild is composed of one integrase strand transfer inhibitor (Elvitegravir), one pharmacokinetic enhancer (Cobicista) and two NNRT's (Emtricitabine and Tenofovir **2**).

1.2.2.2. Side effects of HIV inhibitors

Owing to the success of different combination therapeutic regimens, HIV is now considered to be a manageable disease.⁷⁶ Unfortunately, treatment with HIV-1 inhibitors is not without unpleasant side effects. Many health complications are associated with treatments by various HIV inhibitors. Chronic administration drug toxicity, poor tolerability and therapy adjustment due to treatment failures are some of the consequences.³⁸

Even though inhibitory activities and highest value ranges of the Administration, Distribution Metabolism and Excretion (ADME) profile-related descriptors are taken into consideration when the choice of inhibitors' is made, patients under HAART suffer from a wide range of discomforting body responses.⁷⁷ Cardiovascular disease, hepatitis, pancreas damage, glucose intolerance, kidney stones, rashes, depression, fat accumulation and redistribution, nausea, diarrhea, pain or numbness in the feet, mouth inflammation, blurred vision, headaches, dizziness, anemia, weakness, insomnia, and adverse interaction with non-HIV drugs are some of the common problems experienced during the treatment of HIV with various inhibitors.⁷⁸

Out of all the research work that has been carried out on HIV and the treatment of the disease over the last 30 years, an important conclusion can be drawn: the armory developed for the treatment of HIV infections is not exhaustive. There is much room for improvement in controlling viral replication, avoiding side effects of strenuous treatment protocols and effective elimination of the virus from an infected person.³ An imperative demand for the development of new and safer drugs, emphasizing activity against the currently resistant viral strains is awaited. The critical therapeutic aims are to design compounds with exclusive mechanisms of action with minimal side effects which are effective against drug-resistant HIV-1 variants. A perceptible breakthrough in the HIV-1

therapy could also come from a treatment made of a combination of several HIV-1 enzyme inhibitors in concert.

1.3. BACKGROUND OF RESEARCH AND PROBLEM STATEMENT

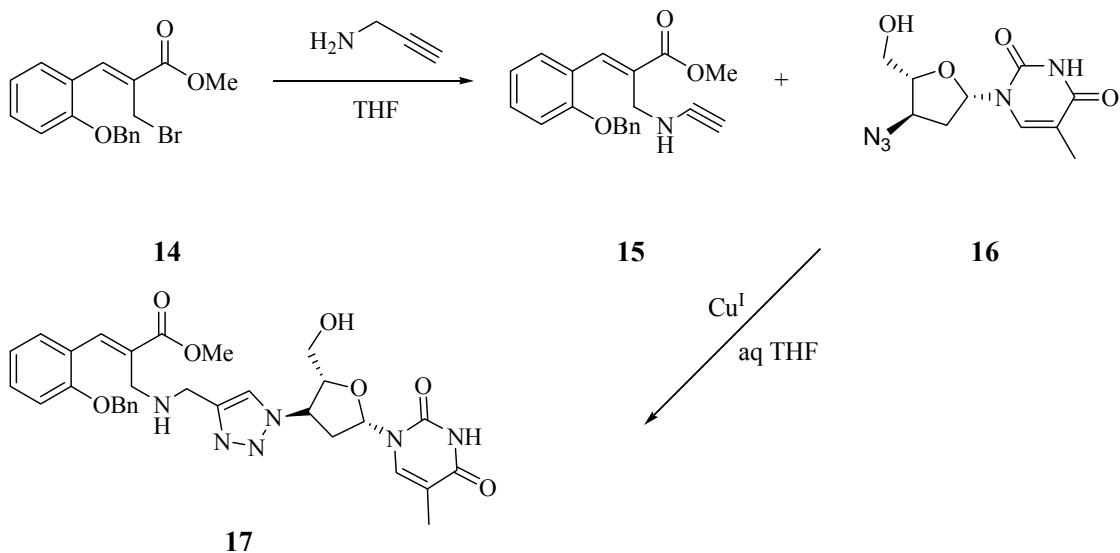
Objective of research

Of the estimated 14.2 million HIV-positive individuals awaiting treatment, nearly 8 million, living in poor African countries, are not currently able to have access to the life-saving antiretroviral treatment because of high cost.⁷⁹ Furthermore, an investigation of 68 approved drugs revealed that it takes an average of 15 years and US\$900 million to successfully generate a new drug, post marketing included. Consequently, the repositioning of old drugs for alternative purposes, to reinforce the treatment of HIV-1 at a low cost, is a timely intervention.⁸⁰

An attractive approach for AIDS treatment is to combine an established anti-HIV drug with novel compounds to generate a new class of drugs. The structure of AZT is such that it contains an azide functionality which obstructs development of the DNA chain, thus inhibiting reverse transcription. Therefore, the chemistry involved in the modification of the structure of AZT can take place at that specific point, including modification of the azide, including Click chemistry. Attempts to synthesize cinnamate esters and binding them to AZT were initiated in our group in 2010.⁸¹⁻⁸³

The geometry of compounds prepared by Olomola in our laboratory was not linear and molecular docking studies of ligands in the active site of the RT and IN enzymes indicated that the compounds did not fit well. Also, an overlay of the docked conformation of the cinnamate ester–AZT conjugates with the well-known integrase inhibitor **5 CITEP** (Structure explained in Section 1.2.2.1.3) revealed that these ligands extend beyond the binding area of **5 CITEP**.⁸¹ This preliminary study laid the foundation for the investigation of the synthesis of more linear derivatives. Prompted by these results, we planned to modify the structure of the target molecule by ensuring linearity between the cinnamate ester and the AZT **1** moiety on an aromatic ring. This could

ensure that the ligand would be buried deeper inside the enzyme pocket and thereby effectively utilize the target area. We expected this strategy to be more efficient.



Scheme 1.1. Synthesis of cinnamate esters-AZT conjugate⁸¹

Further, inspired by the geometry of indenols and benzotriazoles, we also planned to synthesize these compounds and test them as potential PR inhibitors.

Still focussed on the concept of dual action inhibitors, another aim was to target drugs that can be jointly active first against the RT and PR enzymes and second the IN and PR enzymes. Thus, we came up with the aim of joining AZT with benzotriazoles on the one hand to synthesize RT-PR inhibitors and coupling coumarins with activated alkenes to synthesize PR-IN inhibitors as a second strategy.

Particular focus was given to the application of green chemistry principles in the development of synthetic protocols, particularly microwave assisted synthesis and catalytic methods.

CHAPTER TWO

SYNTHESIS OF POTENTIAL PROTEASE INHIBITORS

2.1. INTRODUCTION: PRIVILEGED ORGANIC SCAFFOLDS

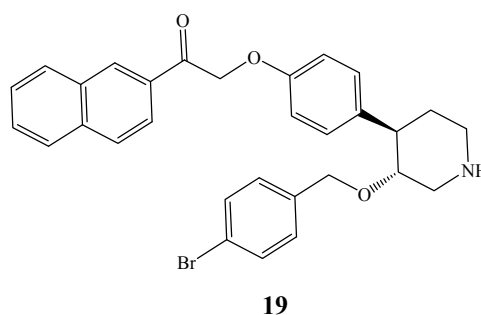
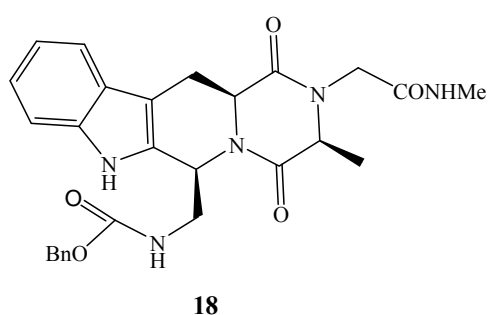
Libraries of compounds impacting biology and medicine in general and more specifically anti HIV treatment are built by using various privileged organic scaffolds. Such molecules include peptidomimetics, indenols, coumarins, cinnamate esters and diketo acids to name just a few.

2.1.1. Peptidomimetics

Peptidomimetics, also called synthetic foldamers, are a class of HIV-1 protease inhibitors.⁸⁴ Due to similarities with their natural peptide counterparts, they can bind to the active site, and thus inhibit the activity of the protease enzyme. Their target is to mimic peptide structure in compounds where the spatial arrangement of functional groups is constrained. Using peptide inhibitors as drugs presents some advantages. The constraints associated with their conformation reduce undesired interactions with other biological receptors and fix the location of some chains of the molecule.⁸⁵ Furthermore, the presence of hydrophobic residues on peptidomimetics plays a crucial role in the enhancement of transport properties of small molecules through biological membranes and they also enhance metabolic stability due to their insensitivity to proteolysis.

However, peptidomimetics also experience significant limitations: poor *in vivo* metabolic stability and potential immunogenicity. Additionally, their permeability across biological barriers is typically very low. Consequently, this results in delivery challenges associated with low oral bioavailability.⁸⁶ In order to circumvent these drawbacks, researchers directed their attention towards the development of a new class of compounds named non-peptide peptidomimetics.

The design of peptidomimetics has led to the development of many scaffolds. The approach of Murphy *et al.* consisted in incorporating β -D-mannopyranose moieties in sugar scaffolds.^{87, 88} Funicello worked on the synthesis of tricyclic heterocycles which can be used as pseudo-peptides in the design of peptidomimetics.⁸⁹ Compound **18** is a THBC-DKP-based peptidomimetic representing a constrained α -turn mimic, an example of a (tetrahydro- β -carboline) (diketopiperazine)-based peptidomimetic scaffold which was recently designed by Airaghi *et al.*⁹⁰

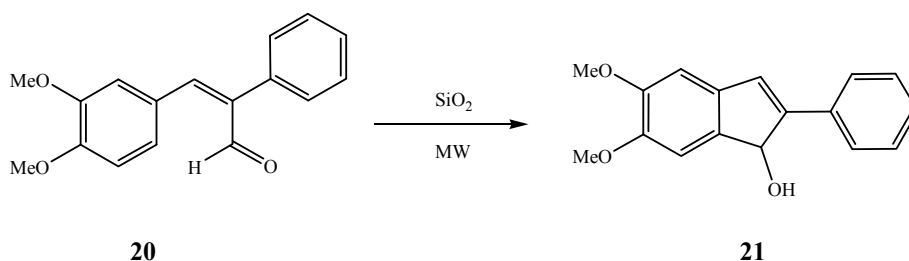


Other non-peptide peptidomimetics have also been evaluated. Bursavich's studies revealed compound **19** (3-alkoxy-4-arylpiperidine) as a new generation of non-peptide peptidomimetic aspartic peptidases.⁹¹ Indinavir, Ritonavir, Saquinavir, and Neflinavir are non-peptidic protease inhibitors currently in clinical use.⁹²

2.1.2. Indenols

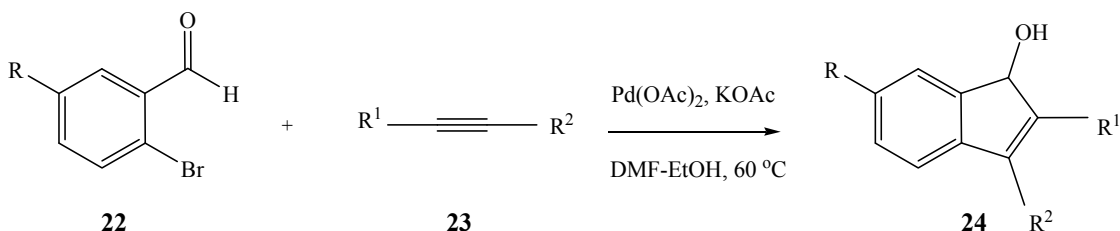
Indenols are an important class of compounds with a wide spectrum of biological activity.⁹³ They are an important structural unit present in various biologically active compounds that possess analgesic, insecticidal, and myorelaxation activities.^{94, 95} They can also be used as intermediates in the synthesis of organic compounds such as indenyl chrysanthemates, which possess insecticidal properties. Because of the aromaticity of indenol systems, hydrophobic interactions with the pocket of the HIV-1 protease enzyme can take place and this qualifies indenols as valuable building blocks to incorporate into the design of peptidomimetic skeletons.

Indenols can be synthesized by different synthetic pathways. Kumar *et al.* reported the synthesis of indenols by silicon dioxide adsorption of unsaturated aldehydes followed by microwave irradiation (Scheme 2.1).⁹³ More recently, Muralirajan *et al.* developed an efficient synthetic strategy for the synthesis of indenols by rhodium-catalyzed C-H activation and carbocyclization of aryl ketones and alkynes.⁹⁴ A Vilsmeier Haack reaction of aromatic Heck adducts can be carried out as well to obtain these compounds.⁹⁶ Many papers have also reported the successful synthesis of indenols by performing an intramolecular Baylis Hillman reaction using various catalysts.⁹⁷⁻¹⁰⁰ Vicente's group prepared a library of indenols by reacting trimethoxyphenyl palladium complexes with a variety of symmetrical and unsymmetrical alkynes.⁹⁵



Scheme 2.1. Microwave promoted synthesis of indenols⁹³

In the same vein, Gevorgyan *et al.* developed a highly efficient variant of the Heck reaction by carrying out a cyclic vinylpalladation of aromatic aldehydes to synthesize indenols using disubstituted alkynes as acceptor molecules (Scheme 2.2).^{101, 102} This synthesis was regioselective and the only regioisomers formed were those having a larger R₁ substituent next to the OH group.



Scheme 2.2. Synthesis of indenols *via* catalytic cyclic vinyl palladation of 2-bromobenzaldehyde¹⁰²

2.1.3. Coumarins

Coumarins are of perennial chemical interest given their long established biological properties. Many of them display important pharmacological effects, including anticoagulant,¹⁰³ anti-inflammatory,¹⁰⁴ estrogenic, antifungal,¹⁰⁵ dermalphotosensitising, antitumor,¹⁰⁶ antimicrobial,¹⁰⁷ antimalarial,¹⁰⁸ vasodilator, molluscicidal, antithelmintic, sedative and hypnotic, analgesic and hypothermic activity.¹⁰⁹ Coumarins also have excellent and well documented photochemical and photophysical behavior.¹¹⁰

In the literature, different reactions are involved in the synthesis of coumarins. They can be either organocatalyzed or metal catalyzed.

2.1.3.1. Organocatalyzed coumarin synthesis

Ranu and coworkers reported the successful synthesis of coumarins by a Knoevenagel condensation of aromatic aldehydes and activated methylene compounds in the presence of a task specific basic ionic liquid (bmin)OH under mild reaction conditions in a maximum time of two hours (A in Scheme 2.3).¹¹¹

The condensation of aroylketene dithioacetals and 2-hydroxybenzaldehydes in the presence of a catalytic amount of piperidine in THF under reflux was also reported to successfully afford 3-aroylecoumarins (B in Scheme 2.3).¹¹²

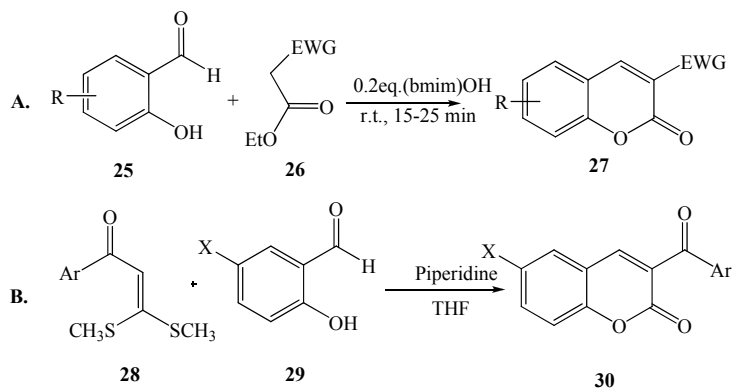
2.1.3.2. Metal catalyzed coumarin synthesis

Coumarins have also been prepared *via* a directed *ortho* metalation-Negishi cross coupling protocol from arylcarbamates.¹¹³ Kalinin described such a synthesis of hydroxycoumarins in three steps. First, the metalation of an arylcarbamate by *sec*-butyl lithium, followed by transmetalation with ZnCl₂, then a cross coupling with an acid chloride in the presence of PdCl₂(PPh₃)₂ to afford an *ortho*-acylated arylcarbamate. Second, a Baker-Venkataraman rearrangement yielded a hydroxyaryl acetamide cyclized by TFA in toluene at the third step to afford hydroxycoumarin (A in Scheme 2.4).

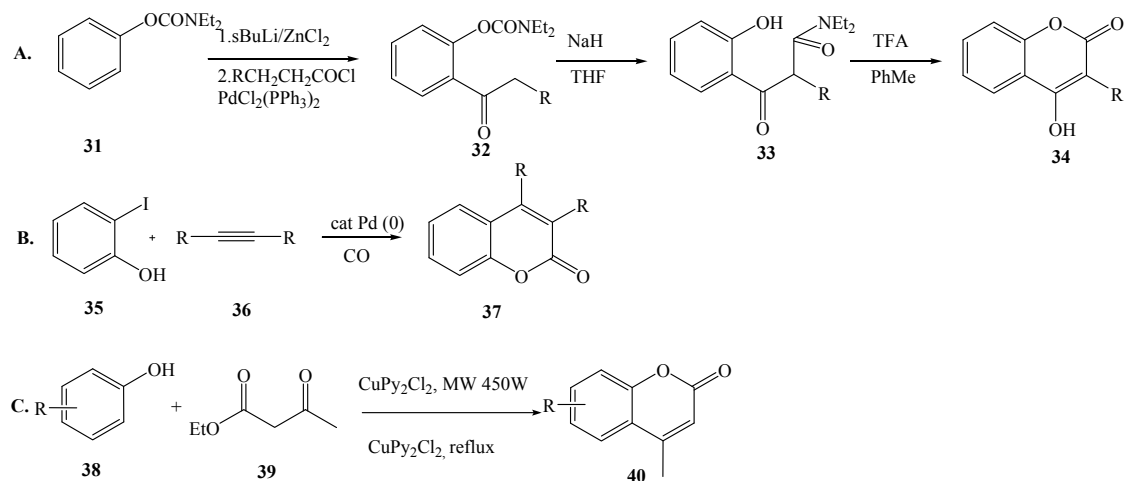
In addition, 3,4-disubstituted coumarins were synthesized by a Larock palladium catalyzed annulation of iodophenol derivatives through the insertion of an internal alkyne

in the presence of carbon monoxide under harsh reaction conditions (reflux at 120 °C in DMF) for 24 hours (B in Scheme 2.4).¹¹⁴

Through the Pechmann synthesis illustrated in C (Scheme 2.4), coumarins were also isolated by reacting different phenols with ethyl acetoacetate in the presence of dipyridine copper chloride for 30 minutes under reflux.¹¹⁵



Scheme 2.3. Organocatalyzed synthetic pathways for coumarins



Scheme 2.4. Metal catalyzed synthetic pathways for coumarins

The properties of these synthetic reactions (Schemes 2.3 and 2.4) were compared.¹¹¹⁻¹¹⁵

- Efficiency

Regardless of the type of catalyst used for the synthesis and the reaction conditions, the above outlined strategies for the synthesis of coumarins exhibited a good yield of 80% on average. Furthermore, the reactions occurred during reasonable reaction times (ten minutes to 24 hours). As far as the cost and the environmental friendliness of the syntheses are concerned, the Knoevenagel condensation (A in Scheme 2.3) is a cheaper and a greener technique since no additional organic solvent is needed and the ionic liquid catalyst is reusable for up to five runs.

While all these syntheses are reasonably efficient, it appears that they present some disparities in selectivity and scope.

- Selectivity

The Negishi coupling demonstrated some selectivity in two aspects. First, the formation of the ortho keto function (compound **32**) on an aryl carbamate was regioselective. Second, the intramolecularity of the Baker-Venkataraman rearrangement of an ortho-acylated arylcarbamate (compound **33**) specifically formed a 2-hydroxyarylacetamide without any side product (A in Scheme 2.4).¹¹³

The Larock annulation presented interesting specificity as well. Kadnicov reported that the insertion of the alkyne to the aryl halide was favored compared to the insertion of CO (B in Scheme 2.4) affording disubstituted coumarins.¹¹⁴

- Scope

Even though the Negishi coupling provided a large scope in aromatic targets, given the number of steps and the metal catalysts involved in this synthesis (A in Scheme 2.4), the Negishi synthesis of coumarins turned out to be expensive. However, the tolerance for a broad variety of functional groups on both readily available alkyne and phenol substrates rendered the Larock annulation very convenient for the synthesis of coumarins bearing multiple functionalities in only one step.

The synthesis of aroylcoumarins *via* pathway B (Scheme 2.3) appeared to be demanding owing to the fact that the synthesis was conducted under inert reaction conditions for 15 hours. In addition, this pathway presented some limitations because the prior synthesis of

arylketene dithioacetals was a prerequisite for the reaction to take place. For this purpose, Knoevenagel synthesis was considered more advantageous as it did not need an inert environment. Also, this condensation has a wide scope on account of the condensation being between an aliphatic or an aromatic carbonyl and easily available methylene compounds. Finally, it is a reaction conducted under mild reaction conditions (room temperature).

2.2. SYNTHETIC STRATEGIES

The synthesis of organic compounds is designed according to various synthetic strategies. For a reaction to be efficient it has to take into consideration atom economy and the transformations taking place have to be chemo-, regio- and stereoselective. Organic synthesis is mostly concerned with functional group modification and/or joining molecular pieces for the construction of molecular frameworks. This can be elegantly achieved through carbon-carbon bond formation between molecules and moreover by expanding the construction on derivatised functional groups. Carbon-carbon bonds can be generated through 1,3-dipolar cycloaddition (Section 2.2.1), the Baylis Hillman reaction (Section 2.2.2), palladium catalyzed reactions (Section 2.2.3) and aldol condensation (Section 3.1) among others, using either conventional energy sources or microwave assisted synthesis. We have focussed on these three carbon-carbon bond forming processes using conventional and microwave methods.

2.2.1. 1,3-Dipolar cycloaddition

The concept of click chemistry was introduced by Sharpless in 2001 to refer to a series of bond forming reactions with wide scope, high selectivity and high yield.¹³⁵ The concern of Sharpless in regards to the slowness and inefficiency of the traditional drug discovery process opened the door to a new approach, where large combinatorial libraries could be readily developed by joining accessible building blocks *via* click reactions.¹³⁶⁻¹³⁸ This reaction has echoed the success associated with the conceptualization and development of asymmetric catalysis which made Sharpless one of the 2001 Chemistry Nobel Prize winners.¹³⁵

Click chemistry is irreversible for practical reactions. They are often cycloaddition reactions, such as the 1,3-dipolar class of reactions, the hetero Diels Alder reactions as well as radical addition, Michael addition, nucleophilic substitution (including ring-opening reactions), carbonyl chemistry and azide-phosphine coupling.^{138, 139}

Click chemistry reactions take place smoothly under mild nontoxic conditions and are usually cited as consistent with the objectives of green chemistry. Click reactions have three main characteristics:

First, they are usually high yielding reactions which require low energy input (can be at room temperature) and are often performed in water, rendering them environmentally safer. Water is a particularly important solvent since it absorbs the heat generated when a reaction is carried out on a large scale, enhancing safety.¹⁴⁰ Click reactions are either addition processes where no by-products are formed or condensation processes with water as the only by-product.^{141, 142} Because they are dependable and completely specific there is often little purification required.¹⁴⁰ The reactions often include a simple product isolation requiring non-chromatographic methods such as crystallization or distillation, affording products stable under physiological conditions.¹³⁷ Often purification can be omitted altogether.

Secondly, other 1,3 dipolar cycloadditions are also used to build carbon-heteroatom-carbon bonds and are tolerant of different functional groups since the functional groups of the reactants and the products do not interact.¹³⁸ As a result, the need for protecting groups is eliminated because most hydroxyl and amide groups involved in click reactions are stable under the reactions conditions.^{135, 137}

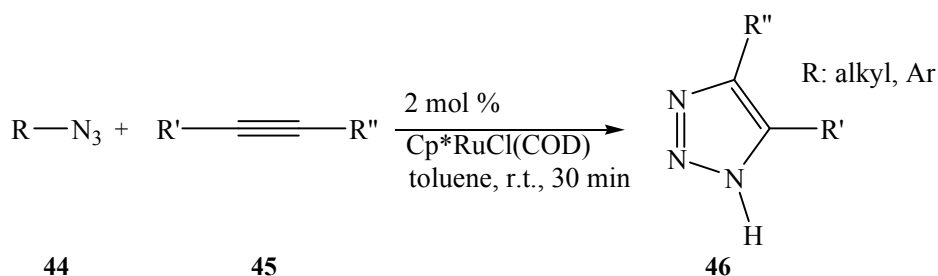
Finally, these reactions generally take place under an oxygenated atmosphere in an aqueous medium using biocompatible reactants and can therefore take place in living cells where these reactions are used to label viruses or biomolecule particles.^{135, 138, 143, 144}

Click chemistry is applicable in polymer synthesis, organic chemistry, bioconjugation, radiochemistry and drug discovery. It can be employed to synthesize a library of small organic compounds, tailor-made macromolecules or bioconjugates in only one or two steps.¹³⁹

From the above mentioned advantages, it can be believed that click chemistry will become a more common approach in the future for a broad range of chemical transformations.

Despite fulfilling all of the aforementioned criteria, the Copper catalyzed click reaction between alkynes and azides has some limitations. The most relevant one was highlighted by Tornøe *et al.* who pointed out that this click reaction is preferably performed between only terminal alkynes and terminal azides. Sterically hindered azides fail to give the target compound.¹⁴⁵ This enforces a geometrical constraint on the structure of the targeted molecule to be isolated *via* this method since only terminal alkynes can be used.

Based on the nature of the catalyst, two types of click reactions can be identified involving azide/alkyne coupling: the copper catalyzed click reaction and the ruthenium catalyzed click reaction. Whereas the Cu(I)-catalyzed reaction is limited to terminal alkynes, the Ru(II)-catalyzed reaction is active with internal alkynes as well (Scheme 2.5).



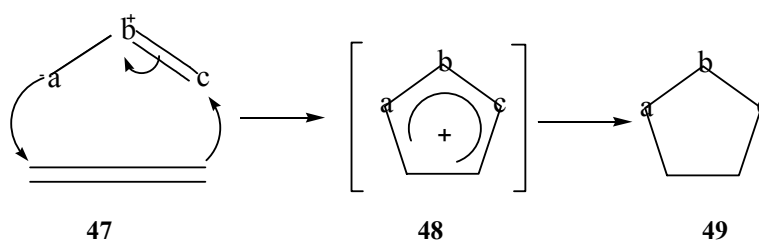
Scheme 2.5. Ruthenium catalyzed cycloaddition of an internal alkyne and an azide ¹⁴⁶

The 1,3-dipolar cycloaddition (1,3-DC) was first applied in organic chemistry by Huisgen in 1963.^{147, 148} Due to requirements such as high temperatures and pressures, this reaction was neglected for decades. In 2001, Kolb and coworkers improved the scope of this coupling reaction considerably by adding a Cu(I) catalyst.¹³⁸ The copper catalyst

decreases the activation barrier by 45.98 kJ/mol and therefore drives the reaction forward with a high selectivity.¹⁴³

2.2.1.1. Characteristics of the 1,3-dipolar cycloaddition

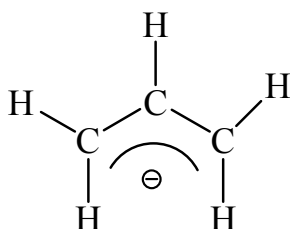
Like the Diels Alder reaction, the 1,3-DC is a $[\pi_4s+\pi_2s]$ concerted reaction between a 1,3-dipole and a dipolarophile through a 6π electron system to give a five-membered cyclic system.^{149, 150} A standard reaction typically requires a dipole and a dipolarophile. Scheme 2.6 portrays a general 1,3-DC reaction.¹⁵¹



Scheme 2.6. a-b-c mechanism of the 1,3-dipolar cycloaddition

The dipolarophile must have at least one π bond. For this reason, alkyne, alkene, carbonyl, imine, azo and nitroso are most indicated.

A 1,3-dipole is a 4π -electron compound composed of a three atom π electron system with one charge-separated resonance structure with opposite charges in a 1-3 relationship. There are two types of 1,3-dipole compounds: the allyl type and the propargyl/allenyl type.¹⁵² The allyl anion has a bent structure with four π electrons in three parallel atomic p_z orbitals.



An allenyl/propargyl dipole is an unsaturated compound with a triple bond in a canonical form. They have a linear structure and possess an additional π orbital orthogonal to the allyl anion type molecular orbital.¹⁴⁹ This and other common 1,3-dipoles are listed in Table 2.1a and 2.1b.

Scheme 2.7. Structure of an allyl anion **50**¹⁵³

Frontier Molecular Orbital (FMO) theory is an excellent tool for understanding the 1,3-DC reaction mechanism. Some 1,3-DC are mainly controlled by a HOMO (dipole)-LUMO (dipolarophile) interaction while others are controlled in the reverse fashion.¹⁵⁴ An electron donating group on the dipole raises the energy of the HOMO and an electron withdrawing group on the dipolarophile lowers the corresponding LUMO, and thus the reduced HOMO (dipole)-LUMO (dipolarophile) controlled scheme results in an accelerated reaction because of the small energy gap between the frontier orbitals.¹⁵⁵ The opposite scenario is observed for a LUMO (dipole)-HOMO (dipolarophile) type reaction.

Table 2.1. Classification of 1,3-dipoles ¹⁴⁸

Table 2.1a. Allyl anion type

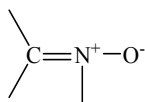
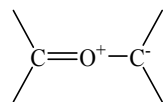
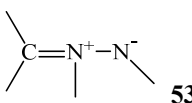
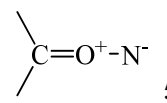
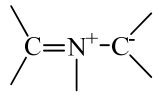
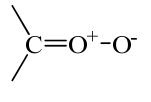
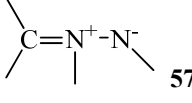
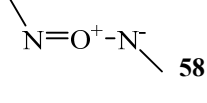
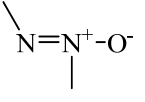
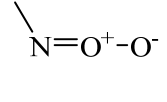
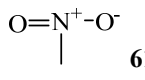
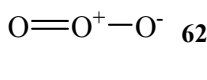
Nitrogen in the middle		Oxygen in the middle	
Nitrones	 51	Carbonyl Ylides	 52
Azomethine Imines	 53	Carbonyl Imides	 54
Azomethine Ylides	 55	Carbonyl Oxides	 56
Azimines	 57	Nitrosimines	 58
Azoxy Compounds	 59	Nitrosoxides	 60
Nitro Compounds	 61	Ozone	 62

Table 2.1b. Propargyl/allenyl anion type

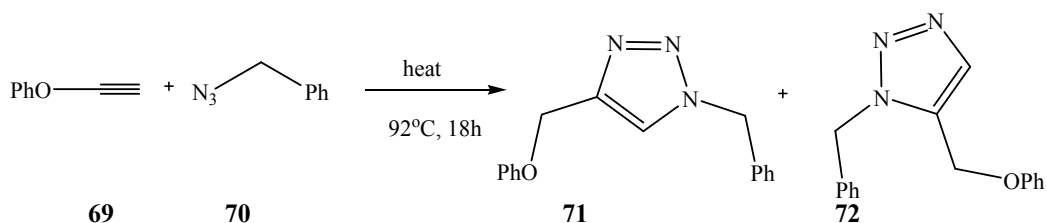
Nitrillium Betaines	Diazonium Betaines
Nitrile Oxides $\text{---C}\equiv\text{N}^+\text{---O}^-$ 63	Diazoalkanes $\text{N}\equiv\text{N}^+\text{---C}^-$ 64
Nitrile Imines $\text{---C}\equiv\text{N}^+\text{---N}^-$ 65	Azides $\text{N}\equiv\text{N}^+\text{---N}^-$ 66
Nitrile Ylides $\text{---C}\equiv\text{N}^+\text{---C}^-$ 67	Nitrous Oxides $\text{N}\equiv\text{N}^+\text{---O}^-$ 68

The 1,3-DC is very useful in organic synthesis for carbon-carbon bond formation.¹⁵⁶ However, a significant limitation of this reaction occurs when terminal alkynes are used as dipolarophiles, since they can interact with each other rather than reacting with the 1,3-dipole, thus leading to alkyne homocoupling.¹³⁷

An application of the 1,3-DC is the Huisgen Cycloaddition which is the first example of a click reaction and is used to synthesize triazoles and benzotriazoles.

2.2.1.2. The Huisgen Cycloaddition

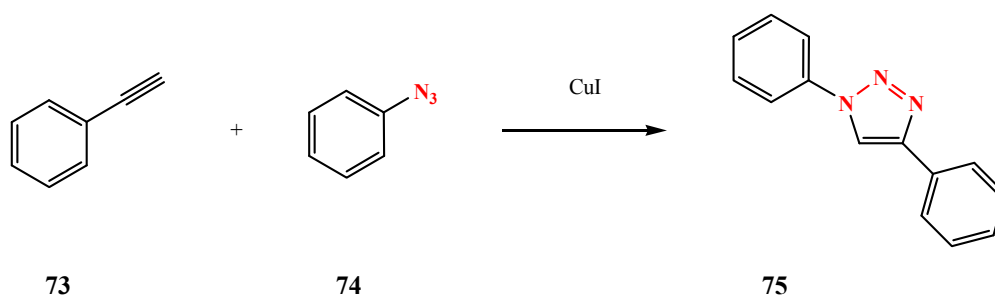
In the Huisgen Cycloaddition the 1,3-dipole is an organic azide and the dipolarophile an alkyne. Generally the azide is heated with the alkyne at above 100 °C in an aqueous-organic solvent mixture, under pressure, for several hours. The product is a mixture of 1,4- and 1,5-substituted 1,2,3-triazoles¹⁵⁷ as illustrated in Scheme 2.8.



Scheme 2.8. Synthesis of 1,4- and 1,5-substituted 1,2,3-triazoles¹⁵⁸

The utility of this reaction became apparent with the discovery of a copper catalyst system by Sharpless and Fokin. This catalyst accelerates the reaction from several hours to a few minutes at room temperature resulting in the formation of 1,4-regioisomers (**71**) of 1,2,3-triazole as the unique product.^{157, 159} This reaction was then named the Copper Catalyzed Azide-Alkyne Cycloaddition (CuAAC). In the presence of a reducing agent, the reaction was even faster when the Cu(I) catalyst was generated *in situ* from a Cu(II) salt (cupric sulfate for instance). This discovery had a great impact on the development of the synthesis of several organic compounds. Recent reports have highlighted the growing utility in drug discovery of Cu(I) promoted [3+2] Huisgen cycloadditions of azides with terminal alkynes popularly known as “the click reaction”.¹⁶⁰

CuAAC has cemented its position at the heart of click chemistry thanks to its wide scope and the orthogonality of the azide and alkyne functionalities to a diverse range of functional groups and reaction conditions.⁴⁸ It is considered to be a powerful linking reaction because of its reliability, specificity and the affinity of the products for biological systems.^{140, 161} As highlighted in Scheme 2.9, azides are the most reliable means of introducing nitrogens into a ring system.¹⁵⁸ A broad range of energy rich organic azide compounds are prepared easily by using sodium azide. Although azides are not the most reactive 1,3-dipole available, they are preferred for their relative lack of side reactions and stability towards water and oxygen under typical synthetic conditions. Azides are also important due to their industrial and biological applications, where they are used as functional groups in pharmaceuticals. For that reason azidonucleosides initially attracted international interest in the treatment of AIDS.¹⁶² As indicated time and again, triazoles and benzotriazoles have been successfully obtained through a 1,3-DC. Their reported important biological activity sparked our interest in the study of their chemistry.



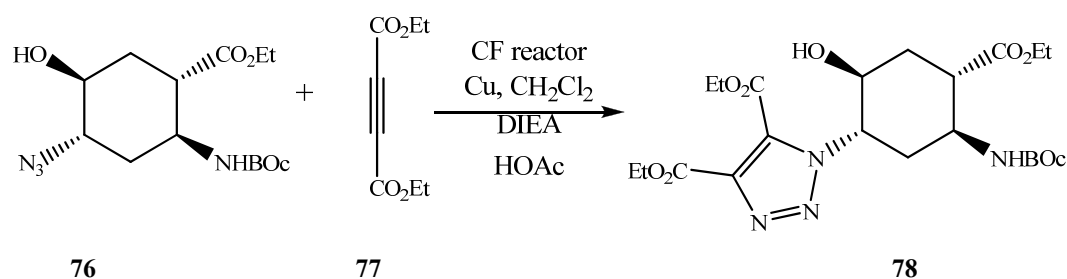
Scheme 2.9. Cu(I) catalyzed azide–alkyne cycloaddition of phenylacetylene with phenylazide ¹⁶³

2.2.1.3. Triazole and benzotriazole chemistry

2.2.1.3.1. Triazoles

Triazoles are five membered nitrogen heteroarenes with a number of interesting pharmaceutical applications.¹⁶⁴ 1,2,3-Triazole derivatives possess powerful antimicrobial, cytostatic, virostatic, and anti-inflammatory activities.¹⁶⁵ They are resistant to metabolic and proteolytic degradation and are capable of hydrogen bonding.¹⁴⁵ This is invaluable for enhancing binding or solubility in biological systems.¹³⁸

By using modern continuous-flow (CF) technologies, Otvos *et al.* reported the synthesis of 1,2,3-triazole-substituted β -aminocyclohexanecarboxylic acid derivatives displaying important antituberculous activity *in vitro*. During their experiment, diethyl acetylenedicarboxylate was subjected to CF CuAAC with azido-functionalized β -amino acid derivatives, with a catalytic amount of acetic acid and *N,N*-diisopropylethylamine dissolved in CH_2Cl_2 (Scheme 2.10).

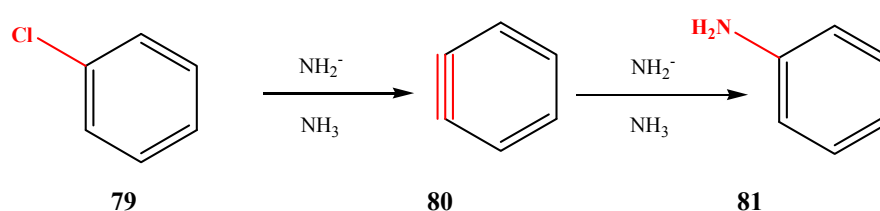


Scheme 2.10. Synthesis of 1,2,3-triazole-substituted β -aminocyclohexanecarboxylic acid derivatives ¹⁶⁶

2.2.1.3.2. Benzotriazoles

Benzotriazoles are bicyclic heterocyclic systems consisting of a triazole ring fused to a benzene ring. By combining the properties of the two rings, they participate actively in hydrogen bonding as well as dipole-dipole and π -stacking interactions thanks to their high dipole moment (about 5 D). They can be prepared by 1,3-DC with benzyne generated *in situ* as an electrically neutral dipolarophile.

Benzyne rings are highly reactive. They are traditionally formed by the treatment of an aryl halide with a very strong basic amide ion (NH_2^- , from an alkali metal amide) used to remove the ortho aromatic proton. The synthesis of aniline from chlorobenzene through a benzyne intermediate was first reported by John D. Roberts in 1953 and marked the real beginning of benzyne chemistry.¹⁶⁷



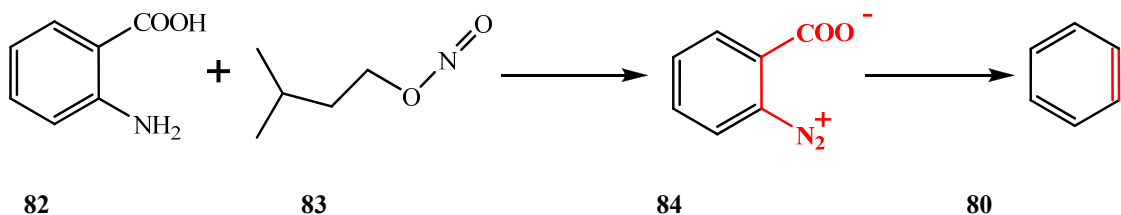
Scheme 2.11. Synthesis of aniline from chlorobenzene *via* a benzyne ring

Benzynes are kinetically unstable, highly strained molecules that readily undergo nucleophilic coupling with various neutral species to form complex organic molecules.

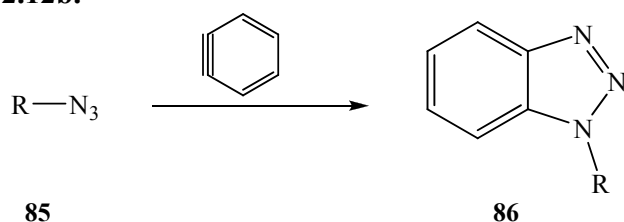
As illustrated in Scheme 2.11, an additional bond is formed between two carbons by sideways overlap of sp^2 orbitals. The new bond is weak and consequently benzyne is highly reactive.¹⁶⁸

Benzyne can also be formed from the diazonium carboxylate intermediate obtained by refluxing anthranilic acid as a benzyne precursor with amyl nitrite.^{169, 170} The reaction sequence is illustrated in Scheme 2.12a. In this case, in the second step, benzyne is consumed by a cycloaddition reaction with an organic azide, as illustrated in Scheme 2.12b.

2.12a.



2.12b.



Scheme 2.12. *In situ* generation of benzyne ring for benzotriazole synthesis

Derivatives of benzotriazole possess a broad range of biological activities including antibacterial, antifungal, antiviral, anti-inflammatory, antihypertensive and analgesic properties.¹⁷¹ This led us to examine their usefulness as potential HIV-1 inhibitors. Indeed, they present an appealing structural motif in peptidomimetic research because their structural and electronic characteristics are close to those of peptides.¹⁷²

2.2.2. The Baylis Hillman reaction

2.2.2.1. Generalities on the Baylis Hillman reaction

As mentioned above, carbon-carbon bonds are built around many different functional groups. When a β -hydroxy carbonyl is required, a Baylis Hillman reaction can be invoked. The Baylis Hillman reaction is widely recognised as a powerful tool for the coupling of aldehydes or imines with activated alkenes.^{173, 174} The reaction is catalyzed by tertiary amines or tertiary phosphines as nucleophilic catalysts and the product is a densely functionalized allylic alcohol or allylic amine.^{175, 176} Several catalytic asymmetric versions have been published as well.¹⁷⁷

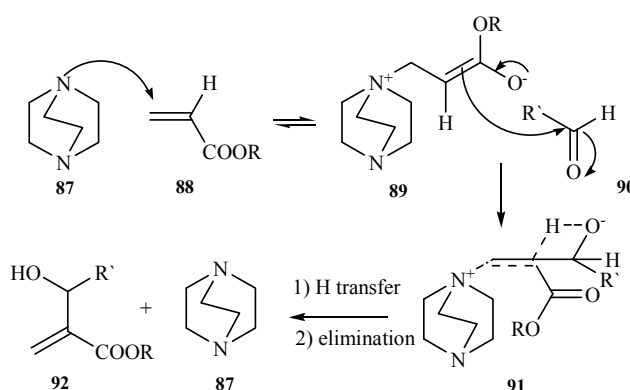
Since its discovery in the early 1970's by Baylis and Hillmann,¹⁷⁵ this reaction has been widely used and continues to inspire researchers due to its immense synthetic efficiency and simplicity.^{178, 179} The Baylis Hillmann reaction is widely used in the synthesis of

quinolones,¹⁸⁰ naphthalenes^{176, 181} and heterocycles such as indoles,¹⁷⁸ pyrazoles and indazoles. It is important to mention that the Baylis Hillman reaction can be used in green chemistry since it is a reasonably atom-economical reaction which can be performed under solvent free conditions and/or using microwave irradiation.¹⁸²

The most important advantage of the Baylis Hillman reaction is to afford highly functionalized molecules, with three chemospecific functional groups in close proximity.¹⁸³ The Baylis Hillman reaction has been successfully used in our research group to synthesize substituted chromenes,^{184, 185} indolizines,¹⁸⁶ hydroxyalkenoate esters,¹⁸⁷ coumarins and quinoline derivatives.¹⁸⁸ These varied applications of the Baylis Hillman adducts in organic transformations prompted us to make use of this reaction for the synthesis of indenols and coumarins as potential HIV-1 protease inhibitors.¹⁷⁹

2.2.2.2. Mechanism of the Baylis Hillman reaction

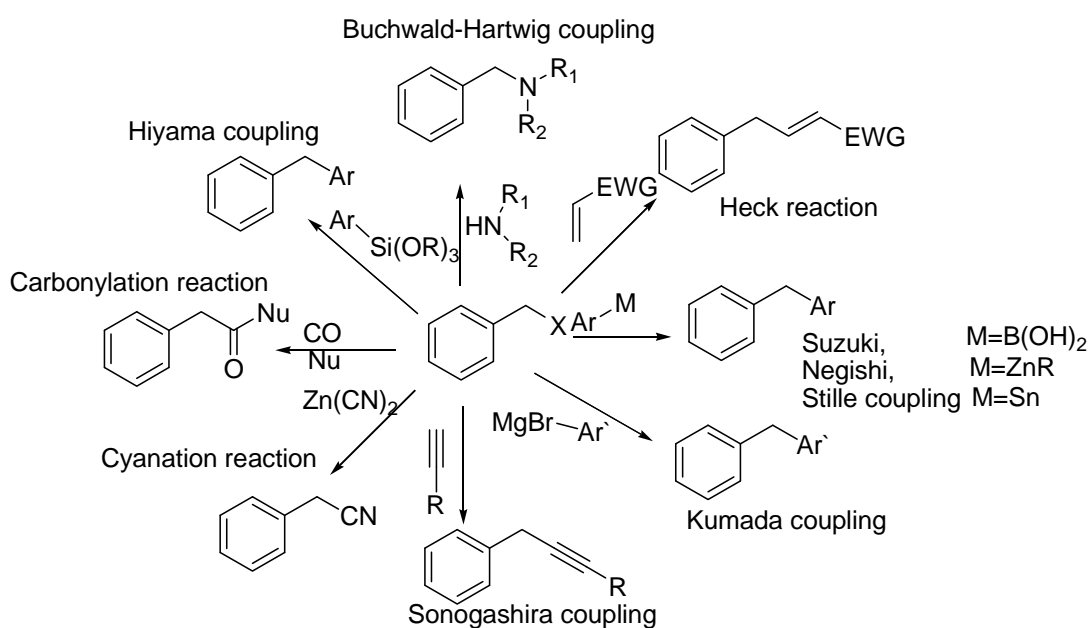
The most generally accepted mechanism of the amine-catalyzed reaction is illustrated in Scheme 2.13, taking as a model case, the reaction between an activated olefin and an electrophile under the catalytic influence of DABCO (**87**).¹⁸⁹ The mechanism reported in Scheme 2.13 follows three steps. The first step is a Michael addition of DABCO (**87**) to the activated alkene to afford a zwitterionic enolate (**89**). In the second step, an aldol type reaction takes place. The enolate is quenched with the aldehyde (**90**) to generate a new zwitterionic enolate (**91**) which undergoes a deprotonation-elimination process at the final step to give the Baylis Hillman adduct (**92**) and regenerate the catalyst.¹⁹⁰



Scheme 2.13. General Baylis Hillmann reaction, with DABCO as tertiary amine catalyst

2.2.3. Palladium catalyzed reactions

Organometallic chemistry is the basis of much of homogeneous catalysis, which is the ideal method for clean and efficient synthesis of fine chemicals, pharmaceuticals and many larger-scale chemical reactions. Organocatalytic transformations also appear to be a powerful means of achieving carbon-carbon bond formation. In many cases, palladium is selected as the metal of choice to carry out organometallic catalysis.^{191, 192} Owing to its high reactivity, palladium catalysis has achieved the status of an indispensable tool for both common and state-of-the-art organic synthesis.^{193, 194} Many palladium catalyzed reactions have been reported. Among the palladium catalyzed reactions used to construct new chemical bonds, we have the Suzuki–Miyaura coupling, the Stille coupling, the Negishi coupling, the Kumada coupling, palladium catalyzed cyanation and carbonylation, the Hiyama coupling, the Sonogashira coupling, the Buchwald-Hartwig coupling, the Heck reaction, the Hiyama coupling, the Sonogashira coupling, the Buchwald-Hartwig coupling and, last but not least, the Heck reaction, which are all illustrated in Scheme 2.14.

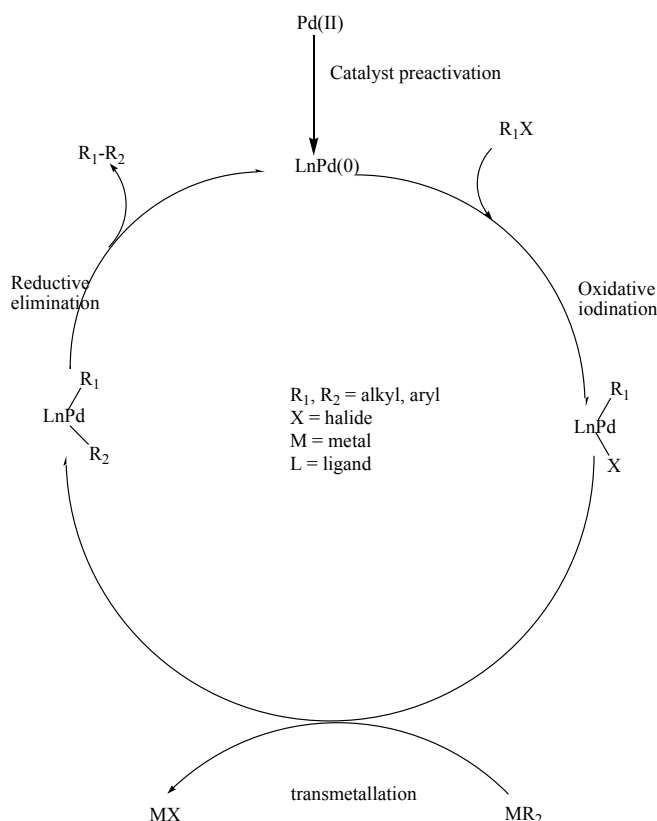


Scheme 2.14. Palladium catalyzed reactions, using benzyl halide as a substrate

In general most of these palladium catalyzed coupling reactions follow similar reaction mechanisms as illustrated in Scheme 2.15. The catalytic cycle of palladium catalyzed coupling takes place in three stages:

First, following the *in situ* activation of the Pd(II) pre-catalyst *via* reduction by phosphines²²⁶, the oxidative addition to the catalytically active $L_nPd(0)$ species takes place. Oxidative addition is formally the insertion of Pd(0) into the organo-halide bond R_1-X .

Second, the transmetalation reaction takes place, which is the transfer of the R_2 group attached to the metal M to the first organo palladium intermediate displacing the halide which then coordinates to the metal M. The nature of M depends on the type of coupling involved. Finally the reductive elimination leading to the product R_1-R_2 formation, with simultaneous recovery of the Pd(0) catalyst.

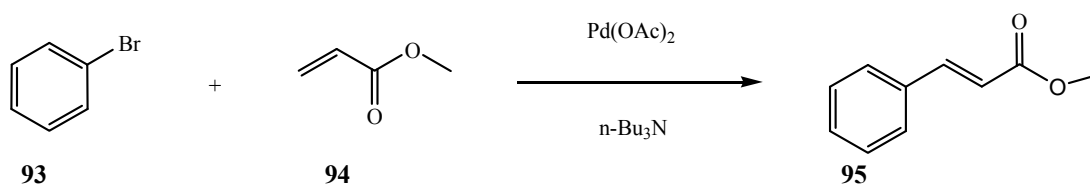


Scheme 2.15. The catalytic cycle of most palladium catalyzed reactions¹⁹⁵

2.2.3.1. The Heck reaction

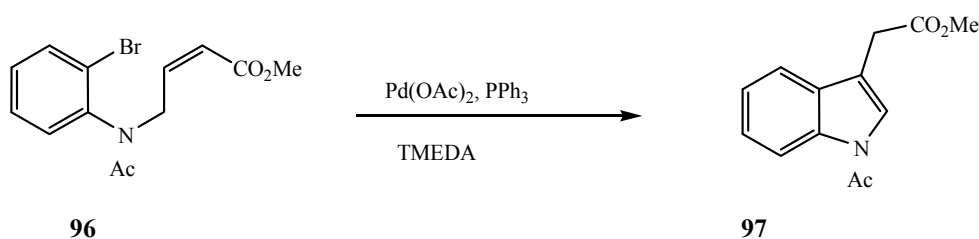
Since its discovery, the Heck reaction has increasingly gained in popularity¹⁹³ and has been used in material science for the efficient elaboration of silicones¹⁹⁶ and for biologically active molecules such as cinnamic acid derivatives and stilbenes.¹⁹⁷

As depicted in Scheme 2.16, palladium-catalyzed coupling of aryl (or vinyl) halides with alkenes is largely employed for the synthesis of substituted olefins, dienes and a wide range of unsaturated compounds *via* the Heck coupling.¹⁹⁸ The easy accessibility of aryl bromides and chlorides and the tolerance of the reaction for a variety of functional groups has lead to the publication of many examples of this reaction.^{194, 199, 200}



Scheme 2.16. Vinyllic hydrogen substitution of bromobenzene²⁰¹

The intramolecular Heck reaction is also possible and has also been applied prolifically, facilitating elegant syntheses of many complex molecules such as carbocyclic and heterocyclic ring systems.^{202, 203} Miwako *et al.* successfully synthesized indoles by using this reaction.²⁰⁴ In most instances, the *exo* mode of cyclization is favored over the *endo* reaction mode (Scheme 2.17).²⁰²



Scheme 2.17. Synthesis of indoles by intramolecular Heck reaction²⁰⁴

The importance of this reaction was recognized when Richard F. Heck was awarded the 2010 Nobel Prize in chemistry, jointly with Ei-ichi Negishi and Akira Suzuki, for the

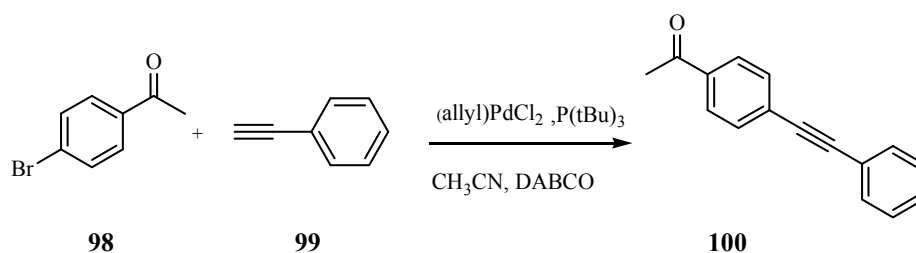
development of Palladium-catalyzed cross-coupling reactions in organic synthesis. Even though the Heck coupling is celebrated as an excellent tool for carbon-carbon bond formation, certain elements combine to inhibit this reaction.

Despite the obvious importance of the Heck reaction in organic synthesis, it is a very poor yielding reaction and there is always a need to perform optimization studies. This can be done by monitoring experimental conditions such as the phosphine ligand, the base, the palladium catalyst and the reaction solvent.²⁰⁵⁻²¹² In the catalytic cycle of the Heck reaction, the palladium catalyst used needs to be stabilised by phosphine ligands.²²⁶ These phosphane compounds are sensitive to oxidation and have to be handled under inert atmosphere. Having an excess of one of the substrates is advised in order to facilitate full conversion. This can be costly in cases where one or more of these substrates are expensive or involve intermediates which are difficult to obtain. Furthermore, since the Heck reaction generally takes place at high temperature, deactivation of the palladium catalyst often arises and many by-products from the oxidation of minor impurities by the palladium catalyst are encountered. It can also happen that a palladium black precipitate is formed. This is due to a sterically induced ligand dissociation leading to the agglomeration of a co-ordinatively unsaturated Pd(0) intermediate.²¹³

2.2.3.2. The Sonogashira coupling

One of the most straightforward methods for the preparation of arylalkynes and conjugated enynes is the palladium-catalyzed coupling of terminal alkynes with aryl or alkenyl halides. This synthesis was described for the first time by Sonogashira *et al.* in 1975.^{214, 215} The coupling is performed with a palladium catalyst, a copper(I) co-catalyst generated *in situ* from a copper(II) salt (CuI or CuCN), and an amine base.

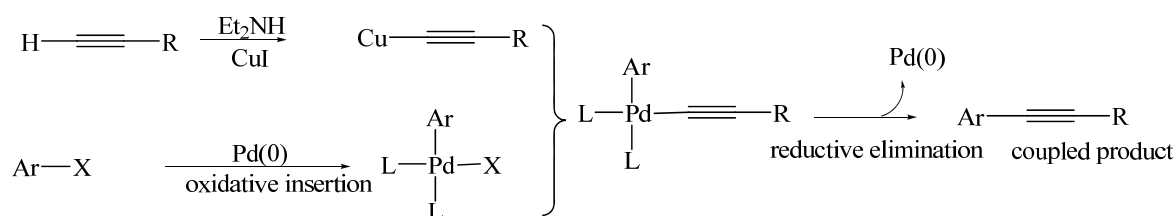
Inspired by this procedure, substituted acetophenone derivatives were successfully obtained by a Sonogashira coupling of bromoacetophenone with phenylacetylene as illustrated in Scheme 2.18.²¹⁶



Scheme 2.18. Sonogashira coupling of phenylacetylene and bromoacetophenone

Scheme 2.19 illustrates the mechanism of the Sonogashira coupling where the first two steps are the same as the general mechanism (Scheme 2.15). The third step involves a base induced elimination of HX which sets up the complex for reductive elimination.²¹⁷ Finally, the formation of the product is mediated by a reductive elimination upon which the palladium(0) catalyst is recovered and the catalytic cycle starts all over again.

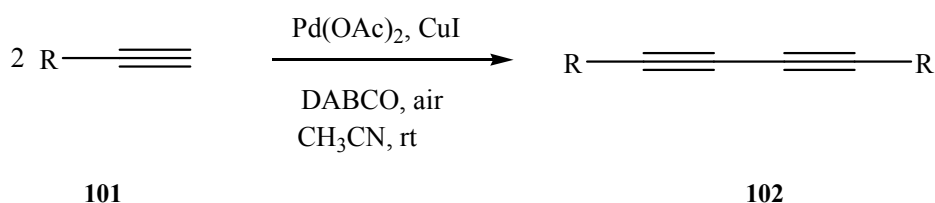
Typically, the reaction requires anhydrous and anaerobic conditions, but over the years, newer procedures have been developed where these restrictions are less important. The recently developed protocols include palladium free, copper free and ligand free reactions. In some cases, the use of a variety of additives have shown some potential.²¹⁸ The original Sonogashira reaction generally proceeds in the presence of a homogeneous palladium catalyst.²¹⁹ However, reports have described an efficient synthesis by using a heterogeneous catalyst instead.²²⁰⁻²²² The syntheses can be carried out in water^{124, 223} as well as in highly polar organic solvents.²²⁴ Although the Sonogashira coupling is known as a high temperature reaction, many examples of cross-coupling reactions have been carried out at room temperature.²²⁵ Surprisingly, in 2000, Kabalka *et al.* reported a solvent free Sonogashira coupling on alumina in the microwave.¹³⁰



Scheme 2.19. Sonogashira coupling reaction mechanism²²⁶

The Sonogashira coupling has been widely studied and expanded to various substrates related to the construction of the complex unsaturated framework of enediyne antibiotics,²²⁷⁻²²⁹ indenones,^{124, 230} isoquinolines and pyridines.²³¹ This synthetic transformation is also a tool of choice for the construction of carbon rich materials (*e.g.* radialenes, graphenes) from simple building blocks.²³² Nonetheless, a number of factors contribute to limitation of the Sonogashira coupling.

An oxidative homocoupling (Glaser coupling) of the alkyne to give the corresponding symmetrical diyne is also catalyzed if oxygen is not completely eradicated during the coupling (Scheme 2.20).^{233, 234} This is the reason why a large excess of the alkyne is usually added very slowly in order to keep its effective concentration in the reaction mixture very low. As an initial solution to this problem, Nolan has indicated that the employment of alkynylsilanes can minimize unwanted side products (homocoupling) during Sonogashira couplings.²³⁵



Scheme 2.20. Homocoupling of terminal alkynes in a Sonogashira Coupling²³⁴

2.3. GREEN CHEMISTRY CONSIDERATIONS

Although many of the previously described methodologies are very efficient in the construction of carbon-carbon bonds, they sometimes have detrimental effects on the environment. Pollution related to organic syntheses is currently under the spotlight and hence the development of synthetic protocols towards greener organic syntheses is more than welcome.¹¹⁶

Green chemistry, also known as benign or sustainable chemistry has attracted substantial interest since it emerged in the early 1990s. Green chemistry is built on a set of principles through which economic and environmental goals can be achieved. These principles of

green chemistry were formalized by Paul Anastas and John Warner and have since been adopted universally.¹¹⁷ They are concerned with the development of procedures and technologies leading to more adequate chemical reactions that produce limited waste and fewer environmental discharges than do conventional methods. The fundamental concern is the eradication of pollution before it arises.

2.3.1. Green chemistry and catalysis

Catalysis is a prominent approach to achieve the goals of green chemistry.^{118, 119} It is used to increase the efficiency and yield of chemical reactions. When reagents are used in catalytic amounts, they can significantly enhance the selectivity of a reaction compared to stoichiometric reagents.¹²⁰ Consequently, energy requirements are reduced and the easy separation of the product can also be realized. In addition, catalysis reduces the amount of reagents needed and promotes the use of less toxic stoichiometric reagents (for instance the use of hydrogen peroxide instead of heavy metals during an oxidation reaction).¹²¹ Even homogeneous and heterogeneous heavy metal complexes meet the needs of green chemistry when they are used in catalytic amounts.¹²²

2.3.2. Alternative green solvents

Organic solvents are commonly employed to carry out organic syntheses and analyses. However, some organic solvents are known to be genotoxic, human carcinogens, irritants, flammable and/or harmful.¹²³ Moreover, they are generally non-biodegradable and expensive to dispose. To address these problems, green chemistry emphasizes on the use of water as a non-toxic, non-flammable reaction solvent which addresses both ecological and cost concerns.¹²⁴ In this line, Zeynizadeh *et al.* reported that water efficiently replaced common ethereal organic solvents in the reduction of carbonyl compounds with sodium borohydride.¹²⁵

In addition, the use of alternative solvents presenting low toxicity, ease of recycling, chemical inertia and ease of removal from the product also promotes greener chemistry. 1,3-Dioxalane, 1,3-propane-diol and *N,N'*-dimethylpropyleneurea are a few of them. It appears that 2-methyltetrahydrofuran is an excellent alternative to THF with a high boiling point, a lower solubility in water and a better ecocompatibility.¹²⁶ In addition,

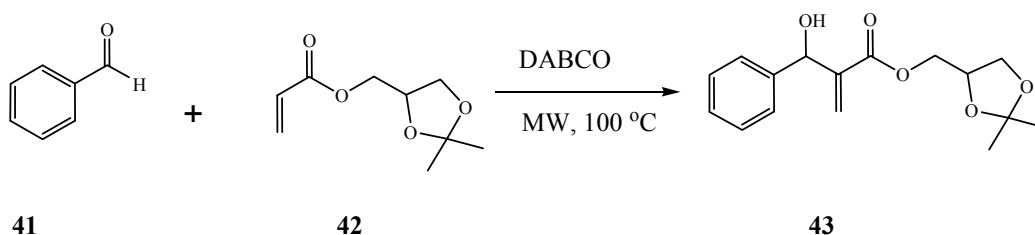
ionic liquids are also possible choices of green solvents. They can be used as liquid supports for re-usable catalytic systems and employed in phase transfer chemistry.¹²⁷

Click chemistry and microwave assisted organic synthesis are two flourishing areas of research working towards clean and less polluting chemistry, and can therefore be considered to be “green” processes.¹²⁸

2.3.3. Microwave assisted organic chemistry

Generating compounds *via* catalysis is a green improvement in organic synthesis but obtaining them in reduced time makes it more efficient and this can be done through microwave assisted reactions.⁹³

Microwave assisted organic chemistry has gained overwhelming popularity as a non-traditional method needing shorter reaction time for performing reactions induced by an increase in molecular fluctuation, giving products in good to excellent yields.^{93, 129-131} A simple explanation is that microwave radiation heats only the reactants and the solvent, and the temperature increase will be uniform throughout the sample, which can lead to less by-products and/or less decomposition of the product.¹³² Suervy *et al.* reported the synthesis of hydrophilic monoacylglycerol by hydrolysis of solketal acrylate through a Baylis Hillman reaction in only fifteen minutes and with 100% conversion (Scheme 2.21).¹³¹



Scheme 2.21. Synthesis of monoacylglycerol using microwave irradiation¹³¹

Considering the fact that Baylis Hillman reactions performed by the conventional method are notorious for being very slow reactions (taking days or even weeks), the improvement in the reaction time observed using the microwave is significant.¹³³

Microwave assisted synthesis satisfies sustainable chemistry principles by addressing the following aspects:

- Use of solvent-free reaction conditions;
- Safety (it reduces the possibility of exposure or discharge of chemicals in the environment and therefore prevents accidents from occurring);
- Clean reaction (less purification and waste produced);¹³⁴
- Green solvent usage (water, ethanol are excellent microwave solvents);
- Use of less energy due to reduced reaction time and greater efficiency in energy transfer;

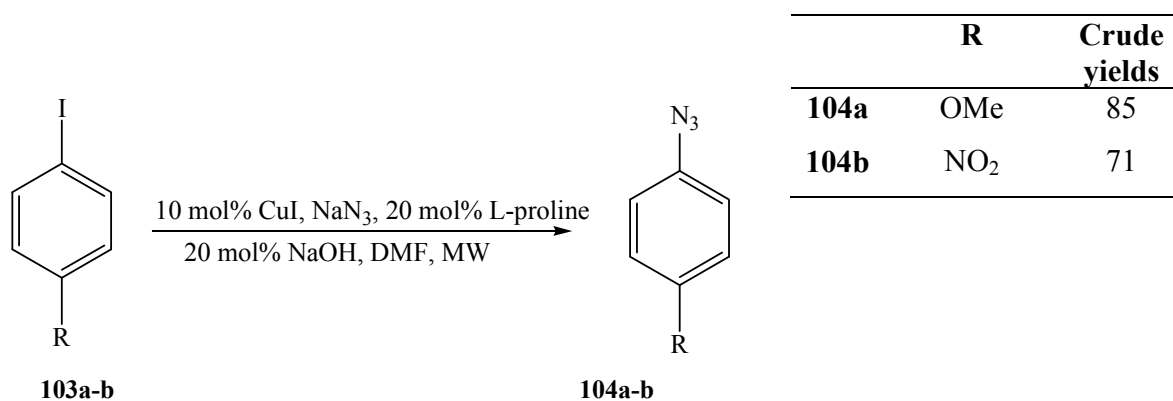
2.4. RESULTS AND DISCUSSION

2.4.1. Synthesis of benzotriazoles

A class of heterocyclic compounds which have been shown to play a role as peptidomimetics are benzotriazoles. One avenue for the synthesis of benzotriazoles is through 1,3-dipolar cycloaddition (1,3-DC) between a dipolarophile derived from an aromatic system and an azide as the electron rich dipole.²³⁶ In the report below, anthranilic acid was chosen as a dipolarophile precursor and the azide was synthesized *via* a range of classical approaches reported in the literature.^{237, 238}

2.4.1.1. Synthesis of azides from iodinated aromatic compounds

Azide compounds can be generated from iodinated derivatives as reported by Zhu and coworkers.²³⁹ Briefly, azide compounds were synthesized in our case using L-proline and catalytic amounts of CuI. NaN₃ was used as the azide source. The mixture was stirred in DMF at 80 °C for one hour under microwave irradiation (Scheme 2.22). The reaction yield was poor when a 1:1 ratio of NaN₃ and iodinated aromatic compound was used (13 to 19%). A 2:1 ratio of NaN₃: iodinated aromatic compound led to a remarkable enhancement on the outcome of the reaction (71 to 85%).



Scheme 2.22. Azide synthesis from iodinated aromatic compounds

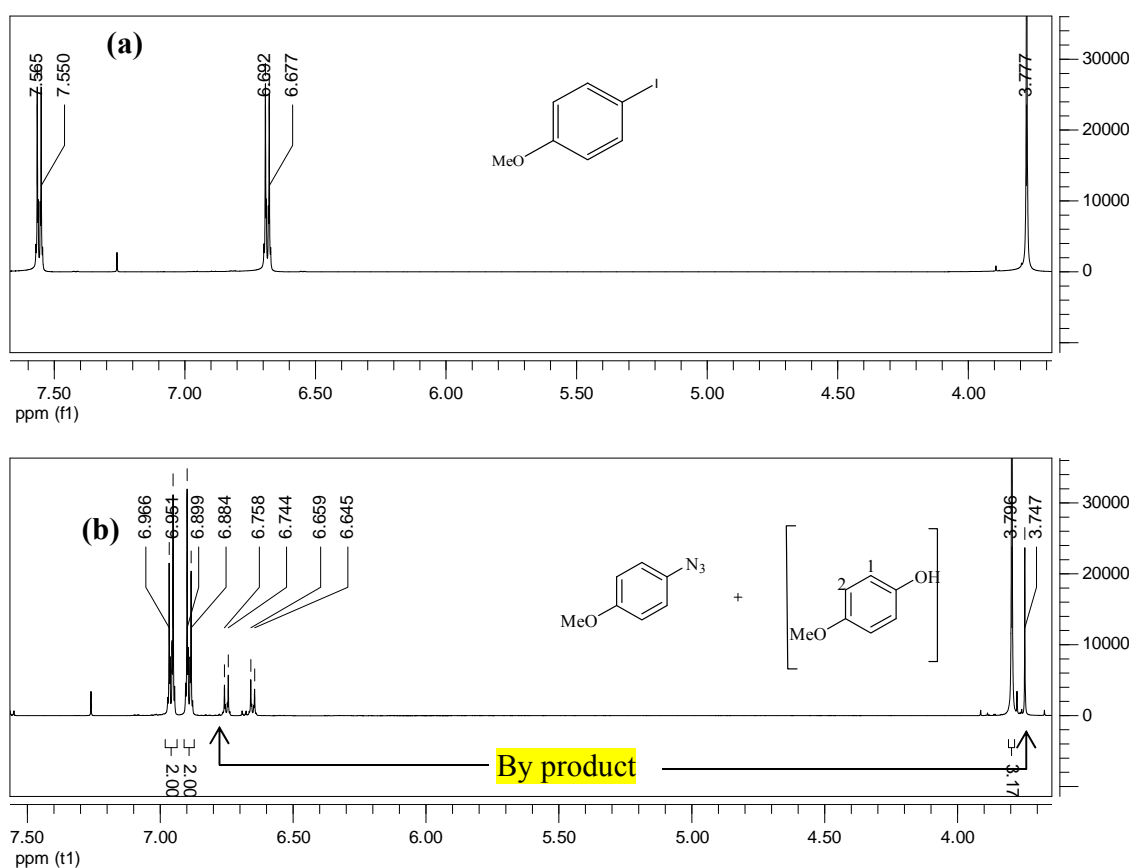


Figure 2.1. Superimposed 600 MHz ¹H NMR spectra of (a) of the iodo starting material and (b) product mixture in CDCl₃

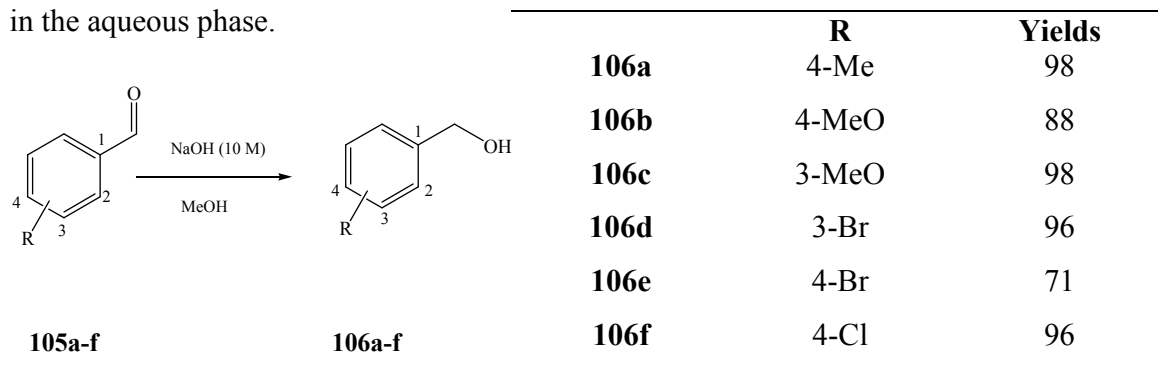
Unfortunately, this improvement was a partial success. As highlighted in the ¹H NMR (Figure 2.1b), the synthesized azides were contaminated by traces of one by-product that we first thought was the starting material. However, after cross-checking the chemical

shift of the aromatic protons of the starting material *p*-iodoanisole (Figure 2.1a) resonating downfield due to the electronegativity of iodine (Ar-H doublets at 6.69 ppm and 7.56 ppm), we observed that the iodo group had been substituted. Uncertainty remains regarding both the origin and the structure of the by-product, although it is apparently a *p*-substituted anisole, although it seems likely that it is a phenol. Water or NaOH present in the medium could be the nucleophiles that have replaced the azide group.

Azides are characteristically explosive, subject to rapid decomposition under the influence of an external energy source to produce nitrogen.¹⁶² This feature made all attempts at purification undesirable and forced us to search for other convenient protocols for their synthesis.

2.4.1.2. Synthesis of azides from benzyl alcohols

The Cannizzaro reaction is a chemical synthesis where aromatic aldehydes are reduced to benzylalcohols and the corresponding carboxylic acids in the presence of a strong base.²⁴⁰ This procedure was followed to generate benzyl alcohols from benzaldehyde derivatives. These aldehydes were reduced by a 10 M solution of NaOH as a reducing agent under reflux in methanol (Scheme 2.23). Any carboxylic acid produced is assumed to have been in the aqueous phase.



Scheme 2.23. Synthesis of benzyl alcohols from benzaldehyde derivatives

The disappearance of the aldehydic proton signal at 9.89 ppm (from the starting material *p*-bromobenzaldehyde) and the appearance of the methylene proton resonating as a

singlet at 4.62 ppm in the ^1H NMR spectrum of compound **106e** (Figure 2.2b) clearly indicated the successful synthesis of the alcohol. Moreover, this was also proved by the methylene carbon signal at 64.6 ppm in the ^{13}C NMR spectrum of compound **106e**. In addition, a broad signal corresponding to a hydroxyl proton at 2.03 ppm appearing on the ^1H NMR of the same compound (Figure 2.2b) further confirmed the formation of the alcohol. A similar pattern from the ^1H and ^{13}C NMR spectra of other derivatives was observed (yields ranging from 71 to 98%).

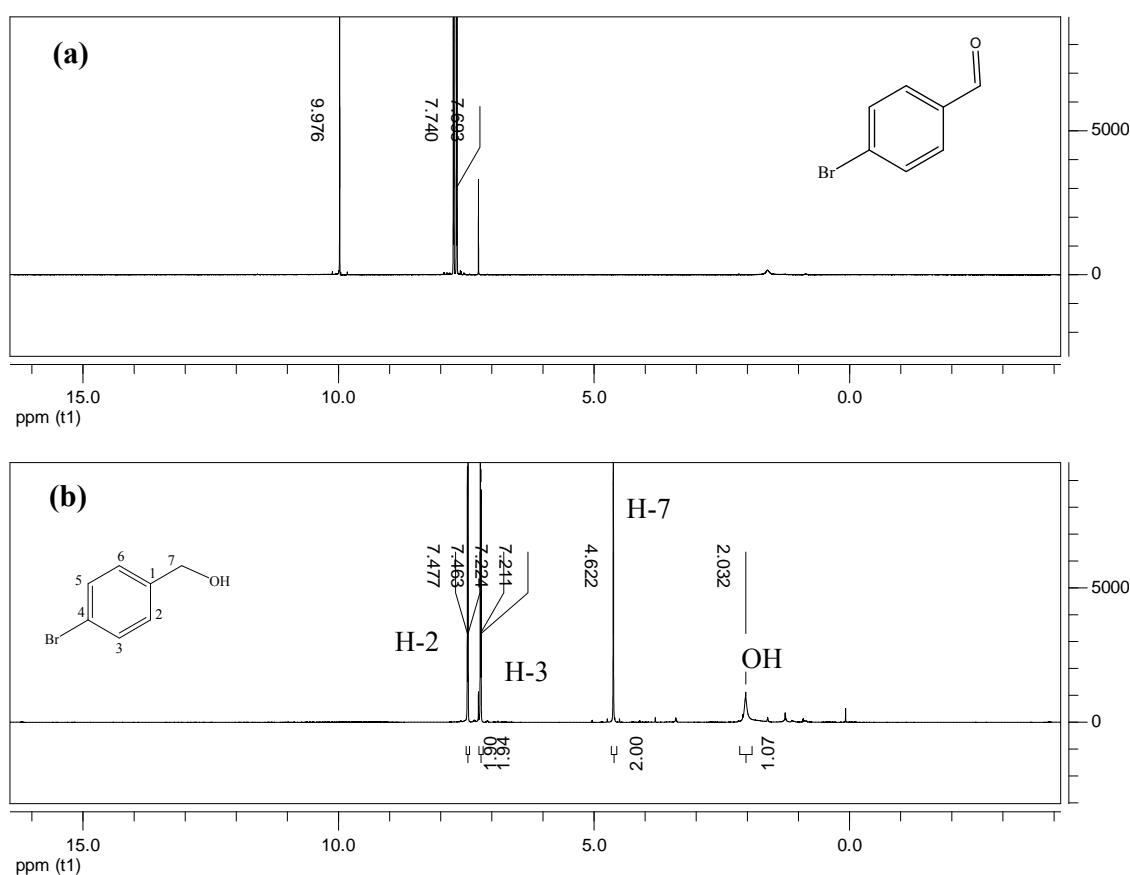
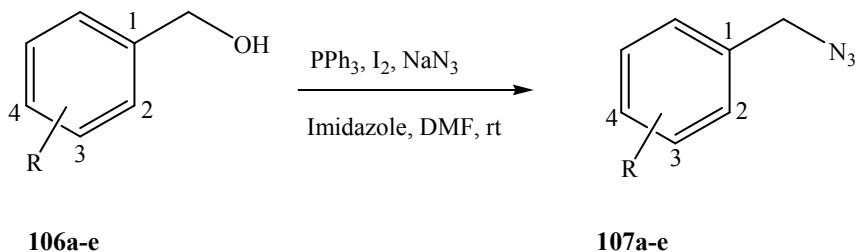


Figure 2.2. 600 MHz ^1H NMR spectra of **105e** (a) and **106e** (b) in CDCl_3

As proposed by Rokhum *et al.*, azides can be generated by reacting the benzyl alcohols with a catalytic amount of PPh_3 , I_2 , and imidazole in DMF *via* a grinding method using NaN_3 as azide source.²⁴¹ The phosphonium salt formed by grinding I_2 , PPh_3 and imidazole activated the alcohol and generated an iodide adduct which, after being stirred

with NaN₃ for half an hour at room temperature, lead to the formation of the analogous azide compound. In our hands, this synthetic approach gave varied results (Scheme 2.24).



Scheme 2.24. Azide synthesis from benzyl alcohols

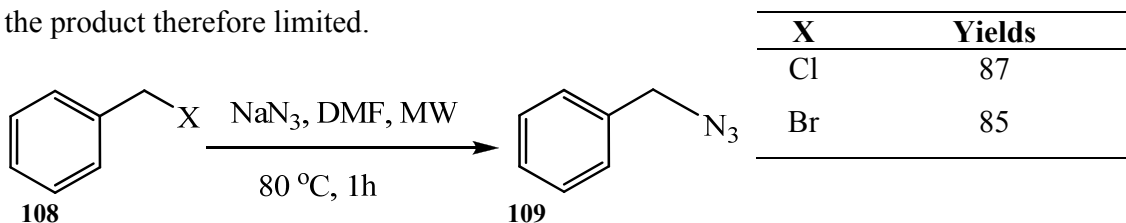
Table 2.2. Yields of benzylazides

	Electron withdrawing group		Electron donating group		
R	4-Br	4-Cl	4-MeO	3-MeO	4-Me
Compounds	107a	107b	107c	107d	107e
Yield (%)	74	96	26	13	12

NMR spectroscopy was used to determine crude yields from the reaction mixture ranging were between 12 and 74%. In spite of the clear structural similarity between the structure of the benzyl alcohol precursors and the benzyl azide products, it appeared that the shielding effect of the azide group caused an upfield shift of the methylene protons of the product (4.35 ppm) compared to the methylene protons of the starting alcohol (4.69 ppm) (Figure 2.3a). Moreover, the aromatic protons of the azide resonate further upfield, between 7.47 ppm and 7.56 ppm. The results contained in Table 2.2 support the theory that an electron withdrawing group (EWG) at the para position of the ring favored the formation of the azide, compared to electron donating groups (EDG) at the same position. Nevertheless, the product was contaminated this time by the starting material. Although several reports in the literature mention that azides can be purified by column chromatography on silica,^{241, 242} all the purification techniques used (column chromatography with hexane and ethyl acetate as solvents, recrystallization in MeOH) to obtain pure compounds were unsuccessful.

2.4.1.3. Synthesis of azides from aryl halides

In 2009, Hansen and coworkers stated that azides can be synthesized under microwave irradiation from aryl halides by using only NaN_3 in DMF (Scheme 2.25).²⁴³ This procedure was attractive since the number of chemicals involved in the synthesis was considerably reduced and the chances of contamination of the product therefore limited.



Scheme 2.25 Azide synthesis from aryl halides

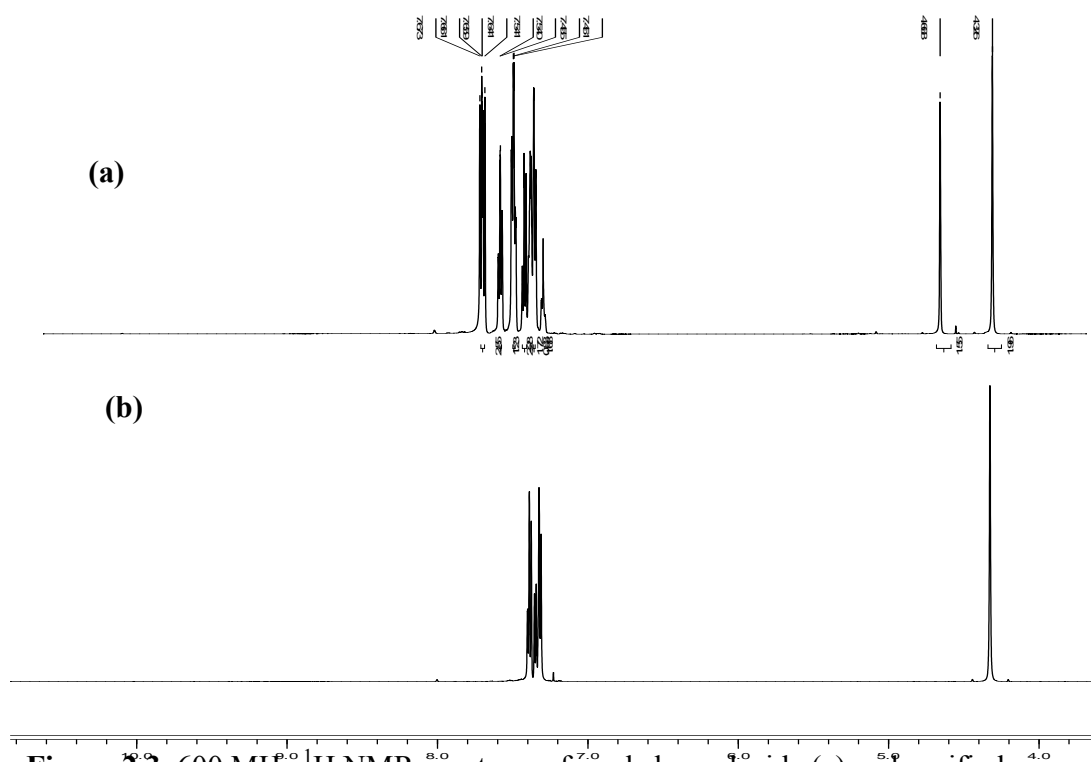


Figure 2.3. 600 MHz ^1H NMR spectrum of crude benzyl azide (a) and purified benzyl azide **109** (b) in CDCl_3

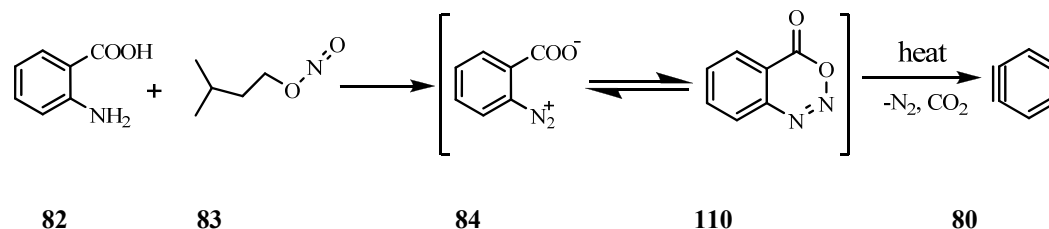
Benzyl chloride and benzyl bromide (compounds **108**, $\text{X} = \text{Cl}$ or Br) were separately mixed with NaN_3 in DMF and irradiated at $80\text{ }^\circ\text{C}$ for an hour in an open vessel in the

microwave. The diethyl ether used for the extraction of the product from DMF was allowed to evaporate at room temperature in order to avoid any external heat and clean benzyl azide **109** (Figure 2.3b) was obtained in good yields of 87% (X = Cl) and 85% (X = Br). This method marked a breakthrough in the efficient, fast, cheap, green and clean synthesis of benzylazides **109** from benzylhalides in this project.

The ^1H NMR of compound **109** (Figure 2.3b) revealed a singlet at 4.39 ppm corresponding to the methylene protons and five aromatic protons overlapping between 7.38 ppm and 7.46 ppm.

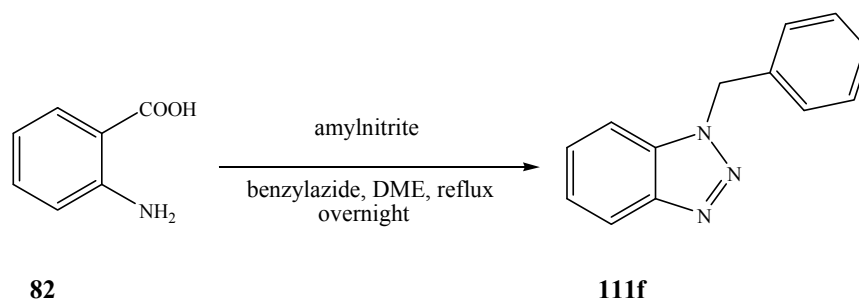
2.4.1.4. The 1,3-Dipolar cycloaddition of anthranilic acid with azides

As previously mentioned, the dipolarophile used was a benzyne **80** generated *in situ* from anthranilic acid **82** in reaction with amyl nitrite **83** (Scheme 2.26). During this process, as proposed by Spiteri *et al.*, a diazonium carboxylate compound **84** formed and underwent subsequently transformation to form complex **110**. After heating, N_2 and CO_2 were released to form a reactive benzyne ring **80**.¹⁷⁰

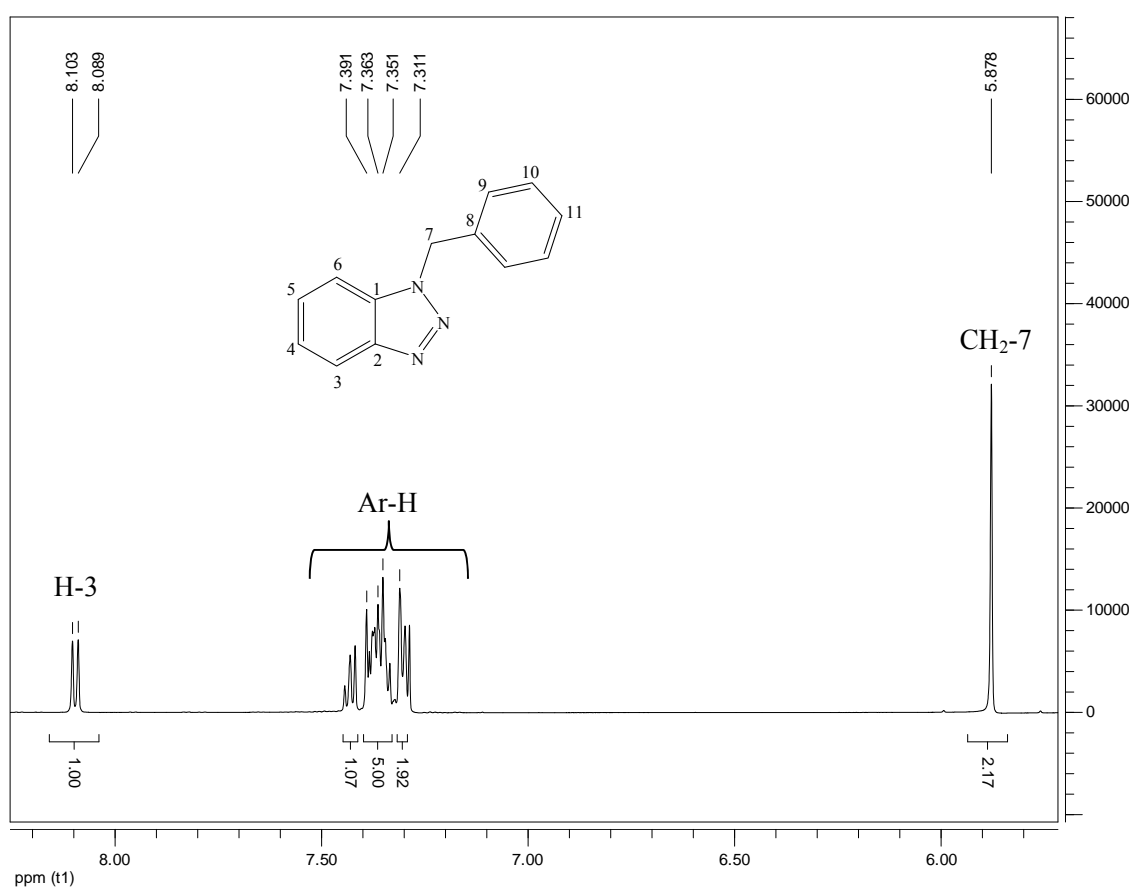


Scheme 2.26. Benzyne ring generation from anthranilic acid

A 1,3-DC of anthranilic acid with benzyl azide **109** in dimethoxyethane (DME) (Scheme 2.27) was performed by simultaneously adding a solution of anthranilic acid and a solution of amyl nitrite **83** to a solution of the azide under reflux. All 11 proton atoms of **111f** were accounted for in its ^1H NMR spectrum (Figure 2.4).



Scheme 2.27. Benzotriazole synthesis from *in situ* generation of a benzyne ring **80** from anthranilic acid **82**



In addition, all 13 carbon atoms of **111f** appeared in its ^{13}C NMR spectrum (Figure 2.5) with the signals of carbons C-9 and C-10 of the phenyl ring corresponding to two symmetrically related carbons each. The methylene proton (H-7), resonating at 5.87 ppm

in the ^1H NMR spectrum of compound **111f** (Figure 2.4) correlates with the methylene carbon resonating at 52.3 ppm in the ^{13}C NMR spectrum. Another proof of the formation of the product was the presence of the characteristic feature of benzotriazole compounds marked by the low intensity of the three quaternary carbons signals C-1, C-8 and C-2 at 132.8 ppm, 134.8 ppm and 146.4 ppm respectively (Figure 2.5).²⁴⁴

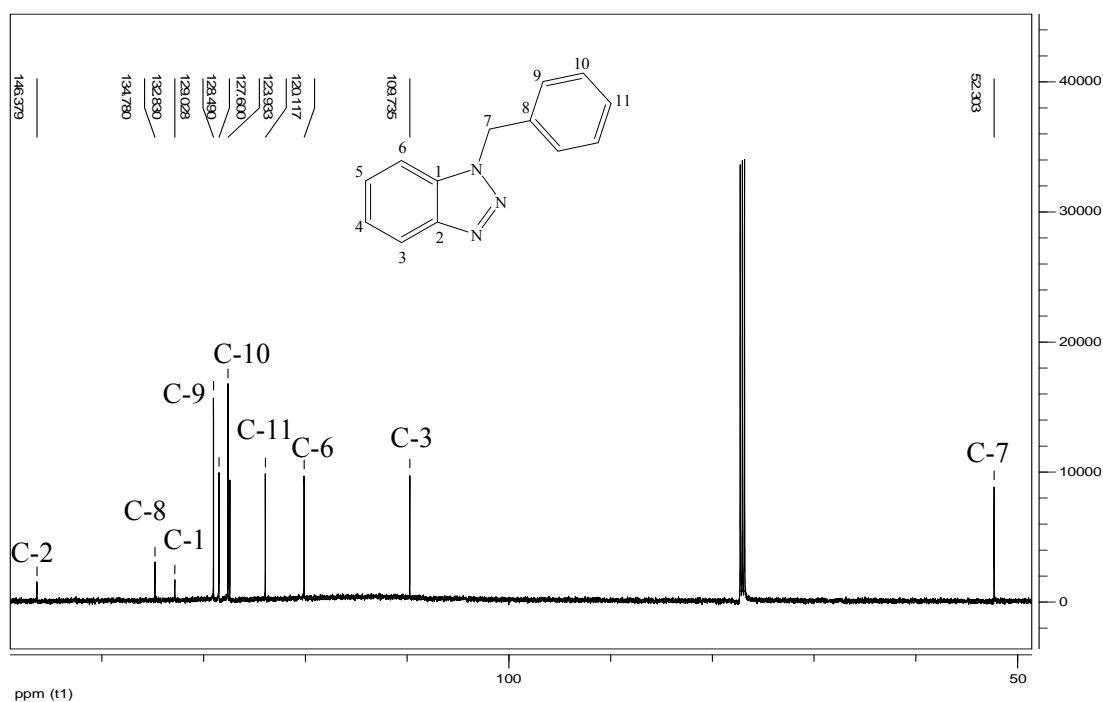
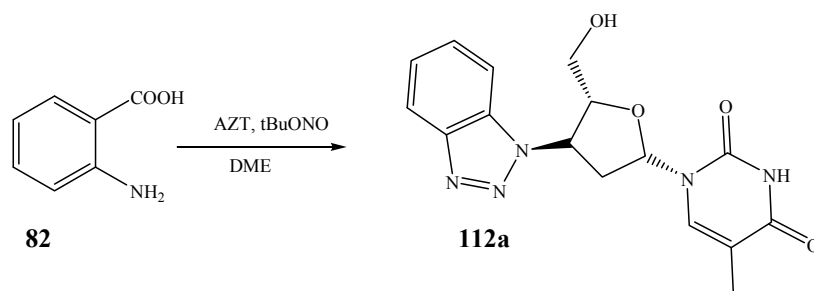


Figure 2.5. 150 MHz ^{13}C NMR spectrum of **111f** in CDCl_3

Given that AZT **1** possesses an azide functionality, we were also interested in testing its behavior when implementing a cycloaddition on anthranilic acid **82** (Scheme 2.28). It is worth mentioning that this idea was already developed by Chandrasekhar *et al.* via a slightly different approach.²⁴⁴ The salient difference from our method was the use of 2-trimethylsilylphenyltrifluoromethanesulfonate as the benzyne precursor in the presence of CsF in CH_3CN at room temperature overnight. Using our approach, we obtained the benzotriazole substituted AZT in 63% yield.



Scheme 2.28. 1,3-DC cycloaddition of AZT **1** with anthranilic acid **82**

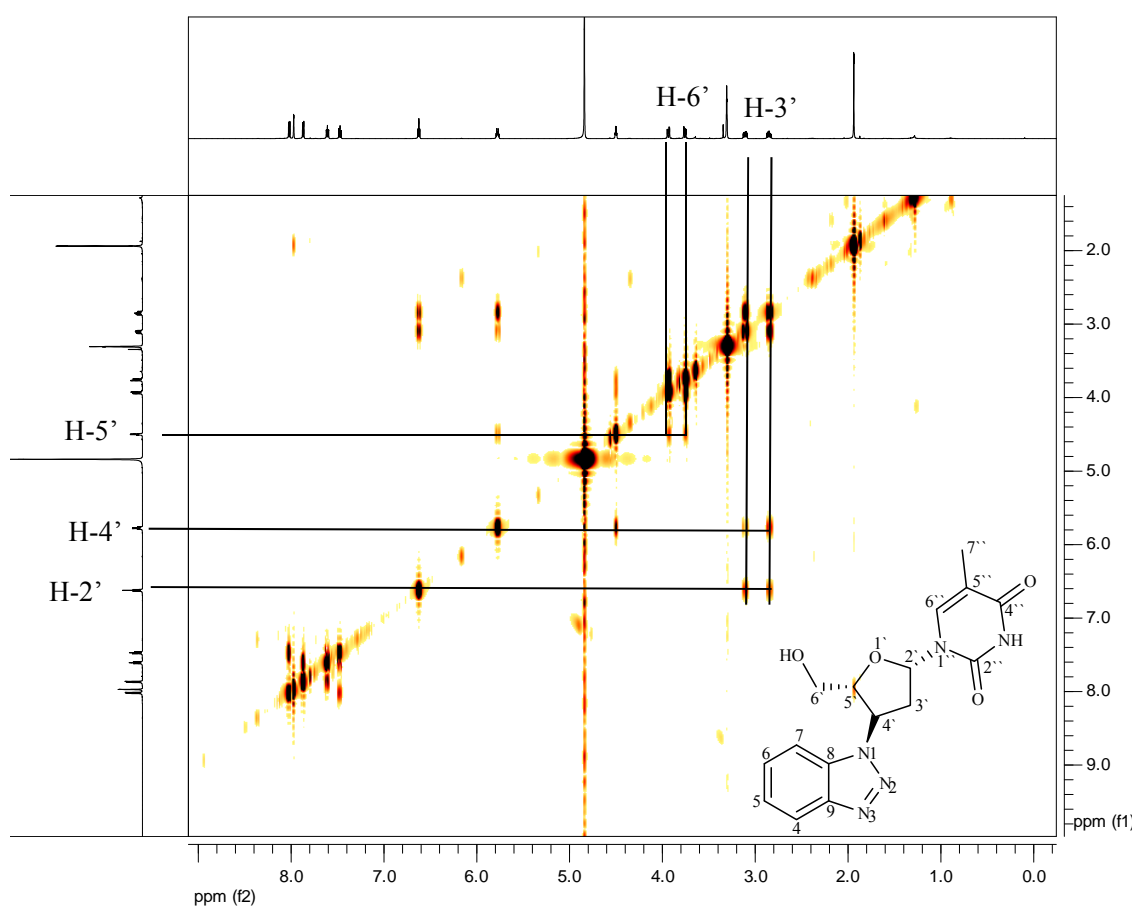


Figure 2.6 ^1H , ^1H -COSY spectrum of **112a** in $\text{MeOH-}d_4$

From the examination of the COSY NMR of compound **112a** (Figure 2.6) we were able to conclusively assign all of the 13 proton signals of **112a**. Two sets of diastereotopic methylene signals were identified at 3.85-3.13 and 3.75-3.95 ppm. The former signals were assigned to H-6 due to its coupling to two different methine protons at 6.62 and 5.77

ppm. These were assigned to H-2' and H-4' respectively, based on their relationship to neighbouring heteroatoms. The second diastereotopic methylene protons of compound **112a**, H-6' appear as a doublet of doublets at 3.76 ppm and 3.93 ppm, due to the proximity of the asymmetric carbon C-5' while the vinylic proton H-6'' resonates as a singlet at 7.97 ppm. Furthermore, the signals of the methine protons H-5' were observed at 4.50 ppm as a doublet of doublets. The signal of the methyl proton H-7'' appears as a singlet at 1.93 ppm. Analysis of this COSY NMR spectrum (Figure 2.6) was completed by the assignment of the aromatic proton signals between 7.46 ppm and 8.02 ppm.

The HSQC NMR spectrum of compound **112a** (Figure 2.7) confirmed the analysis of the ¹H NMR first by the presence of a methyl resonating at 12.54 ppm. Second, the vicinal vinylic carbons signals of C-5'' and C-6'' resonated at 111.8 ppm and 138.4 ppm respectively, the nitrogen atom deshielding C-6'' more than the deshielding effect of carbonyl C-4'' on C-5''. Finally, the three asymmetric carbon signals of C-4', C-5' and C-2' appeared distinctly at 59.1 ppm, 86.3 ppm and 87.1 ppm respectively, C-2' being more deshielded than C-5' because of the neighboring nitrogen atom. Signals corresponding to methylene carbons C-3' and C-6' resonated at 38.5 ppm and 62.4 ppm respectively. Correlations on the HSQC spectrum (Figure 2.7) confirmed these assignments which were in satisfactory agreement with the structural pattern of compound **112a** reported by Chandrasekhar and obtained in almost the same yield (63%).²⁴⁴ We went a bit further with Chandrasekhars' strategy and cyclised AZT **1** iodoanthranilic acid (80%) and bromoanthranilic acid (79%) and we generated novel compounds **112b** and **112c**.

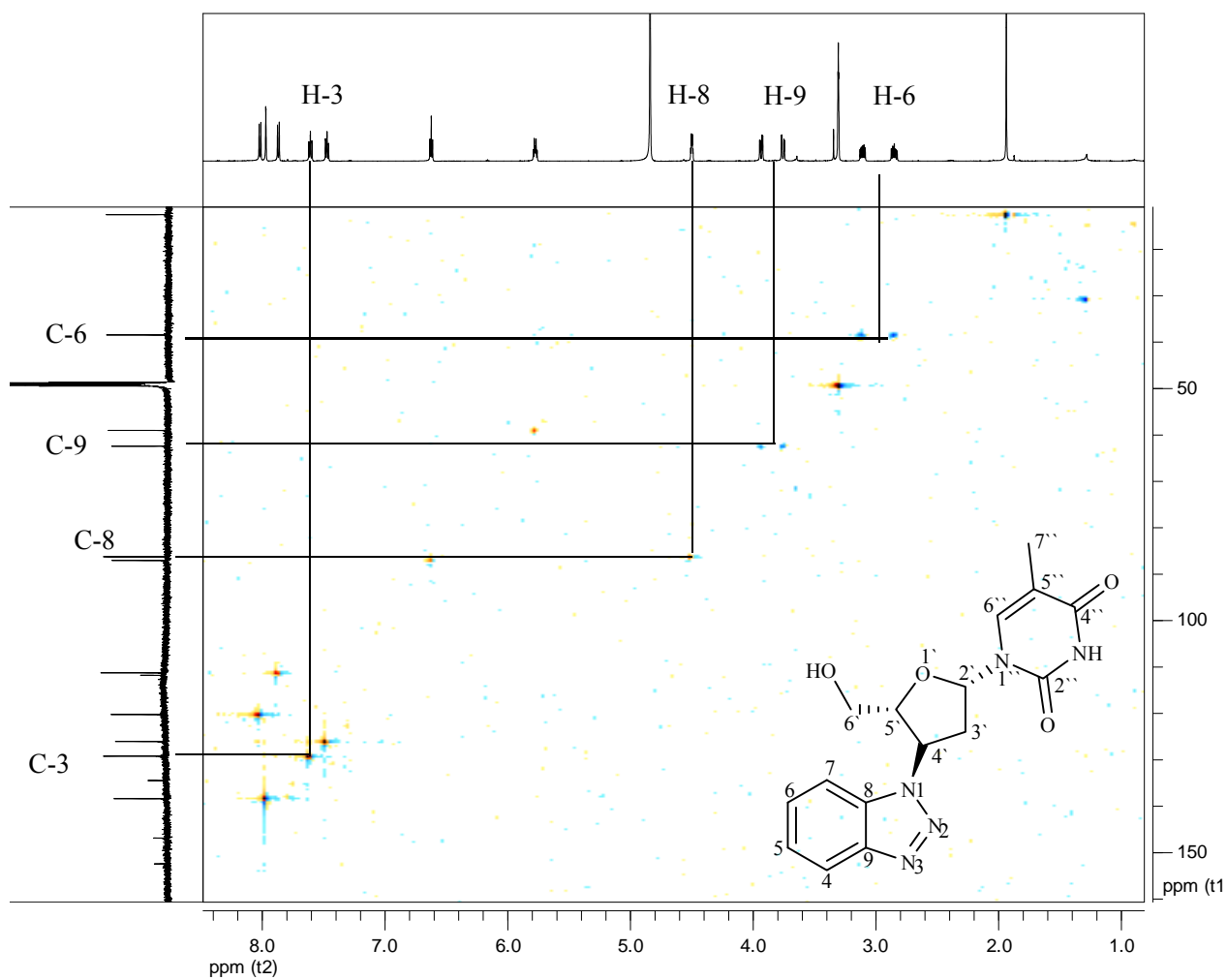


Figure 2.7. HSQC NMR spectrum of compound **112a** in MeOH- d_4 showing selected assignments

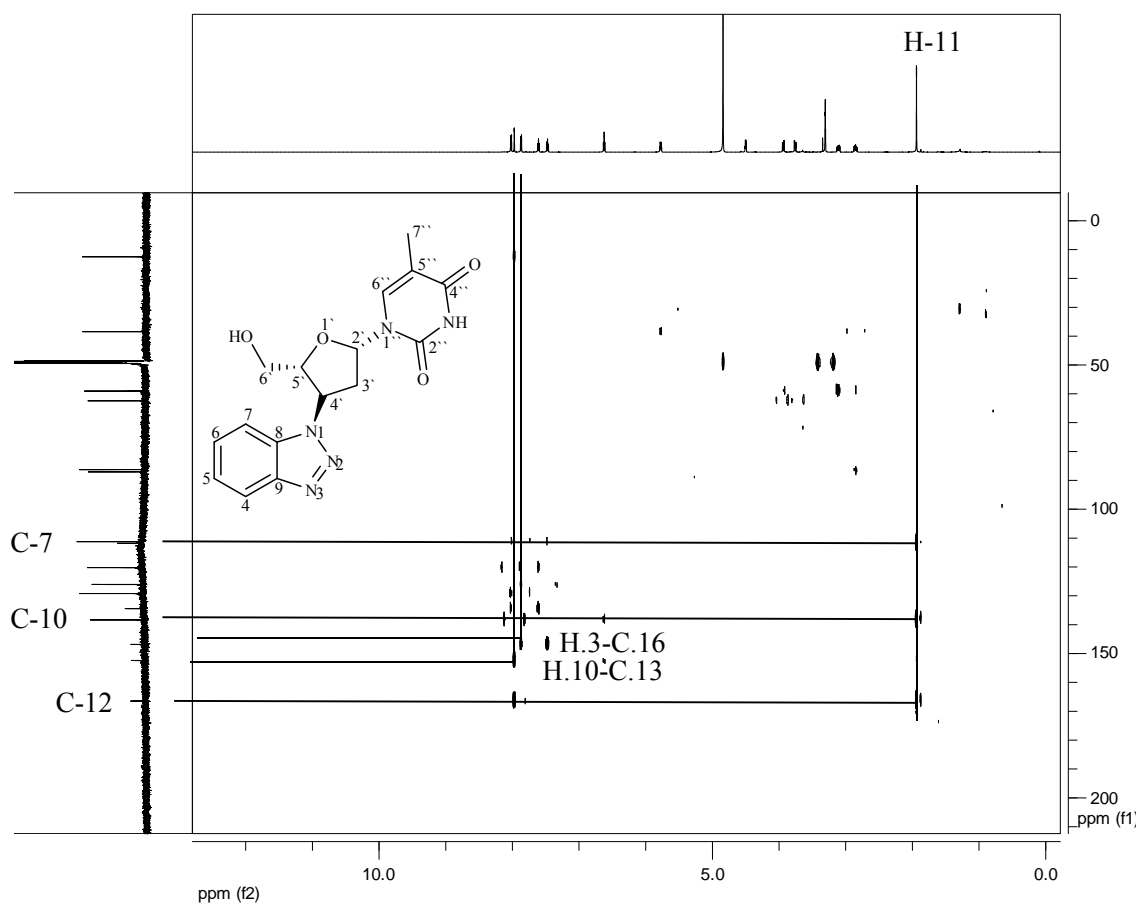
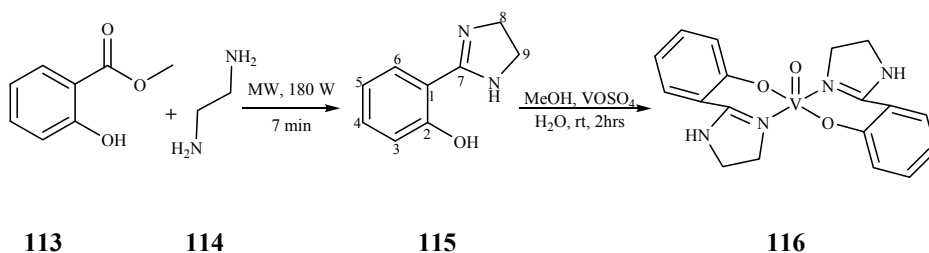


Figure 2.8. HMBC NMR spectrum of compound **112a** in MeOH- d_4

The assignments of the quaternary carbons were accomplished with the aid of an HMBC spectrum (Figure 2.8). A correlation between the signal of the methyl protons H-11 and the signal of the vinylic carbon C-14 and also a predictable 3-bond correlation to the methine carbon C-10 and the carbonyl C-12 were observed. In addition, a correlation between the vinylic proton H-10 and the carbonyl C-13 as well as between the aromatic proton H-3 and the quaternary carbon C-16 were observed.

- **Synthesis of the Vanadium catalyst**

Iodinated aromatic compounds are prohibitively expensive. In order to satisfy the demand for cheaper chemistry, the iodination of anthranilic acid **82** was carried out using a vanadium catalyst that was previously reported by Walmsley *et al.* (Scheme 2.29).²⁴⁵



Scheme 2.29. Synthesis of the vanadium catalyst **116**

Under microwave irradiation, methyl salicylate **113** was reacted with ethylene diamine **114** for seven minutes at 180 W to give compound **115**. To compound **115** was added an aqueous solution of MeOH and vanadium oxide. The mixture was stirred at room temperature for two hours and the product was filtered off and recovered as a blue precipitate.

The ^{13}C NMR spectrum of the intermediary **115** revealed the presence of eight carbon nuclei, where the two methylene carbon signals of C-8 and C-9 appeared isochronously at 40.3 ppm, the methine quaternary carbon C-2 was present at 161.3 ppm (being deshielded by the attached oxygen atom), followed by the signal of the methine carbon C-7 (highly deshielded by the two nitrogen atoms) resonating at 171.6 ppm. This confirmed the synthesis of the desired intermediate **115**.

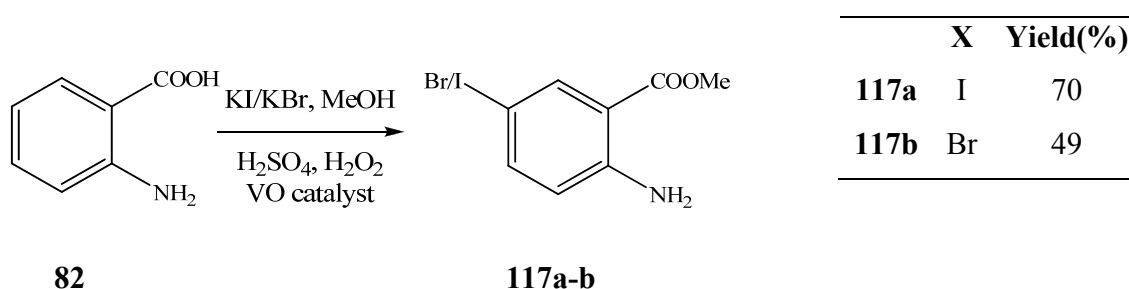
Because of the paramagnetic nature of the vanadium metal, NMR analysis could not be performed on this catalyst. However the IR spectrum revealed the presence of the N-H stretch at 3248.82 cm^{-1} , the C=N stretch at 1575.62 cm^{-1} and the V=O stretch at 929.56 cm^{-1} , characteristic bands of this vanadium based catalyst (see appendix A.1).

- **Oxidative iodination and bromination of anthranilic acid**

It is necessary to understand the mechanism behind this oxidative iodination, specifically, the role of the catalyst. The dioxygen present in hydrogen peroxide is activated by the vanadium catalyst to give a peroxovanadium intermediate (Scheme 2.30). An electrophilic iodinium ion is generated by the interaction of the peroxovanadium compound with the iodide source KI, followed finally by the iodination of the aromatic compound by standard aromatic electrophilic substitution.²⁴⁶ This reaction is therefore

subject to the same substituents effect as other electrophilic substitution. The bromination of anthranilic acid was also possible by pursuing the same route, using KBr as the bromide source.

Unexpectedly, the use of MeOH as solvent caused the esterification of the acid to take place and inevitably compounds **117a** and **117b** were formed instead (Scheme 2.30). The success of the synthesis was thus demonstrated by a methyl resonating at 3.91 ppm in the ^1H NMR and at 52.1 ppm in the ^{13}C NMR spectrum (Figure 2.9).



Scheme 2.30. Iodination/bromination of anthranilic acid **82** in MeOH

The signal of the carbon bound to iodine in aromatic compounds is easily identified around 80-100 ppm in CDCl_3 .²⁴⁷ Focussing in that region in the ^{13}C NMR spectrum of compound **117a** (Figure 2.9) it was thus trivial to assign the C-I signal resonating at 78.1 ppm. The remaining signals were assigned by analogy with anthranilic acid. The multiplicity of H-6 resonating as a singlet at 8.22 ppm, H-3 resonating as a doublet at 6.74 ppm and H-4 resonating also as a doublet at 7.55 ppm further gave evidence of the formation of **117a** (Figure 2.10). The COSY NMR spectrum (Figure 2.10) indicated a correlation between signals H-4 and H-3 (with a coupling constant of 8.8 Hz corresponding to an ortho relationship between the two protons). These assignments confirmed that the electrophilic substitution took place at carbon C-5.

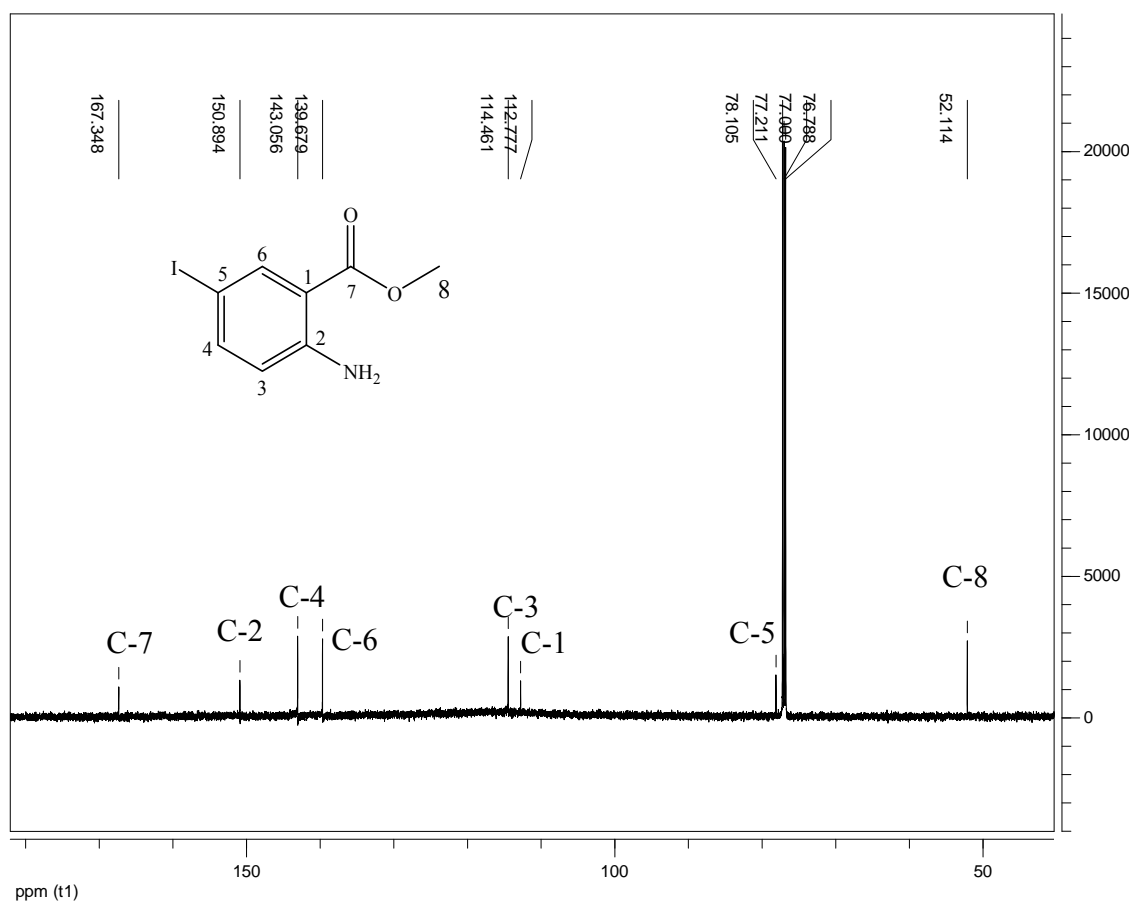


Figure 2.9. 150 MHz ^{13}C NMR spectrum of **117a** in CDCl_3

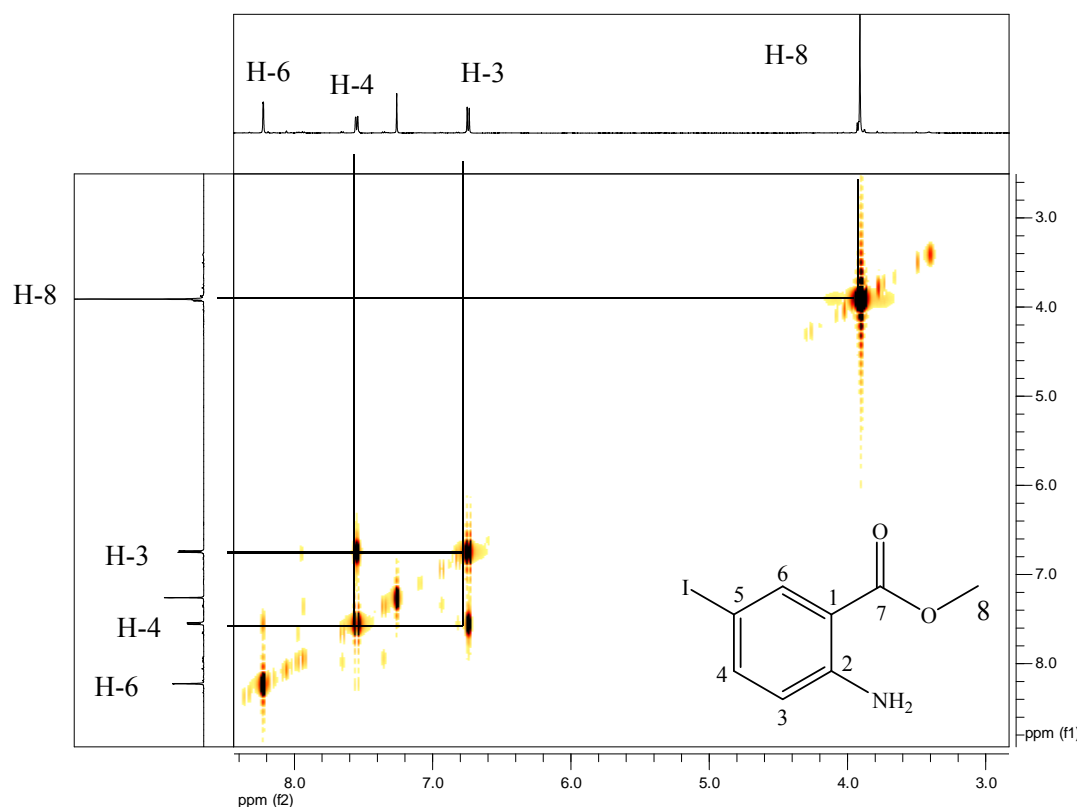
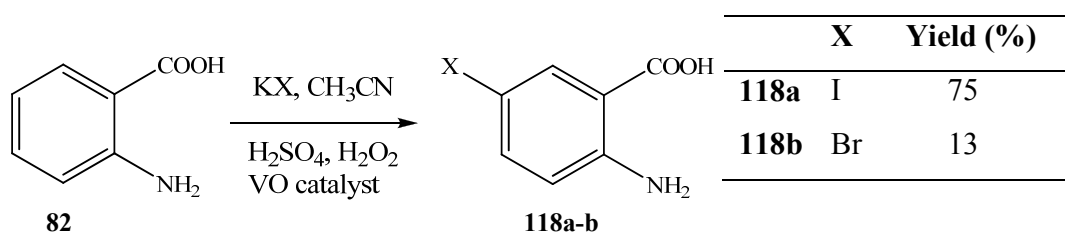


Figure 2.10. ^1H , ^1H -COSY NMR spectrum of **117a** in CDCl_3

Since iodinated anthranilic acid was needed in order to generate an iodobenzene ring for the cycloaddition, the ester we accidentally synthesized was not considered useful at this stage of our strategic plan. Acetonitrile was our second solvent of choice and under the same reaction conditions, **117a** was obtained in a yield of 75% (Scheme 2.31). In the ^{13}C NMR (Figure 2.11) the absence of the carbon methyl signal was unambiguously clear.



Scheme 2.31. Oxidative iodination and bromination of anthranilic acid **82** in CH_3CN

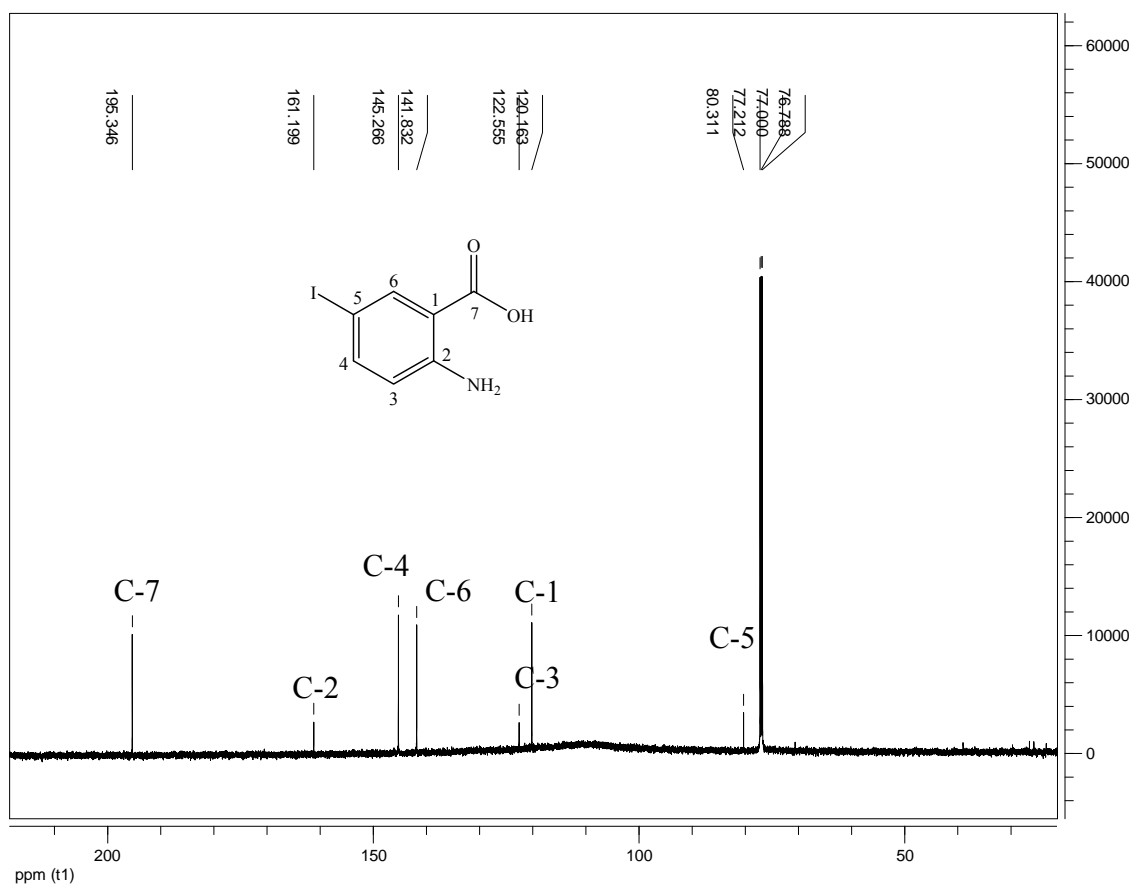


Figure 2.11. 150 MHz ^{13}C NMR spectrum of compound **118a** in CDCl_3

Anthranilic acid was also brominated following the same procedure. However we only obtained **118b** in a yield of 13%. In an attempt to optimize the yield of the reaction, we discovered an eco-friendly oxidative bromination of aromatic system recently published by Bhunia *et al.*²⁴⁸ At room temperature, a catalytic amount of V_2O_5 in water, hydrogen peroxide and perchloric acid as oxidizing agent and KBr as the bromide source produced **118b** in an improved yield of 71% after two hours.

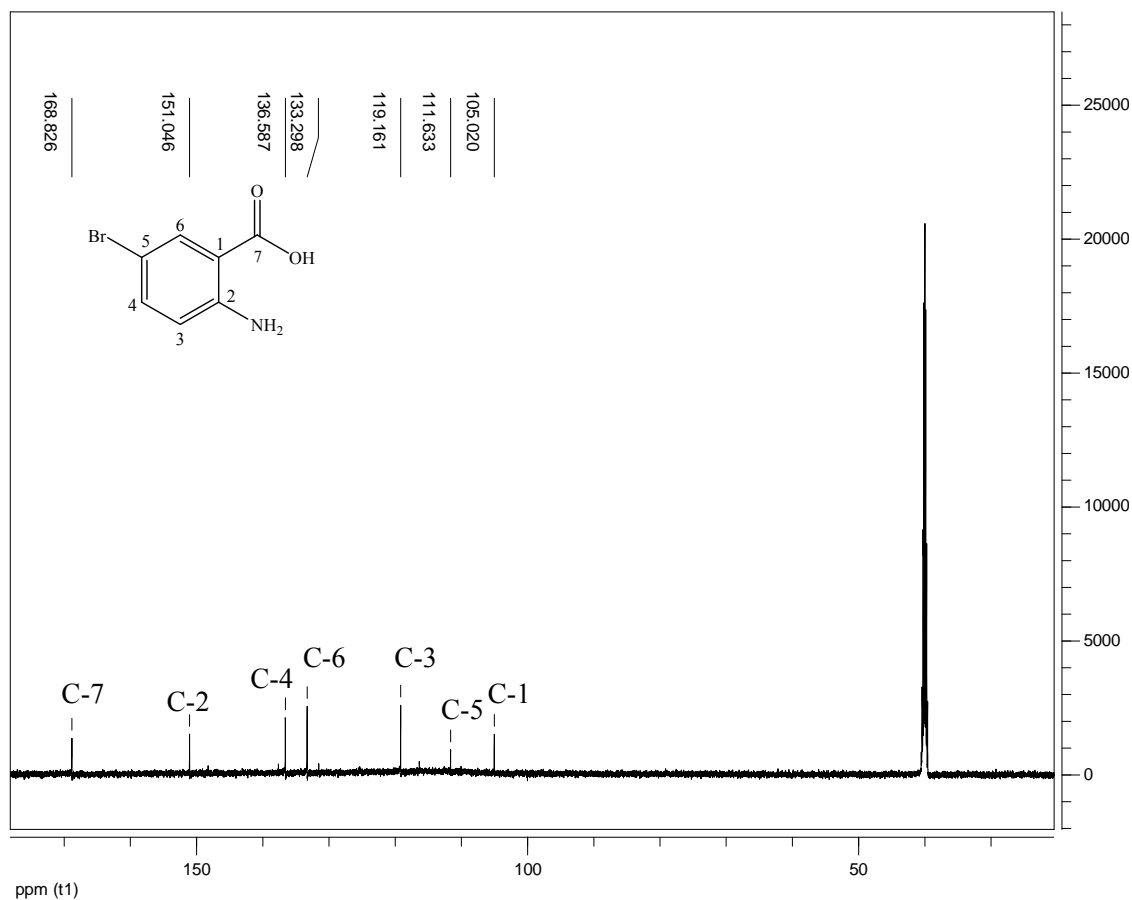
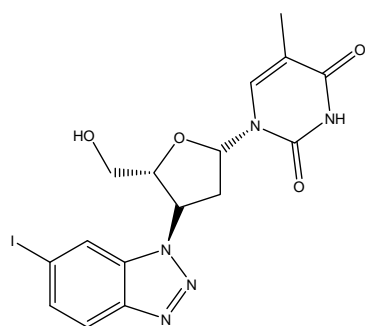


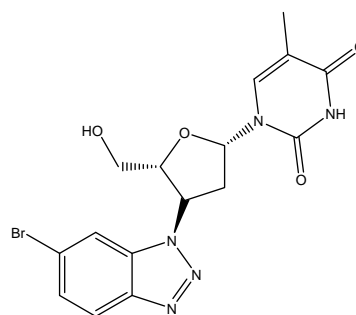
Figure 2.12. 150 MHz ^{13}C NMR spectrum of compound **118b** in $\text{MeOH-}d_4$

Due to the high electronegativity of bromine compared to iodine and confirmed by Chemdraw® predictions, the signal of the carbon bound to bromine appeared downfield relative to C-I and resonated at 111.6 ppm (Figure 2.12).

The iodoanthranilic acid and the bromoanthranilic acid synthesized were then cyclized with AZT according to method described in Scheme 2.28 to afford compound **112b** (80%) and compound **112c** (79%), both new compounds which were fully characterized.



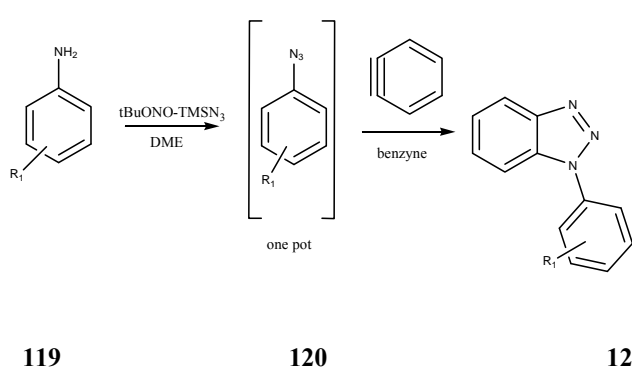
112b



112c

2.4.1.5. The 1,3-dipolar cycloaddition of anthranilic acid derivatives with aromatic amines

Since the synthesis of different azide analogs proved difficult, we searched for alternative methods to access the target compounds. Several reports indicated that azides can be generated *in situ* from aniline derivatives.²³⁷ Thus, different azides were generated by reacting aniline derivatives with amyl nitrite to form diazonium compounds. The addition of trimethylsilylazide (TMSN₃) as the azide source followed and the mixture was allowed to stir at room temperature for an hour. The azide formed was immediately coupled with anthranilic acid **82** by following the method previously described in Scheme 2.32 to afford compounds **121a-g**.



119

120

121

Scheme 2.32. *In situ* synthesis of azides from aniline derivatives for 1,3-DC

	R	Yield (%)
121a	H	44
121b	2-Me	52
121c	4-Me	50
121d	3-MeO	38
121e	3-Br	57
121f	3-F	64
121g	4-Cl	55

The confirmation of the structure of **121d** was achieved using NMR spectroscopy. The structure of benzotriazoles comprises at least two aromatic rings (Scheme 2.32) and, it

was difficult to identify all the proton signals without ambiguity due to the overlap of the aromatic protons resonating in the same region (Figure 2.13). It was much easier to resolve their structure based on the ^{13}C NMR where at least the three quaternary carbons of all the compounds in the series consistently appeared between 135 ppm and 150 ppm as a set of signals diagnostic of the skeleton of a benzotriazole.

With the aid of HSQC NMR of compound **121d** we were able to assign the methyl singlet at 3.91 ppm, and H-12 appeared as a doublet at 7.04 ppm while the aromatic protons signals H-3 and H-6 were clearly resolved as doublets at 7.77 ppm and 8.14 ppm respectively (Figure 2.13).

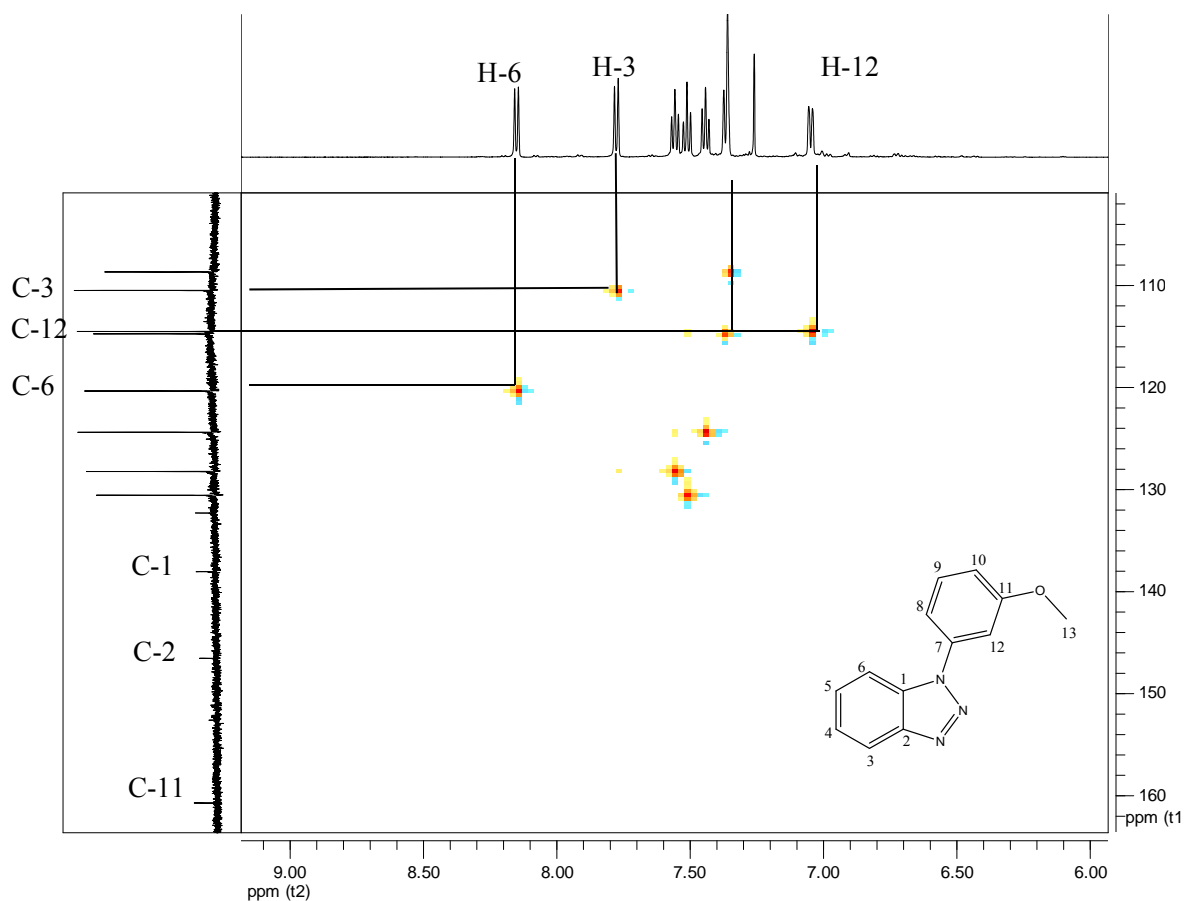
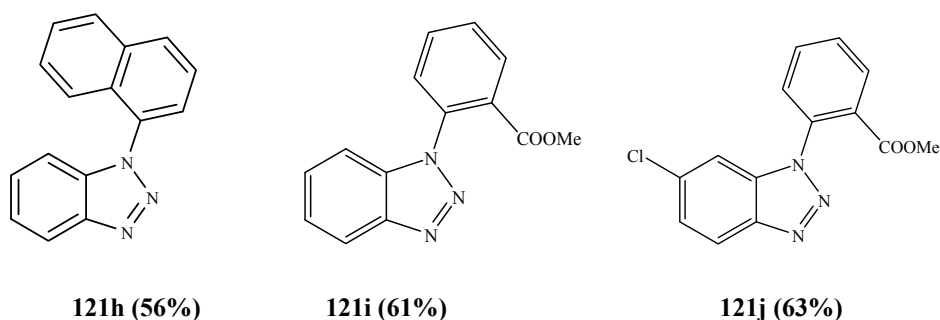


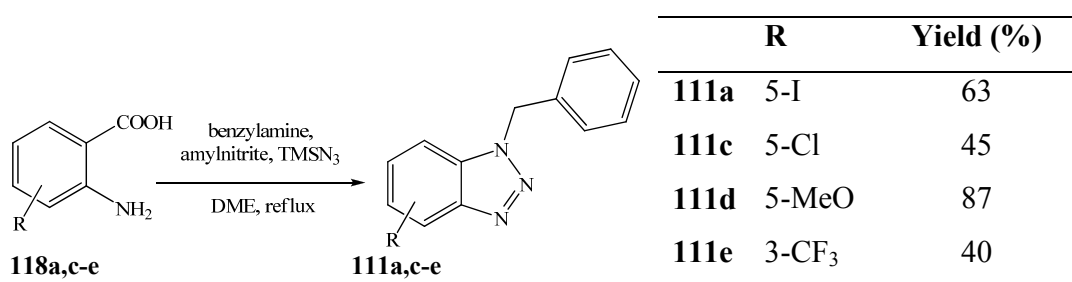
Figure 2.13. HSQC NMR spectrum of compound **121d** in CDCl_3

Careful inspection of the HSQC NMR of analog **121d** (Figure 2.13) also revealed the presence of 13 carbon signals with a methyl carbon signal at 55.6 ppm and the four quaternary carbon signals of the compound C-7, C-1, C-2 and C-11 at 132.3 ppm, 138.1 ppm, 146.5 ppm and 160.7 ppm respectively as expected.

Besides the aniline derivatives mentioned in Scheme 2.32, 1-naphtholamine and anthranilic acid itself were used to afford compounds **121h**, **121i** and **121j** by following the same methodology. The interesting factor about using anthranilic acid **82** as the azide precursor was the esterification of the acid functionality by the solvent dimethoxyethane under reflux to form the corresponding methyl esters.



In addition to compound **118a**, other commercially available anthranilic acids for instance, 5-chloroanthranilic acid (**118c**), 5-methoxyanthranilic acid (**118d**) and 3-trifluoromethylantranilic acid (**118e**) were used and cyclized with benzylamine to complete this series of substituted benzotriazole analogs (Scheme 2.33).



Scheme 2.33. Synthesis of benzotriazole analogs from different anthranilic acid derivatives as benzyne precursors with benzylamine as the azide source

The proton NMR of compound **111e** displayed 10 protons as expected. The singlet corresponding to the methylene (H-7) appeared at 5.34 ppm and a triplet at 6.67 ppm corresponding to H-5 were relatively easy to assign due to their multiplicities. Using a COSY spectrum (Figure 2.14) we were then able to identify H-4 (8.13 ppm) and H-6 (7.6 ppm) by correlation with H-5. Similarly, since the signals between 7.26 ppm and 7.44 ppm only showed correlations to each other, they were assigned to the five aromatic protons (H-9 to H-13) on the unsubstituted ring.

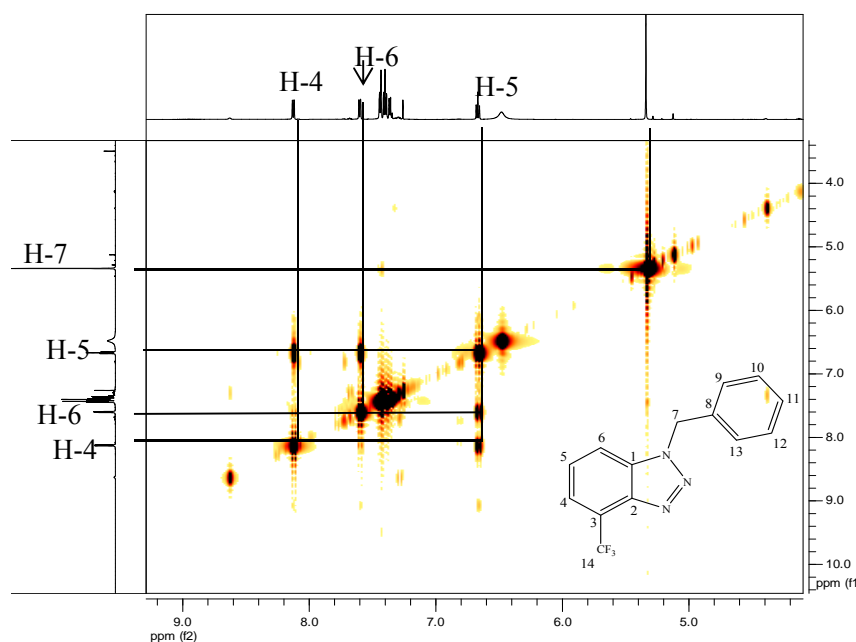


Figure 2.14. ^1H , ^1H -COSY NMR spectrum of compound **111e** in CDCl_3

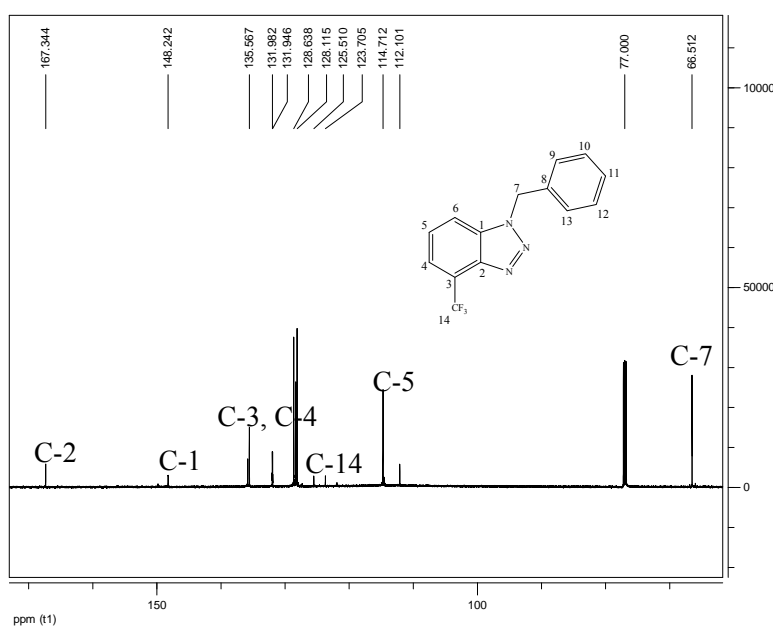


Figure 2.15. 150 MHz ^{13}C NMR spectrum of compound **111e** in CDCl_3

In the ^{13}C NMR spectrum of compound **111e** (Figure 2.15) the simplest carbon to assign was a methylene carbon resonating at 66.5 ppm. In addition a quaternary CF_3 carbon resonating as a quartet at 123.7 ppm due to the coupling of the carbon with the three fluorine atoms and also highly deshielded by these fluorine atoms was observed. A closer examination of the ^{13}C NMR spectrum revealed the presence of three multiplets overlapping between 128.1 ppm and 128.6 ppm which indicates the presence of the aromatic carbons of the substituted ring (C-10, C-12, C-11, C-9 and C-13). A correlation in the HMBC spectrum (Figure 2.16) of the methine proton H-4 and the quaternary carbon C-2 further confirmed its assignment. The HMBC spectrum also indicated a correlation between the methine proton H-6 and the quaternary carbon C-1 resonating at 148.2 ppm. Therefore the quaternary carbon resonating at 135.6 ppm was assigned to C-3, slightly deshielded by the CF_3 group attached to it and correlating with the methine proton H-4 in the HMBC spectrum (Figure 2.16).

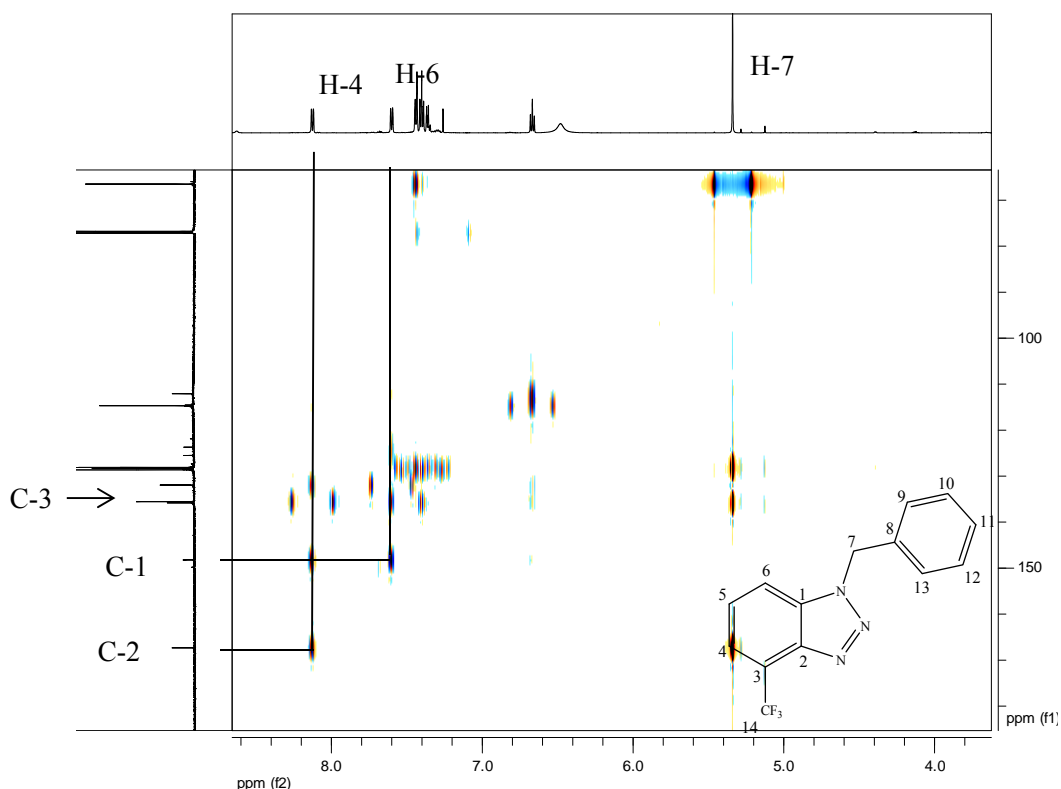
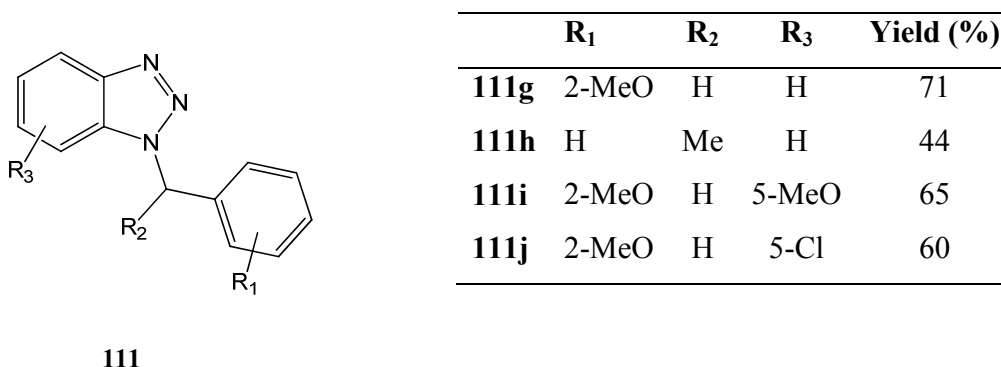


Figure 2.16. HMBC NMR spectrum of compound **111e** in CDCl_3

Substituted benzylamines were also cyclized with substituted anthranilic acid using an analogous process (Scheme 2.34). Substituted benzylamines were chosen because the benzyl group fits well in the hydrophobic pocket of the HIV 1 PR enzyme.



Scheme 2.34. Benzotriazole analogs from anthranilic derivatives and substituted benzylamine

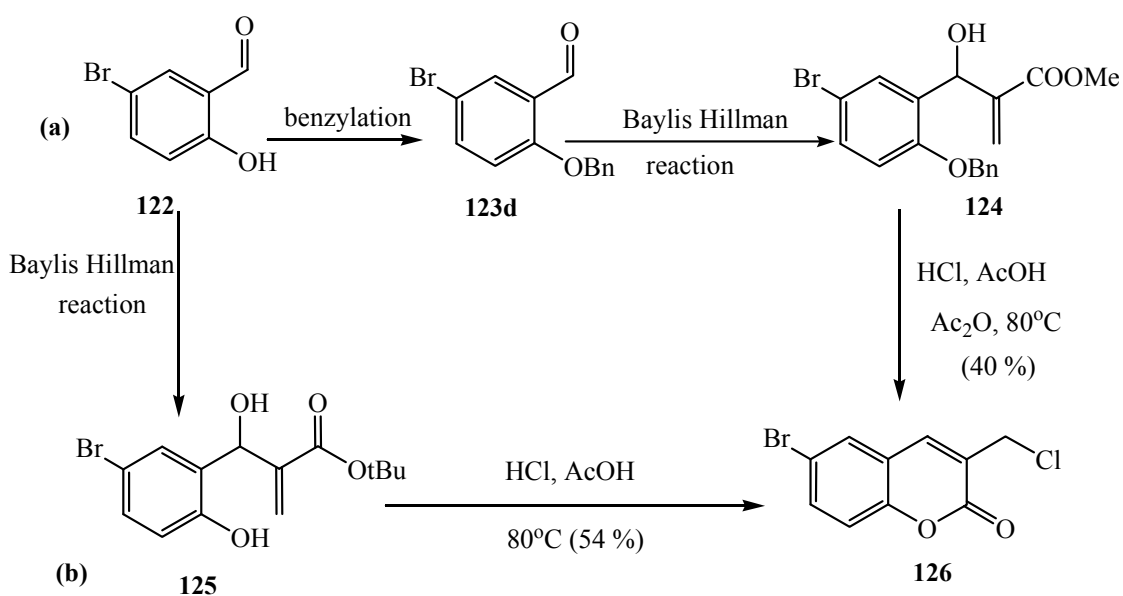
2.4.2. Synthesis of coumarins

Several reports claim that some coumarins are active inhibitors of the HIV-1 protease enzyme.²⁴⁹⁻²⁵¹ In our research group, coumarin and cinnamate ester-AZT conjugates have already been shown to be active inhibitors against HIV-1 enzymes.^{81, 83} In this section we present the synthesis of coumarin derivatives with functionalities that could enhance their anti-HIV activity (described in Section 2.1.3). We first present the synthesis of coumarins followed by their derivatisation *via* palladium catalyzed reactions.

2.4.2.1. Synthesis of coumarins from Baylis Hillman adducts

The starting point for this work was an earlier study by Musa *et al.* where 3-bromomethylcoumarin derivatives were synthesized using a Baylis Hillman methodology (Scheme 2.35a).^{252, 253} In our hands the first step following Musa's procedure,²⁵² involved a benzylation reaction of 5-bromosalicylaldehyde to afford compound **123d** as described in Section 3.2.1 (synthesis of acrylamide). The benzylation was performed in order to avoid the formation of by-products during the Baylis Hillman reaction. The Baylis Hillman reaction with methylacrylate (Scheme 2.35a) gives mixture of compounds while the use of tertbutyl acrylate (Scheme 2.35b) results exclusively in the formation of the

Baylis Hillman product. Using substrates thus formed, we performed a solventless Baylis Hillman reaction under microwave conditions where compounds **122** and **123d** were mixed with acrylate and a catalytic amount of 1,4-diazabicyclo [2.2.2] octane (DABCO) **87** and irradiated for six hours to afford compounds **124** and **125** in an average good yield of 71%.



Scheme 2.35. Synthesis of coumarins from Baylis Hillman adducts ^{252, 253}

The ^1H NMR spectrum of compound **124** (Figure 2.17) indicates the presence of 17 protons as expected with a broad singlet resonating at 3.32 ppm corresponding to the benzylic OH and a methyl singlet at 3.74 ppm. The three characteristic Baylis Hillman protons (BH protons) H-7 and H-9 (a and b) resonate as singlets at 5.66 ppm, 5.89 ppm and 6.29 ppm respectively while 8 aromatic protons appear between 6.79 ppm and 7.37 ppm.

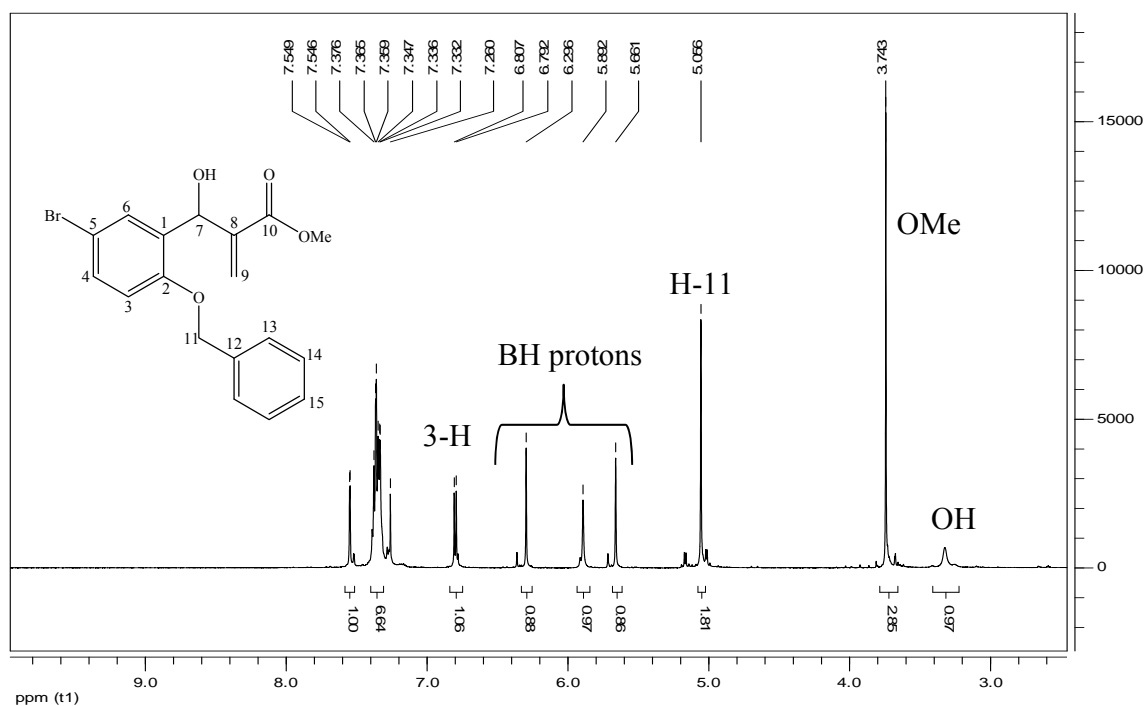


Figure 2.17. 400 MHz ^1H NMR spectrum of compound **124** in CDCl_3

The ^{13}C NMR spectrum of **124** (Figure 2.18) revealed 18 carbons as forecast. The easily identified signals were of a methyl carbon at 52.0 ppm, a methine carbon (C-7) appearing at 67.7 ppm, a methylene carbon C-11 resonating at 70.5 ppm and a carbonyl (C-10) resonating at 166.9 ppm.

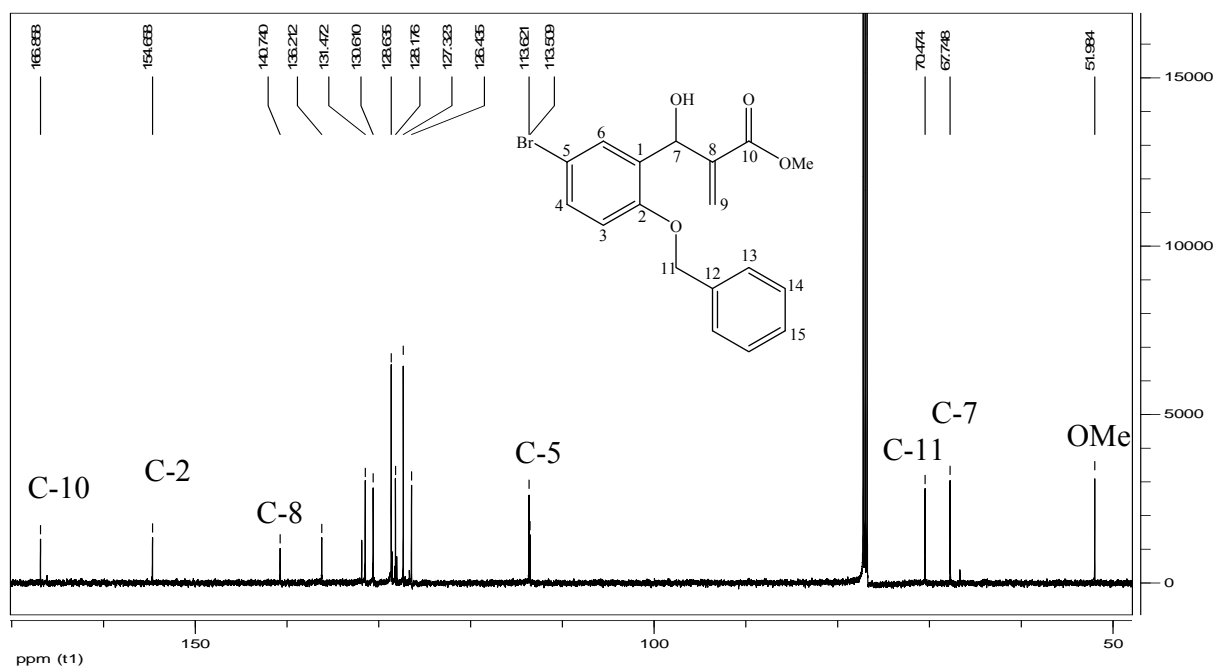


Figure 2.18. 100 MHz ^{13}C NMR spectrum of compound **124** in CDCl_3

Finally, coumarin **126** was obtained by refluxing the Baylis Hillman adducts **124** or **125** in a mixture of hydrochloric acid, acetic acid and acetic anhydride for two hours at 80 °C in yields of 40% and 54% respectively.

The ^1H NMR spectrum of compound **126** indicated the presence of six unique proton signals as expected. While signals corresponding to H-11 appeared at 4.57 ppm, four aromatic protons resonate between 7.28 ppm and 7.84 ppm, the signals corresponding to the Baylis Hillman methyl and methylene protons, and those corresponding to the benzyl group, have disappeared.

The ^{13}C NMR spectrum (Figure 2.19a) confirmed the presence of 10 carbons of compound **126** as expected. The DEPT-135 NMR spectrum (Figure 2.19b) further confirmed the identity of the methylene carbon C-11 resonating at 41.2 ppm and the five quaternary carbons including the carbonyl C-2 resonating at 159.8 ppm.

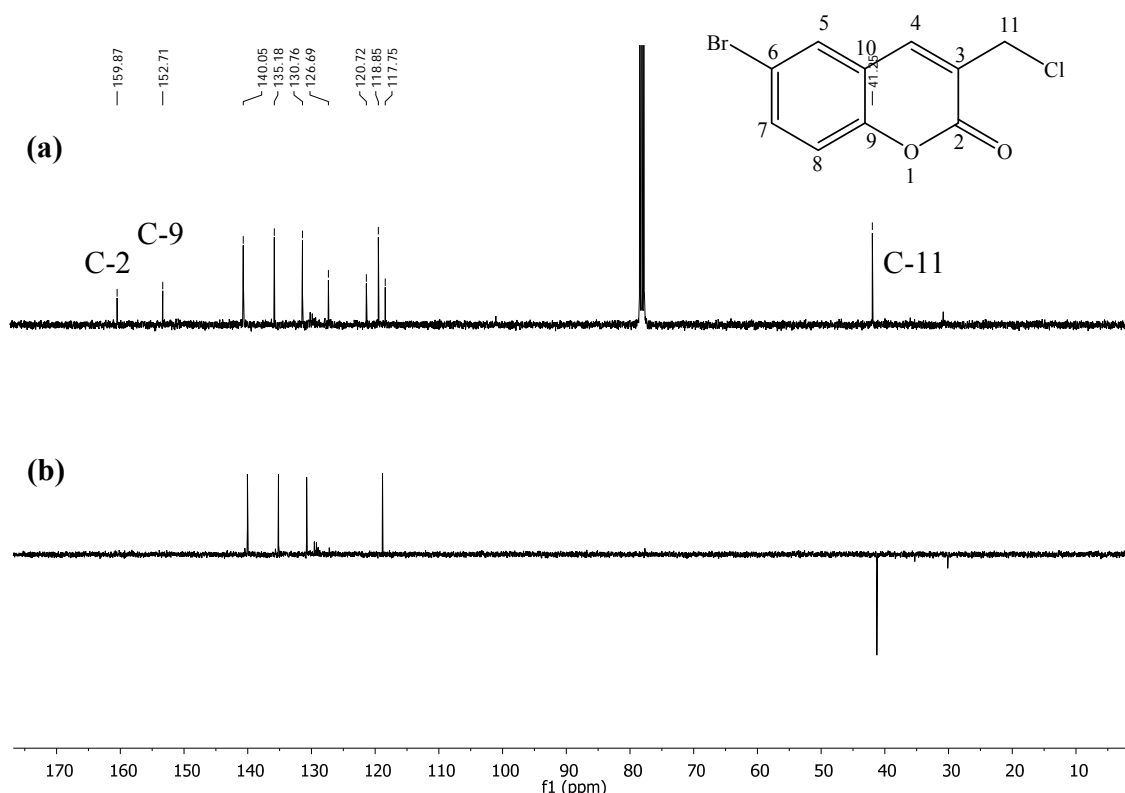
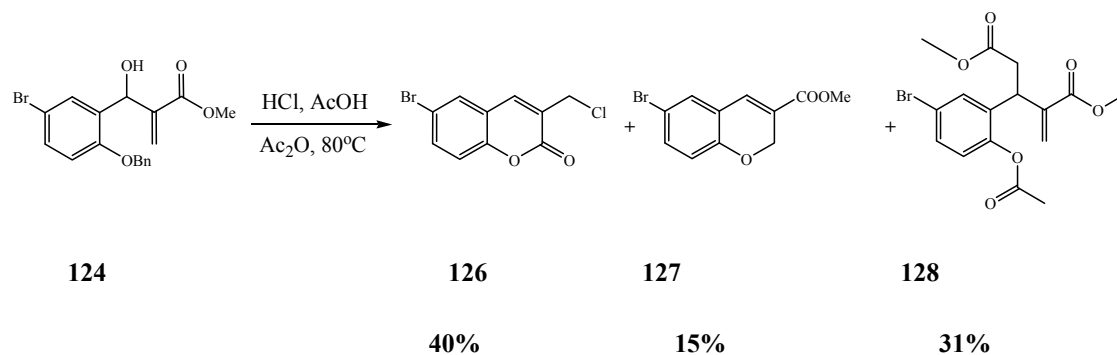


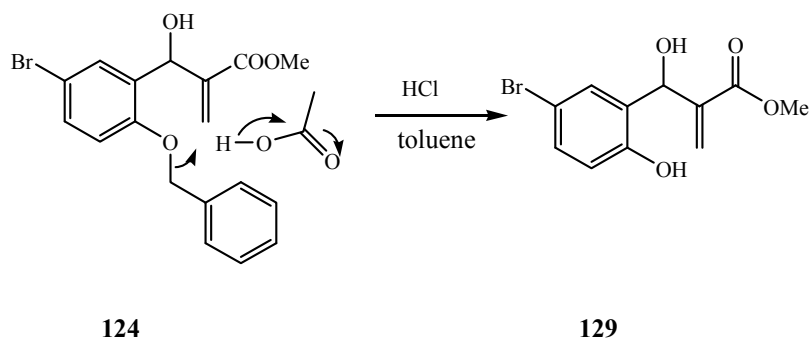
Figure 2.19 100 MHz ^{13}C NMR (a) and DEPT-135 NMR (b) spectra of compound **126** in CDCl_3

By following the approach outlined in Scheme 2.35a, we observed that a number of transformations took place during the cyclisation of the methyl acrylate adduct (**124**), as depicted in Scheme 2.36 and besides compound **126**, minor competition products were also isolated in sufficient purity and quantity for identification.



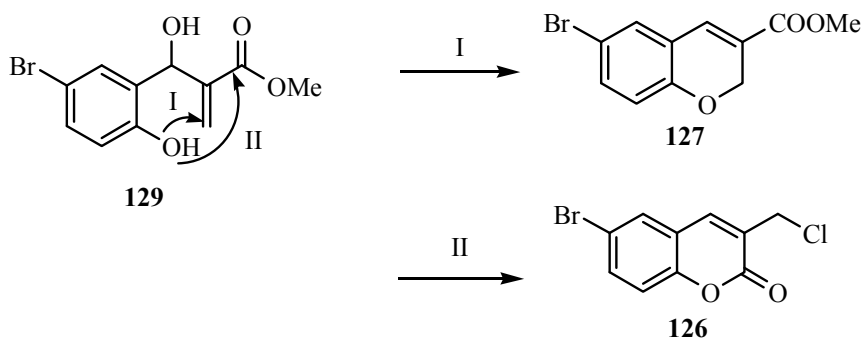
Scheme 2.36. Coumarin synthesis by acid catalyzed cyclisation of Baylis Hillman adducts

During this reaction, an acetic acid mediated debenzylation (deprotection) of compound **124** occurred following the reaction mechanism outlined in Scheme 2.37, proposed by Fletcher *et al.*²⁵⁴



Scheme 2.37. Debenzylation of the Baylis Hillman adduct

Musa *et al.* demonstrated that the Baylis Hillman intermediate **129** underwent a conjugate addition of the nucleophilic hydroxyl group to the alkene double bond followed by an elimination (dehydration) which afforded chromene **127** (Scheme 2.38, Path I), while a nucleophilic attack of the carbonyl by the hydroxyl group with subsequent HCl addition to the alkene double bond afforded compound **126** (Path II).^{253, 255}



Scheme 2.38. Cyclisation of Baylis Hillman adduct to afford chromenes (I) and coumarins (II)

The ¹H NMR spectrum of compound **127** (Figure 2.20) indicates the presence of nine protons as expected with a methyl ester singlet appearing at 3.82 ppm and two methylene protons at 4.90 ppm. The disappearance of the benzyl group from the Baylis Hillman adduct and appearance of the methylene protons of compound **126** was also observed.

The ^{13}C NMR spectrum (Figure 2.21) reveals the presence of eleven carbons as forecast. Of particular interest were the carbonyl (C-11) resonating downfield at 166.0 ppm and the methylene carbon signal C-2 at 66.0 ppm.

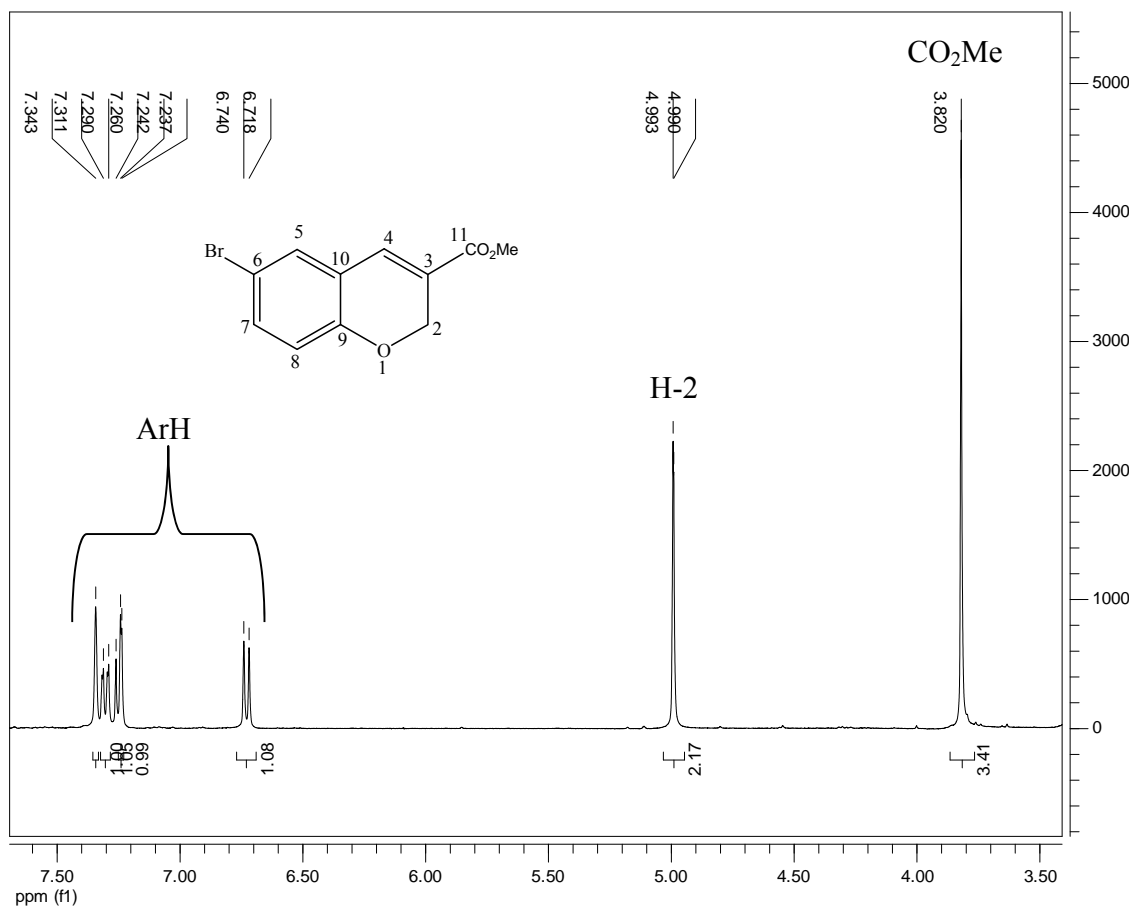


Figure 2.20. 400 MHz ^1H NMR spectrum of compound **127** in CDCl_3

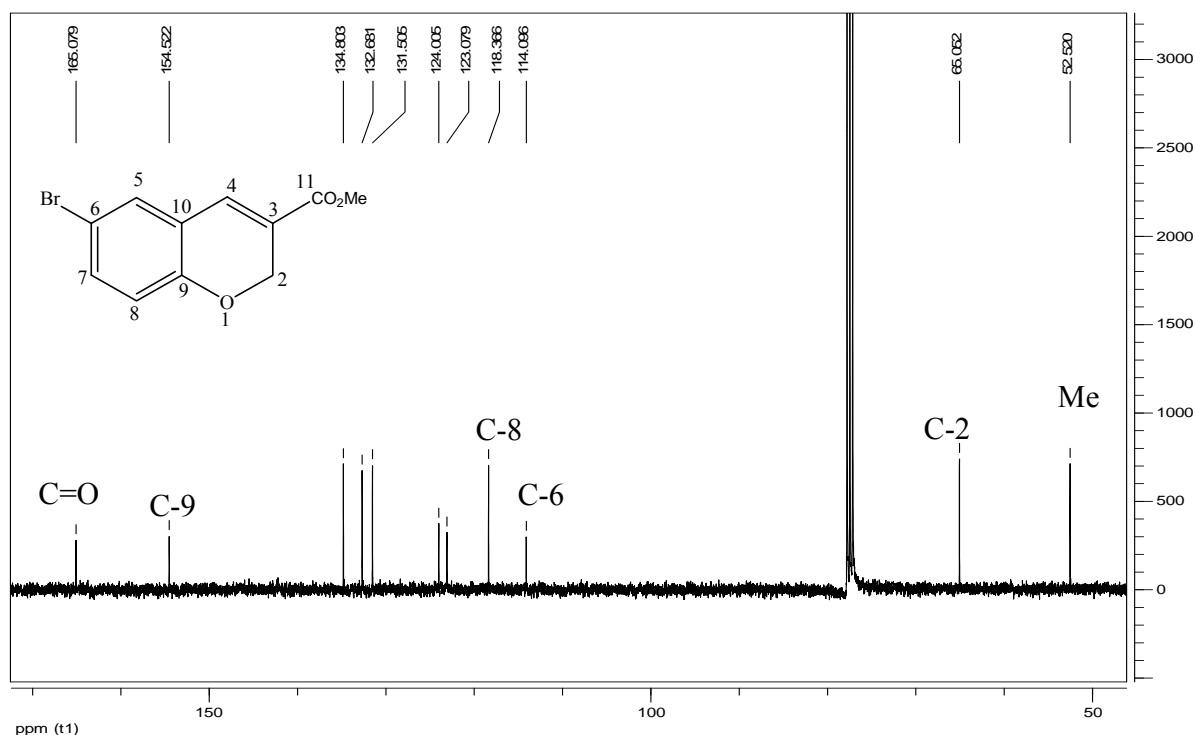


Figure 2.21. 100 MHz ^{13}C NMR spectrum of compound **127** in CDCl_3

In addition to compound **126** and compound **127**, novel compound **128** was formed (Scheme 2.36). The formation of the $\text{C}_7\text{-C}_{12}$ carbon bond (Figure 2.22) was unprecedented. Future research will focus on understanding the mechanistic details involved in the formation of compound **128**.

NMR spectroscopy facilitated the elucidation of the structure of compound **128**. In the COSY NMR spectrum of compound **128** (Figure 2.22) appear seventeen proton signals. The presence of a sharp methyl singlet at 2.14 ppm corresponding to H-14 and two methoxy proton signals at 3.68 ppm and 3.73 ppm indicated the likely presence of an acetyl methyl and two methoxy groups. Furthermore, vinylic methylene signals (H-9) appeared as two singlets at 5.45 ppm and 6.08 ppm. Surprisingly, the methine proton (H-7) resonated as a triplet at 4.48 ppm, more than 1 ppm upfield from where expected. From the COSY NMR spectrum of compound **128** (Figure 2.22) it was furthermore apparent that H-7 was coupling with the methylene protons H-12 and this could explain its multiplicity.

The ^{13}C NMR spectrum of compound **128** (Figure 2.23a) reveals the presence of 16 carbon signals while the HSQC and DEPT-135NMR spectra (Figure 2.24 and Figure 2.23b) confirmed the presence of an acetyl carbon C-14 resonating at 13.9 ppm, a methylene carbon C-12 appearing at 33.1 ppm, a methine carbon signal C-7 at 44.2 ppm and two methoxy carbon signals C-16 and C-11 at 52.2 ppm and 52.8 ppm respectively. In addition, the methylene carbon signal C-9 appeared at 129.3 ppm while 6 aromatic carbon signals appeared between 116.9 ppm and 135.8 ppm. From the DEPT-135 NMR spectrum of compound **128** (Figure 2.23b) and its ^{13}C NMR spectrum (Figure 2.23a), the carbonyl carbon signals C-13, C-10 and C-15 were identified at 161.1 ppm, 166.8 ppm and 171.8 ppm respectively. The HMBC NMR spectrum (Figure 2.25) confirmed these assignments by showing a correlation between the methoxy proton signals H-16 and H-11 with the carbonyl signals C-15 and C-10 respectively while a correlation between the acetyl methyl singlet H-14 and the carbonyl signal C-13 was also observed. In addition, a correlation between the Baylis Hillman protons H-7 and H-9 with the methylene carbon C-12 was observed.

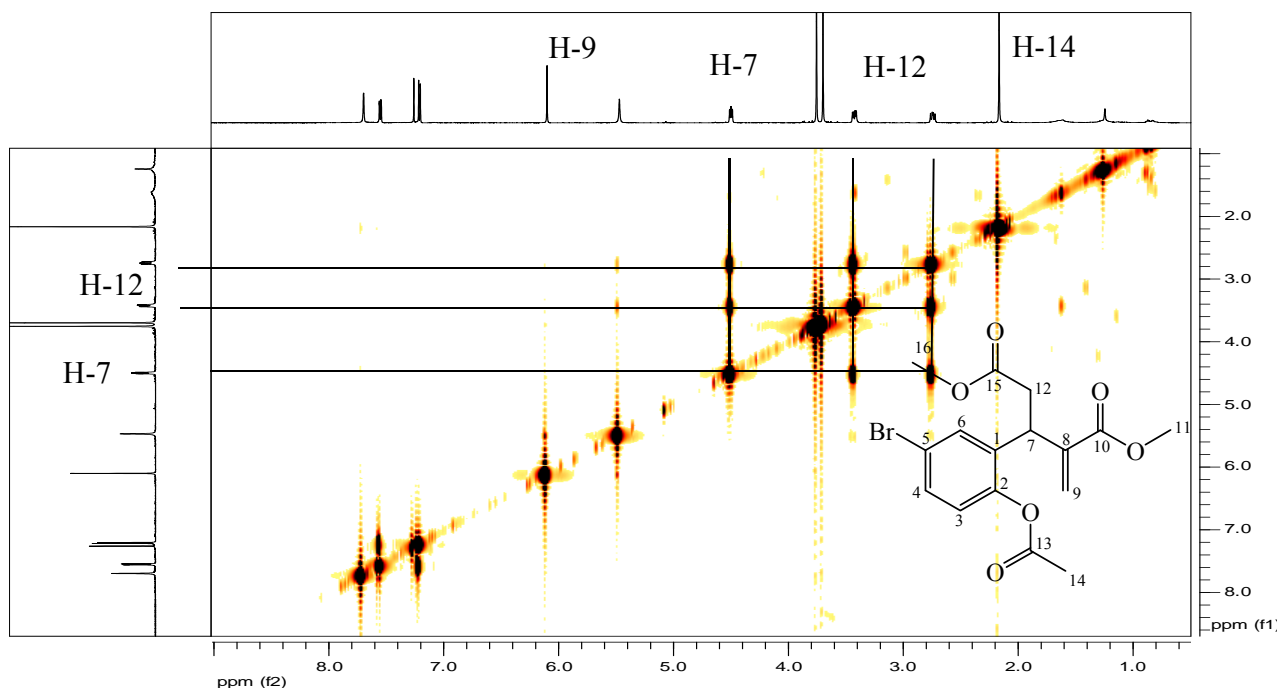


Figure 2.22. ^1H , ^1H -COSY NMR spectrum of compound **128** in CDCl_3

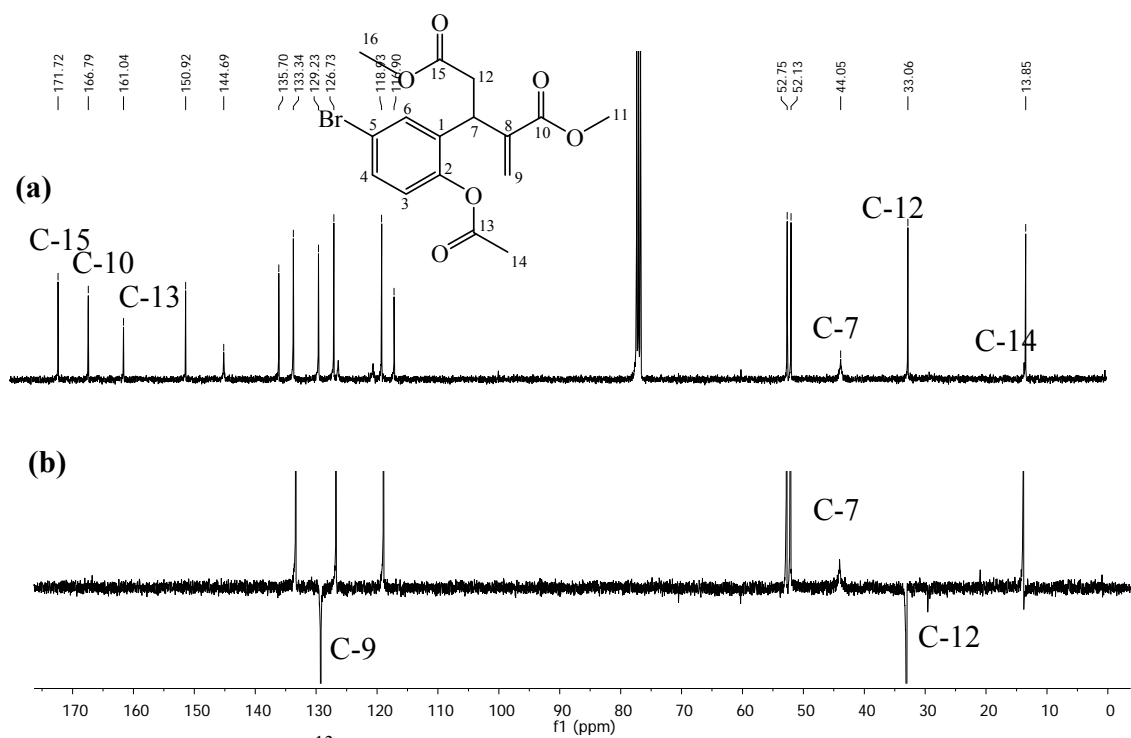


Figure 2.23. 100 MHz ^{13}C NMR (a) and DEPT-135 NMR (b) spectra of compound **128** in CDCl_3

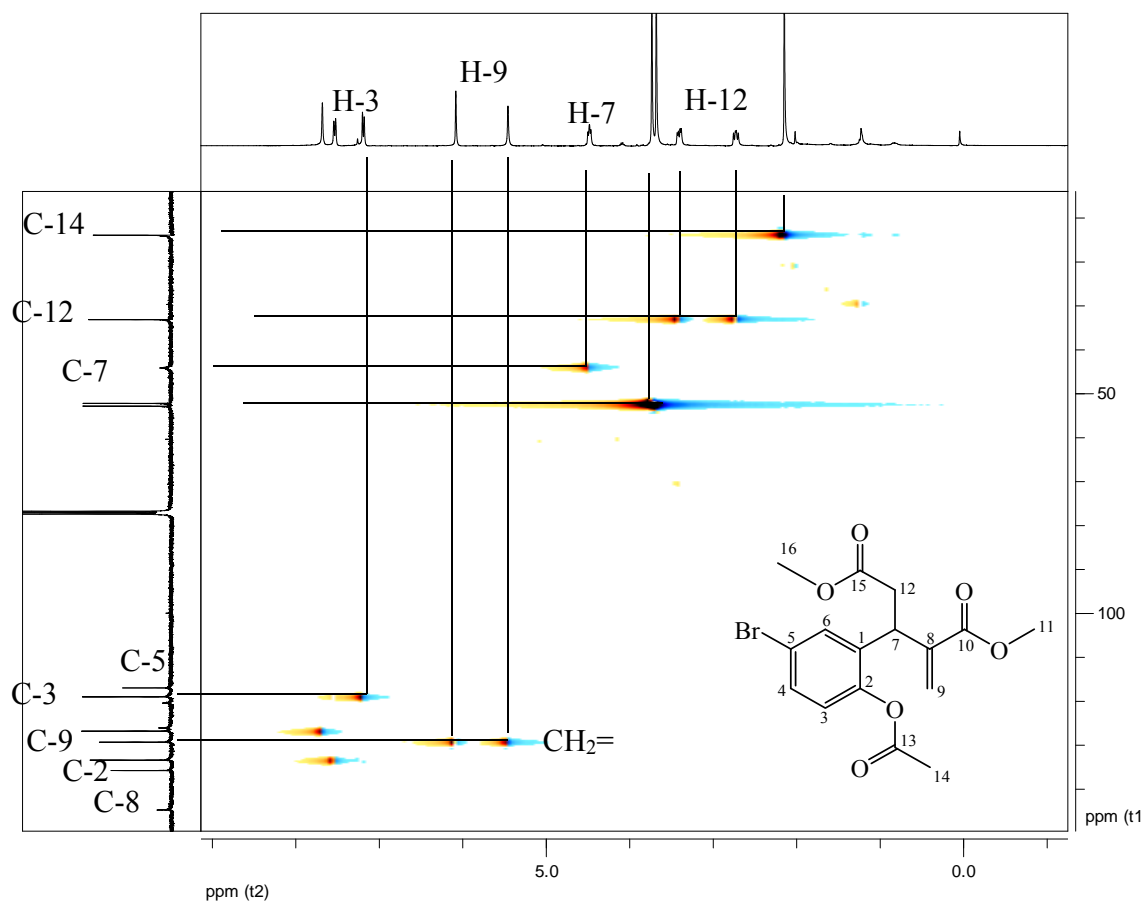


Figure 2.24. HSQC NMR spectrum of compound **128** in CDCl₃

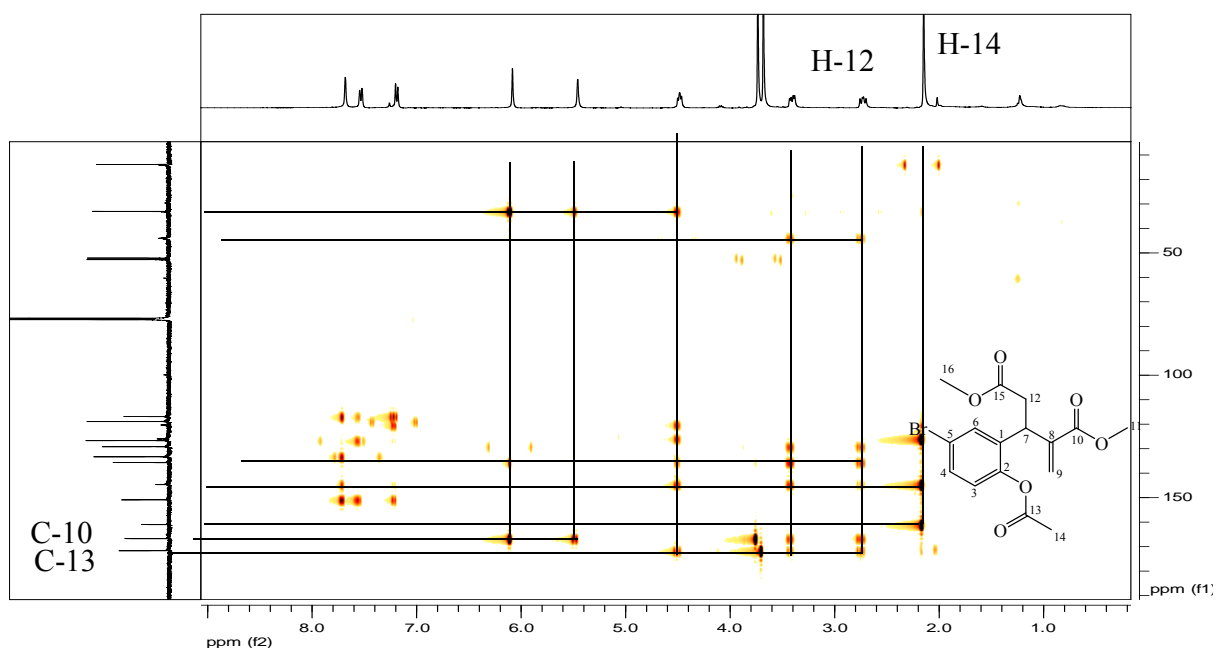


Figure 2.25. HMBC NMR spectrum of compound **128** in CDCl_3

Because of these competitive side reactions, compound **126** was also synthesized by the pathway described in Scheme 2.35b. A Baylis Hillman reaction of 5-bromosalicylaldehyde with *tert*-butylacrylate since it is more reactive than methyl acrylate afforded compound **125** which was cyclized under acidic conditions to afford compound **126** as the only product with an improved yield of 54%.

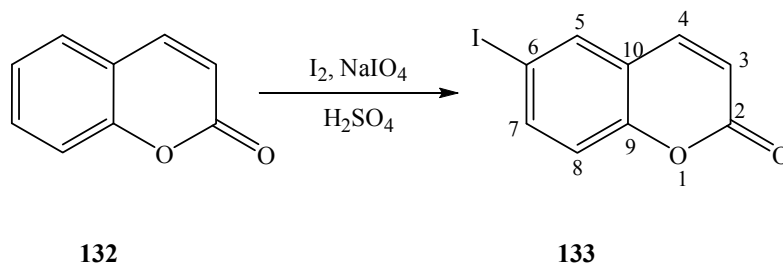
2.4.2.2. Derivatization of coumarin by palladium catalyzed reactions

Having bromine at carbon 6 (see compound **126** in Figure 2.19), suggested the possibility of palladium catalyzed Heck and Sonogashira coupling reactions to extend the carbon scaffold. However, after many attempts no reaction was observed under either condition. It appeared that in compound **126**, bromine was not a sufficiently good leaving group to favor carbon-carbon bond formation.

2.4.2.2.1. Oxidative iodination of coumarin

We hypothesized that iodine would be more amenable to this type of reaction allowing us to generate a new library of coumarin compounds. Thus, we attempted to iodinate

commercially available coumarin according to an oxidative iodination procedure reported by Kraszkievicz *et al* as outlined in Scheme 2.39.²⁵⁶



Scheme 2.39. Oxidative iodination of coumarin

Stirring coumarin with iodine in a catalytic amount of sodium iodate in H_2SO_4 regioselectively afforded compound **133** in a good yield of 72% after an hour. To confirm the attachment of iodine, high resolution mass spectroscopy (HRMS) was carried out and the signal at 272.9409 was a proof of the success of the synthesis since the exact mass predicted by Chemdraw® was $[\text{M}+\text{H}] = 272.9379$.

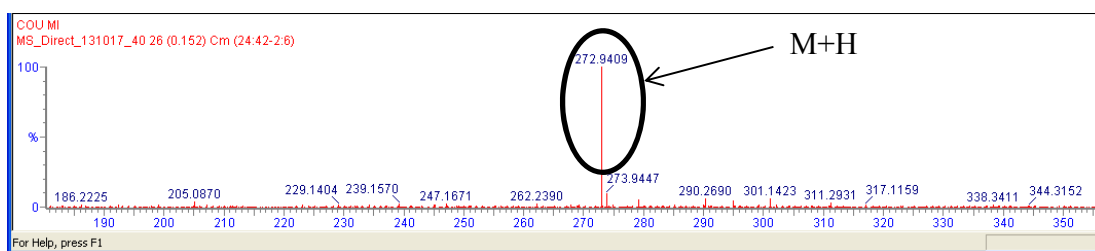
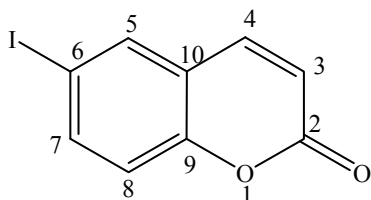


Figure 2.26. HRMS spectrum of compound **133** obtained using electron spray ionization positive source conditions



133

Molecular formula: $\text{C}_9\text{H}_5\text{IO}_2$

Requires: 272.9379

In order to identify the position of iodine on the coumarin ring, NMR spectroscopy was used. The ^1H NMR spectrum of compound **133** indicates the presence of 5 protons as expected with H-3 and H-4 resonating as doublets at 6.44 ppm and 7.62 ppm respectively

with the same coupling constant of 9.56 Hz. The methine proton (H-5) resonated as a doublet at 7.81 ppm while the methine proton (H-8) resonated as a doublet at 7.09 ppm. Finally, the methine proton (H-7) resonated as a doublet of doublets at 7.79 ppm (indicating both *meta* and *ortho* coupling). A quaternary carbon for C-6 resonating at 87.3 ppm in the ^{13}C NMR spectrum was a diagnostic signal consistent with an aryl carbon bearing iodine.

Correlation on the COSY NMR spectrum (Figure 2.27) confirmed the position of the C-I bond by showing only one correlation of the methine proton signal H-7 and its vicinal proton H-8 beside correlations of the vinylic protons H-3 and H-4. H-5 exhibited no cross peaks, consistent with its isolation.

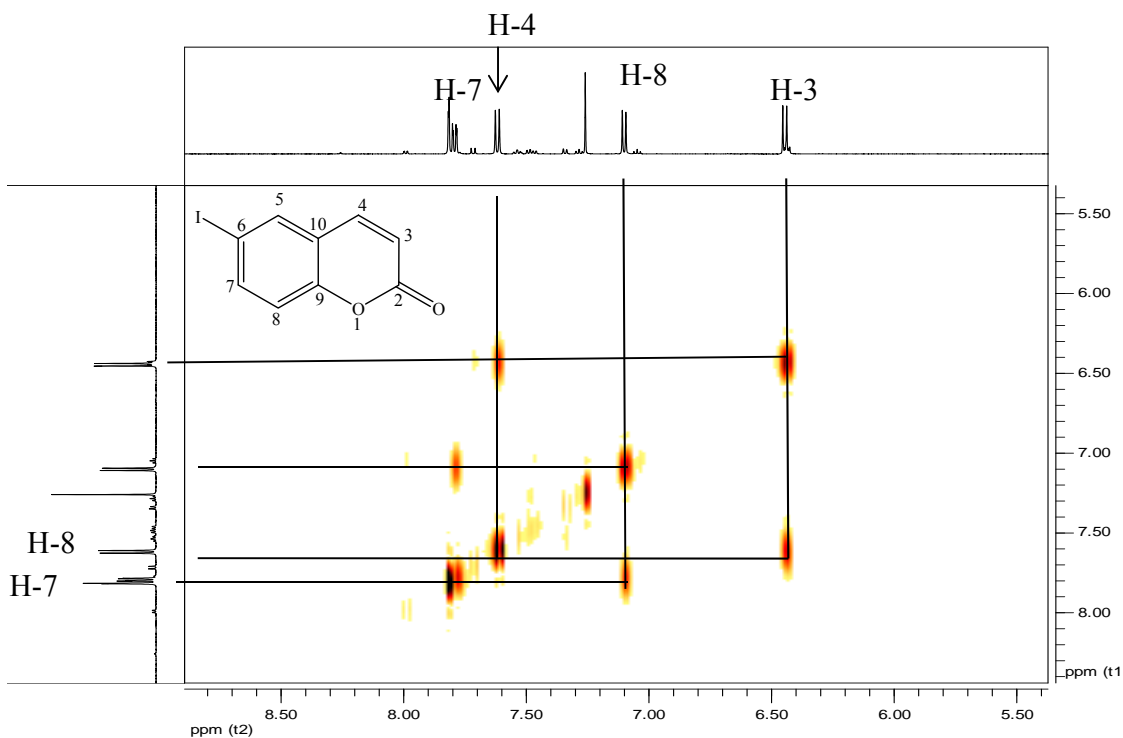
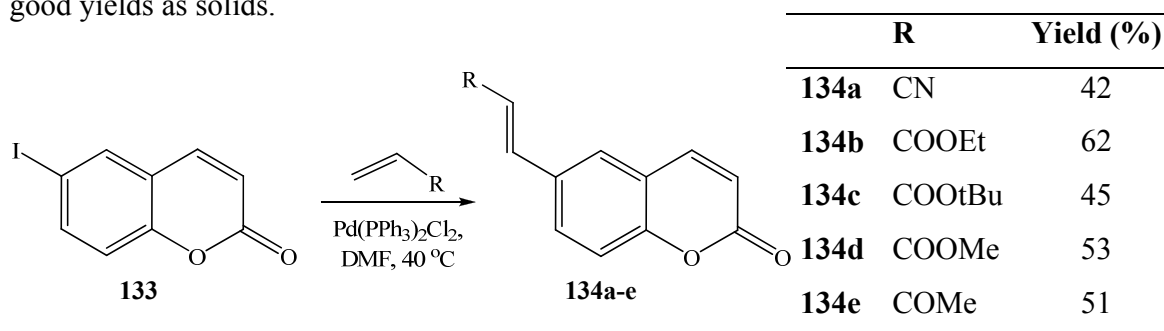


Figure 2.27. ^1H , ^1H -COSY NMR spectrum of compound **133** in CDCl_3

2.4.2.2.2. Coumarin scaffolds in the Heck reaction

We hypothesized that attaching activated alkenes to a coumarin to afford new coumarin scaffolds could not only improve their activity as potential PR inhibitors but perhaps also show a dual action against the IN enzyme since these novel scaffolds possess a

cinnamoyl fragment in their structure. For this purpose, a Heck reaction was performed on compound **133** with activated alkenes in the presence of a catalytic amount of $\text{Pd}(\text{PPh}_3)_2(\text{Cl})_2$ in dry DMF, under argon for 48 hours (Scheme 2.40), as put forward by Jiang *et al.*²⁵⁷ After work-up of the reaction, novel compounds **134a-e** were obtained in good yields as solids.



Scheme 2.40. Heck reaction on coumarin derivatives

The COSY NMR spectrum of compound **134b** (Figure 2.28) indicates the presence of a methyl triplet resonating at 1.30 ppm and a methylene quartet at 4.23 ppm. Furthermore, the COSY NMR spectrum of compound **134b** (Figure 2.28) also shows a correlation between signals at 6.42 ppm and 7.70 ppm, which were therefore assigned to H-2' and H-1' respectively, H-1' being deshielded by the conjugation of the alkene double bond and the carbonyl C-3' of the acrylate. Correlations observed in the HSQC NMR spectrum of compound **134b** (Figure 2.29) confirmed the presence of a methyl carbon signal at 14.2 ppm and a methylene carbon signal at 60.6 ppm while the two expected carbonyl signals C-2 and C-3' at 160.0 ppm and 166.4 ppm respectively. The quaternary carbon signal C-9 was observed downfield at 154.8 ppm due the electron withdrawing effect of the coumarin lactone group.

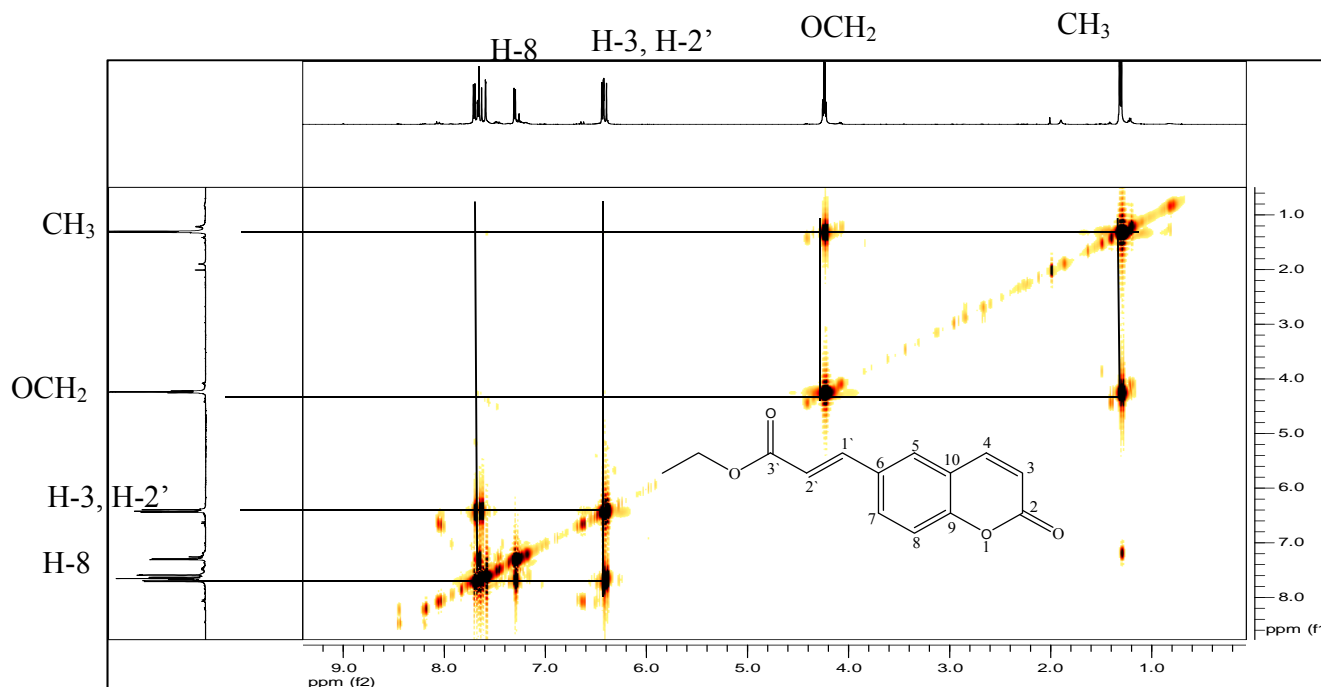


Figure 2.28. ^1H , ^1H -COSY NMR spectrum of compound **134b** in CDCl_3

The C-2' and C-1' alkene carbon signals were assigned to resonances at 119.0 ppm and 142.9 ppm using correlations in the HSQC spectrum (Figure 2.29). Also according to the HSQC spectrum (Figure 2.29), the methine proton H-8 resonates as a doublet at 7.30 ppm and the corresponding methine carbon signal C-8 appeared at 117.3 ppm. This assignment was confirmed in the HMBC NMR spectrum (Figure 2.30) where a correlation between H-8 and the quaternary carbon C-9 was observed. Due to conjugation of the alkene double bond with the carbonyl C-2, the signal corresponding to the methine proton H-4 was shifted downfield to 7.59 ppm while the methine proton H-3 was observed as a doublet overlapping with the methine proton signal H-2' farther upfield at 6.42 ppm. Finally, the methine aromatic protons signals H-5 and H-7 overlapped in the region between 7.61 ppm and 7.65 ppm and their corresponding carbon C-5 and C-7 resonate at 130.7 ppm and 130.9 ppm respectively. A correlation between the methine proton signal H-2' with the carbon signal C-5 and C-3' in the HMBC spectrum (Figure 2.30) further confirmed the above assignments.

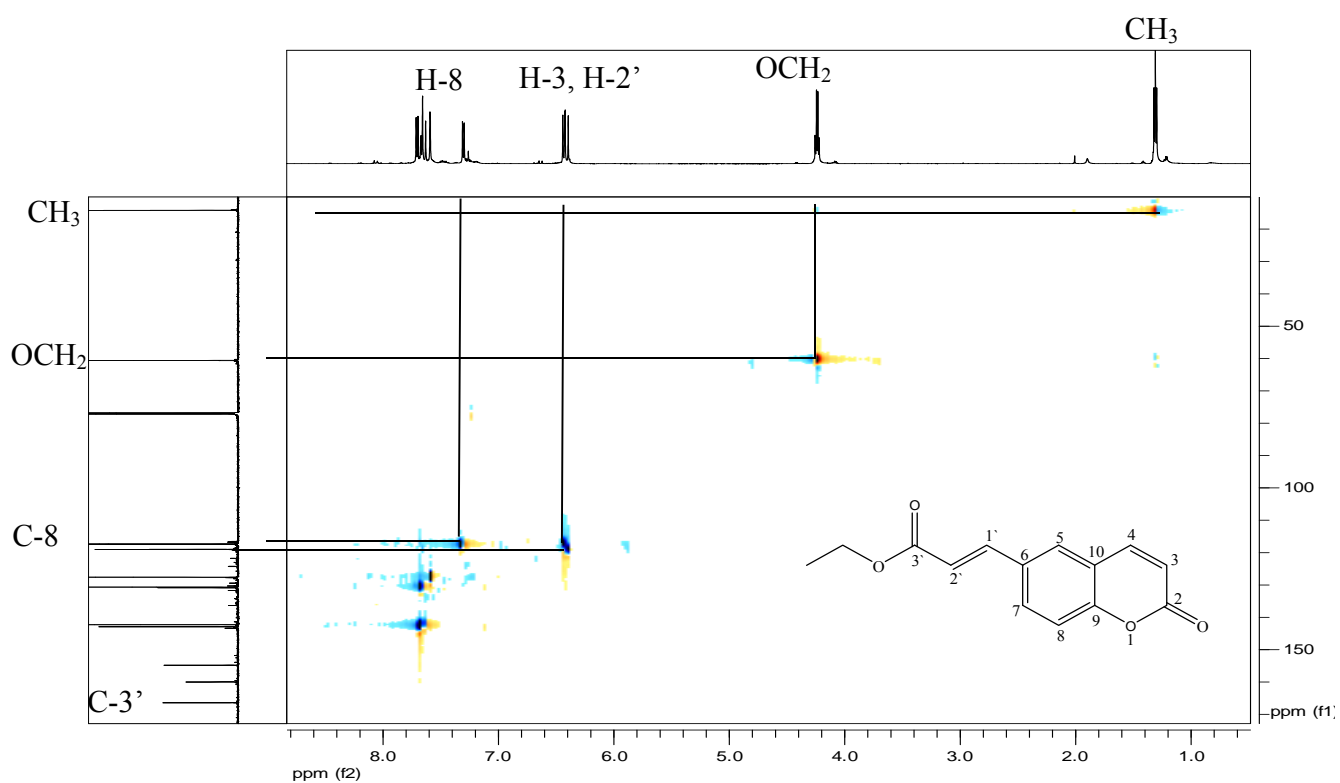


Figure 2.29. HSQC NMR spectrum of compound **134b** in CDCl_3

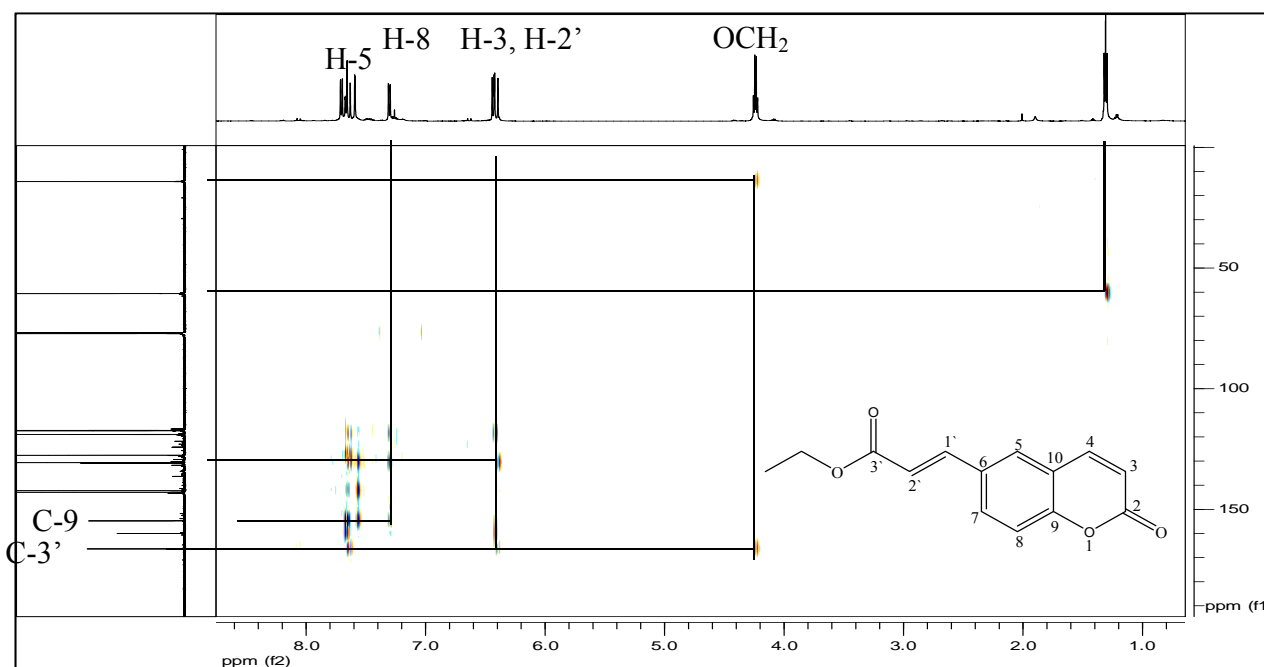
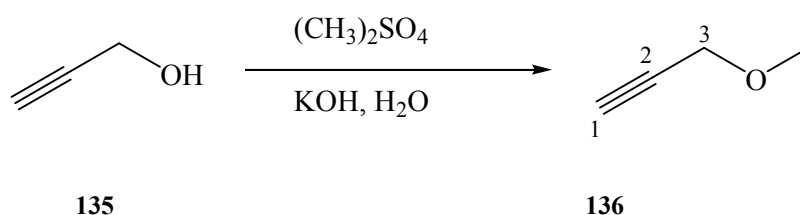


Figure 2.30. HMBC NMR spectrum of compound **134b** in CDCl_3

2.4.2.2.3. Derivatization of coumarin by a Sonogashira coupling reaction

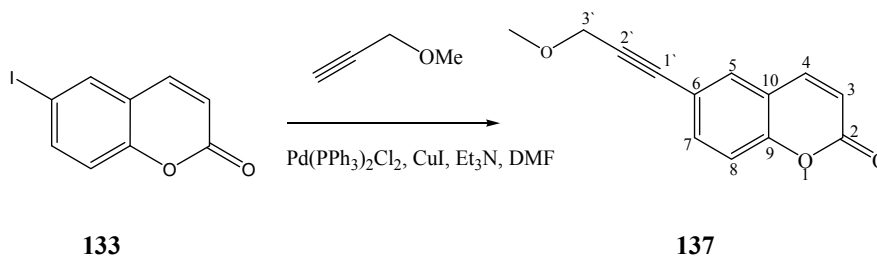
Finally, we also intended to carry out a Sonogashira coupling on compound **133** with a propargyl derivative. First, propargyl alcohol was methylated by a strong methylating agent dimethylsulfate as reported by Fall *et al.*, according to the pathway described in Scheme 2.41.²⁵⁸ This was to protect the hydroxyl group through the course of the subsequent reactions.



Scheme 2.41. Methylation of propargyl alcohol

Beside the expected methine proton H-1 resonating at 2.41 ppm and the methylene proton signal H-3 appearing at 4.06 ppm, a sharp methyl signal was clearly identified at 3.36 ppm in the ^1H NMR spectrum of compound **136** hence proving that the methylation was successful.

A Sonogashira coupling was then performed by following a method proposed by Larock *et al.*²²⁴ As described in Scheme 2.42, a catalytic amount of CuI and the palladium catalyst $\text{Pd}(\text{PPh}_3)_3\text{Cl}_2$ was added under argon with a stoichiometric amount of Et_3N and the terminal alkyne (to a mixture of the iodinated coumarin in dry DMF). After three hours of reflux novel compound **137** was isolated in a yield of 53%.



Scheme 2.42. Sonogashira coupling of ether **136** with 6-iodocoumarin **133**

The ^1H NMR spectrum of compound **137** reveals the presence of 10 protons. A methyl singlet appeared at 3.36 ppm and a methylene proton singlet at 4.27 ppm. In the ^{13}C NMR spectrum (Figure 2.31a), the disappearance of the C-I signal at 87.3 ppm was observed along with the appearance of two methine carbons C-1' and C-2' resonating at 84.6 ppm and 85.8 ppm respectively. Furthermore, beside a methyl carbon signal assigned at 57.9 ppm, a methylene carbon signal C-3' appeared at 60.3 ppm in the DEPT-135 NMR spectrum (Figure 2.31b).

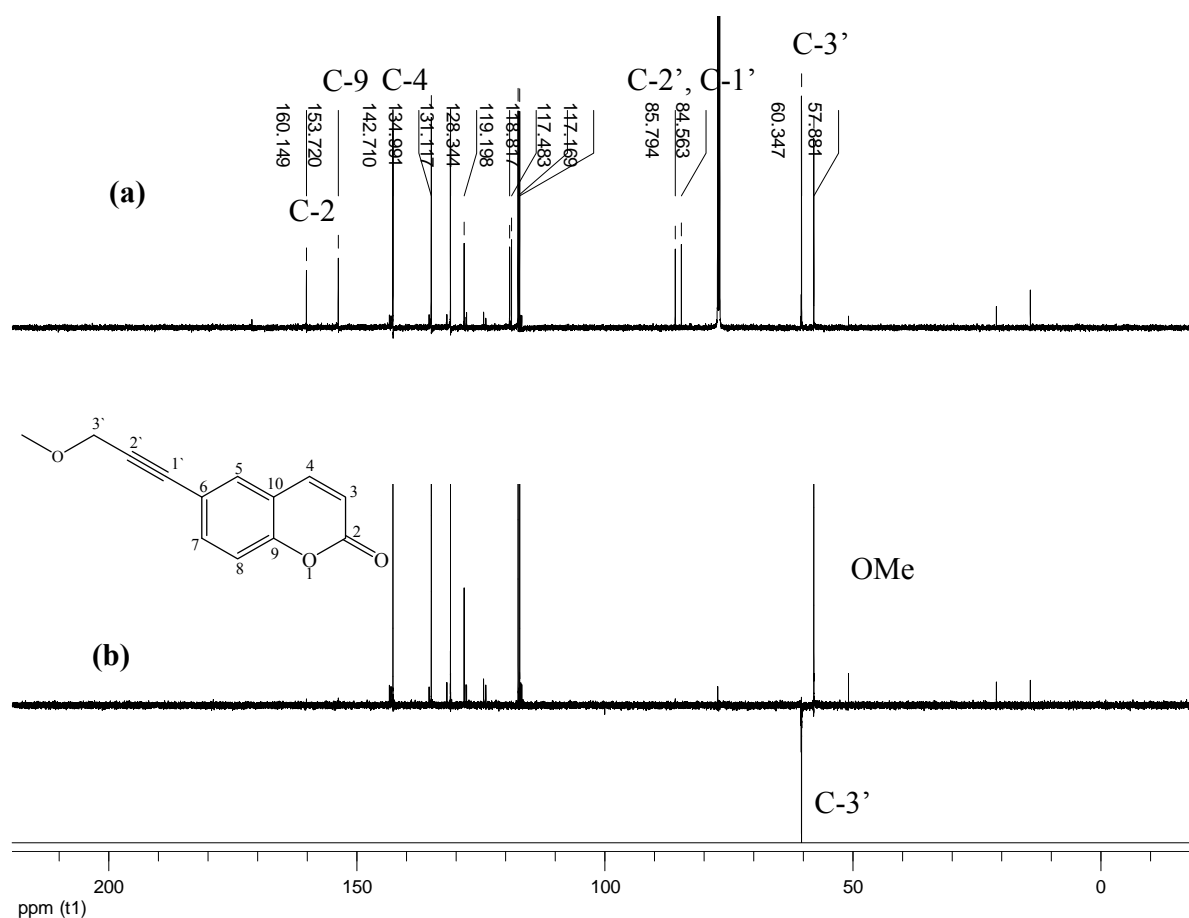


Figure 2.31. 150 MHz ^{13}C NMR (a) and DEPT-135 NMR (b) spectra of compound **137** in CDCl_3

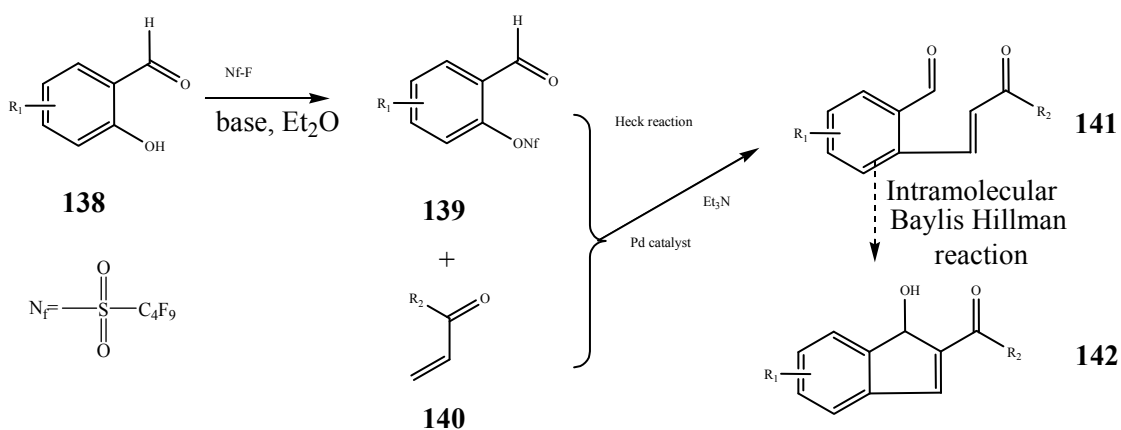
2.4.3. Application of the Heck reaction

In this study the Heck reaction was used to provide access to two, very different, molecular scaffolds, both of which have demonstrated useful biological activity. Indenols are reported to possess analgesic and myorelaxation activity.^{95, 259} Thanks to their fused electron rich cyclic ring system bearing a hydroxyl substituent which can bind to the active site of the PR enzyme, they could also be valuable building blocks to be tested as potential HIV-1 protease inhibitors. To the best of our knowledge, this particular property has not yet been reported and therefore we decided to explore the synthesis of novel indenol derivatives from appropriately functionalized cinnamate esters.

2.4.3.1. Synthesis of indenols from 2-formyl cinnamate esters

It was proposed that indenols could be synthesized from cinnamate esters, themselves prepared by the Heck reaction illustrated in Scheme 2.43.

Since a good leaving group is needed for the Heck reaction to take place, the first step of the strategic plan was the generation of a highly electronegative substituent in the ortho position to the formyl group. Nonaflation of salicylaldehyde was used as a strategy to improve the leaving potency of the hydroxyl group. This approach enabled us to make use of a readily available substrate and reasonably well established chemistry.²⁶⁰



Scheme 2.43. Synthetic pathway (A) to indenol derivatives

2.4.3.1.1. Nonaflation of salicylaldehyde derivatives

The nonaflation involved the protection of the hydroxyl of the salicylaldehyde derivatives by using perfluoro 1-butane sulfonyl fluoride (N_f -F) as a protecting agent.²⁶¹ According to a procedure described by Rottlander *et al.*, salicylaldehyde was stirred for 12 hours in absolute Et_2O (diethylether) with Et_3N as a base under argon.²⁶² The N_f -F was subsequently added gradually at 0 °C since the reaction is exothermic. The nonaflated salicylaldehyde derivative, compound **139a**, was obtained in a yield of 57%. Further optimization studies of the nonaflation reaction conditions were carried out, examining the influence of the solvent and the base on the outcome of the synthesis.

- **Influence of the solvent on the nonaflation**

A polar solvent (DMF) and a series of medium polarity solvents (dioxane, acetonitrile and ether) were assessed and the yields obtained are reported in Table 2.3.

The results demonstrated that the polarity of the solvent has a significant effect on the yield of the reaction. Highly polar solvents such as DMF resulted in higher yields of the fluorinated benzaldehyde derivative when triethylamine was used. However, this was not applicable for all the bases involved in the reaction. During similar studies, Vorbruggen stated that non polar solvents work better for the N_f protection of 5 α -cholestane-3 β -ol alcohol derivatives when DBU (1,8 –diazodicyclo[5.4.0]undec-7-ene) was used as a base. He hypothesized that the high polarity solvent affects the nucleophilicity and the basicity of the base, which in this case gave poor yields.²⁶¹ Based on our success in using DMF as a solvent for the nonaflation, the next objective was to determine the most suitable base.

Table 2.3. Yields of nonaflyl benzaldehyde upon optimization of the solvent

Solvent	Polarity index	Yield (%)
DMF	6.4	99
Acetonitrile	5.8	90
Dioxane	4.8	85
Et ₂ O	2.8	57

- **Influence of the base on the nonaflation**

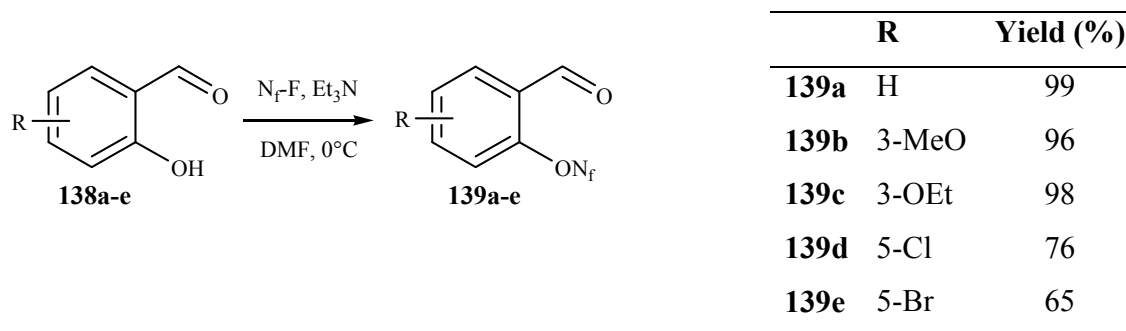
A wide range of bases were compared in DMF. Included in this survey were nucleophilic amine bases such as *N,N*-(dimethyl)-4-aminopyridine (DMAP), 1,4-Diazabicyclo[2.2.2]octane (DABCO), 3-hydroxyquinuclidine (3HQ), a Bronsted base Et₃N and a moderately strong inorganic base K₂CO₃.

Table 2.4. Yields of nonaflyl salicylaldehydes using different bases

Base	Et ₃ N	3HQ	DMAP	DABCO	K ₂ CO ₃
Yield (%)	99	81	80	73	70

Electron donating groups on the nitrogens present in DABCO and 3HQ could explain their lower efficiency compared to Et₃N. The ethyl groups of Et₃N donate fewer electrons to the nitrogen whose lone pair of electron is less basic and nucleophilic to favor the attack of the hydroxyl hydrogen of salicylaldehyde. Because of problems related to solubility, K₂CO₃ was not very efficient for this synthesis.

Having these optimized reaction conditions in mind, salicylaldehyde derivatives were converted to their corresponding novel nonaflyl derivatives in relatively good yields (Scheme 2.44).



Scheme 2.44. Nonaflation of salicylaldehyde derivatives using optimized reaction conditions

A deuterium exchange of salicylaldehyde in CDCl_3 proved that the hydroxyl group resonates at 9.9 ppm. From the ^1H NMR of compound **139a** (Figure 2.32b) the disappearance of the hydroxyl hydrogen signal was a clear sign that the protection of the alcohol was successful. As expected, five proton signals appear. Beside four aromatic protons resonating between 7.38 ppm and 7.97 ppm, an aldehydic proton H-7 resonates at 10.24 ppm in the nonaflate and 11.01 ppm in salicylaldehyde **138a**.

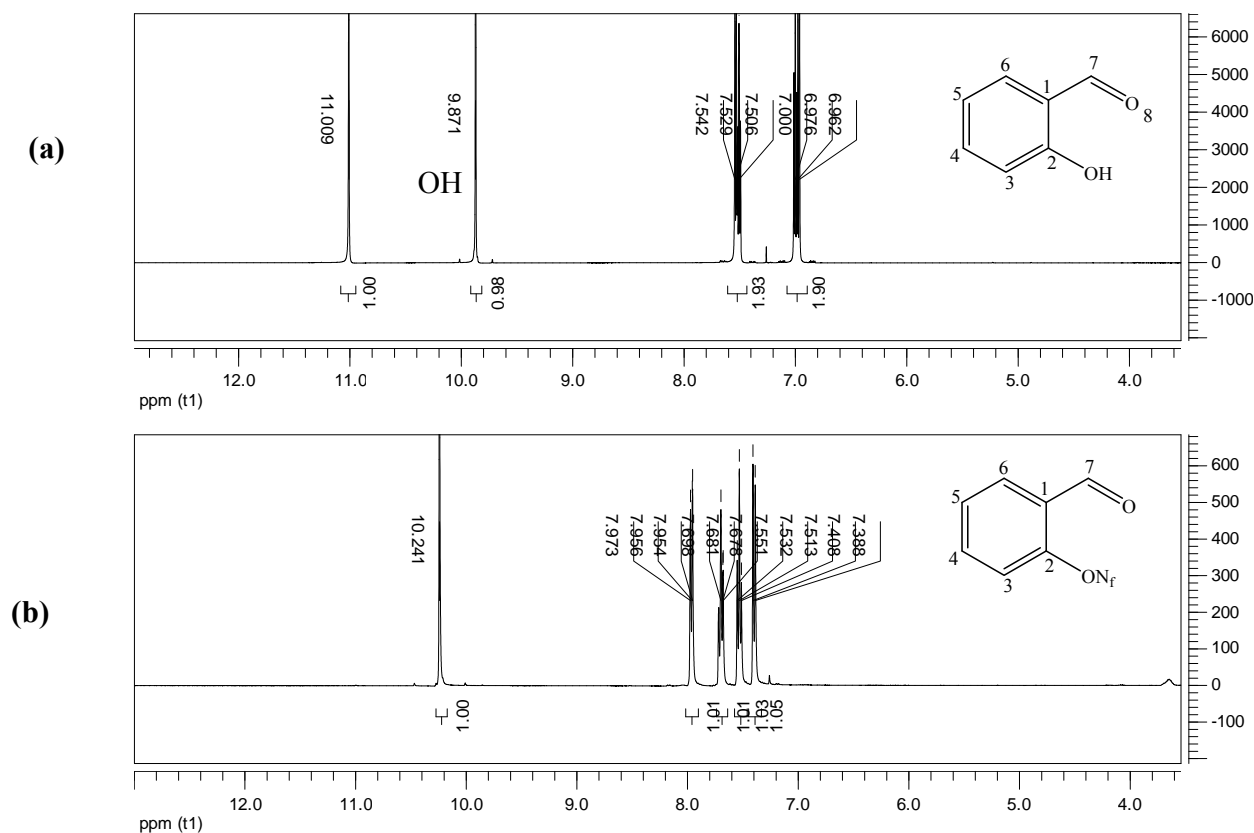


Figure 2.32. 400 MHz ^1H NMR spectrum of salicylaldehyde **138a** (a) and compound **139a** (b) in CDCl_3

The ^{13}C NMR spectrum of compound **139a** (Figure 2.33) provided further useful structural information. Owing to the coupling of the four carbon atoms with the nine fluorine atoms of N_f in the aromatic region (between 100-120 ppm) an aggregation of small carbon signals showed evidence that the bond between C-2 and ON_f was formed and the fluorinated moiety was attached. Furthermore, the signal of C-2 was shifted from 161.4 ppm to 149.9 ppm. The conjugation of the lone pair of electron of the hydroxyl oxygen of salicylaldehyde with C-2 formed a carbonyl and contributed to deshielding C-2 while with N_f , no conjugation was possible and C-2 resonated upfield.

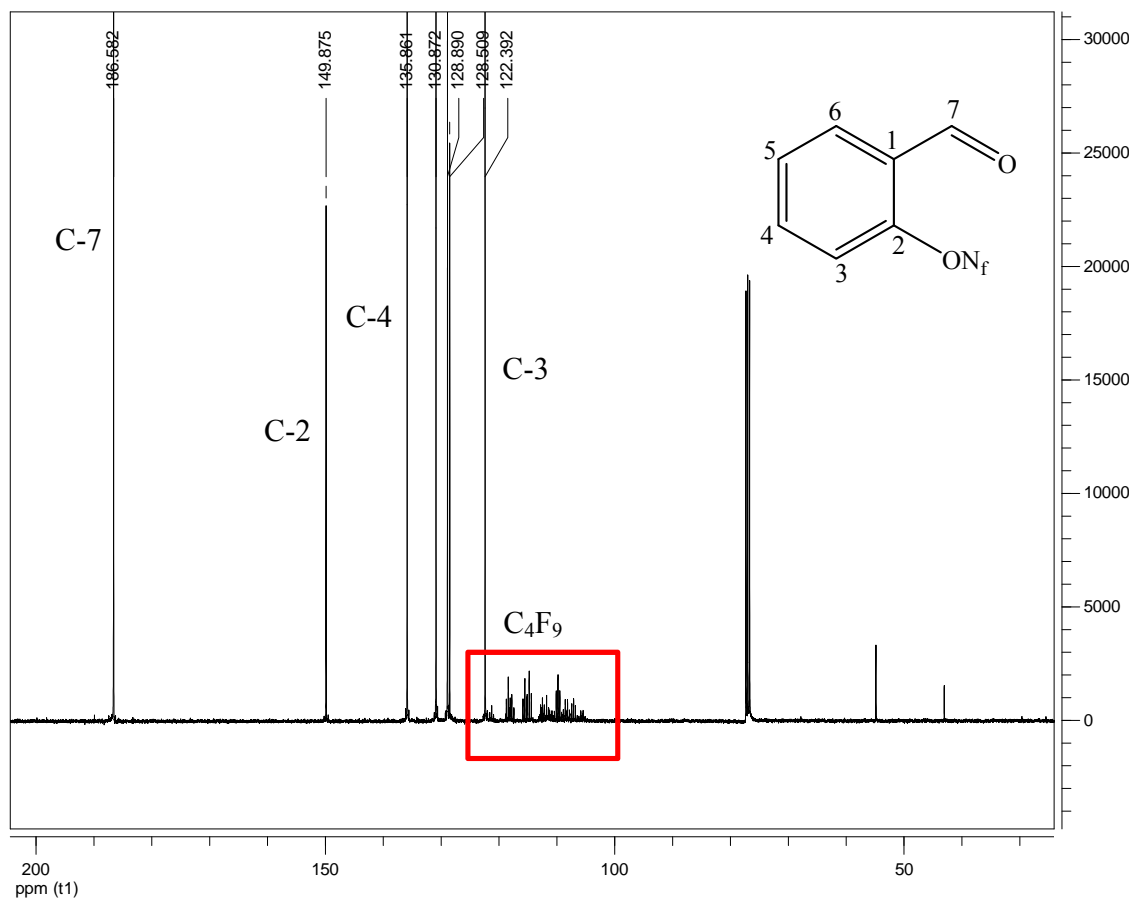


Figure 2.33. 100 MHz ^{13}C NMR spectrum of compound **139a** in CDCl_3

2.4.3.1.2. The Heck reaction on nonafllyl benzaldehyde

The following step involved a Heck coupling reaction of the nonafllyl benzaldehyde derivatives with activated alkenes. A catalytic amount of $\text{Pd}(\text{OAc})_2$ and PPh_3 were added to a mixture of compound **139a**, Et_3N and methyl acrylate in DMF. The reaction mixture was heated under reflux at 120 °C for 72 hours. The reaction was carried out under N_2 since PPh_3 is air sensitive and hence prone to oxidation.²⁶³ The synthesis was successful and afforded compound **141a** whose identification was possible by NMR spectroscopy.

The ^1H NMR spectrum of compound **141a** (Figure 2.34) reveals the presence of 10 protons as expected. A sharp methyl singlet was observed at 3.78 ppm beside two vinylic protons H-3' and H-4' resonating as doublets at 6.33 ppm and 8.48 ppm respectively with

the same coupling constant of 15.9 Hz. Furthermore, four aromatic protons appear between 7.56 ppm and 7.83 ppm and an aldehydic proton H-5' resonates at 10.23 ppm.

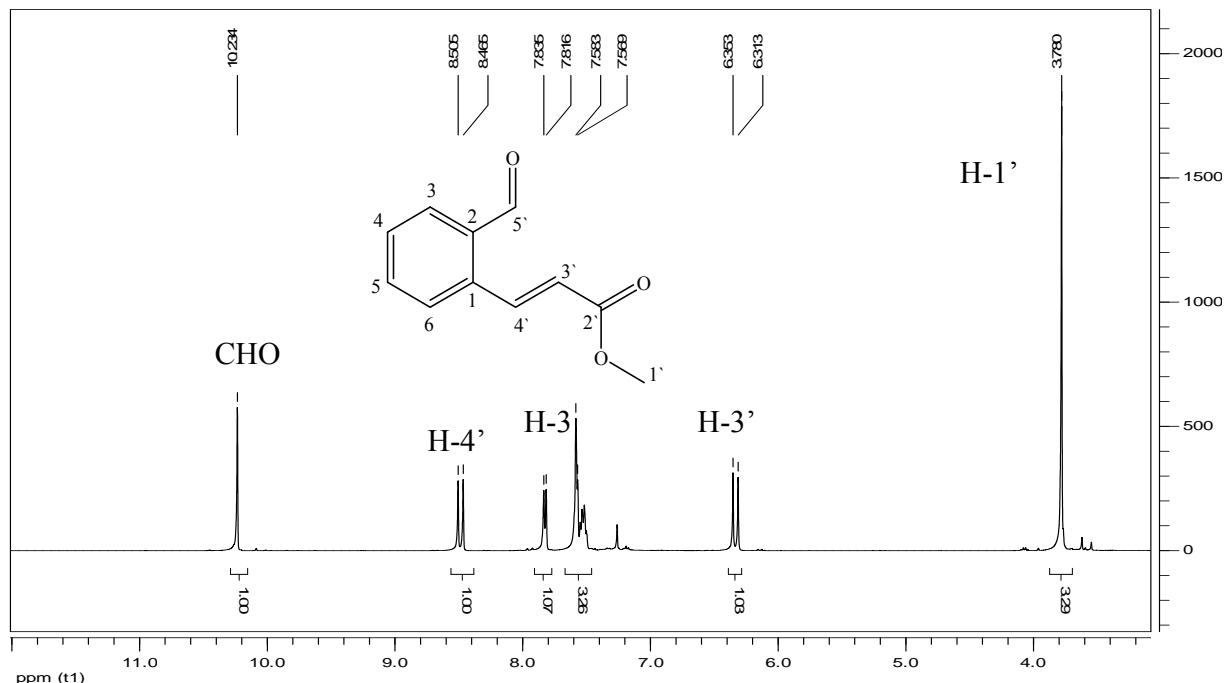


Figure 2.34. 400 MHz ^1H NMR spectrum of compound **141a** in CDCl_3

In the ^{13}C NMR spectrum (Figure 2.35), ten carbon signals were observed with the methyl carbon (C-1') at 51.7 ppm and two carbonyls (C-2' and C-5') resonating at 166.4 ppm and 191.6 ppm. In addition, five aromatic carbon signals appeared between 127.8 ppm and 141.1 ppm. Correlations in the COSY NMR spectrum (Figure 2.36) confirmed the presence of two vinylic protons H-3' and H-4' whose carbons C-3' and C-4' resonate at 122.5 ppm and 141.1 ppm respectively. The ^{13}C NMR spectrum (Figure 2.35) indicated the presence of 3 quaternary carbons, where besides the carbonyl signals of C-2' and C-5', the quaternary carbons C-1 and C-2 were deduced to resonate isochronously at 136.3 ppm

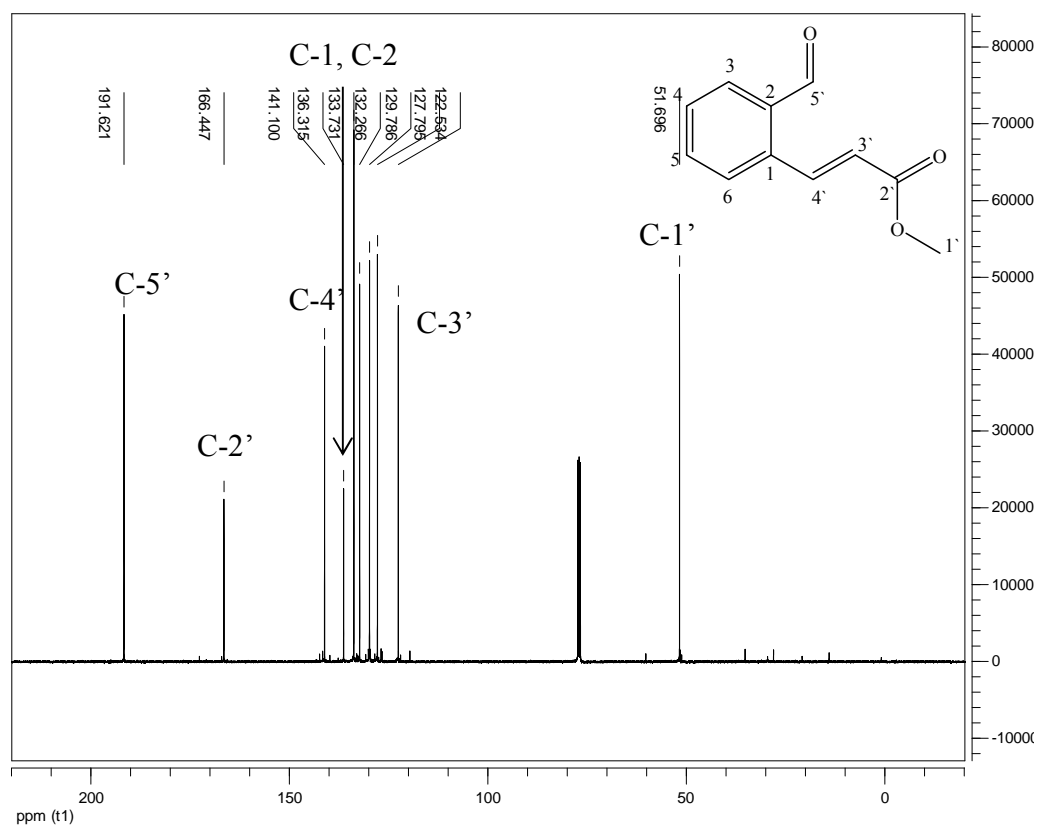


Figure 2.35. 100 MHz ^{13}C NMR spectrum of compound **141a** in CDCl_3

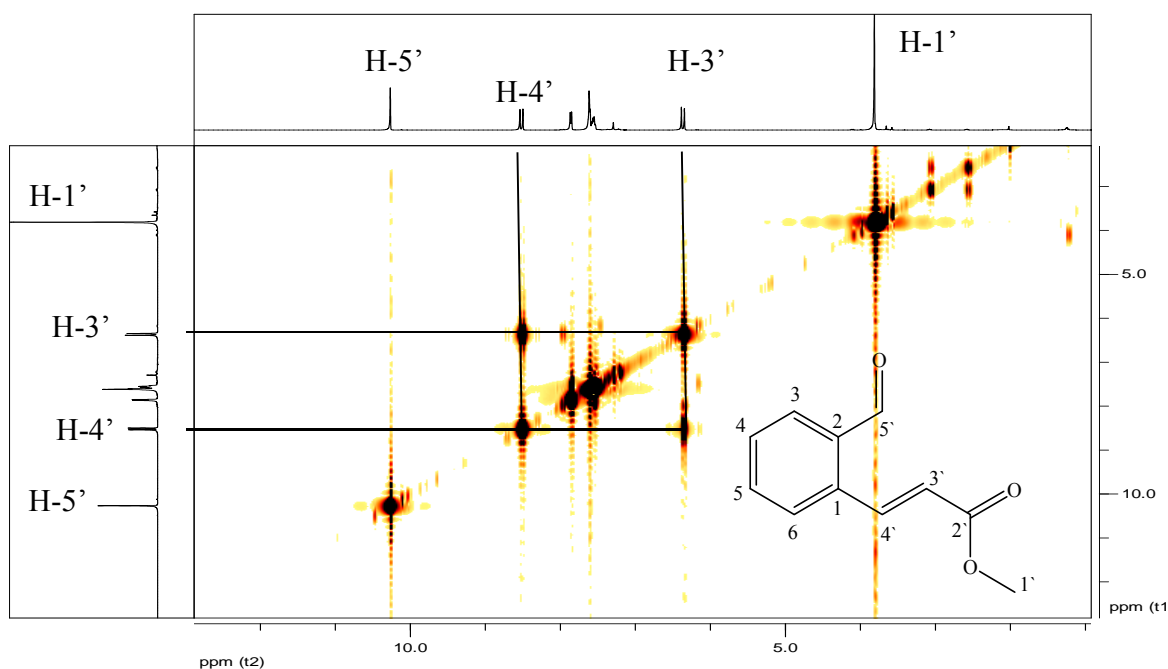
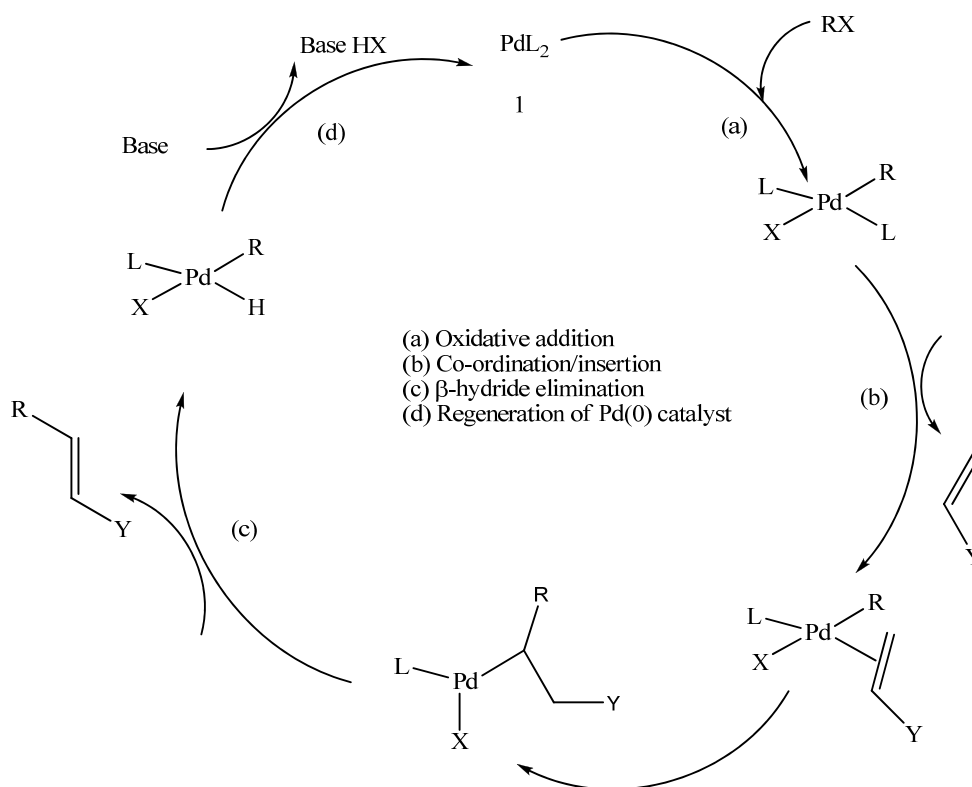


Figure 2.36. ^1H , ^1H -COSY NMR spectrum of compound **141a** in CDCl_3

2.4.3.1.3. Heck reaction optimization

As reported in the literature, the Heck reaction is a very poor yielding reaction depending on the nature of the substrates involved.²⁶⁴⁻²⁶⁷ This was confirmed by the poor yield (6%) obtained for compound **141a**. It was therefore necessary to assess whether changes in reaction conditions could lead to an improved yield. The mechanism of the catalytic cycle of the Heck coupling reaction is well understood (Scheme 2.45).^{268, 269} The main steps involved are the oxidative addition of the organo halide to the palladium catalyst, followed by the coordination/insertion of the alkene double bond to form an organo halide palladium complex which is stabilized by solvent. β -Hydride elimination delivers the product and is finally followed by the regeneration of the palladium(0) catalyst. This reaction can be significantly affected by the base, the phosphine ligand, the palladium catalyst and the solvent used.



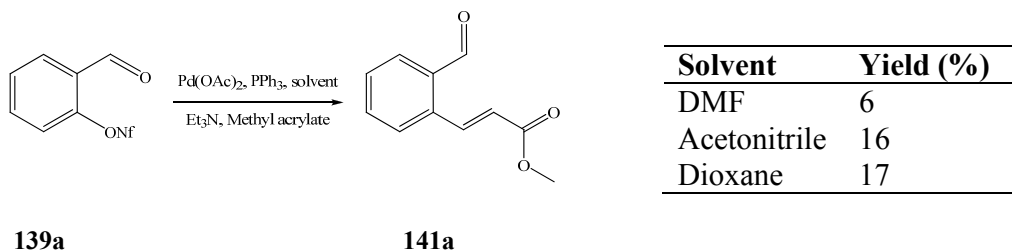
Scheme 2.45. General mechanism for the palladium catalyzed Heck reaction ²⁶⁹

Our attention was focussed on examining the effect of the phosphine ligand, the catalyst and the solvent on the outcome of the reaction. Triethylamine was used as the standard base for the optimisation studies. These studies were all performed on the reactive **139a** and the electron deficient alkene methyl acrylate. Since tetraalkylammonium salts possess an accelerating effect in Heck reactions by increasing the polarity of the medium, a catalytic amount of triethylammonium bromide was added to the reaction mixture in every case.²⁰⁶

- **Effect of the solvent**

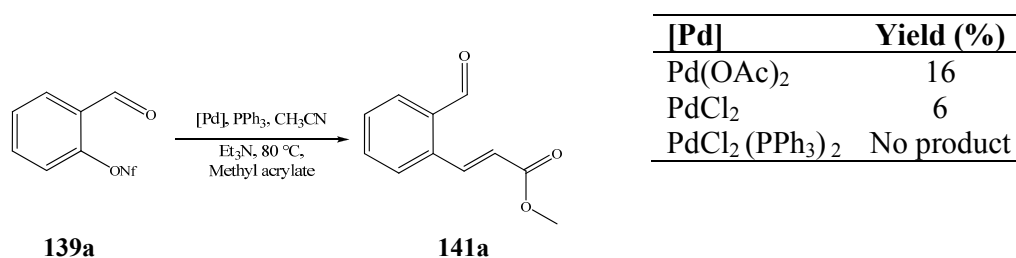
According to previous studies the Heck reaction is most successful in polar aprotic σ -donor-type solvents such as dimethylformamide (DMF), acetonitrile and dioxane.²⁰⁴ When these solvents were used for our study, the yields of the cinnamate ester **141a** ranged from 6-17% (Scheme 2.46). Even though dioxane was the best solvent for the

coupling, its environmental toxicity was considered an important factor. Therefore, acetonitrile was used as the preferred solvent for the study at hand.



Scheme 2.46. Influence of solvent on the Heck reaction of nonaflaldehyde **139a** to give **141a**

- **Effect of the palladium source**

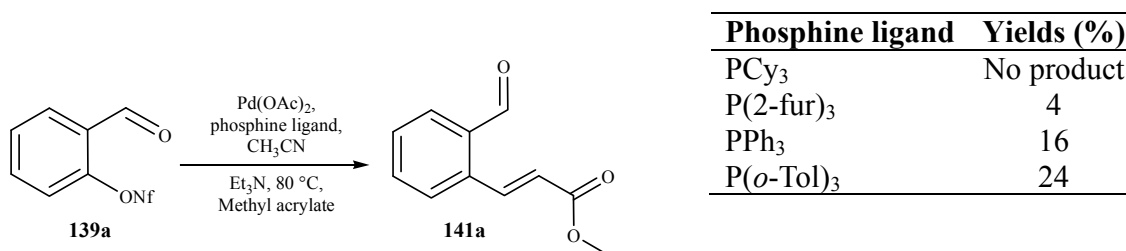


Scheme 2.47. Influence of the palladium catalyst on the Heck reaction of nonaflaldehyde **139a** to yield **141a**

Although none of the readily available complexes were very efficient, the most effective palladium source was Pd(OAc)₂, while PdCl₂(PPh₃)₂ was completely ineffective. In every case, at the end of the reaction the precipitation of palladium metal as palladium black apparently stopped the reaction and could account for the poor yields observed. The formation of elemental metal could be explained by limited catalyst stability leading to palladium precipitation due to the oxidation of PPh₃ by oxygen. Heck suggested that two factors can be at the origin of this phenomenon: first, the conversion of the phosphine ligands into phosphonium salts; second, the sterically induced ligand dissociation resulting in agglomeration of a coordinately unsaturated palladium(0) intermediate.²⁰⁹

- **Effect of the phosphine ligand**

The phosphine ligand plays two essential roles in the Heck reaction. Since the palladium salts need to be reduced to Pd⁰ in order to become activated, phosphines act as reducing agents, being oxidized to phosphine oxides. They also stabilize the catalyst in its zero oxidation state in the form of stable PdL₂ species, which subsequently enter the catalytic cycle.²⁷⁰ It was thus necessary to examine the effect of variation of the phosphine ligand.



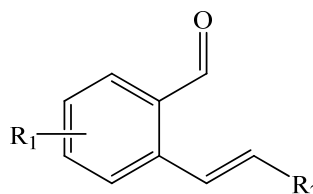
Scheme 2.48. Influence of the phosphine ligand on the Heck reaction of nonaflaldehyde **139a** to yield **141a**

The results indicated in Scheme 2.48 were in agreement with Heck and coworkers' observations. Heck reported that in a Heck reaction, triarylphosphines are preferred over trialkylphosphines and triphenyl phosphite.²⁰⁹ In our study, tri(*o*-tolyl)phosphine appeared to give better yields compared to triphenylphosphine, probably because the larger tri(*o*-tolyl)phosphine ligands dissociate more readily and thus promote the initial oxidative addition of C-ON_f bonds.^{209, 271}

After a detailed study of parameters that influence the Heck coupling namely the solvent, the phosphine ligand and the pre-catalyst, the best system overall was palladium acetate as the pre-catalyst, Et₃N as the base with tri(*o*-tolyl)phosphine as the phosphine ligand in acetonitrile as solvent. Having that in mind, the Heck coupling of four nonaflaldehyde derivatives **139a-d** with activated alkenes was performed and novel formyl cinnamate esters were obtained (Table 2.5).

Table 2.5. Yields (%) of Heck adducts under optimal conditions

$R_1 \backslash R_2$	CO ₂ Me	CO ₂ Et	CO ₂ tBu	COMe
H	24	47	11	24
OMe	12	22	6	12
OEt	18	5	10	
Cl	5	11	16	



141a-n

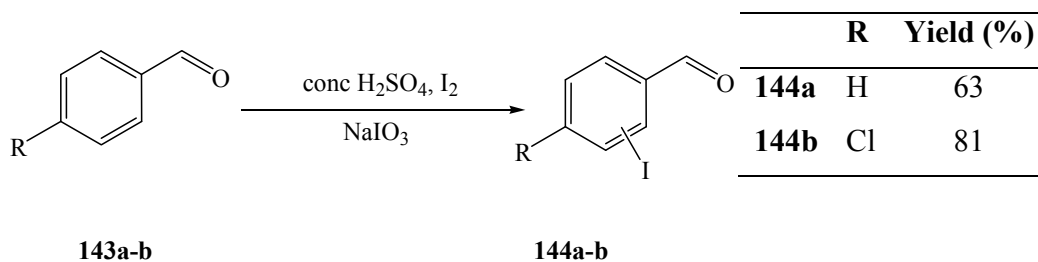
With regard to the results appearing in Table 2.5, the optimization studies performed led to a significant improvement in the yield of the Heck adducts (From 6 to 24% for R_1 =H and R_2 = CO₂Me). However, substrates bearing electron withdrawing groups still gave poor yields.

During oxidative addition in the Heck reaction, the relative reactivity of organohalides decreases in the order of $I > ON_f > Br \gg Cl$.²⁷² Thus, iodine was also of interest in this study.

- **Effect of aniline on the Heck reaction under optimized conditions**

Iodine is an excellent chemical element for further elaboration through transition-metal catalyzed cross-couplings, especially palladium catalyzed transformations.²⁷³ Due to its high electropositivity relative to the other halides and as an extension of the above strategy, the Heck reaction on 4-chloro 2-iodobenzaldehyde with methyl acrylate was carried out. It was necessary to first synthesize the iodinated aromatic aldehyde. A report by Kraszkiewick *et al.*, on effective oxidative iodination of deactivated arenes indicated that iodobenzaldehyde derivatives could be synthesized as indicated in Scheme 2.49.²⁵⁶ In our hands, the iodination of two benzaldehyde analogs was clean and proceeded smoothly to give the corresponding iodinated aryl in a good yield (63% and 81%).

This iodination reaction was regioselective and resulted in the formation of 3-iodobenzaldehyde (**144a**) and 4-chloro-2-iodobenzaldehyde (**144b**).



Scheme 2.49. Oxidative iodination of benzaldehyde derivatives

The ^{13}C NMR spectrum of compound **144b** (Figure 2.37) indicated the presence of five aromatic carbons resonating between 128.9 ppm and 144.5 ppm beside the signal of C-2 (carbon attached to iodine) at 98.2 ppm as expected and a carbonyl signal appearing at 188.8 ppm.

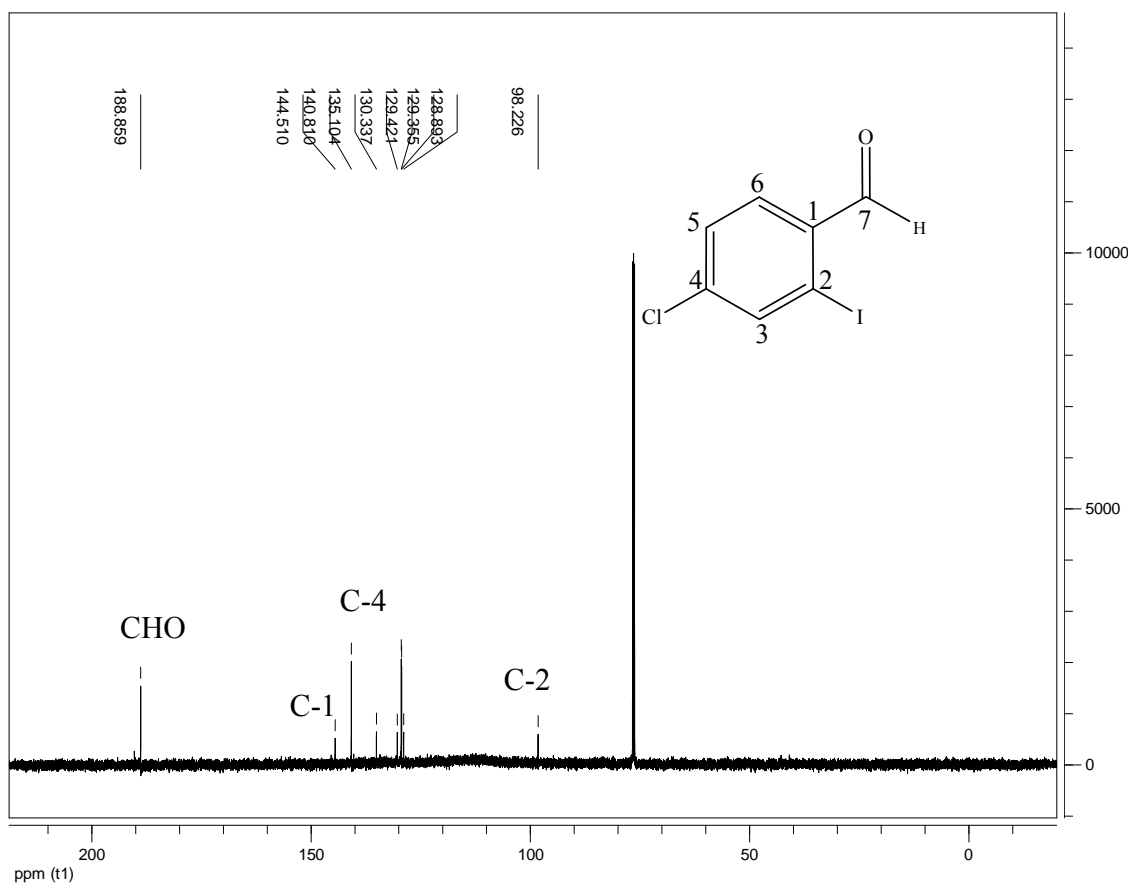


Figure 2.37. 150 MHz ^{13}C NMR spectrum of compound **144b** in CDCl_3

144a **140c** **145** **144a**

Scheme 2.50. Conjugate addition of aniline to *tert*-butylacrylate

The ^1H NMR spectrum of compound **145** (Figure 2.38) indicates the presence of 18 protons. While five aromatic protons resonate between 6.62 ppm and 7.18 ppm, two methylene protons resonate as triplets at 2.51 ppm and 3.39 ppm with corresponding coupling constants and finally nine methyl proton signals appear as a singlet at 1.46 ppm, corresponding to the tertiary butyl group.

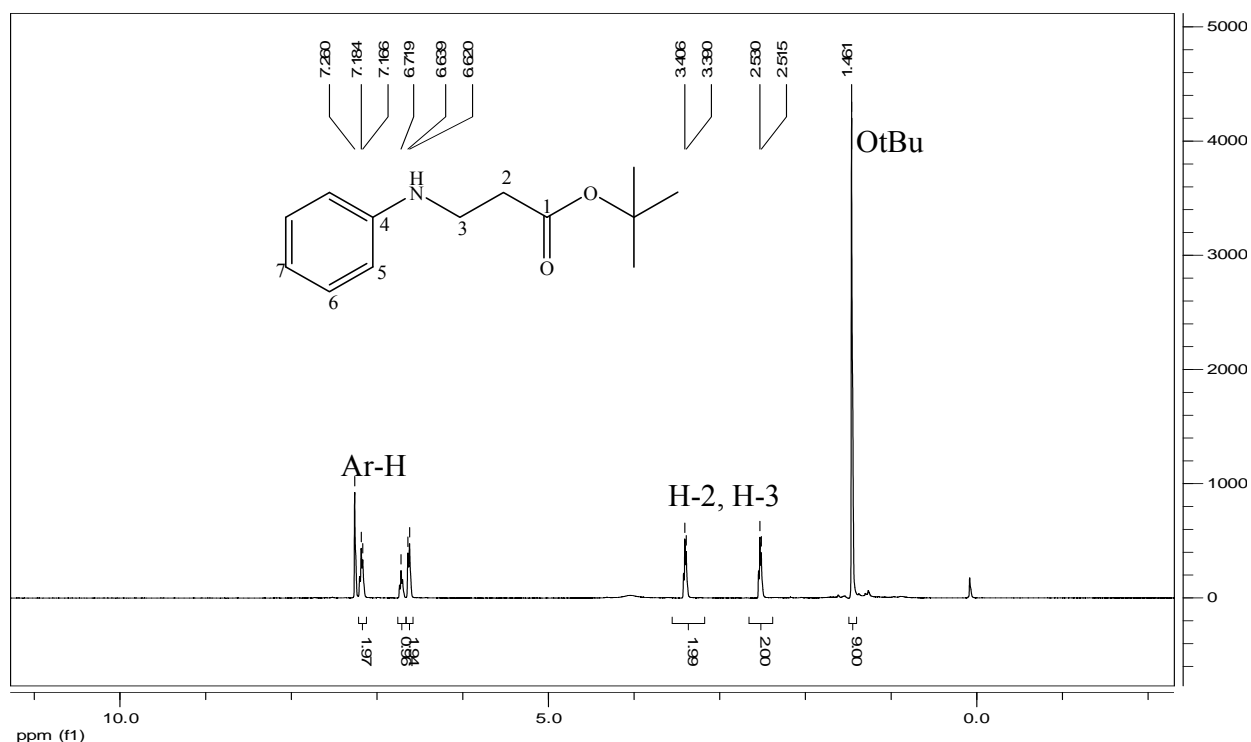
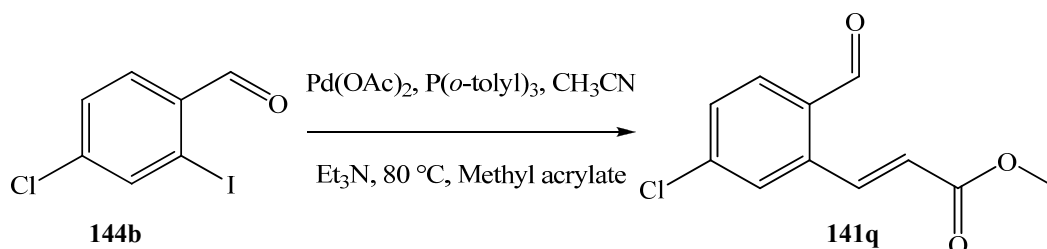


Figure 2.38. 400 MHz ^1H NMR spectrum of compound **145** in CDCl_3

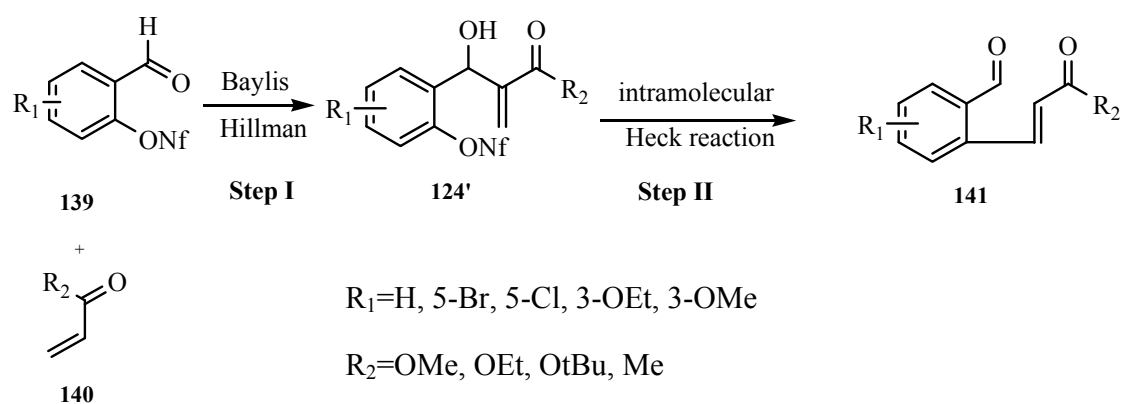
2.4.3.1.4. Synthesis of Heck adduct from iodobenzaldehyde derivatives

The promising catalytic system comprising tri(*o*-tolyl)phosphine, tetraethylammonium bromide and palladium acetate in acetonitrile, was employed for the Heck olefination of 4-chloro-2-iodobenzaldehyde with methyl acrylate. Under reflux at 80 °C for 72 hours, the arylated alkene compound **141q** was isolated in a satisfactory yield of 83% if compared to the 5% yield obtained with nonafllyl chlorobenzaldehyde as starting material. The results clearly demonstrated that the compatibility of the leaving group has a significant effect on the yield of the reaction.



Scheme 2.51. Heck reaction of 4-chloro-2-iodobenzaldehyde **144b** to afford **141q**

In order to close the five membered ring system, the proposed final step included an intramolecular Baylis Hillman reaction between the aldehyde and the α,β -unsaturated electron-withdrawing group assembled in the Heck reaction (Scheme 2.43). Common Baylis Hillman catalysts such as DABCO, DBU and 3-HQ failed to give the desired indenol product **142**. We reasoned that using a Lewis acid such as scandium(III) triflate would cause the two carbonyl oxygens to be closer together and hence facilitate the intramolecular Baylis Hillman and thus the closure of the ring. However, the cyclisation was still unsuccessful and this motivated us to modify our strategic plan.

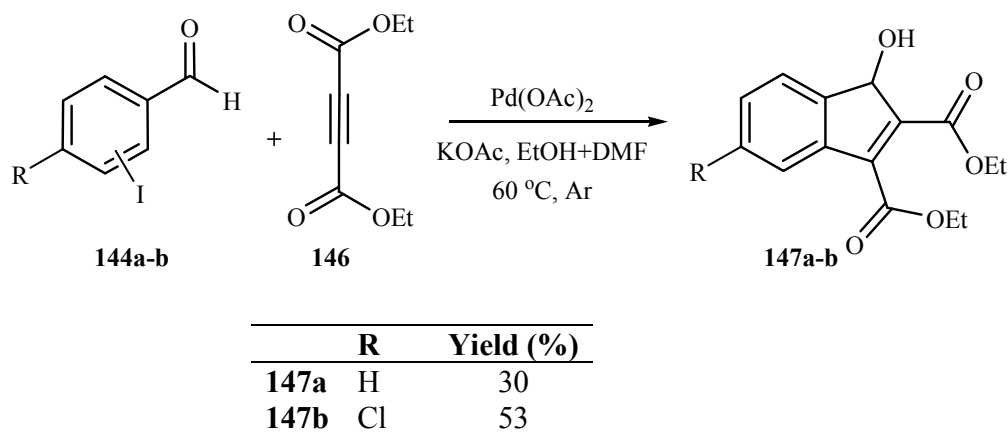


Scheme 2.52. Synthetic pathway (B) to indenol derivatives

A Baylis Hillman reaction was carried out on compound **139** to afford a nonaflyl Baylis Hillman adduct **124'** and an intramolecular Heck reaction was performed (Scheme 2.52). Surprisingly, a retro-Baylis Hillman reaction took place at step II and instead of obtaining an indenol compound **142**, cinnamate ester analog **141** was formed (Scheme 2.52). This observation indicated that indenol compounds are not stable, decompose easily and therefore qualify as poor drug candidates. This could probably explain the difficulty in obtaining these indenol compounds by following the multi-step reactions designed in strategic plans A and B (Scheme 2.43 and Scheme 2.52).

2.4.3.2. Synthesis of indenols by catalytic cyclic vinyl palladation

A literature search revealed a simple one-step protocol for the synthesis of indenols by catalytic cyclic vinyl palladation. Gevorgyan *et al.* reported that *o*-iodinated benzaldehyde derivatives react with a internal alkynes at 60 °C in the presence of palladium acetate and potassium acetate in a solvent mixture of DMF-EtOH.¹⁰² As indicated in Scheme 2.53, the same procedure was followed successfully to afford novel compounds **147a** and **147b** in a yield of 30% and 53% respectively with the *ortho* and the *meta* iodinated benzaldehydes (compounds **144a** and **144b**). Apparently, palladium inserted into the carbon-iodine bond at the *meta* position and underwent a regioisomerisation to give the indenol product from 3-iodobenzaldehyde.



Scheme 2.53. Synthetic pathway (C) to indenol derivatives

The ¹H NMR spectrum of **147b** (Figure 2.39) indicates the presence of 14 protons as expected. Six methyl protons resonate together as a triplet at 1.23 ppm and 4 methylene protons resonate as two quartets around 3.54 ppm corresponding to the two ethyl groups. One methine proton (H-3) resonated at 5.42 ppm and three aromatic proton signals appeared between 7.41 ppm and 7.96 ppm.

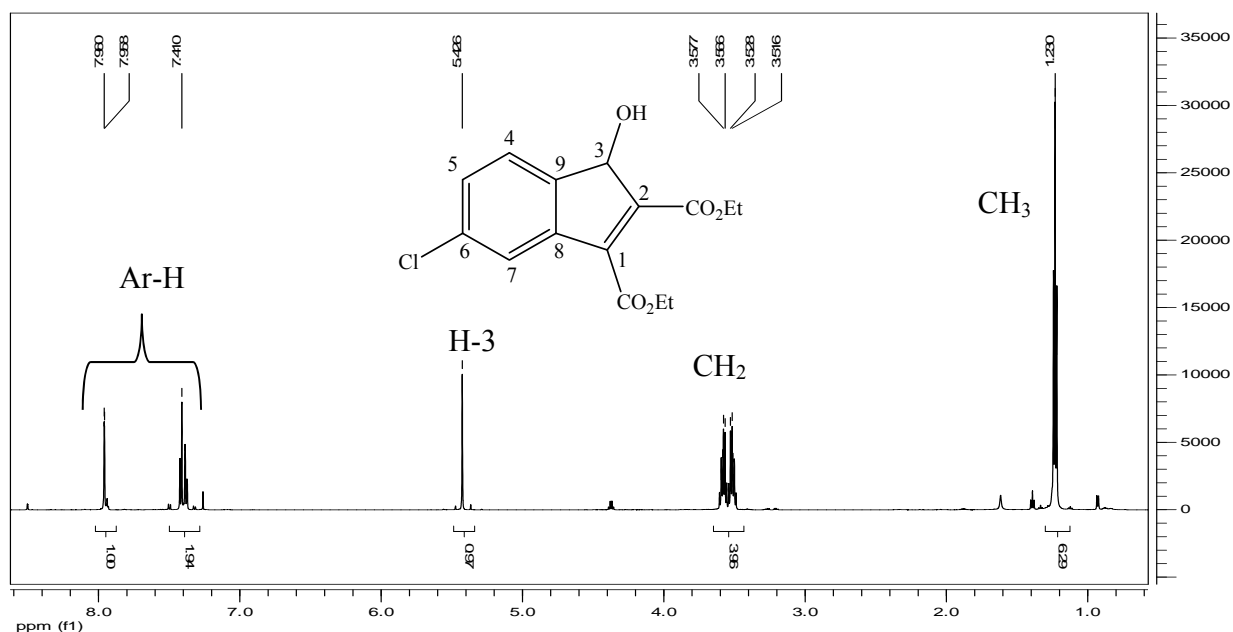


Figure 2.39. 600 MHz ^1H NMR spectrum of compound **147b** in CDCl_3

Examining both the HSQC NMR spectrum (Figure 2.40) and the DEPT-135 NMR spectrum (Figure 2.41) revealed the presence of four quaternary carbon signals. Carbons C-1 and C-2 resonate isochronously at 99.7 ppm while C-6 appears at 138.2 ppm because of the electron withdrawing effect of the chlorine atom. Carbons C-8 and C-9 resonate isochronously at 139.3 ppm and a carbonyl signal of the ester groups further downfield at 141.2 ppm. The HSQC NMR spectrum (Figure 2.40) confirmed the identity of a methyl carbon signal at 15.1 ppm whilst a methylene carbon was recorded at 61.1 ppm and three aromatic methine carbon signals C-5, C-4 and C-7 were confirmed at 127.8 ppm, 128.9 ppm and 138.5 ppm respectively. The methine carbon C-3 was also assigned at 97.8 ppm by means of HSQC correlation.

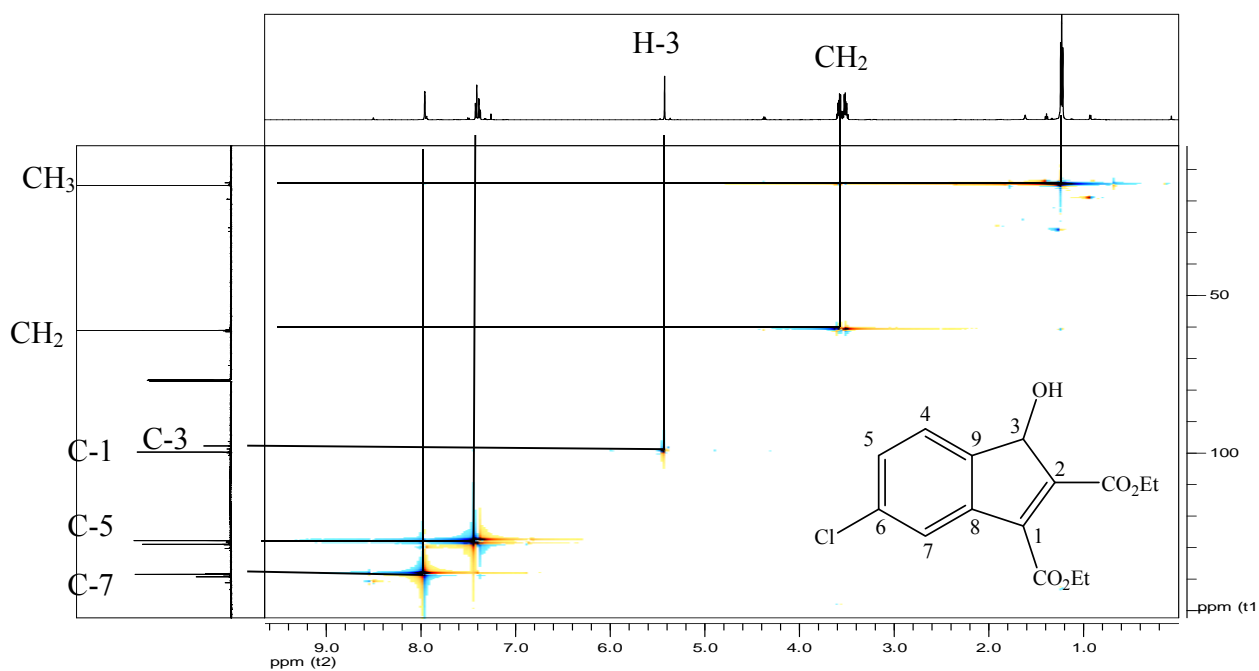


Figure 2.40. HSQC NMR spectrum of compound **147b** in CDCl_3

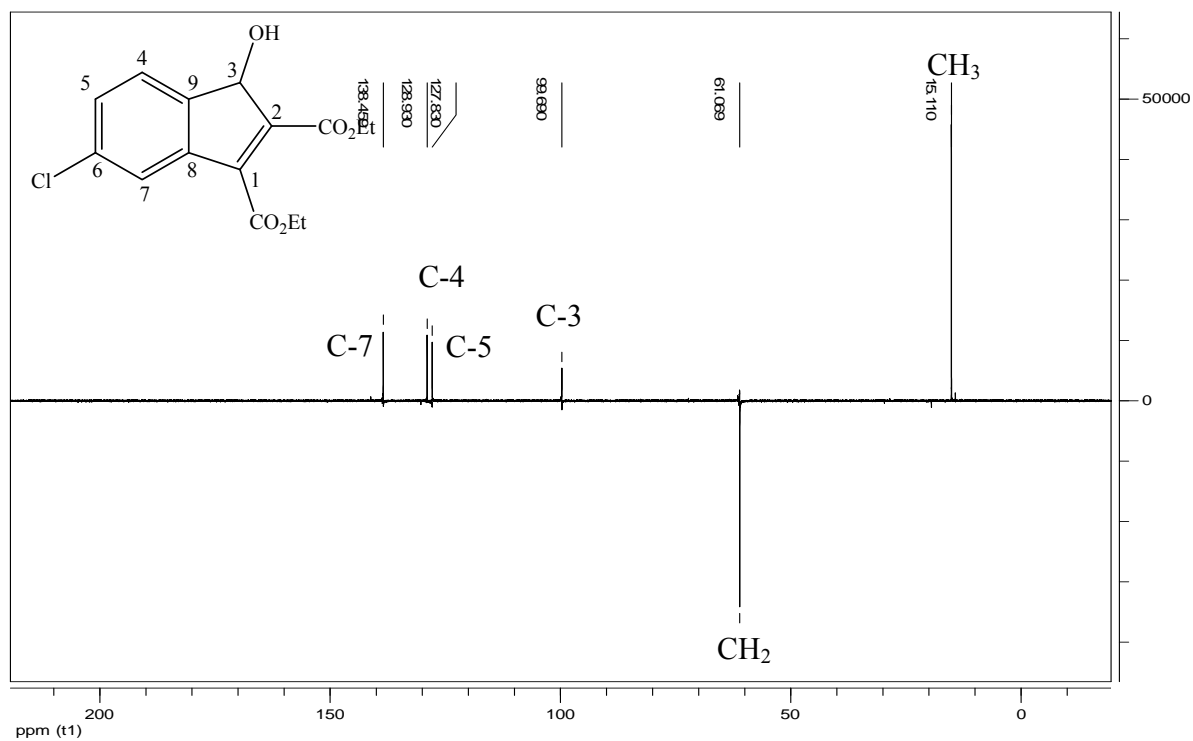


Figure 2.41. 150 MHz DEPT-135 spectra of compound **147b** in CDCl_3

Because of the quick decomposition of compounds **147a** and **147b** as explained in Scheme 2.52, building a substantial library of these novel indenols analogs was not possible.

2.5. SUMMARY

The 1,3-DC paved the way for the elegant synthesis of a library of 22 different benzotriazole analogs among which eight are new. Novel coumarin, substituted formyl cinnamate and indenol compounds were synthesized *via* palladium catalyzed reactions and their structure elucidation was made possible by interpreting NMR, IR and HRMS analysis data.

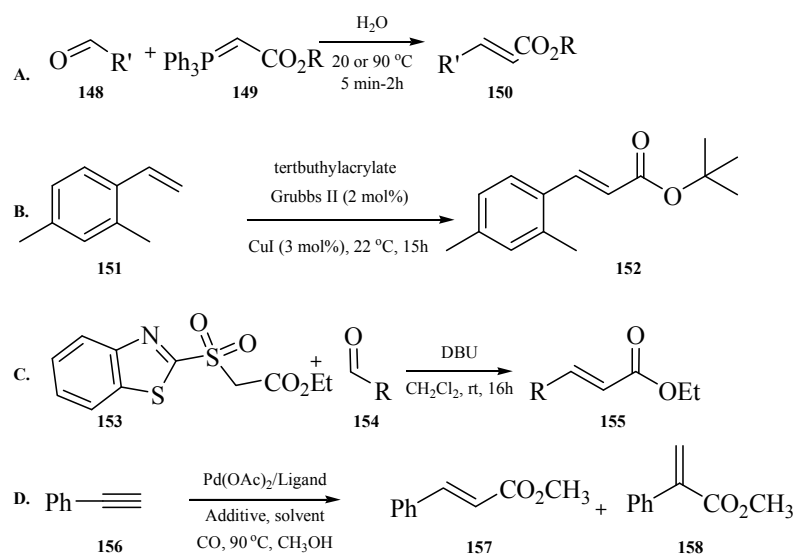
CHAPTER THREE

SYNTHESIS OF POTENTIAL INTEGRASE INHIBITORS

3.1. INTRODUCTION

It has been demonstrated that cinnamoyl compounds possess the capacity to inhibit the HIV-1 integrase enzyme.^{15, 22, 50, 274-277} For this reason, we intended to synthesize various cinnamoyl-based compounds in order to explore their variation in activity as a result of different functionalities attached to them. Since cinnamate esters are widespread in pharmacopeia, attention was given to their synthesis. Several methods have been developed to afford cinnamate esters.^{35, 278-284} Among them, the most common are the Wittig reaction, olefin cross metathesis, the Julia olefination and the palladium-dppb-borate catalyzed synthesis.

El-batta *et al.* reported cinnamate esters formed by a Wittig reaction of stabilized ylides and aldehydes in an aqueous medium (A in Scheme 3.1).²⁸⁵ More recently, Voigtritter and coworkers described the synthesis of cinnamate esters by olefin cross-metathesis (B in Scheme 3.1) of terminal alkenes with type II and type III olefinic conjugates, in the presence of a catalytic amount of a Grubbs-II catalyst.²⁷⁹ Along these lines, a Julia olefination of ethyl (benzothiazol-2-ylsulfonyl)acetate with benzaldehyde also yielded α,β -unsaturated esters (C in Scheme 3.1).²⁸⁶ Also, a palladium catalyzed alkoxycarbonylation of phenyl acetylene gave *trans* cinnamate esters (D in Scheme 3.1).²⁸⁷



Scheme 3.1. Syntheses of cinnamate esters

- Efficiency

All these syntheses were reported to be high yielding under reaction conditions optimized as indicated. The rate of the Wittig reaction (Scheme A) was found to be considerably accelerated in an aqueous medium owing to the stabilizing effect of water on the polar transition state while the type of palladium catalyst and the ligand involved determined the reaction outcome in D (Scheme 3.1).

Furthermore, the olefin cross metathesis synthesis of cinnamate esters (Scheme B) indicated that because iodine stabilizes Ruthenium in the Grubbs catalyst, using CuI as a co-catalyst enhanced the yield of the reaction.

- Selectivity

The Wittig synthesis of cinnamate esters (Scheme A) showed a high E selectivity with a strong attraction between the hydrophobic moieties of the aldehyde and the ylides. On the other hand, during the Julia olefination (Scheme C) both *cis* and *trans* cinnamate esters were produced with stereoselectivity dependant on the nature of the substrate.

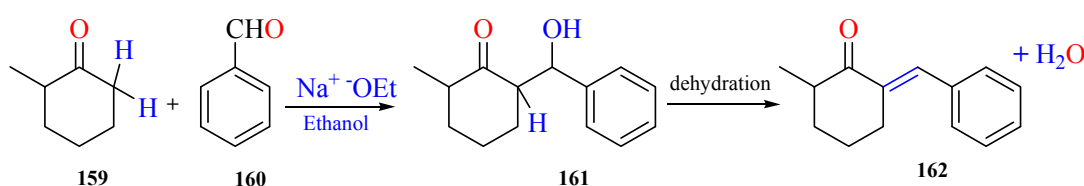
A study of the effect of the solvents involved in the palladium catalyzed syntheses of cinnamate esters (Scheme D) suggested that polar coordinating solvents were more

effective compared to non-polar solvents and polar non coordinating solvents with respect to the regioselective syntheses of the esters.

- Scope

The Wittig reaction can generally tolerate carbonyl compounds containing several kinds of functional groups such as OH, OR, aromatic nitro and even ester groups. This reaction appears to be a very cheap reaction (Scheme A) if compared to the palladium catalyzed alkoxy carbonylation (Scheme D) where a palladium catalyst, a phosphine ligand and an additive need to be added. On the other hand, the palladium catalyzed reactions are limited to the use of terminal alkynes. In the Julia olefination, branched aliphatic and aromatic aldehydes are used to afford alkenes with all types of semi-stabilized heteroaryl sulfonyl anions (Scheme C). In the olefin cross metathesis synthesis, Michael acceptors such as 2,4 –dimethyl-1-vinylbenzene is cross coupled with activated alkenes as olefinic partners (Scheme B).

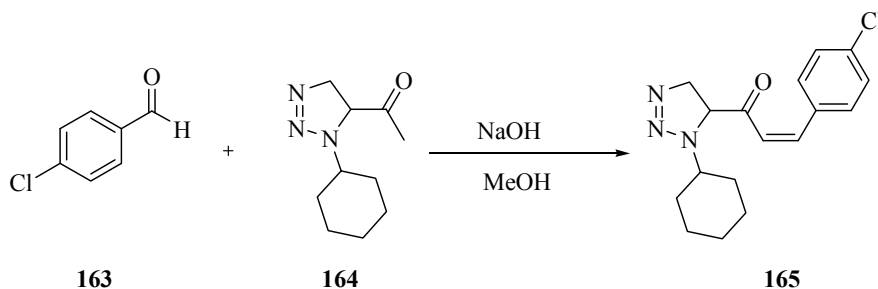
Cinnamate esters can also be obtained *via* aldol condensation of an aldehyde and a methyl ketone.²⁸⁸ It is a useful atom-economical strategy of a carbon-carbon bond forming reaction, in which an active enolate is generated *in situ* from a methyl ketone and undergoes a subsequent addition to an aldehyde or a ketone to form a β -hydroxy carbonyl compound (aldol adduct).^{289, 290}



Scheme 3.2. Aldol condensation of benzaldehyde and 2-methylcyclohexanone¹⁵¹

The condensation is often followed by spontaneous dehydration to produce an α,β -unsaturated carbonyl compound. The alkene formed is very stable since its double bond is conjugated to the carbonyl group. An aldol condensation reaction can be either acid or base catalyzed. While bases activate the nucleophile, acids activate the electrophile during the synthesis.

Stevens' group implemented this general strategy and reported the synthesis of compound **165** via a base catalyzed aldol condensation of compound **164** with *p*-chlorobenzaldehyde.²⁹¹



Scheme 3.3. Synthesis of an aromatic α , β -unsaturated ketone by aldol condensation²⁹¹

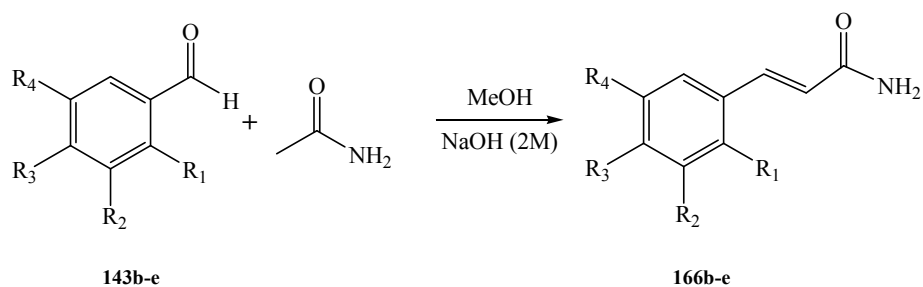
This condensation has also been used to synthesize polymers,²⁹⁰ polyols,²⁹² chalcones and chiral (R)-dihydroxycarboxylic acids.²⁹³

In this project, the aldol condensation and click chemistry were employed for the synthesis of cinnamoyl derivatives.

3.2. RESULTS AND DISCUSSION

3.2.1. Synthesis of acrylamide

Our strategic plan to explore peptidomimetics included the development of acrylamide derivatives. This approach began with a base-catalyzed aldol condensation of aromatic aldehydes with acetamide to yield aromatic acrylamides (Scheme 3.4) following the approach reported by Stevens *et al.*²⁹⁴ As indicated in Scheme 3.4, benzaldehyde derivatives and acetamide were mixed in MeOH. An aqueous solution of 2 M NaOH was added and the reaction mixture was stirred under reflux in MeOH for three hours.



	R₁	R₂	R₃	R₄	Yield (%)
166b	H	H	Cl	H	71
166c	H	H	Br	H	96
166d	OH	H	H	Br	31
166e	OH	Br	H	Br	25

Scheme 3.4. Aldol condensation of benzaldehyde derivatives **143b-e** with acetamide (crude yields obtained from NMR)

In the ^{13}C NMR spectrum of compound **166b** (Figure 3.1), all the 9 carbon atoms are accounted for with the carbonyl C-9 resonating at 188.3 ppm while the quaternary carbons C-1 and C-4 resonate at 136.5 ppm and 133.2 ppm respectively. The vinylic carbon C-8 resonates at 125.7 ppm while C-7 resonates at 142.1 ppm. Due to the electron withdrawing effect of the chlorine atom, the aromatic carbon C-3 resonates at 129.5 ppm while C-2 resonates at 129.3 ppm.

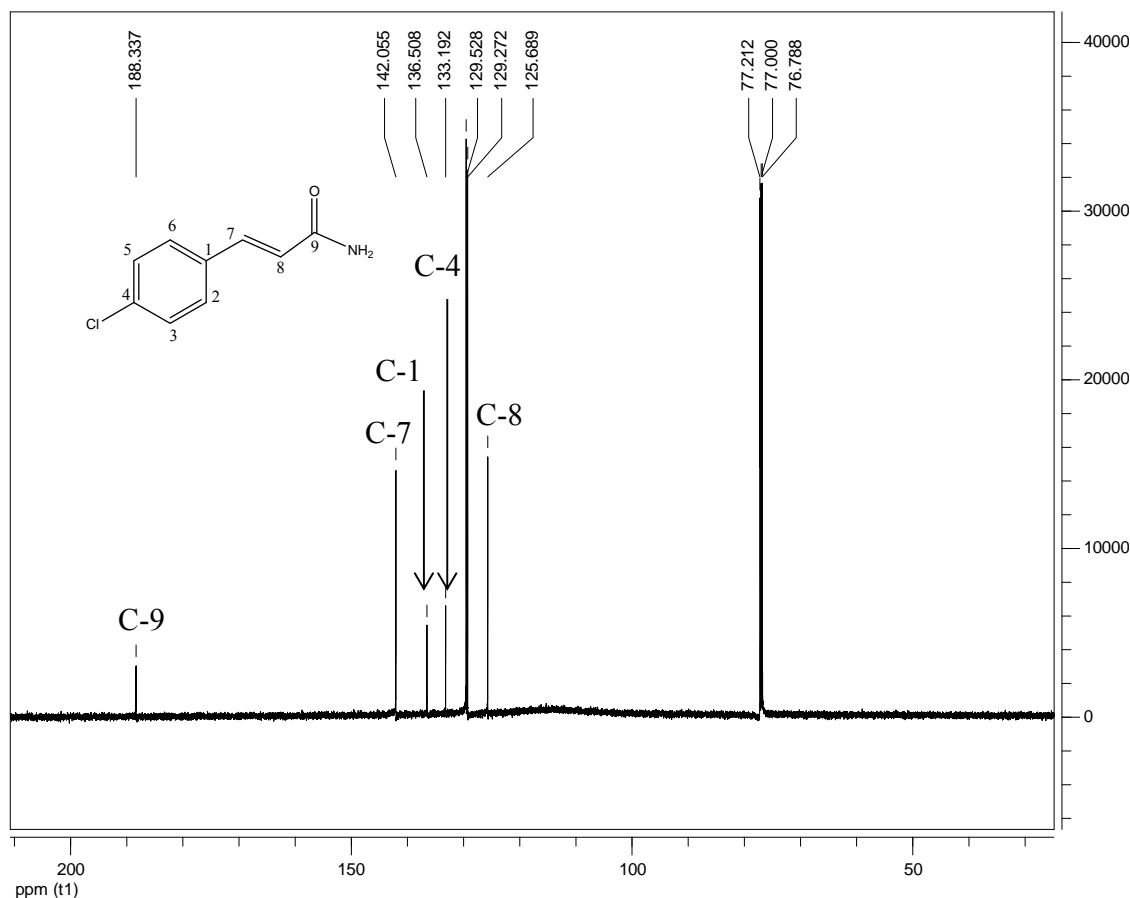
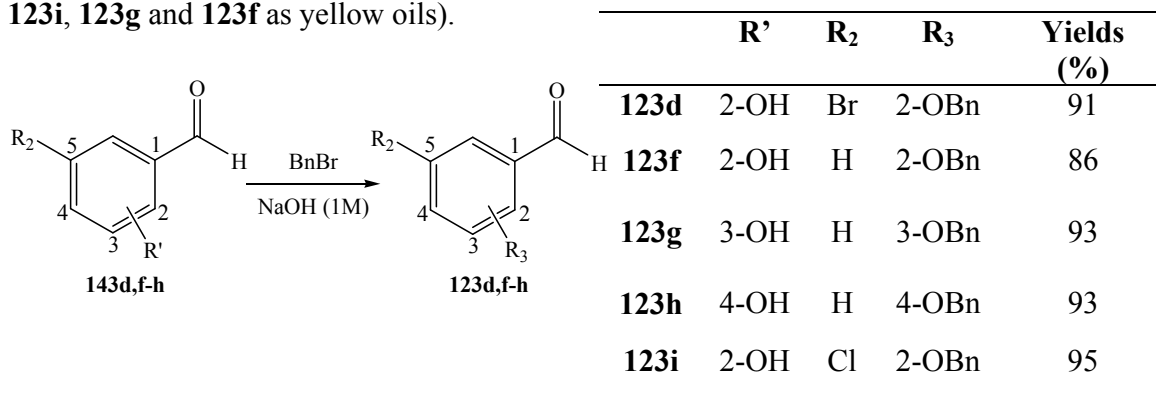


Figure 3.1. 150 MHz ¹³C NMR spectrum of compound **166b** in CDCl₃

On the basis of the data recorded in Scheme 3.1, the syntheses where salicylaldehyde analogs were involved (compound **166d** and compound **166e**) produced aldol adducts in very low yields (25% and 31%). These poor yields could be explained by a competition between the aldol condensation reaction and the deprotonation reaction of the phenolic hydroxyl group R₁ by NaOH. In order to circumvent this side reaction, the protection of those hydroxyl groups (R₁) was necessary. This was possible by performing a benzylation reaction (Scheme 3.5) of the salicylaldehyde derivatives.

The method used required the addition of an aqueous solution of NaOH (1M) and a slight excess of the protecting agent (benzyl bromide) to each salicylaldehyde derivative. The mixture was allowed to reflux for 30 minutes and the compounds indicated in Scheme 3.5

were isolated in excellent yields (Compounds **123d** and **123h** as solids and compounds **123i**, **123g** and **123f** as yellow oils).



Scheme 3.5. Benzylation of benzaldehyde derivatives

In the ^1H NMR spectrum of compound **123d**, the disappearance of the alcoholic proton of the starting material (5-bromosalicylaldehyde) around 11 ppm was observed. Similarly, the appearance of the methylene protons H-8 resonating as a singlet at 5.18 ppm showed the introduction of the benzylic group. In addition, five aromatic proton signals overlapping between 7.37 ppm and 7.42 ppm could be ascribed to the pendant phenyl moiety. In the IR spectrum of **123d**, the disappearance of the hydroxyl signal (of the starting material **143d**) at 3380.22 cm^{-1} was also observed.

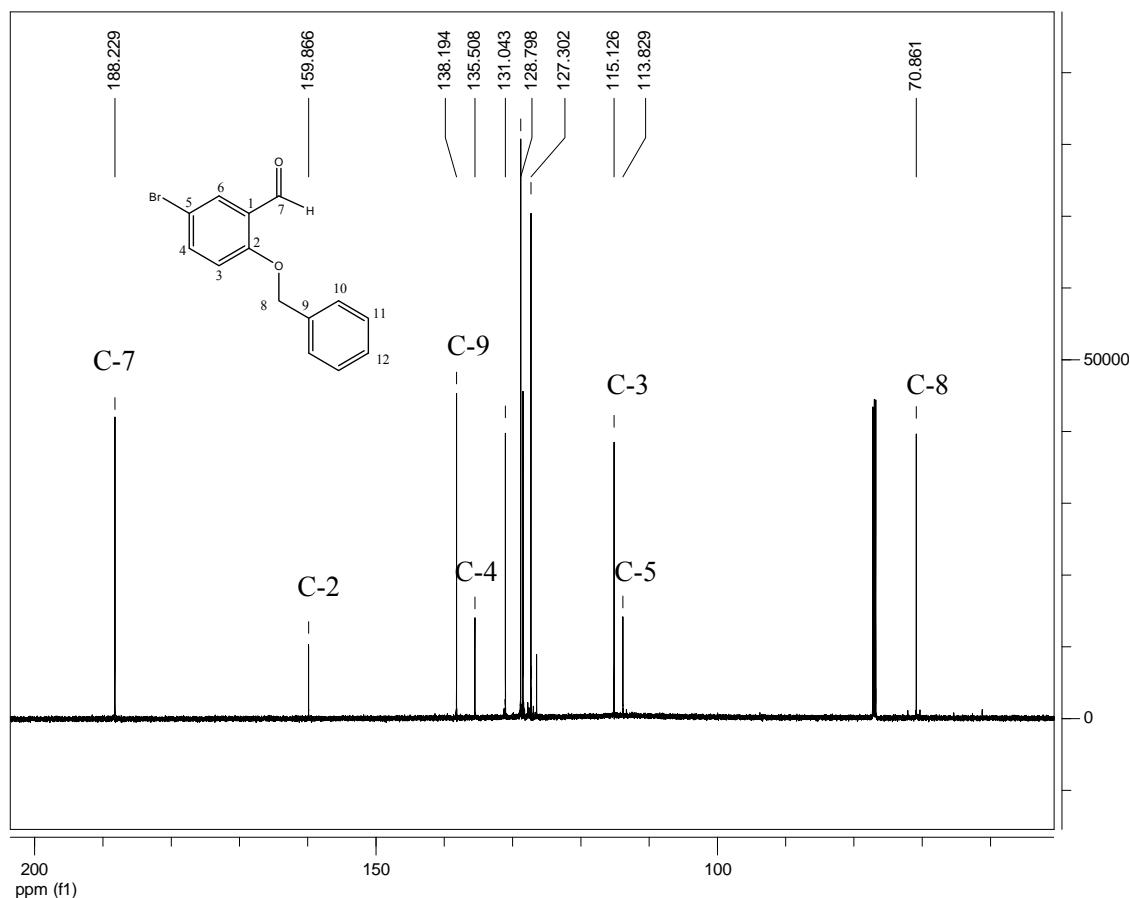
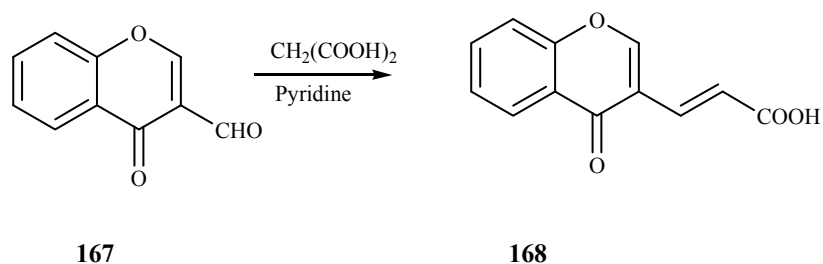


Figure 3.2. 150 MHz ^{13}C NMR spectrum of compound **123d** in CDCl_3

The ^{13}C NMR spectrum of compound **123d** (Figure 3.2) further confirmed the attachment of the benzyl group by accounting for all the 12 carbon signals of compound **123d** among which the presence of the methylene carbon resonating at 70.9 ppm was diagnostic. Compound **123d** was previously used as a substrate in the synthesis of cinnamate ester–AZT conjugates by Olomola. In the procedure described by Olomola, K_2CO_3 was used as the base and NaI as a promoter in absolute ethanol. The chemical shifts observed are in agreement with those reported by Olomola.⁸¹ Unfortunately, benzylated aromatic aldehydes compounds appeared to be unsuitable substrates for an aldol condensation involving acetamide and after several attempts, only an intractable mixture of products could be obtained.

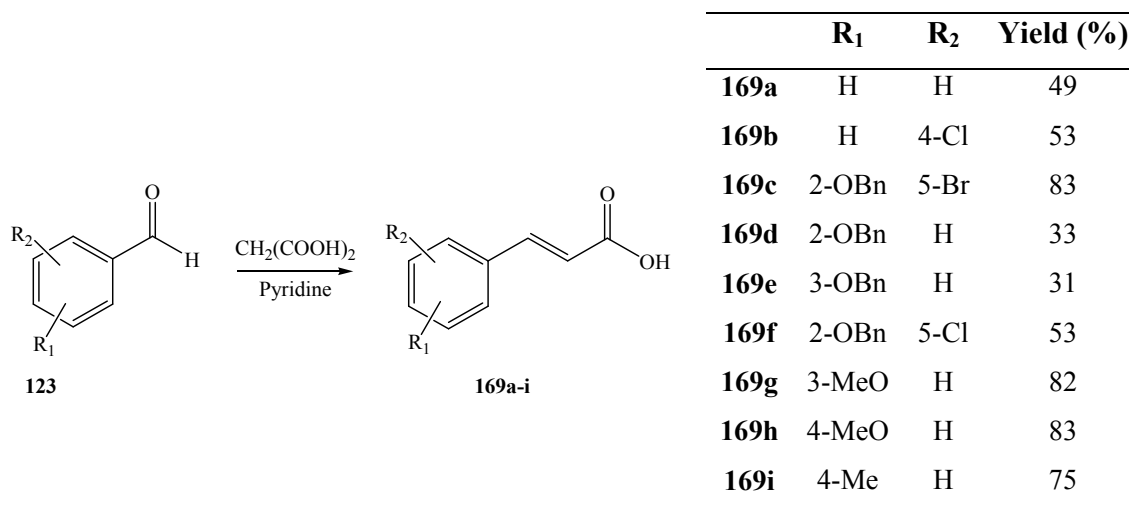
3.2.2. Synthesis of cinnamic acid derivatives

The conjugated cinnamate moiety remained a desirable target and, consequently, we decided to utilize these protected aldehydes (**123d**, **123f**, **123g** and **123i**) with other acid derivatives. In 1975, Nohara reported the successful synthesis of 3-(4-oxo-4*H*-1-benzopyran)acrylic acids **168** by a base-catalyzed aldol condensation of 4-oxo-4*H*-1-benzopyran-3-carboxaldehyde **167** with malonic acid and pyridine under reflux for 30 minutes (Scheme 3.6).²⁹⁵



Scheme 3.6. Synthesis of acrylic acids by aldol condensation²⁹⁵

We followed the same protocol by using benzaldehyde derivatives as aldehydes of interest in order to synthesize functionalized cinnamic acids (Scheme 3.7). From a mechanistic point of view, we hypothesized that the nucleophile formed by the abstraction of the acidic methylene protons of malonic acid would react with the carbonyl of the aldehyde derivative to form a 2-(-[hydroxy(phenyl)methyl-])malonic acid derivative. A subsequent decarboxylation reaction followed by dehydration gave compounds **169a-i**.



Scheme 3.7. Synthesis of cinnamic acids by aldol condensation

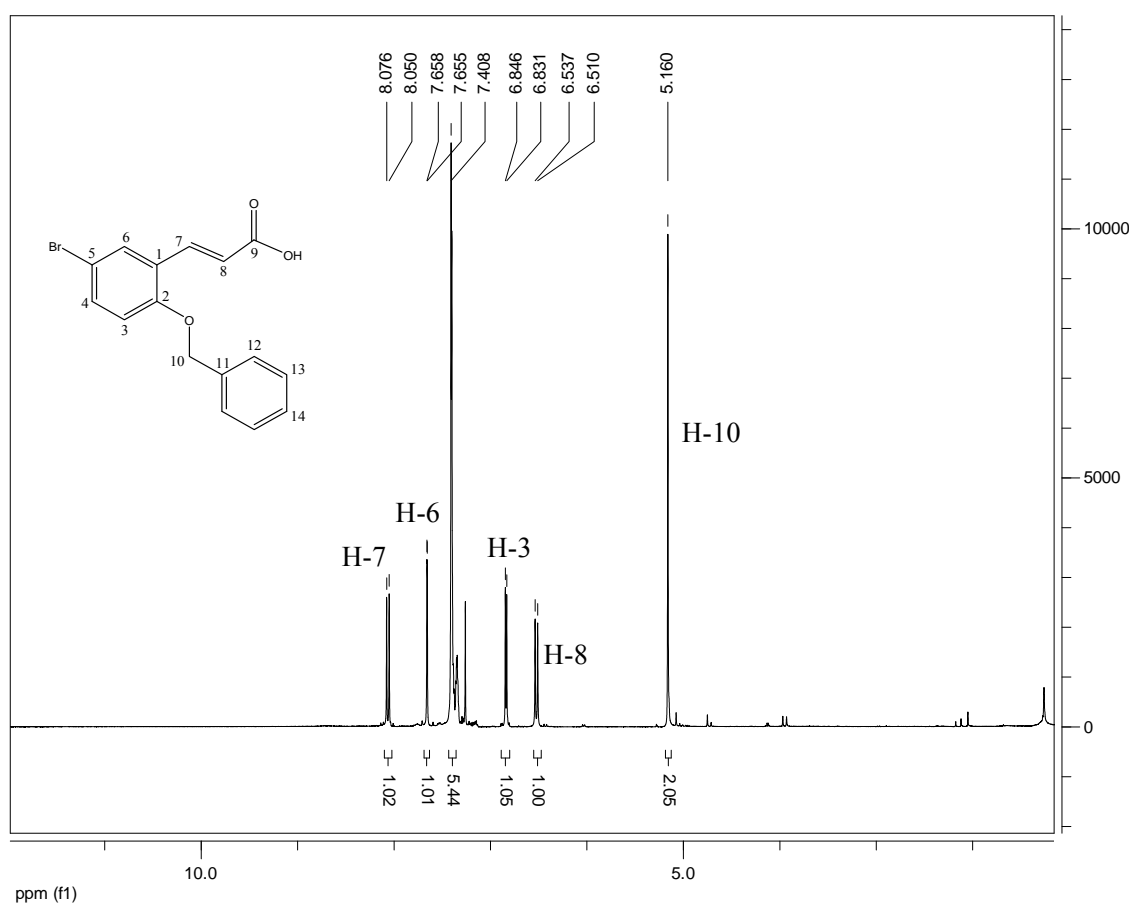


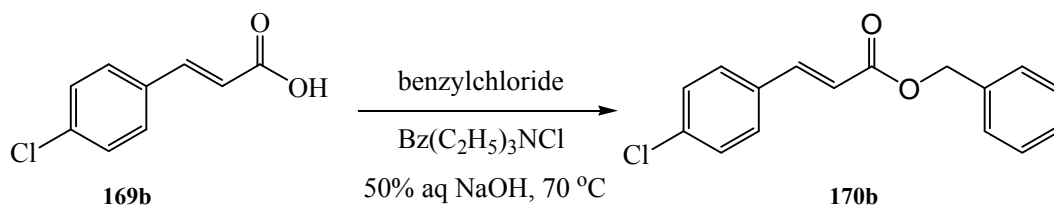
Figure 3.3. 600 MHz ^1H NMR spectrum of compound **169c** in CDCl_3

The ^1H NMR spectrum of compound **169c** (Figure 3.3) indicates the presence of 13 protons with the vinylic protons H-8 and H-7 resonating as doublets at 6.51 ppm and 8.07 ppm respectively, H-7 being more highly deshielded because it is attached to the electrophilic carbon conjugated to the carbonyl. This observation was in agreement with Chemdraw® predictions. Also of interest was the disappearance of the aldehydic proton at 10.46 ppm indicating that the condensation had successfully occurred. In the ^{13}C NMR spectrum of the same compound, the 16 carbon atoms were all accounted for with the new carbonyl signal of the carboxylic acid C-9 at 171.8 ppm and two new vinylic carbons C-8 and C-7, at 114.6 ppm and 140.6 ppm respectively.

The synthesis of compound **169c** was first reported by Breitenbach *et al.*,²⁹⁶ by following a similar approach, the only difference being the addition, in their case, of a stoichiometric amount of piperidine.

3.2.3. Synthesis of benzyl cinnamate esters

Most HIV-1 IN inhibitors bear pendant aromatic groups probably accounting for an enhancement in binding of drug candidates in the active site of the IN enzyme.^{15, 297} Consequently, we decided to prepare benzyl protected esters. The synthesis of compound **170a** was high yielding by following the benzylation reaction outlined in Scheme 3.8 (75%). However, applying the same procedure for the synthesis of compound **170b** appeared to be very low yielding. The literature revealed that compound **170b** could be synthesized by a different route established by Wang and coworkers who reported the synthesis of benzyl esters from a phase transfer catalyzed alkaline hydrolysis of benzyl chloride (Scheme 3.8).²⁹⁸ Following this protocol we obtained compound **170b** in a good yield of 87%.



Scheme 3.8. Synthesis of benzyl 3-(4-chlorophenyl)acrylate **170b**

The ^1H NMR spectrum of compound **170b** (Figure 3.4) revealed the presence of nine aromatic protons between 7.34 ppm and 7.45 ppm and a singlet at 5.25 ppm corresponding to the methylene group H-10. These assignments confirmed the formation of the expected product. As expected, in the ^{13}C NMR spectrum of compound **170b** (Figure 3.5) a new methylene carbon C-10 resonating at 66.5 ppm and the carbonyl (C-9) shifted slightly upfield at 166.5 ppm were observed, confirming the proposed structure.

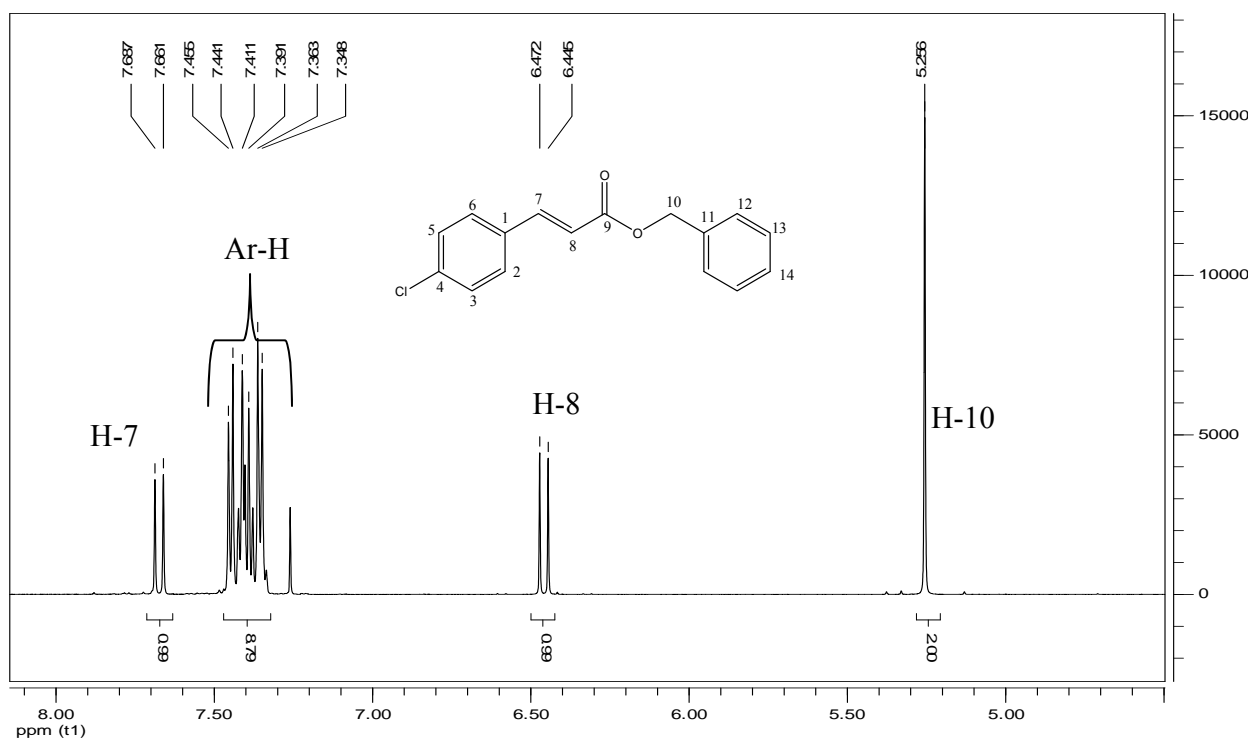


Figure 3.4. 600 MHz ^1H NMR spectrum of compound **170b** in CDCl_3

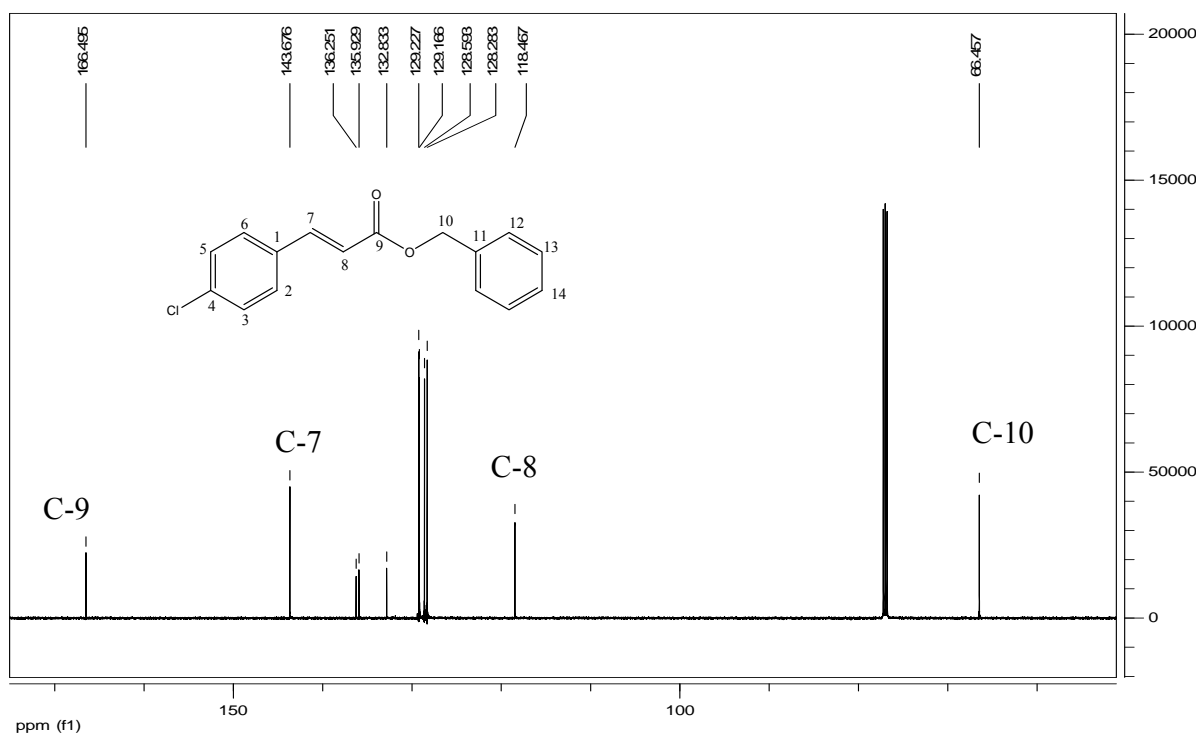


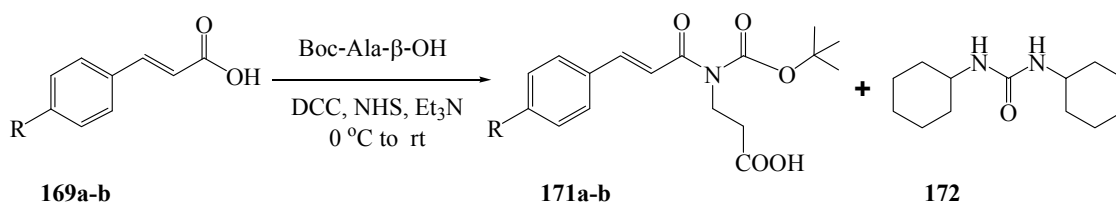
Figure 3.5. 150 MHz ^{13}C NMR spectrum of compound **170b** in CDCl_3

3.2.4. Synthesis of protected amino acid cinnamate conjugates

Peptides are excellent delivery vehicles in a biological context owing to their ability to cross cell membranes and are therefore favored therapeutic agents.²⁹⁹ Most of the peptide based integrase inhibitors currently identified are natural compounds derived from the IN coding region.²⁹⁹⁻³⁰¹ In an effort to combine the effectiveness of peptide-based inhibitors and cinnamates, we chose to prepare a series of cinnamic acid peptide analogs in order to test their potential activity.

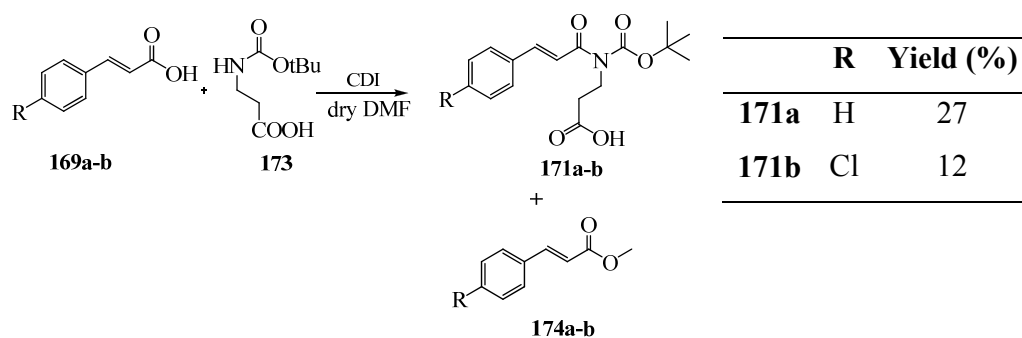
Cinnamic acid derivatives (compounds **169a-b**) were coupled with *N*-Boc- β -alanine in order to generate a peptide bond. A Boc-protected amino acid was used to ensure selective coupling of a single amino acid to each cinnamic acid. In addition, Boc protected amino acids are good partners in the syntheses of peptides since they present the advantage of being unreactive under basic conditions and resistant to other nucleophiles.^{302, 303} In our first attempt at making peptide bonds, we implemented a procedure reported by Joullié *et al.*³⁰⁴ As outlined in Scheme 3.9, Et_3N was used as a

base and *N*-hydroxysuccinimide (NHS) and dicyclohexyldiimide (DCC) as coupling reagents, at 0 °C in dry DCM. Unfortunately, the cinnamate substituted amino acid **171a** was obtained in a poor yield of 9% with compound **172** as a by-product and unreacted starting material was recovered.³⁰⁴ Dicyclourea is formed by the reaction of the key intermediate *O*-acylisourea produced from carboxylic acid reacting with DCC and the amine. We reasoned that this very low yield could be explained by the poor nucleophilicity of the Boc protected amino acid.



Scheme 3.9. Synthesis of peptidomimetics by coupling of cinnamic acid derivatives with Boc-β-alanine

The poor outcome of this synthesis motivated a search for different coupling reagents. The following method was first employed in 2001 by Nchinda³⁰⁵ for the synthesis of chromones containing analogs of ritonavir by coupling a diamine with chromone 2-carboxylic acid. 1,1'-Carbonyl diimidazole (CDI) was used to promote the coupling reaction by enhancing the electrophilicity of the carboxylate group of the acid derivative. After stirring the mixture of the cinnamic acid derivative and *N*-Boc-β-alanine in dry dimethyl formamide (DMF) at room temperature, under argon for 48 hours as outlined in Scheme 3.10, novel compounds **171a** and **171b** were isolated. Besides the expected products (compounds **171a** and **171b**), methylated cinnamic acid derivatives were also formed.



Scheme 3.10. Synthesis of *tert*-butylamido cinnamate peptide adducts

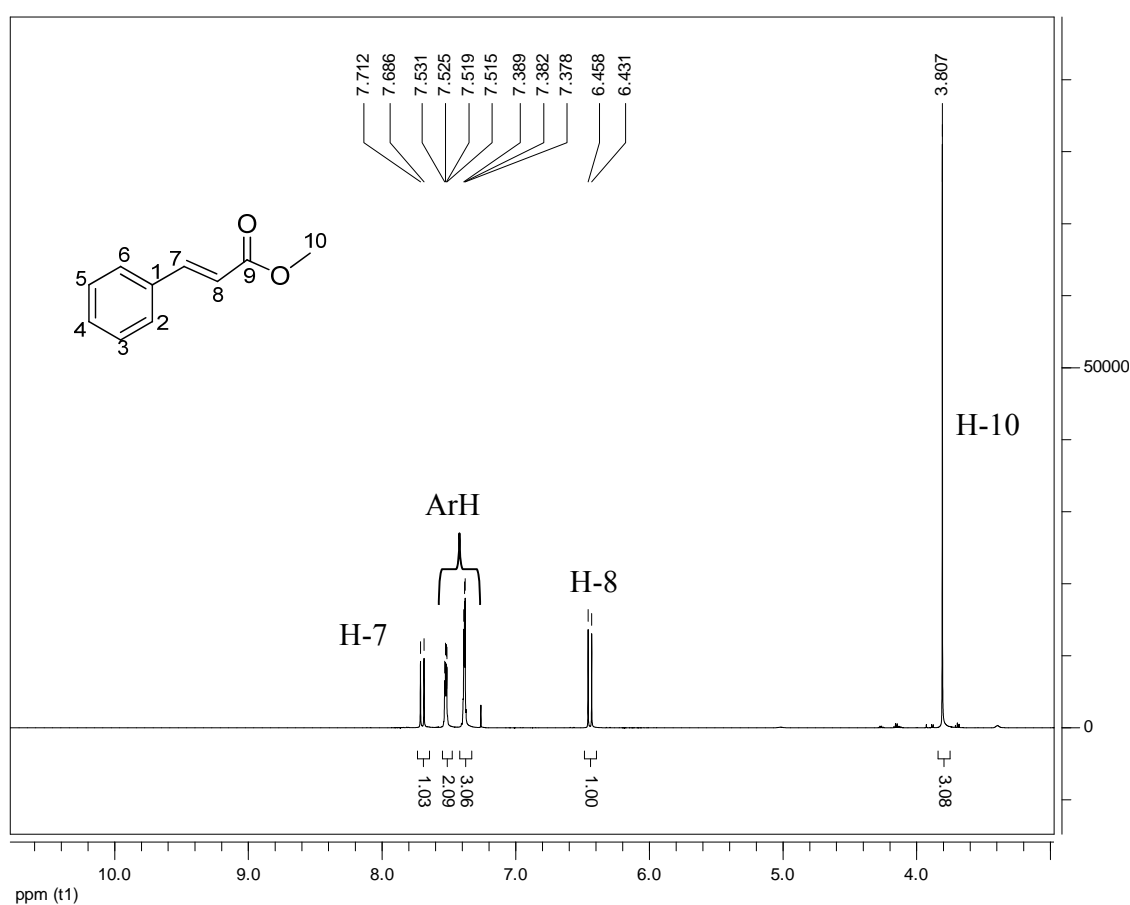


Figure 3.6. 600 MHz ^1H NMR spectrum of compound **174a** in CDCl_3

The methylation was confirmed by a sharp methyl singlet resonating at 3.81 ppm in the ^1H NMR spectrum (Figure 3.6), with the vinylic protons H-8 and H-7 at 6.44 ppm and 7.70 ppm respectively, and the aromatic protons between 7.37 ppm and 7.53 ppm.

The ^1H NMR spectrum of compound **171a** (Figure 3.7) revealed the presence of 9 *tert*-butyl protons resonating as a singlet at 1.41 ppm and two methylene protons H-13 and H-14 resonating as triplets at 2.50 ppm and 3.37 ppm respectively, H-14 being more deshielded by the acid group. A broad singlet at 5.05 ppm confirmed the presence of a hydroxyl group. These signals confirmed the presence of the amino acid. The two doublets resonating at 6.43 ppm and 7.68 ppm correspond to the vinylic protons H-8 and H-7, where H-8 is shielded by conjugation with the acrylamide group. The aromatic protons which appear in the region between 7.36 ppm and 7.51 ppm further confirmed the integrity of the cinnamate moiety.

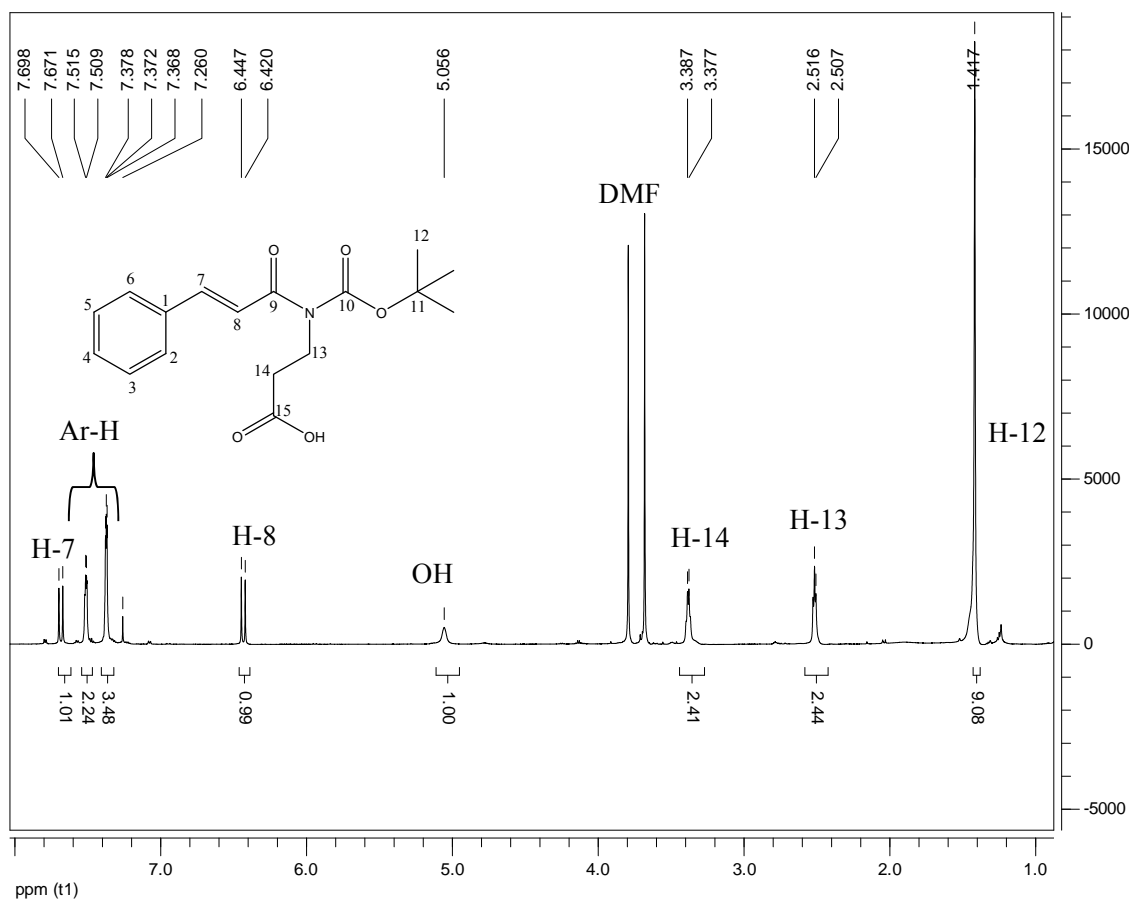


Figure 3.7. 600 MHz ^1H NMR spectrum of compound **171a** in CDCl_3

The presence of a *tert*-butyl signal was supported by a methyl carbon and a quaternary carbon C-11 resonating at 28.3 ppm and 79.3 ppm respectively in the ^{13}C NMR spectrum

(Figure 3.8). The DEPT-135 NMR spectrum (Figure 3.9) of compound **171a** also confirmed the presence of the two methylene carbons C-14 and C-13 at 34.3 ppm and 35.9 ppm respectively. These assignments were facilitated by observing their correlations in the HSQC NMR spectrum (Figure 3.10). These correlations revealed that the carbons C-8 and C-7 resonate as expected at 117.8 ppm and 144.8 ppm respectively, very close to their original positions. Furthermore, the DEPT-135 NMR spectrum confirmed (by their absence on this spectrum) the presence and position of three carbonyl signals at 155.7 ppm, 167.4 ppm and 172.9 ppm. In the HMBC NMR spectrum (Figure 3.11), correlations between the carbonyl signals C-15 and C-9 and the methylene proton H-13 and the methine proton signal H-7 confirmed the assignments of the corresponding signals at 172.9 ppm and 167.4 ppm respectively. By a process of elimination, the signal of carbonyl C-10 was assigned at 155.7 ppm.

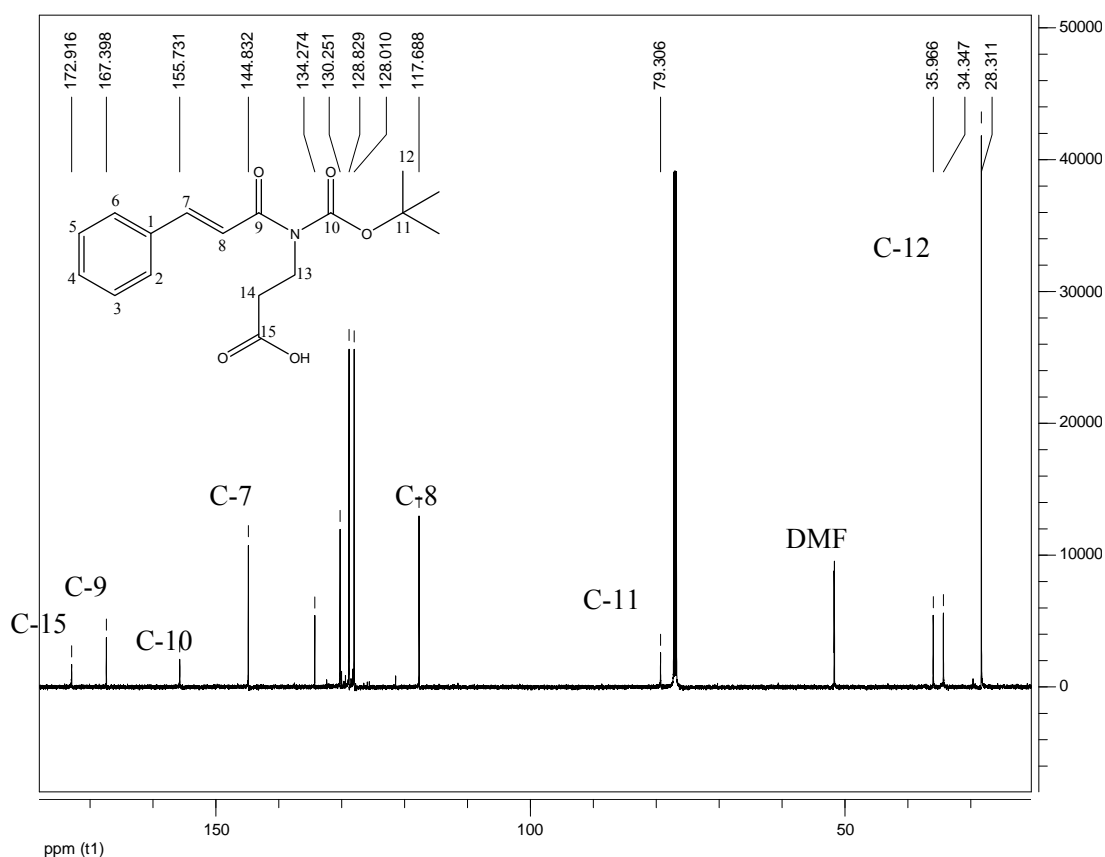


Figure 3.8. 150 MHz ^{13}C NMR spectrum of compound **171a** in CDCl_3

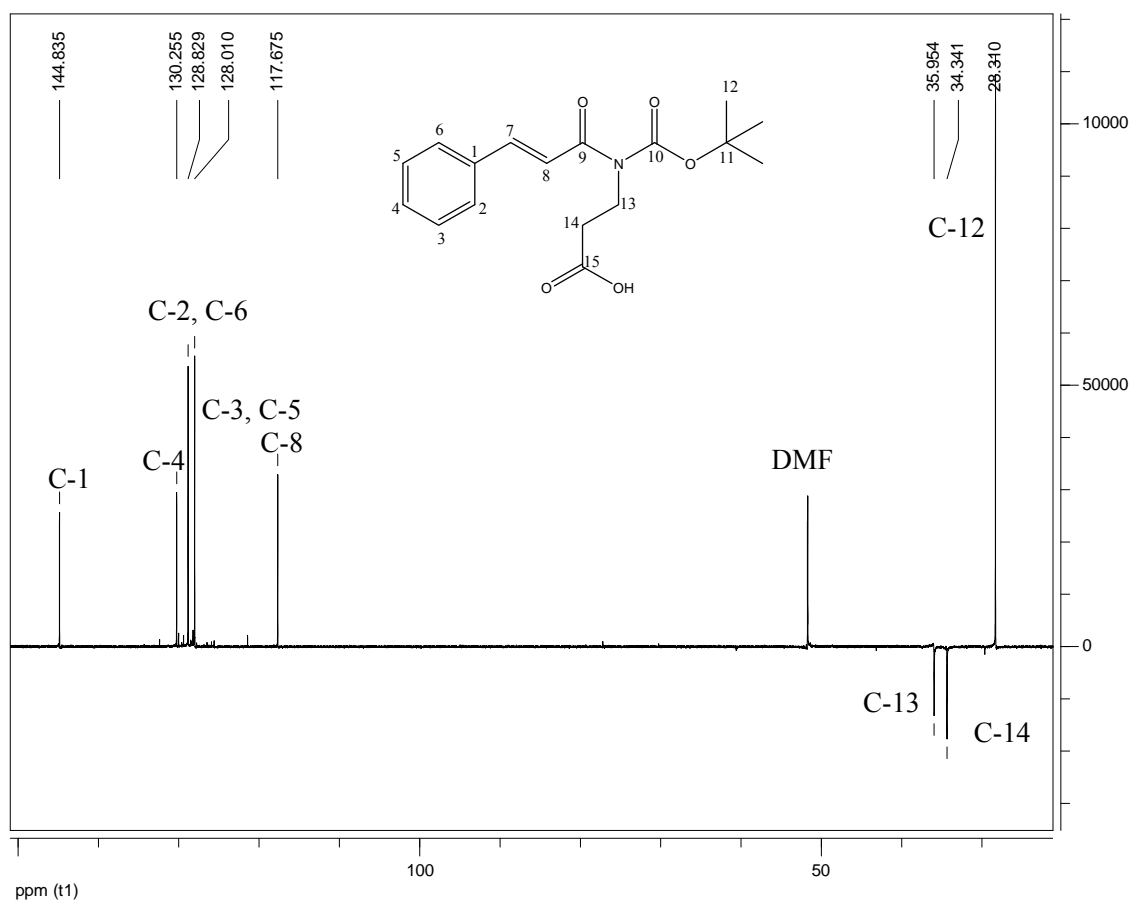


Figure 3.9. DEPT-135 NMR spectrum of compound **171a** in CDCl_3

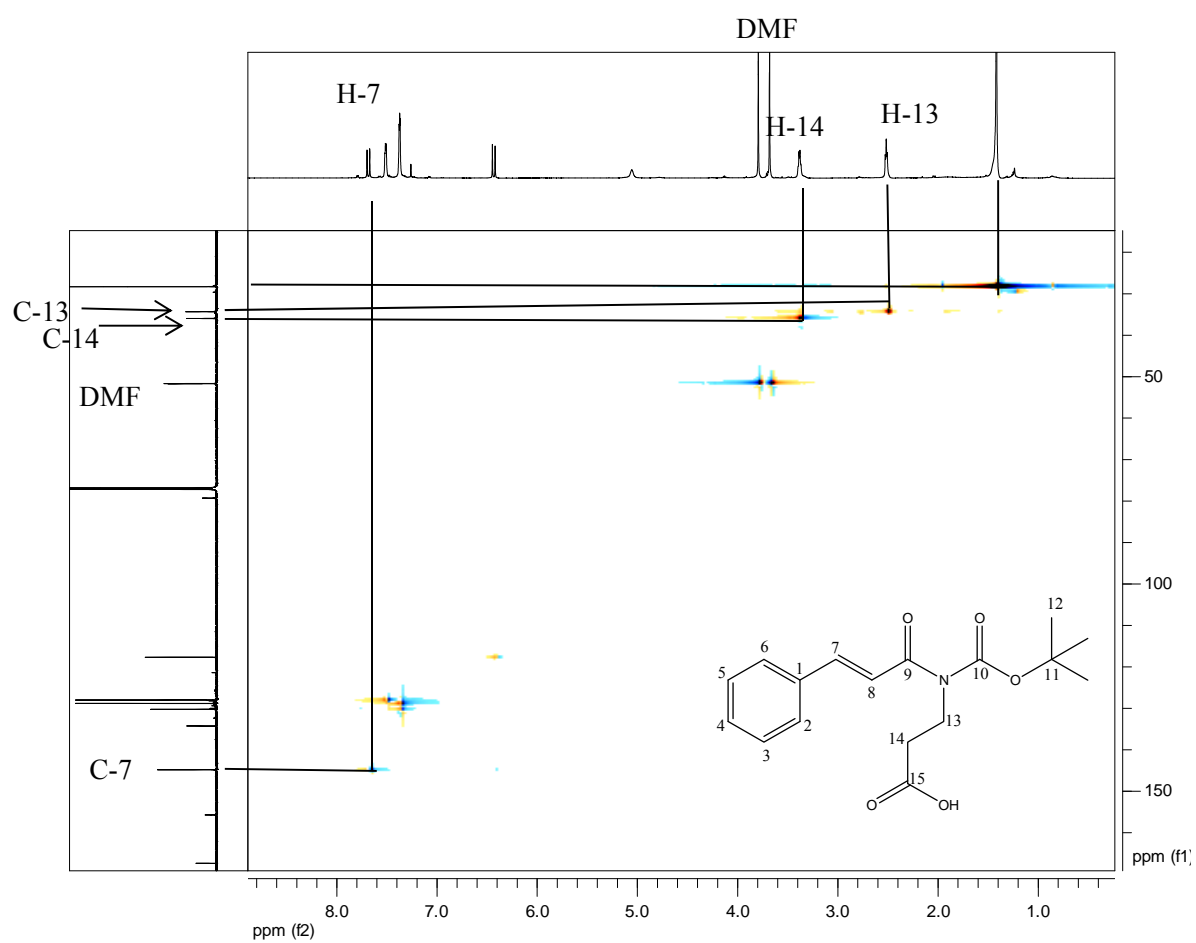


Figure 3.10. HSQC NMR spectrum of compound **171a** in CDCl_3

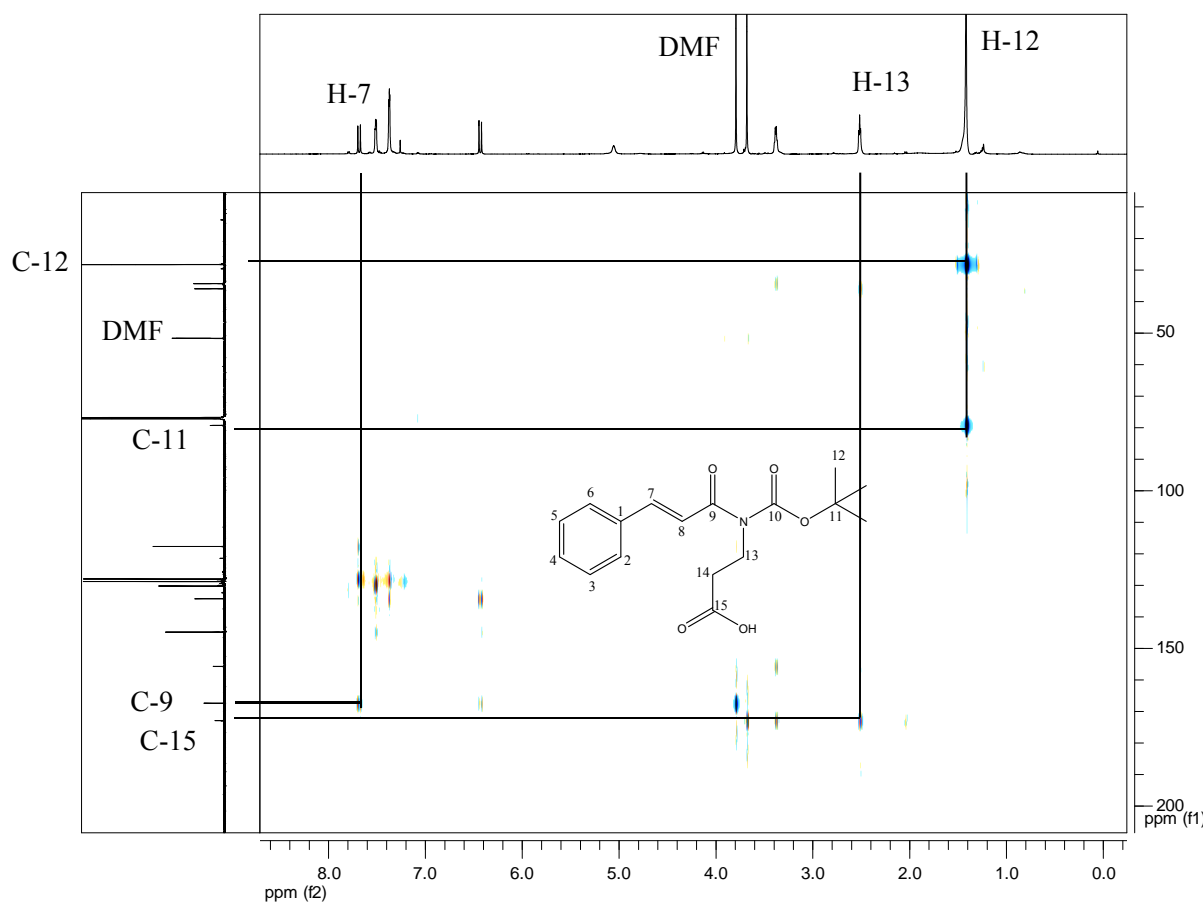
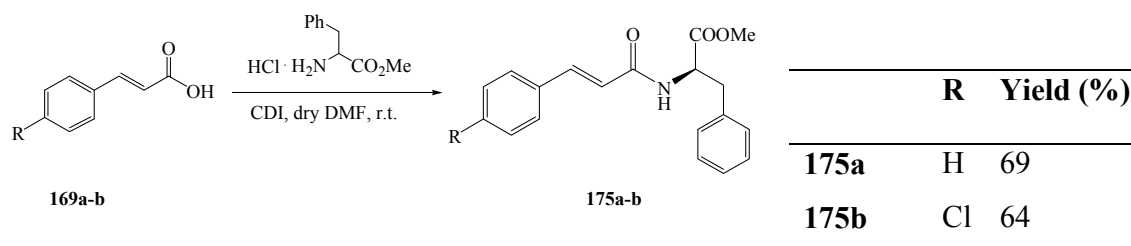


Figure 3.11. HMBC NMR spectrum of compound **171a** in CDCl_3

As depicted in Scheme 3.10, compounds **171a** and **171b** were obtained with a marginal improvement but still in a low yield. We speculated that reactivity associated with the structure of Boc- β -alanine could also account for that (Scheme 3.10) since a Boc substituted nitrogen has reduced nucleophilicity due to delocalization of the lone pair into the carbamate protecting group. Therefore, attention was given to L-phenylalanine methyl ester hydrochloride which is a highly nucleophilic, carbonyl protected amino acid. The same coupling procedure was followed. As expected, compounds **175a** and **175b** were isolated in good yields of 69% and 64% respectively as indicated in Scheme 3.11.



Scheme 3.11. Synthesis of phenyl alanine cinnamate adducts

The ^1H NMR spectrum of compound **175a** (Figure 3.12) reveals the presence of 19 protons as forecast. A methyl singlet resonating at 3.77 ppm and a methine proton signal (H-8) appearing as a doublet of doublets at 5.06 ppm were easily assigned. In addition, two diastereotopic methylene protons resonate as two doublets of doublets at 3.18 ppm and 3.26 ppm due to the proximity of the asymmetric carbon C-8. The aromatic protons are overlapping between 7.10 ppm and 7.51 ppm while the vinylic protons H-6 and H-5 resonate at 6.44 ppm and 7.65 ppm respectively as doublets. Finally, a less well-resolved NH signal was observed at 6.31 ppm.

The assignment of the diastereotopic methylene proton (H-9) at 3.25 ppm facilitated the attribution of the signal at 39.7 ppm in the ^{13}C NMR spectrum to C-9, by means of the HSQC correlation (Figure 3.13). Similarly, cross peaks corresponding to the asymmetric centre (C-8) and the vinylic protons (H-5 and H-6) facilitated the assignment of the corresponding carbons C-8, C-5 and C-6 at 53.4, 141.8 and 120.0 ppm respectively. These assignments were in agreement with those reported by Bornaghi *et al.* where compound **175a** was first synthesized by coupling L-phenylalanine methyl ester hydrochloride with cinnamoyl chloride.³⁰⁶

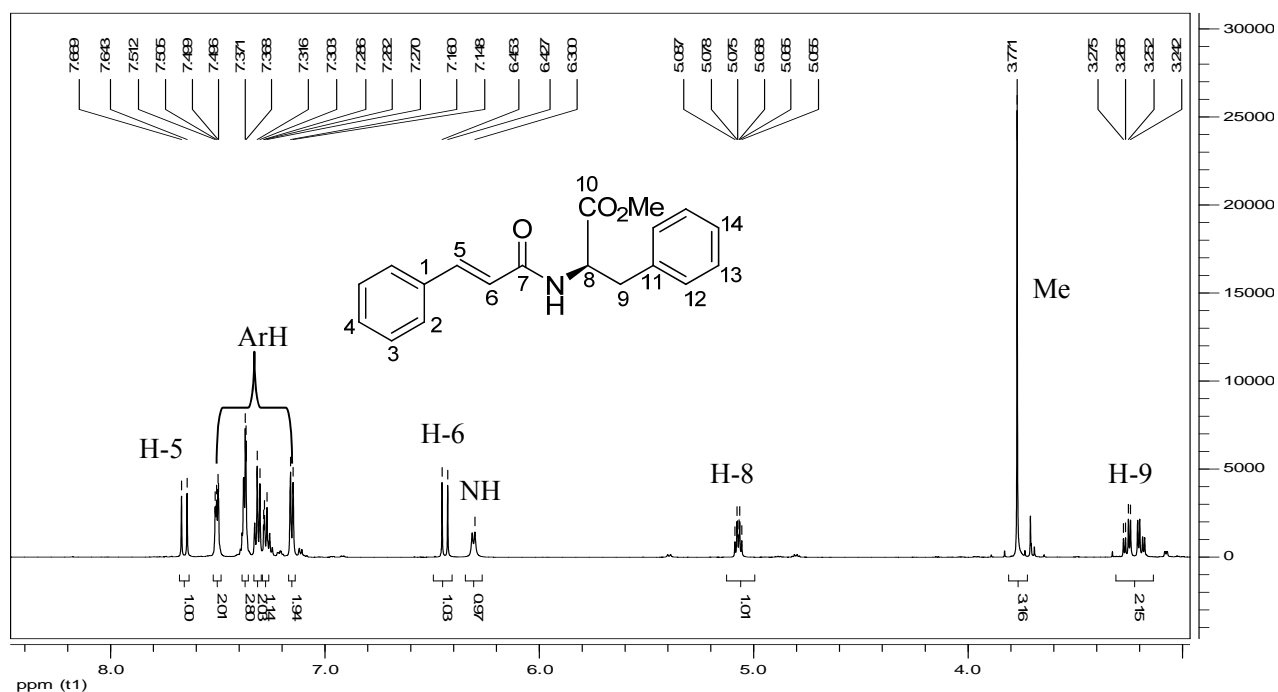


Figure 3.12. 600 MHz ¹H NMR spectrum of compound **175a** in CDCl₃

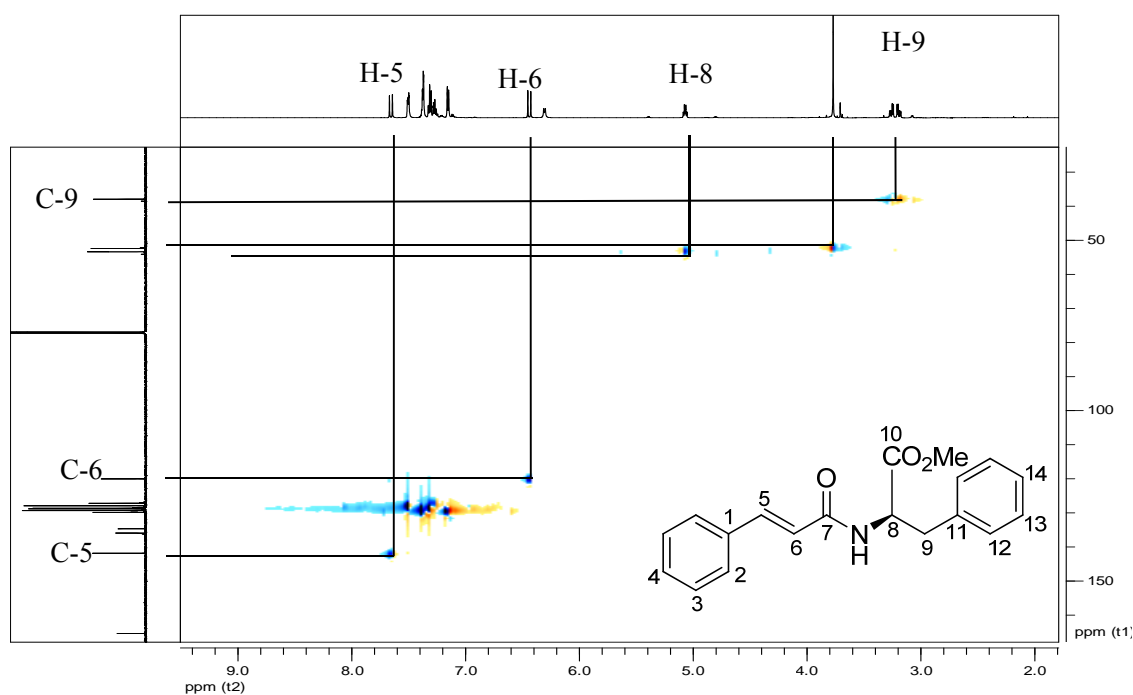
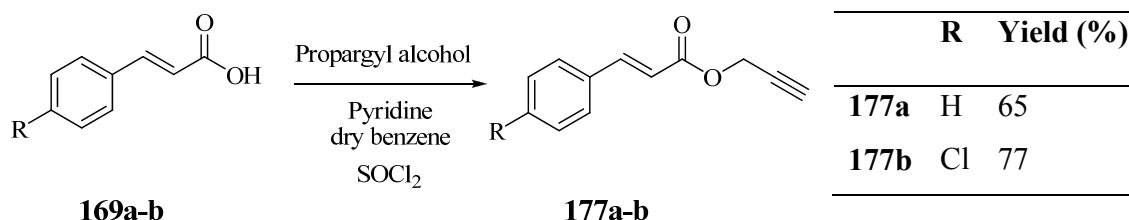


Figure 3.13. HSQC NMR spectrum of compound **175a** in CDCl₃

A similar synthesis where a primary amine (benzylamine) was coupled with cinnamic acid afforded compound **176** in a yield of 47% (Scheme 3.11).

3.2.5. Synthesis of cinnamate ester-AZT conjugates

Boudreau *et al.*, established a synthetic pathway for the synthesis of caffeoyl and cinnamoyl clusters with a step involving the synthesis of cinnamic esters from propargyl alcohol with cinnamic acid derivatives in the presence of SOCl_2 and pyridine (Scheme 3.12).³⁰⁷ This approach was attractive as a means of designing linear cinnamate ester-AZT analogs as part of the aims of this project (Section 1.3).



Scheme 3.12. Synthesis of propynyl cinnamate

The ^{13}C NMR spectrum of compound **177a** (Figure 3.14a) revealed the presence of 12 carbon signals with two carbon signals (C-12, C-11) in the alkyne carbon region at 74.9 ppm and 77.8 ppm respectively and a quaternary carbon signal C-1 at 134.1 ppm. A carbonyl signal at 165.9 ppm and a methylene carbon signal at 51.9 ppm belonged to the ester group, while the two vinylic carbon C-8 and C-7 resonate at 116.9 ppm and 145.9 ppm respectively. In addition, the presence of a methylene carbon signal C-10 was confirmed in the DEPT-135 NMR spectrum (Figure 3.14b). In the DEPT 135 NMR spectrum, the quaternary carbon C-11 resonates at 77.50 ppm. This unexpected signal has been shown to be due to a polarization transfer from the alkyne proton H-12 situated two bonds away resulting from the large two bond coupling constant.⁴¹⁹ These chemical shifts were in agreement with those reported by Boudreau *et al.*³⁰⁷

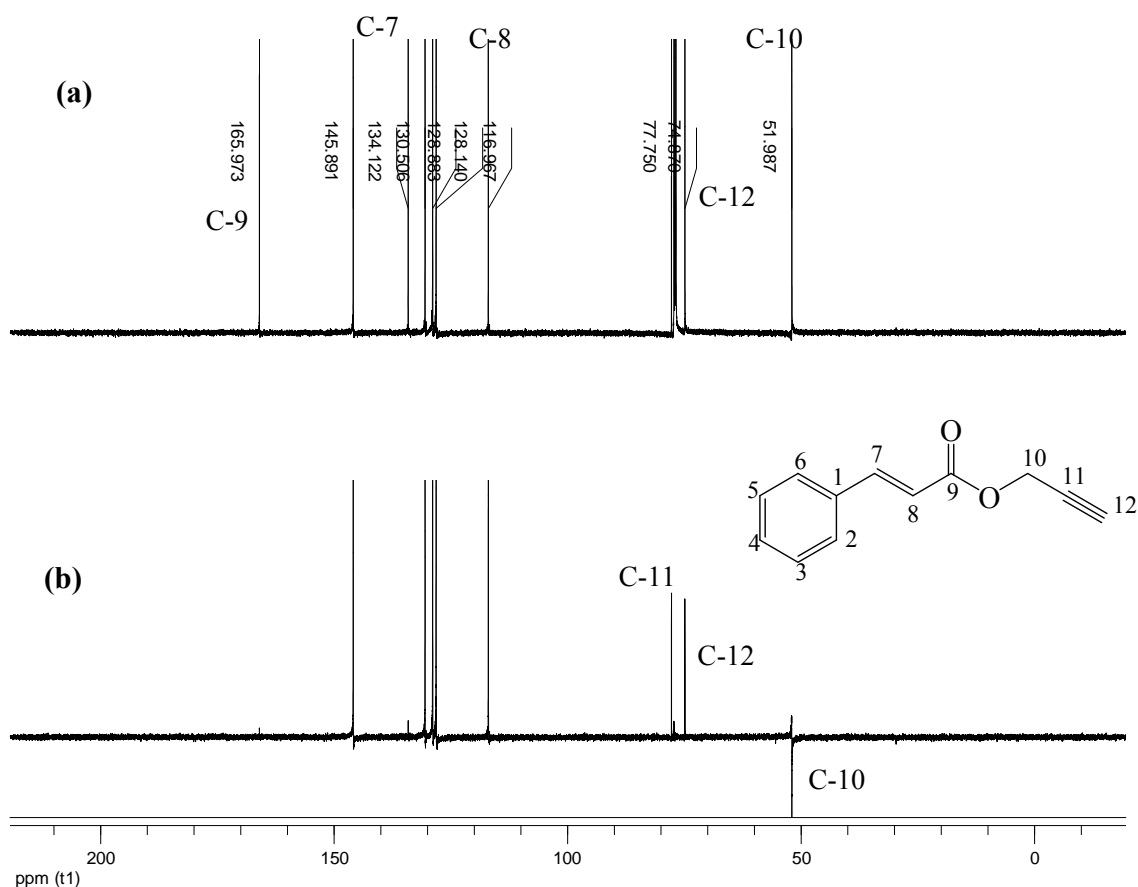
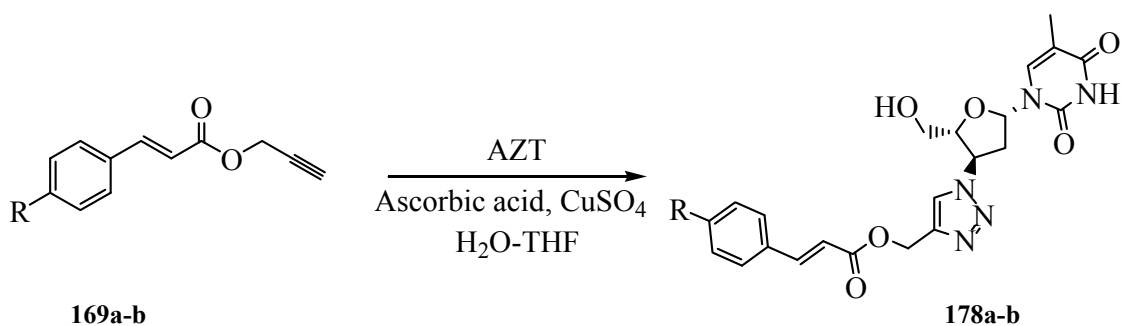


Figure 3.14. 150 MHz ^{13}C NMR (a) and DEPT-135 NMR (b) spectra of compound **177a** in CDCl_3

The final step in this pathway was a click reaction of compound **177a** with AZT according to a method used by Olomola for the coupling of cinnamate ester conjugates with AZT.⁸¹ To a stirred solution of AZT and propargyl derivatives (compounds **177a** and **177b**) dissolved in a 1:1 mixture of H_2O -THF were sequentially added CuSO_4 (0.1 mmol, 0.02 g) and ascorbic acid (0.1 mmol, 0.025 g) and the reaction mixture was stirred at room temperature for 24 hours (Scheme 3.13). After work-up and purification by chromatography, novel compounds **178a** and **178b** were isolated in decent yields as reported in Scheme 3.13.



	R	Yield (%)
178a	H	57
178b	Cl	71

Scheme 3.13. Click reaction of cinnamate esters derivatives

In the HSQC NMR spectrum of compound **178a** (Figure 3.15), the fingerprint of the AZT moiety was clearly observed (see ^1H NMR of compound **112a**, section 2.3.1.4) with only slightly different chemical shifts. The disappearance of the alkyne carbons C-12 and C-11 from compound **177a** at 74.8 ppm and 77.8 ppm were noticed while new alkene signals at 125.8 ppm and 144.4 ppm appeared in the HSQC and the DEPT-135 NMR spectra (Figure 3.15 and Figure 3.16). Correlations in the HSQC NMR spectrum of compound **178a** (Figure 3.15) confirmed the presence of the vinylic proton H-12 correlating with the carbon signal at 118.4 ppm. The vicinal vinylic carbon C-21 resonates at 138.2 ppm while the three asymmetric carbon signals of C-13, C-16 and C-15 appear distinctively at 61.2 ppm, 86.4 ppm and 86.8 ppm respectively. Signals at 168.1 ppm, 167.1 ppm and 152.8 ppm correspond to the carbonyl quaternary carbons C-9, C-19 and C-18 whose presence was also confirmed in the DEPT-135 NMR spectrum (Figure 3.16). The HMBC spectrum (Figure 3.17) revealed a correlation between the vinylic carbon C-12 and the methyne proton H-13. Correlations on the COSY NMR spectrum also confirmed these assignments.

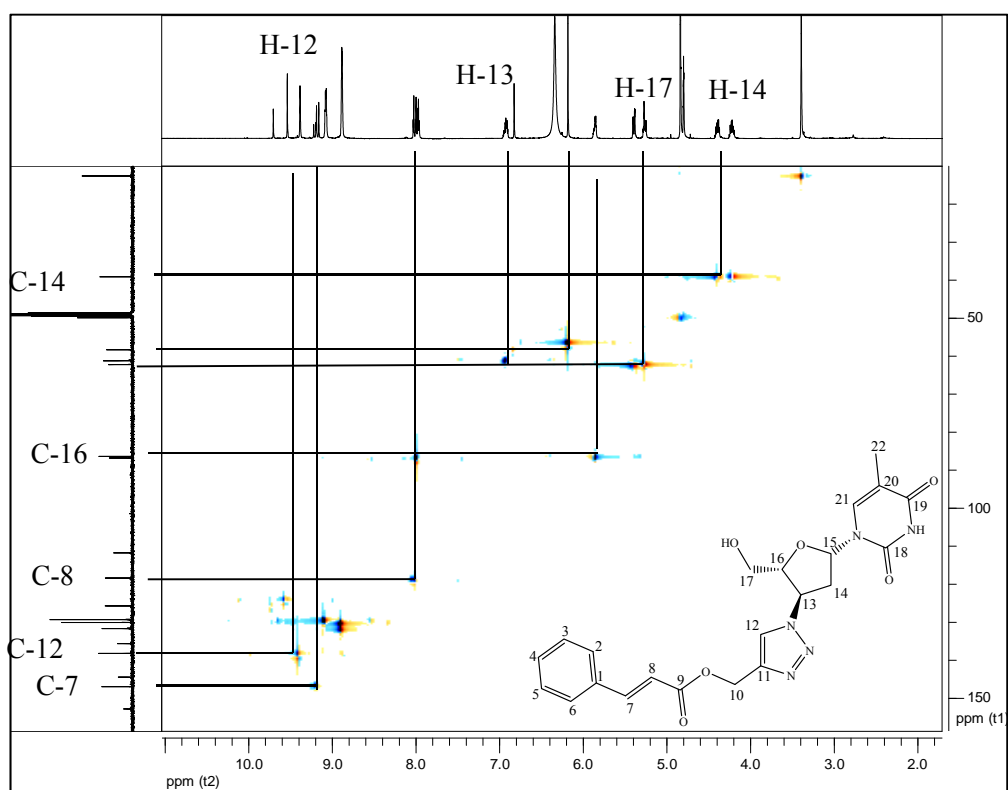


Figure 3.15. HSQC NMR spectrum of compound **178a** in $\text{MeOH-}d_4$

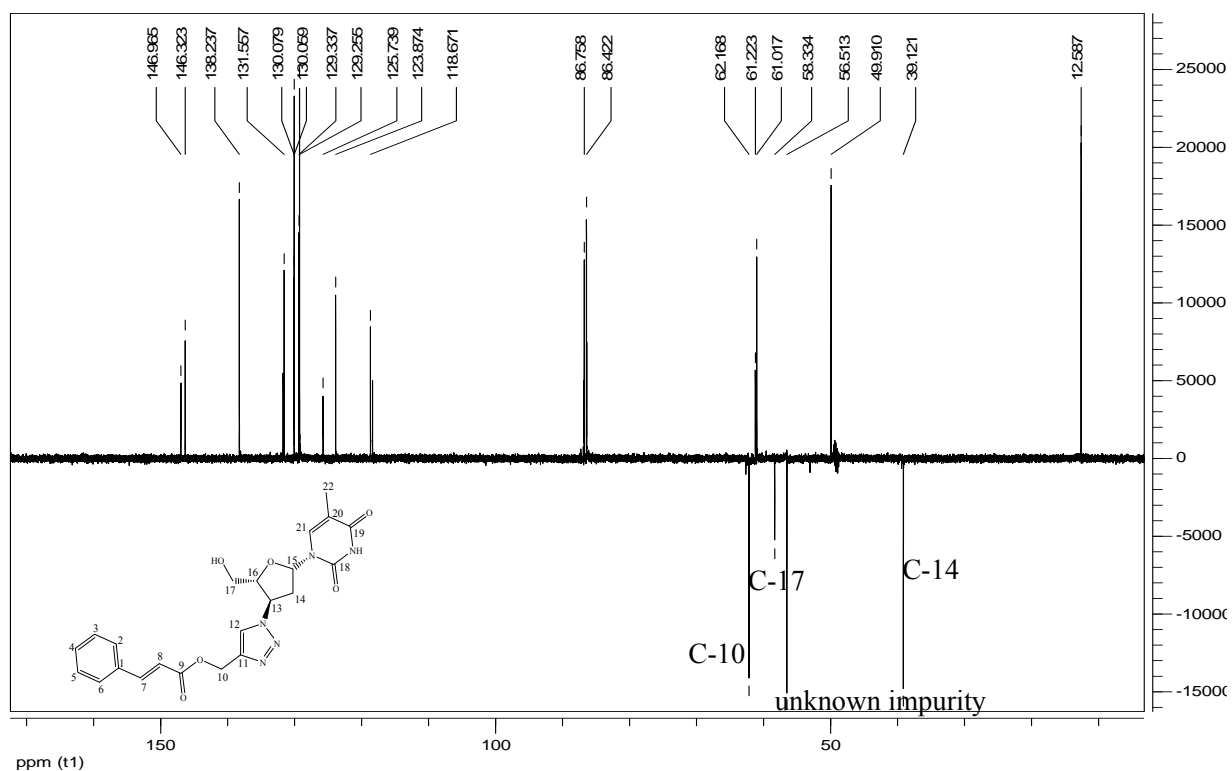


Figure 3.16. DEPT-135 spectrum of compound **178a** in MeOH- d_4

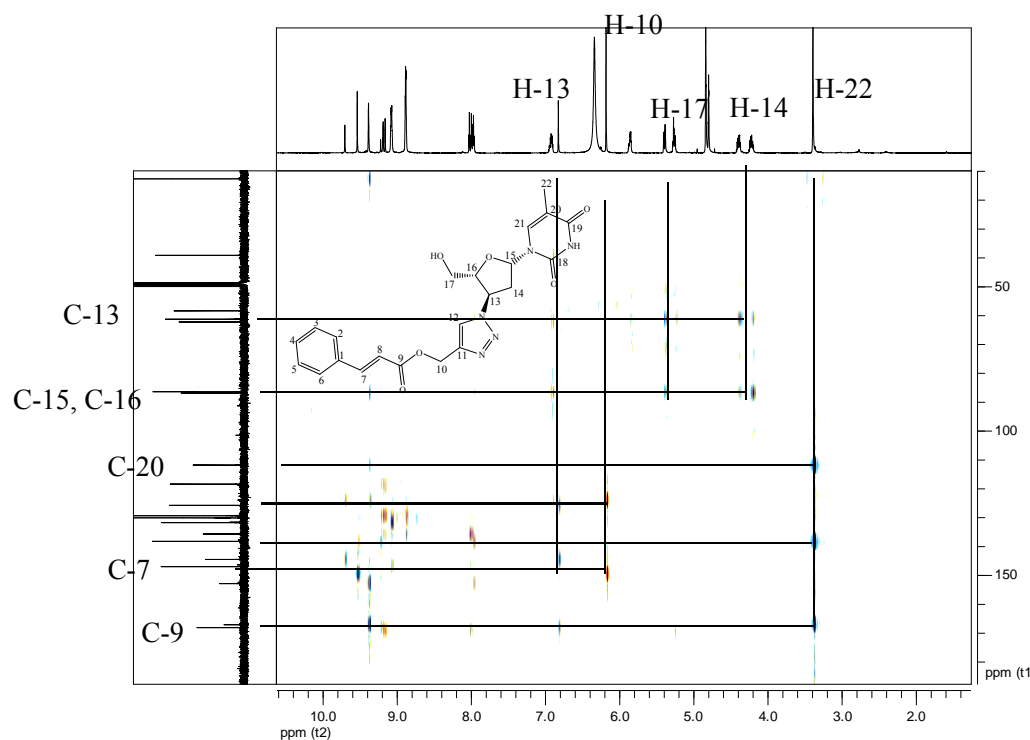


Figure 3.17. HMBC NMR spectrum of compound **178a** in $\text{MeOH-}d_4$

3.3. SUMMARY

Cinnamoyl derivatives including acrylamides, acrylic acids, cinnamate esters, protected amino acid cinnamate analogs and cinnamate-AZT conjugates were successfully synthesized in good yields *via* aldol condensation, peptide chemistry and click chemistry. These compounds were fully characterized by means of NMR spectroscopy and IR.

CHAPTER FOUR

EVALUATION OF COMPOUNDS AS HIV-1 ENZYME INHIBITORS

4.1. INTRODUCTION

Computer-aided drug design is an exceptionally powerful tool to visualize and explore the activity profile of a suggested compound within a known receptor. Computational approaches such as molecular modelling are capable of predicting ligand-receptor interactions at the active binding sites of a biological protein target. The strength of these interactions can be predicted and compared across a range of ligands.

4.1.1. Background: Molecular modelling

Drug discovery is hampered by the screening processes and clinical trials through which drug candidates are selected. Even though these processes are essential for safety concerns, they are time consuming and costly.³⁰⁸ Pharmaceutical companies spend more than 403 million dollars for each new drug to become commercially available.³⁰⁹ In addition, according to the California Biomedical Research Association it takes an average of 12 years for a drug to move from the research laboratory to the patient.³¹⁰

Proteins are macromolecules possessing a defined three dimensional structure composed of a sequence of linear chains of 20 unique amino acids. Enzymes are functional proteins operating as biological catalysts in biochemical reactions in the human body. On the other hand, ligands (drug candidates) are small molecules that interact with proteins by either inhibiting or improving their activity. The binding property of a ligand to a protein is used *in silico* in docking-based screening of drug candidates against a specific protein and has been shown to be a very useful approach in drug discovery.³¹¹ The exact complex structure of the atoms of a drug candidate and a protein can be visualized by performing docking studies and hence the functionalities of ligands can be modified in order to enhance their binding affinity and consequently their activity.³¹¹

In the process of designing an inhibitor against an enzyme, a drug has to selectively inhibit a protein without affecting alternative structures present in the system such as

glands, organs etc. Through binding, an inhibitor can stop a natural substrate from entering the active site of an enzyme and/or hinder the enzyme from catalyzing a reaction. Thus, molecular docking is a fast and efficient screening methodology since the strength of interactions and the activity of a large database of ligands can be predicted before carrying out their syntheses against the targeted protein.³¹²⁻³¹⁴ With the rapid development of computer technology in the past three decades and the easy accessibility of programs performing complicated computer calculations, Computer Aided Molecular Design (CAMD) has become an excellent means to explore the molecular design of some novel drugs. Hence, it is an important route to the inexpensive identification of lead compounds and therefore helps in saving resources.³¹⁵

4.1.1.1. Molecular modelling principles

The aim of docking studies is to fit a compound into an established three-dimensional binding site in order to analyze ligand conformation, orientation and possible molecular interactions such as hydrogen bonding, hydrophobic interactions and bonds to metals.^{312, 316} In addition, docking results can also suggest relative orientations of functional groups within a ligand with desirable binding interactions.³¹⁶ The best orientation of the ligand forms a complex with the protein and bears an overall minimum energy. In principle, molecular modelling is based on calculations performed by algorithms which determine the energy minimization of the protein-ligand complex. Energy minimization is essential since it involves repeated evaluation of various bonded and non-bonded interactions of a complex. Since the optimal orientation of the ligands in the receptor is required, their flexibility facilitates the interactions with the binding site of the protein. Binding site mapping is used to identify the region of the macromolecule presenting a high affinity for the ligand and hence confines the determination of binding interactions to a specific region.

4.1.1.2. Chemical interactions in molecular modelling

During the docking process, two interacting molecules exhibit a range of intermolecular forces.

Electrical forces: Depending on their electrical charges, the molecules interacting are either drawn together or pulled apart.

Electrodynamic forces: These are van der Waals (VDW) interactions. They are most significant when the two atoms are close and have a large contact surface area since they represent the sum of the attractive or repulsive forces between dipoles in the interacting molecules.

Steric forces: These occur when the proximity of the interacting atoms in the two molecules start affecting their reactivity. Consequently, chemical reactions and the free energy of a system can be modified.

Solvent related forces: These forces appear during chemical reactions between the solvent, the ligand and the macromolecule. The interaction of a protein with a ligand is a coordinated process that involves the breakage and formation of several hydrogen bonds, including the reorganization of water molecules around the ligand and within the protein active site.³¹⁵ Solvent related forces involve covalent and non-covalent bonds including hydrophilic (Hydrogen bonds occurring between the hydrogen atom of the donor interacting with an atom of the receptor) and hydrophobic interactions. Hydrogen bonds are considered to be the most important interactions to consider when docking studies are performed.³¹¹ Hydrophobic interactions are associated with the release of water molecules from the protein active site and the ligand. They play a significant role in complex formation, predominantly contributing to the total entropy change and, in some cases, to the total free energy of binding.³¹⁵

Pi stacking (or π - π stacking): Peptides are made of arrangements of aliphatic and aromatic amino acids. The aromatic rings interact with each other within the protein backbone and with aromatic ligands through π - π stacking interactions. These attractive non-bonding interactions between aromatic systems are important in stabilizing the conformations of the macromolecule-ligand complex.³¹⁷

4.1.2. Docking modes

According to molecular dynamic theory, the intermolecular interfaces between the ligand and the macromolecule can lead to a rigid or a flexible docking mode.

4.1.2.1. Rigid body docking

The search for strong interactions based on energy levels is achieved by using various docking modes. Two molecules interacting can exhibit billions of different possible conformations. The evaluation of these conformations by using energy functions requires long computational runtime. To circumvent this problem, some approximations can be made. A lock-and-key model, where the protein/enzyme is the lock and the ligand/drug is the key, can be adopted with the two molecules considered rigid. This approach is named a rigid body docking mode. However, this method is not accurate since a precise prediction of protein–ligand interactions requires the flexibility of the ligand and the protein surface in the docking protocol. The reason being that an optimal flexibility of the ligand and the macromolecule will lead to maximum interactions of the ligand with the binding site of the enzyme.³¹⁸

4.1.2.2. Flexible ligand docking

Considering the disadvantages of rigid body docking, a full flexibility of the ligand can be considered. If the macromolecule is maintained in a rigid state, then the computational time required for the process is reasonable. The reason is that by considering the flexibility of the entire macromolecule, the calculation of the receptor energy will require computing power beyond that of common personal computers since flexible regions must be evaluated by a full pairwise energy evaluation.³¹⁹ In this case, the macromolecule is maintained rigid in a conformation corresponding to the crystallographic structure determined for the enzyme with a known inhibitor (eg ritonavir, 5 CITEP) which is removed *in silico* before the docking. The new ligand occupies the active site where the original inhibitor was located.³²⁰ This method is more reliable, since the multiple conformations adopted by the ligand in the binding site can be evaluated.

4.1.2.3. Flexible protein docking

Nonetheless, during real molecular docking, the protein and the ligand are in constant motion.³²¹ In order to adequately approximate this computationally, programs have been devised which take into account some degree of flexibility of the protein (Molecular

dynamics, Monte Carlo methods).³²² However, docking simulations with a fully flexible target are still not feasible.

4.1.3. Major steps in molecular docking

For the purpose of our study, a flexible ligand docking mode was used. In order to carry out this docking mode, important steps need to be followed.

Data on the shape of a protein and drug are usually available separately. Docking studies help to tie a protein and a drug together and visualize them in three dimensions. For this purpose, each component involved in the docking process has to go through some preparatory steps discussed below.

4.1.3.1. Preparation of the receptor

The Protein Data Bank (PDB) is a large database of protein-ligand complexes accessible online.³²³ It is a bank of biological macromolecular crystal structures established at the Brookhaven National Laboratories (BNL) in 1971. A cursory glance through the PDB revealed that it contains approximately 1200 protein structures. The aim of the PDB is to develop a means of exchanging information between databases. The Research Collaboratory for Structural Bioinformatics (RCSB) is the system responsible for the management of PDB data deposition, processing and distribution.³²⁴ The 3D structure of the receptors used in this study were downloaded from the PDB. However, X-ray crystal structures usually have to go through some modifications before being operational in docking software. Such modifications include removing unnecessary molecules such as water, ligands, atoms and ions, stabilizing charges, filling in the missing atoms (hydrogen), assigning atom types and generating side chains according to the parameters available.

4.1.3.2. Active site identification

It can happen that a receptor has many active sites and the one of interest should be identified. The dimensions of the cuboid grid box defining the active site of the macromolecule are more accurate when they are centered on the coordinates of the ligand in the original PDB file and also when they provide enough space for the ligand to rotate

freely.³²⁵ Alternatively, a “*blind docking*” could be executed with default parameters in order to first identify the favorable binding site of the ligand. A smaller grid volume could then be built around the ligand-binding site located afterwards (Figure 4.1).

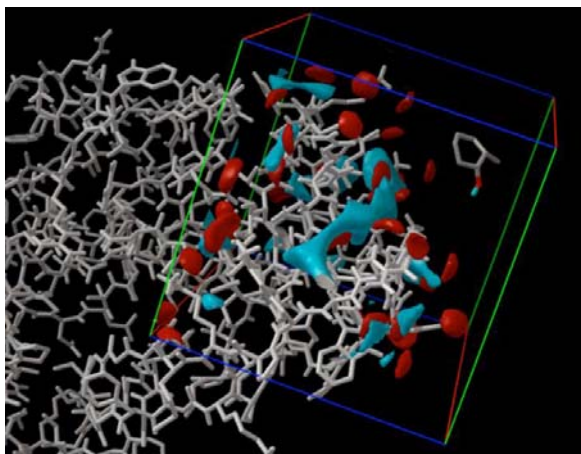


Figure 4.1 Viewing grids in AUTODOCK tools. The protein backbone is shown in white bonds. The grid box is represented as a cuboid in red/blue/green lines. A ligand is shown in the grid box at the upper right

4.1.2.3. Preparation of the ligand

Chemical compounds used for virtual screening can be obtained from various databases such as ZINC and PubChem.³²⁶ They can also be drawn by using chemical drawing tools such as Chems sketch®³²⁷ or Chemdraw®³²⁸ and imported into Vega ZZ®³²⁹ where charges on the ligand can be calculated, torsions edited around rotatable bonds and conformational searches executed to find those conformers with lowest energy. Another route could be to simply draw the structure of the ligand in Discovery Studio Visualizer (DSV)³³⁰, clean up the structure and save it as a pdb file for use in a further docking procedure. In order to fit in an enzyme active site, a ligand must not be too large or have a wrong shape. After these steps, the calculation is carried out and the results interpreted.

4.1.4. Docking calculations

This is the step where the ligand is actually docked into the receptor active site using any of various docking programs.

4.1.4.1. Docking programs

A range of nearly 60 different docking programs are currently available.³¹⁴ AUTODOCK, Genetic Optimization for Ligand Docking (GOLD), FlexX, DOCK and ICM (Internal Coordinate Mechanics) are the most popular software packages used and they all address the flexible ligand docking mode.³³¹ Based on the conformational search of the flexible ligand, they can be split into two groups: the first case is where the ligand fits into the macromolecule active site by matching (DOCK and FlexX) whereas in the second scenario the ligand fits by optimal ligand conformation search through global energy optimization (AUTODOCK, GOLD and ICM).³³² Since AUTODOCK is the most cited docking software in scientific publications and therefore the program used in our study, the characteristics of Autodock will be discussed below while the characteristics of the other software cited above are mentioned in Appendix (A.2).

AUTODOCK

The program AUTODOCK was developed by Morris in 1998 as an improvement of the first version written in 1990 by Goodsell.³³³ One of the most powerful features of AUTODOCK is that, it is not only possible to dock a flexible ligand into a rigid macromolecule, but also to select amino acid residues of the macromolecule that can be considered flexible during the docking.

AUTODOCK 4.0 software is constituted of two main sub-programs running in tandem: autodock and AutoGrid. Autodock combines a rapid grid-based method for energy evaluation and pre-calculation of ligand-protein pairwise interaction as a 3-dimensional energy grid of equally spaced discrete points for a rapid energy evaluation. To achieve this objective, it uses AutoGrid, whose function is to pick out interesting parts of the active site giving favorable interactions.^{246, 311, 333} The grids allow a quick computation of the interaction energy of the protein-ligand complex (Figure 4.1). AUTODOCK combines an empirical free energy force field with a Lamarckian Genetic Algorithm (LGA), providing fast prediction of bound conformations with predicted free energies of association.³¹⁹

AUTODOCK uses a molecular mechanics model for enthalpic contributions such as VDW interactions, hydrogen bonding, and an empirical model for entropic changes upon

binding. Torsion angles are randomly assigned to rotatable bonds and the overall rotation is arbitrarily specified as well. The docking is done by using the Monte Carlo method or the Simulated Annealing (SA) method where, at each point, the program adjusts each of the degrees of freedom of the ligand or the flexible residue of the macromolecule and searches for the global minimum of the energy function.³³² A maximum of 100 million energy evaluations are allowed for each docking. A scoring function identifies good docked conformations based on their energy level.

Even though AUTODOCK seems to be the more reliable program in docking studies, depending on the nature of the ligand, a different program could be more indicated since each program possess a different algorithm.³³⁴ Furthermore, it is also important to always find a right balance between the results of AUTODOCK simulations and biological experiments which at times are different.

4.1.4.2. Evaluation of the docking results

The conformer of the protein-ligand complex with the lowest energy out of all the docked conformers obtained is selected and opened in Discovery Studio Visualizer. Several parameters can be of interest during this analysis:

The analysis of the receptor-ligand complex model relies on parameters such as binding energy, ligand efficiency, inhibition constants, intermolecular energy, electrostatic energy, torsional energy between bonds, unbound energy, π - π stacking interactions, hydrogen bonds and hydrophobic interactions.^{313, 335}

Inhibition constant IC₅₀: The effectiveness of a potential drug is expressed as a measure of enzyme inhibition.³³⁶ The half maximal inhibitory concentration (IC₅₀) is a measure of the effectiveness of a compound in inhibiting biological or biochemical functions (catalysis for instance). A prediction of that value can be obtained by processing docking results. It has been established that highly active drugs possess IC₅₀ values within nanomolar range.^{337, 338}

Atom-atom distance interaction: The existence of interactions between two atoms is determined by the energy produced by the interaction. This energy is affected by many

variables, particularly the distance between the two atoms. The interaction energy is inversely proportional to the distance (within Å unit area) between two intermolecular atoms. Thus, the closer the atoms are, the stronger is their interaction.

4.1.5. Limitations of molecular modelling

Even though molecular modelling provides a useful framework for the generation of hypotheses in the design of new drugs, numerous (and often unreported) limitations are encountered.^{339, 340} Scoring functions used in docking programs make a number of simplifications and assumptions to allow a more computationally efficient evaluation of ligand affinity, often at the cost of the accuracy of the results.

- Most of the structures from the PDB do not meet the quality criteria required for modelling studies. For instance, some atoms in the flexible part of the protein have limited resolution and consequently their corresponding spatial coordinates are omitted in the pdb file.
- The different conformational states of the protein which have similar energies are often not taken into consideration in docking studies.³²⁰
- Force fields are generally not reactive, therefore bond breakage and bond formation are not possible to simulate.³³⁹ This automatically excludes protein-ligand interactions which result in covalent bond formation.
- Electrostatics has a tremendous role in molecular recognition, in the dynamics of protein folding, and in protein-ligand interactions. However, in molecular modelling, electrostatic interactions rely only on the concept of charges associated with the nuclei. The representation of electrostatics with a charge on each atom fails to reproduce the electrostatic potential surrounding a molecule as estimated by quantum mechanics. In addition, since molecular orbitals are not spherically symmetrical, the implicit assumption of monopole electrostatics is not correct.
- One of the potentially significant errors in these predictions is the common assumption that the ligand binding affinity contributions of non-covalent interactions are additive.³⁴⁰
- Polarizability effects are not taken into consideration in van der Waals interactions since fixed parameters are used during the simulations.

- The transferability of the typical atom parameter sets of different force fields is not always precise.
- Water molecules play a significant role in protein–ligand docking, either as intermediaries, by establishing hydrogen bonds between the protein and the ligand or by being displaced by the ligand. However, explicit water molecules are usually not taken into account in docking studies.

In general, the limiting assumptions are not always compatible with the system under investigation. These disadvantages indicate that computational results do not necessarily accurately predict the experimental data. Efforts to overcome these inadequacies could include multipole electrostatics and polarizability through the use of more sophisticated, second-generation force fields such as AMOEBA.³⁴¹ Also, *in vitro* assays need to be carried out in order to verify docking data. Nevertheless, HIV protease drug development has been significantly improved by performing docking studies on potential drug candidates.³⁴²⁻³⁴⁴

4.1.6. *In vitro* biological assays

It is important to understand the mechanism of action of a target enzyme for the development of drug candidates through Structure-Activity Relationship (SAR) studies but it is also important to carry out assays which test their potential inhibitory activity in enzymatic reactions in a real system. These biological tests are used to study how synthetic compounds at physiological concentrations will inhibit enzymatic activity and finally conclude if the target inhibitors have any medicinal potency.

4.1.6.1. HIV-1 protease fluorometric analysis

Several methods have been developed for the assay of HIV-PR activity. These include a chromatographic assay with ultraviolet (UV) detection for HIV-PR activity, colorimetric assay using two non-enzymatic reactions in a microtiter plate for the high-throughput screening of HIV-PR inhibitors, a solid-phase immunoassay, an enzyme-linked immune-sorbent assay (ELISA) and a fluorescence resonance energy transfer (FRET)-based assay.³⁴⁵ Since fluorometric FRET peptide assays are subject to less interference from the

autofluorescence of test compounds and cellular components involved in the enzymatic reaction, they provide better sensitivity than colorimetric assays.

The FRET based fluorogenic peptide used in this study is derived from the native P17/P24 cleavage site on the precursor polyprotein Pr^{gag} of the HIV-1 protease. As illustrated in Figure 4.2, the fluorescence of Hilyte Fluor 488 is quenched by QXL 520 until the peptide is cleaved into two separate fragments by HIV-PR. Incubation of the HIV-1 PR with the FRET peptide substrate results in specific cleavage and a time-dependent increase in fluorescence intensity linearly related to the extent of substrate hydrolysis. Consequently there are changes in fluorescence which can be monitored by excitation/emission at 490 nm/520 nm. Thus, any inhibitory activity corresponds to the formation of a plateau or a decrease in the rate of change of fluorescence.

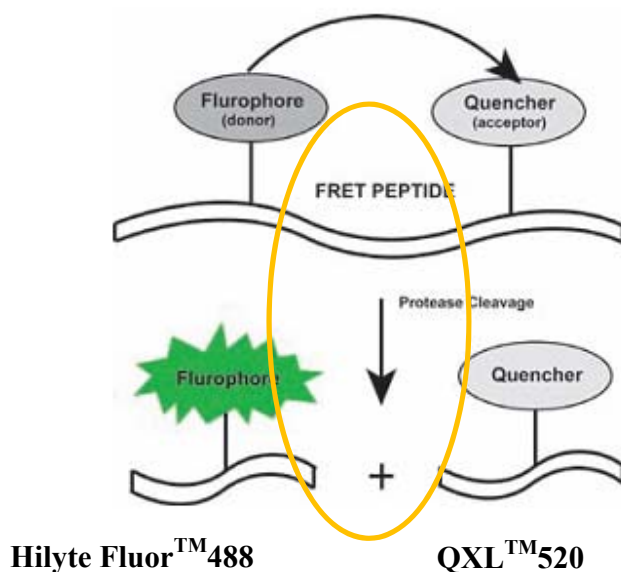


Figure 4.2. Schematic representation of a FRET peptide proteolytic cleavage by HIV-1 protease

When the FRET peptide and the PI are excited at 490 nm, photons are emitted spontaneously at 520 nm. In this study, a continuous enzyme assay with regular readings of activity was used to perform kinetics studies of the fluorescence intensities as a

function of time which gave the rate of inhibition of PIs from a non-linear regression analysis of the Michaelis-Menten equation.³⁴⁶

4.1.6.2. HIV-1 reverse transcriptase colorimetric analysis

As already mentioned in Section 1.1.1, the HIV-1 RT enzyme catalyses both RNA directed DNA synthesis and DNA directed DNA synthesis in the host cell.²⁹⁹ Retroviral propagation *in vitro* has been used to test HIV-1 RT activity *via* scintillation proximity assay,³⁴⁷ reporter ribozyme assay³⁴⁸ and a colorimetric assay.³⁴⁹ In these assays, the use of RT as a marker for DNA production is used as a parameter to determine its activity.³⁵⁰ The method is described in Figure 4.3. A biotin-labeled DNA/RNA hybrid complex bearing digoxigenin (DIG) and the RT enzyme are bound to a streptavidin coated microplate in the first step. Next, a DIG antibody conjugated to peroxidase (anti-DIG-POD) binds to the digoxigenin-labeled DNA. Subsequent to the addition of the peroxidase substrate ABTS, the peroxidase enzyme catalyses the cleavage of the substrate and the colored reaction product whose absorbance is detected in solution by using a microplate reader. Since the role of the inhibitor is to prevent the RT from cleaving the substrate, a correlation between the RT activity and the absorbances of the products of the enzymatic reaction can be drawn. When no DNA is formed due to the activity of an inhibitor, there is no attachment of anti-DIG-POD to the hybrid complex and DIG is washed away when the plates are rinsed by the washing buffer solution.

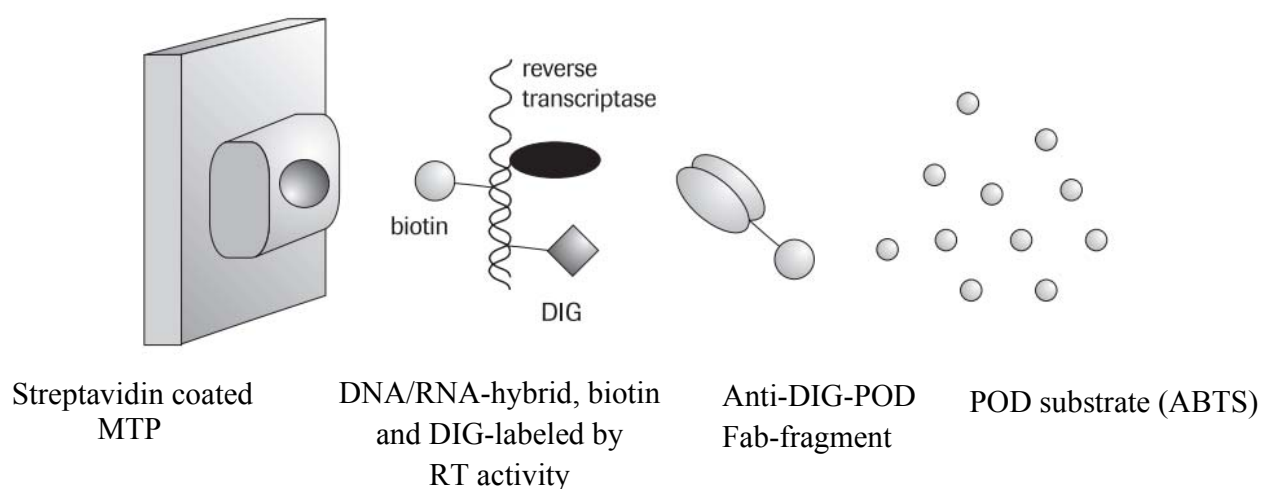


Figure 4.3. Schematic representation of the RT colorimetric assay

4.1.6.3. HIV-1 integrase colorimetric analysis

IN activity can be determined in a variety of ways, namely a cell-based assay,¹⁵ a fluorescent HIV-1 IN DNA binding assay,³⁵¹ a subviral preintegration complex (PICs) assay,³⁵² a non-radioactive enzyme-linked immunosorbent assay (ELISA) based on HIV-1 integrase^{23, 353} and an HIV-1 IN colorimetric assay.³⁵⁴

The principle of these assays share the common characteristic of mimicking the processing and joining reactions of the HIV-1 IN enzyme during the HIV-1 replicative cycle in a biological system (see Section 1.1.1.2).

The protocol for this assay is outlined as follows: first, streptavidine-coated 96-well plates are loaded with a double stranded donor substrate HIV-1 DS DNA. Second, HIV-1 IN enzyme is loaded onto the DS DNA and a target substrate TS DNA is added. During, the enzymatic reaction, IN cleaves the 3'-end of the DS DNA and integrates the DS DNA into the TS DNA by strand transfer recombination.^{23, 355} UV/Vis absorbance is used in conjunction with an HPR-labeled antibody targeting modifications on the TS DNA 3'-end are carried out and when the IN enzyme is interacting with IN inhibitors, a decrease in absorbance is observed.

4.1.7. Saturation Transfer Difference (STD) NMR experiments

Saturation Transfer Difference (STD) is a ligand-based NMR technique used to determine the binding or interactions of small molecules (ligands) to a targeted protein.³⁵⁶⁻³⁵⁸ This technique has been widely employed not only to identify bioactive compounds but also to elucidate which ligands are binding in a mixture of several ligands.^{359, 360} The concentrations required are optimised under weak binding conditions with a dissociation constant (K_d) between 10^{-3} to 10^{-7} M.³⁶¹ The principle behind STD NMR experiments is simple: upon irradiation of a mixture of a protein with up to 7 different ligands, there is intermolecular transfer of magnetisation from the protein to the bounded ligands. Consequently, a fast chemical exchange of ligand molecules from the bound to the free-state takes place and the saturation is transferred into solution where the STD effect is detected.^{359, 362} The difference spectrum is obtained by subtracting the

saturated spectrum from the spectrum without protein saturation and the STD spectrum will only show the signals of the ligands which experience intensity changes and are therefore at some stage in the proximity of the protein.³⁶¹ Additionally, the ligand protons close to the protein will have the strongest signal in the STD spectrum since they are saturated to the highest degree.³⁶³ Quantitative analysis can be carried out on an STD NMR experiment in order to gauge more detail about ligand binding to the enzyme but for the purpose of this project, the focus was on qualitative STD analysis where the emphasis was placed on the structure of the ligand binding to the protein.

4.2. BIOLOGICAL RESULTS AND DISCUSSION

4.2.1. Qualitative assessment of binding by STD NMR

4.2.1.1. STD NMR on BSA (Bovine Serum Albumin)

It is known that L-tryptophan binds to BSA while glucose does not.³⁶⁴ Inspired by an experiment previously carried out in our research group by Conibear, the binding affinity of L-tryptophan to BSA was analyzed as a model system to confirm the parameters of the STD pulse program.³⁶⁵

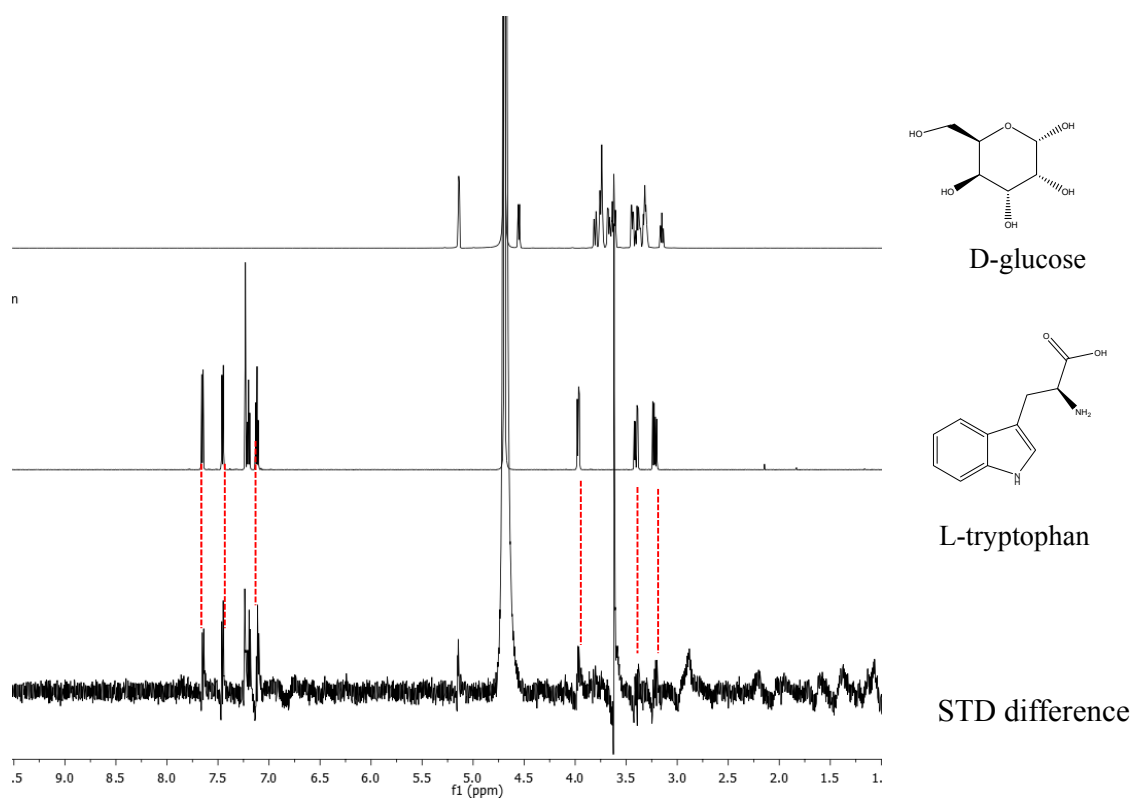


Figure 4.4. BSA STD difference spectrum (bottom) in D₂O with ¹H NMR spectra of ligands **D-glucose** (top) and **L-tryptophan** (middle). L-tryptophan signals are shown in the difference spectrum (red dotted lines)

As indicated in Figure 4.4, whilst the protons signals from L-tryptophan were clearly identified on the STD NMR spectrum, the absence of the glucose signals was consistent with the fact that glucose does not bind to BSA.

4.2.1.2. STD NMR on HIV-1 IN

Using the same parameters for the STD experiment carried out with BSA, D-glucose and L-tryptophan, an STD experiment was conducted with ligands **178a**, **170b**, **169e**, **169d** and HIV-1 IN. In this case a spin lock filter was incorporated in order to suppress the enzyme signals.

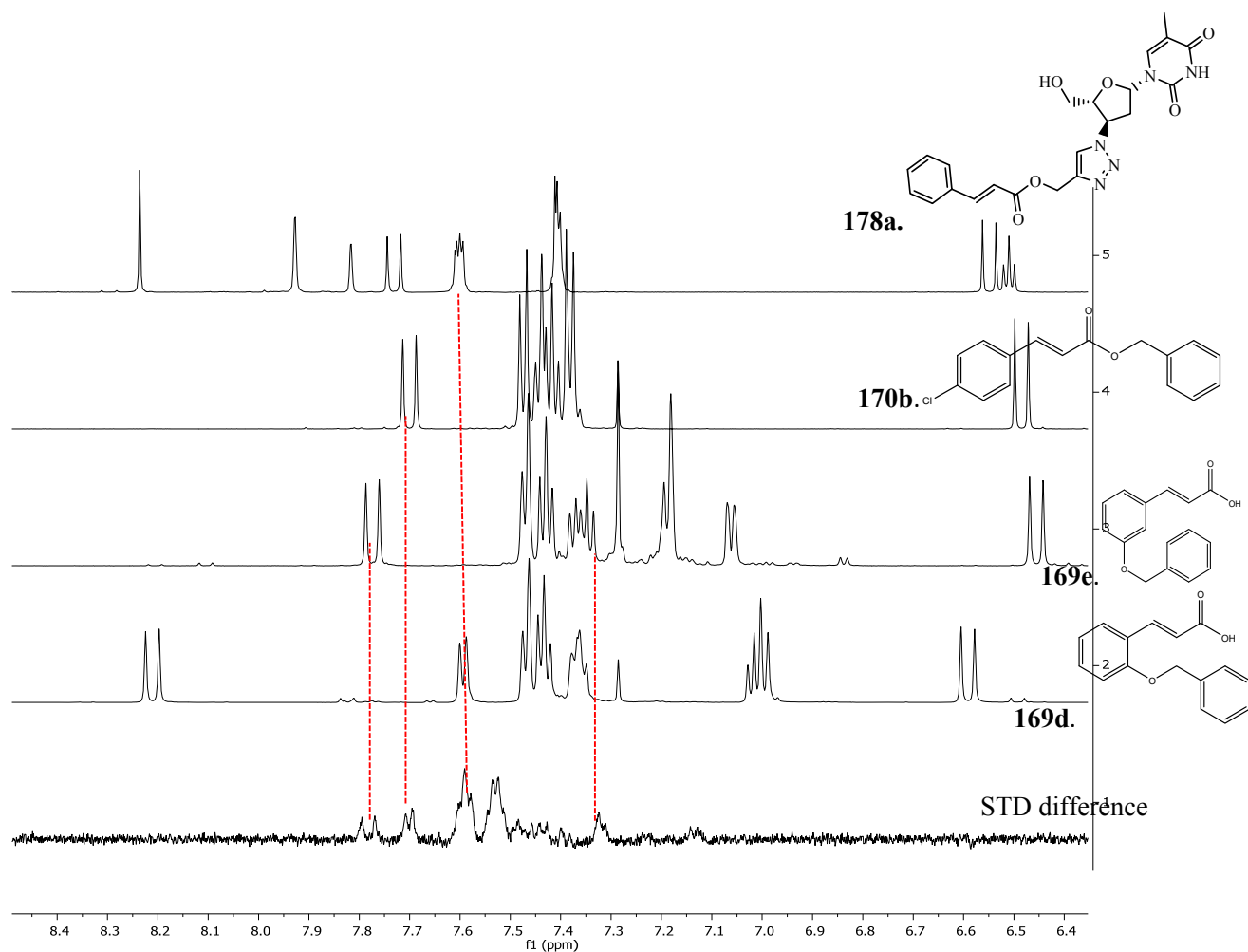


Figure 4.5. HIV-1 IN STD difference spectrum of compounds showing correlations between characteristic ligand signals and signals in the STD difference spectrum (red dotted lines) in D₂O.

The individual stacked spectra of the ¹H NMR of ligands **178a**, **170b**, **169e**, **169d** and the HIV-1 IN STD spectrum showed some correlations between the ligands **170b**, **169e**, **169d** and the difference spectrum, indicative of ligand binding (Figure 4.5). This was due to the fact that only some functionalities of the ligand effectively bind in the active site of the enzyme and not the entire molecule. Thus, we noticed that only the aromatic rings of the ligands were bound to the IN enzyme. Ligand **178a** showed a very weak binding compared to the other ligands studied. Also, the similarity of the ¹H NMR signals of ligands **178a**, **170b**, **169e**, **169d** between 7 ppm and 8 ppm contributed to ambiguity in identifying which of the ligands was actually binding to HIV-1 IN. TOCSY (Total Correlation Spectroscopy) experiments using the MLEV pulse sequence (Malcolm Levitt's CPD sequence) are long range heteronuclear correlation 2D NMR experiments,

which show correlations between successive protons (over 5 to 6 bonds) within a given spin system.^{366, 367, 368} Since an STD TOCSY NMR experiment also depends on saturation transfer, this experiment was therefore carried out in order to increase the strength of the signals showing interactions of the ligands with HIV-1 IN. The ligand resonances were assigned using TOCSY spectroscopy.

To increase the spectral resolution, an HIV-1 IN STD TOCSY experiment of the IN enzyme and ligands **178a**, **170b**, **169e**, **169d** was conducted at body temperature (310 K). The spectrum of HIV-1 IN STD TOCSY was superimposed onto the TOCSY NMR spectra of ligands **178a**, **170b**, **169e**, **169d** (Figure 4.6) in order to find matches between the signals of the ligands with those of the HIV-1 IN STD TOCSY as a proof of the binding of the ligands to the IN enzyme. The superimposed spectra (Figure 4.6) showed a congested coupling network of the signals of the 4 ligands with the IN enzyme.

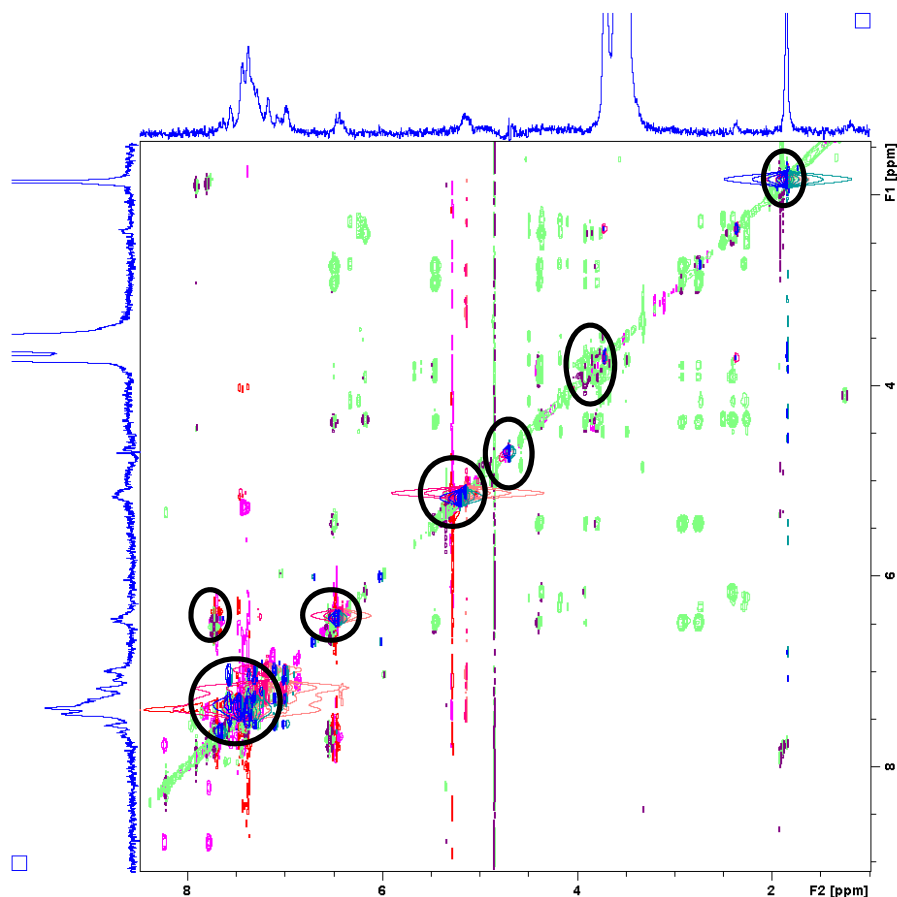


Figure 4.6. Superimposed spectra of HIV-1 IN STD TOCSY and TOCSY NMR spectra of ligands **178a**, **170b**, **169e**, **169d**. HIV-1 IN STD TOCSY spectrum is blue, TOCSY NMR spectrum of ligand **178a** is green, TOCSY NMR spectrum of ligand **170b** is pink, TOCSY NMR spectrum of ligand **169e** is red and TOCSY NMR spectrum of ligand **169d** is brown

Nevertheless, as highlighted in Figure 4.6 (black circles), the colored signals assigned to ligands **178a**, **170b**, **169e**, **169d** matched well with the blue signals of the STD TOCSY experiment. This observation also provided evidence that ligands **178a**, **170b**, **169e**, **169d** are in equilibrium with bound ligands attached to HIV-1 IN.

4.2.2. Computer modelling and biological assay studies

4.2.2.1. Docking studies of heterocycles for inhibition of HIV-1 PR (1HXW)

Docking simulations are receptor based methods in computer assisted drug design.³⁶⁹ Their value is in exploration of the binding mode of a ligand within the active site of an enzyme substrate.³⁷⁰ Docking simulations can also be used to monitor the effect of chemical changes in a class of ligands on their activity by examining the receptor ligand interactions. More interestingly, new synthetic targets can be explored *in silico* either to develop new inhibitors with potential activity or by enhancing existing lead compounds through modification.³⁷¹

Upon successful synthesis of a range of functionalized aromatic compounds, we proceeded to perform docking studies and subsequent evaluation of the structure–activity relationship of these compounds binding in the active site of the HIV-1 protease enzyme. As mentioned previously, there has been an ongoing interest in our research in the development of inexpensive compounds showing activity against PR which are robust to mutations. Consequently, we addressed the question of how the binding pattern, the conformational behavior and the chemical substitution of a protease inhibitor affect its activity. For this purpose, our attention was drawn to three different types of heterocycles: coumarins, indenols and benzotriazoles.

Software employed: *AUTODOCK 4.2 and Discovery Studio Visualiser 3.5 were the two software packages used to perform docking studies. AUTODOCK 4.2 was downloaded from www.scripps.edu, while Discovery Studio Visualiser 3.5 was downloaded from www.accelerys.com.*

4.2.2.1.1. Docking studies of coumarin-alkene derivatives

In the following study, attention was given to two classes of activated alkenes: nitriles and esters. Four different acrylates and acrylonitrile were substituted on the coumarin ring and the coumarin-alkene conjugates formed were docked in the active site of the protease enzyme 1HXW (PR) in order to study the effect of these substituents on their activity.

The docking of the coumarin-acrylonitrile compound **134a** in 1HXW (Figure 4.7) revealed that carbonyl C-2 was hydrogen bonded to the hydroxyl hydrogen of ASP 30 at a distance of 1.94 Å (A in Figure 4.7) while the oxygen atom O-1 interacted with the hydroxyl hydrogen of ASP 29 at the same distance (B). Furthermore, hydrophobic interactions of the coumarin ring with ASP 30, ASP 29 and ALA 28 residues were observed whilst the nitrile group was located in the hydrophobic pocket framed by ILE 50, THR 80, PRO 81 and VAL 82. The predicted inhibitory concentration was 55.08 μ M.

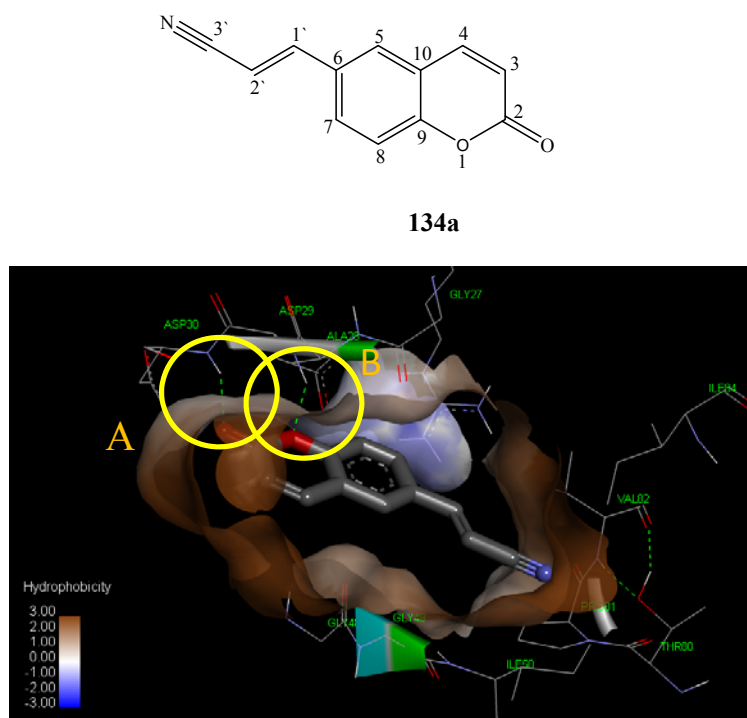


Figure 4.7. Three dimensional representation of compound **134a** in the active site of the HIV-1 protease enzyme (1HXW). Oxygen atoms are red, nitrogen atom is blue, carbon atoms of the protein and the ligand are grey, hydrogen bonds appear as green dots. (Predicted inhibitory concentration: **55.08 μ M**)

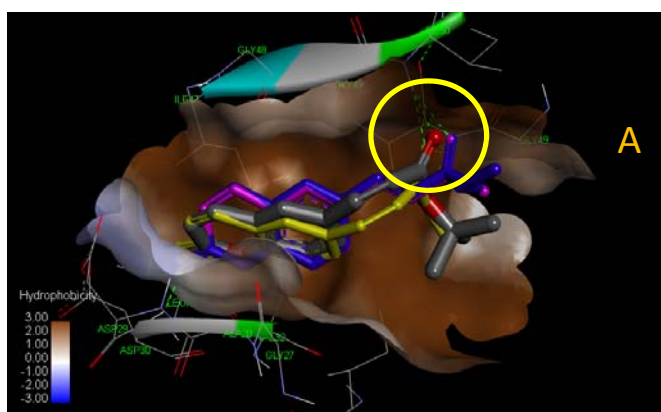
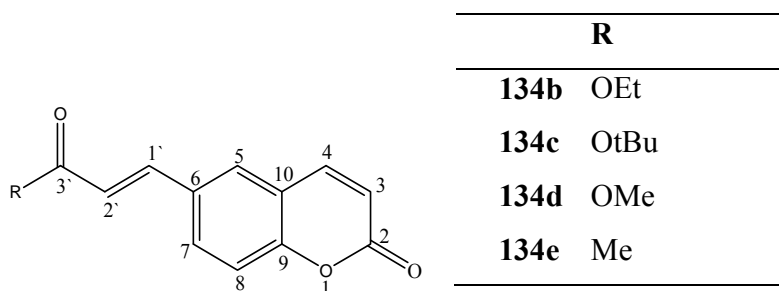


Figure 4.8. Superimposed three dimensional representation of compounds **134c**, **134b**, **134e** and **134d** in the active site of the HIV-1 protease enzyme (1HXW). Oxygen atoms are red, carbon atoms of the protein and the ligand are grey, hydrogen bonds appear as green dots, compound **134b** is blue, compound **134e** is purple and compound **134d** is yellow

Table 4.1. Interactions between HIV-1 PR and coumarin alkene derivatives

		134e	134c	134d	134b
Interactions	Hydrogen bonds	ASP 30, ILE 50	ILE 50	ILE 50	ILE 50, ASP 30
	Hydrophobic interactions of the coumarin ring	ASP 30, VAL 32, ILE 47	LEU 76, ASP 30, ASP 29, ALA 28, VAL 32	ILE 47, GLY 48, ASP 30	ILE 47, VAL 32, ILE 84
	Hydrophobic interactions of the R group	GLY 49, ILE 50	GLY 49, ILE 50	GLY 49, ILE 50	ILE 84, ILE 50
Predicted IC₅₀ (μM)		24.00	3.55	15.15	30.36

The docking of four coumarin alkene derivatives in 1HXW (PR) was examined (Figure 4.8). Carbonyl C-3' of these compounds were all hydrogen bonded to ILE 50 (A in Figure 4.8) while hydrophobic interactions occurred between the coumarin ring and the cavity formed by ASP 30, ILE 47 and VAL 32, and the R substituents buried in the hydrophobic pocket built by GLY 49 and ILE 50. A common observation was the interaction of all the ligands with either ASP 30 or ASP 29, reported as important amino acid residues in binding to the PR enzyme.^{372, 373} Although these compounds presented, more or less, the same mode of interaction, a significant increase in activity was observed in compound **134c** probably due to the spatial orientation of the methyl groups which increased the hydrophobicity. The good activity predicted for compound **134c** (Table 4.1) and the presence of a cinnamoyl fragment prompted us to investigate its activity in the integrase enzyme (1QS4). The cinnamoyl functional group is a structural feature reported to be active against the HIV-1 integrase enzyme.³⁷⁴ (See compound **134c**).

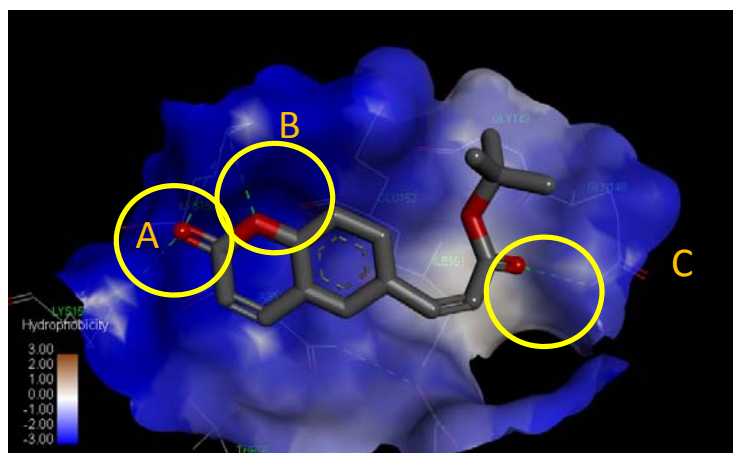
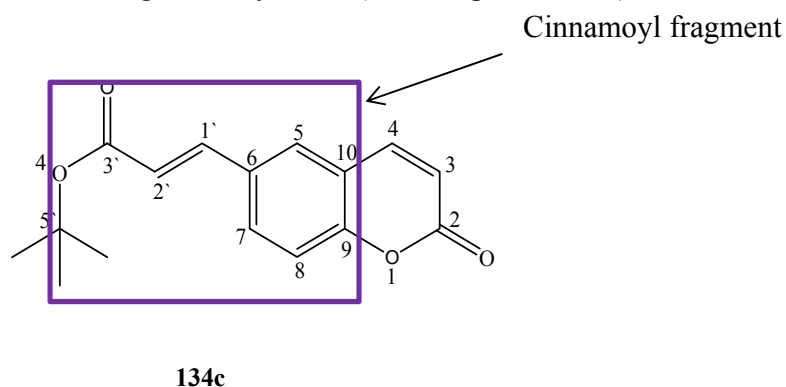


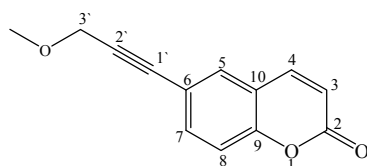
Figure 4.9. Three dimensional representation of compound **134c** in the active site of the HIV-1 integrase enzyme (1QS4). Oxygen atoms are red, carbon atoms of the protein and the ligand are grey, hydrogen bonds appear as green dots. (Predicted inhibitory concentration: **155.46 μ M**)

As indicated in Figure 4.9, compound **134c** showed some interactions in the active site of 1QS4 (IN). While the carbonyl C-2 interacted with the hydroxyl hydrogen of LYS 156 and LYS 159 (3.17 Å and 3.12 Å respectively) (A in Figure 4.9), oxygen O-2 was bound to the hydroxyl hydrogen of LYS 159 (2.75 Å) (B), and carbonyl C-3' to the hydroxyl hydrogen of GLN 148 (2.77 Å) (C). In the 1QS4 active site, hydrophilic interactions of the coumarin ring with TRH 66, LYS 156 and LYS 159 residues were observed instead when the *tert*-butylacrylate moiety was inserted in the pocket formed by GLY 149 and GLN 148. However, it turned out that the inhibition constant of compound **134c** in the integrase enzyme was drastically increased from 3.55 µM to 155.56 µM and therefore appeared to be a poor drug candidate for the inhibition of the HIV-1 integrase enzyme. Since the *tert*-butyl group was buried in an hydrophilic pocket, in order to increase the hydrophilicity of this ligand, we replaced the *tert*-butyl group by a methyl group (Compound **134d**) and a very poor inhibitory activity against HIV-1 IN upon docking was still observed (predicted IC₅₀ = 251.09 µM), indicating no improvement.

4.2.2.1.2. Docking studies of coumarin-alkyne analog

We were also interested in studying the behavior of an alkyne substituent on the coumarin backbone.

Compound **137** was also docked in 1HXW (PR) (Figure 4.10) and it appeared that besides having the same mode of hydrogen bonding and hydrophobic interactions as the coumarin-alkene derivatives, the methoxy substituent was located in the pocket delimited by ASP 30, LEU 76 and ILE 47 (B in Figure 4.10). The activity of compound **137** (IC₅₀ = 49.93 µM) was not predicted to be as good as the coumarin-acrylate analogs (see Table 4.1) but was slightly better than coumarin-acrylonitrile conjugate **134a** (IC₅₀ = 55.08 µM).



137

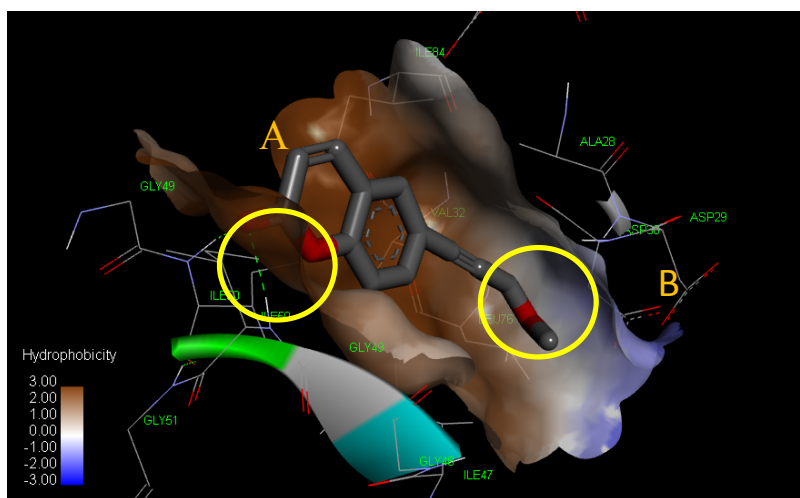
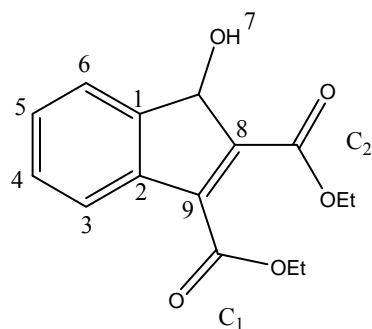


Figure 4.10. Three dimensional representation of compound **137** in the active site of the HIV-1 protease enzyme (1HXW). Oxygen atoms are red, carbon atoms of the protein and the ligand are grey, hydrogen bonds appear as green dots. (Predicted inhibitory concentration: **49.93 μ M**)

4.2.2.1.3. Modelling studies of indenol analogs

Given the geometry of indenols, it was expected that some hydrogen-bonding interactions would be observed between the hydroxyl group and ester group adorning these scaffolds. In addition, probable π - π interactions between the benzene ring and a particular subsite pocket of the protease enzyme could also occur. These assumptions prompted us to study their inhibitory effect against the HIV-1 protease enzyme.



147a

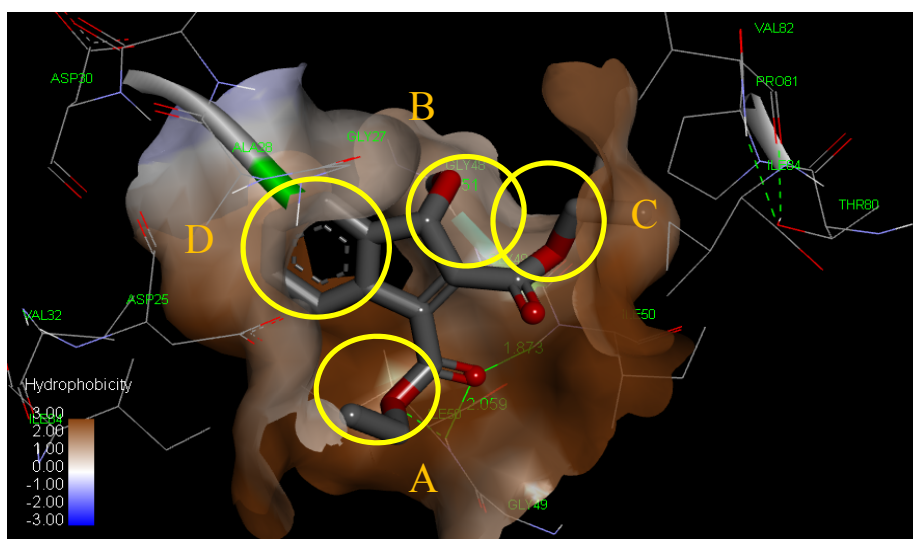


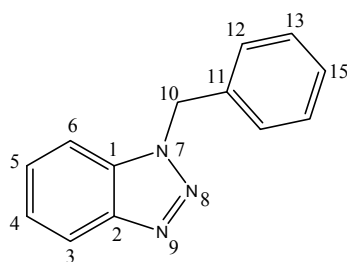
Figure 4.11. Three dimensional representation of compound **147a** in the active site of the HIV-1 protease enzyme (1HXW). Oxygen atoms are red, carbon atoms of the protein and the ligand are grey, hydrogen bonds appear as green dots. (Predicted inhibitory concentration: **45.91 μM**)

Careful inspection of compound **147a** bound to 1HXW (PR) indicated that the oxygen atom of one of the ester side chains (C_1) exhibited potential hydrogen bonding with ILE 50 (A in Figure 4.11) (a distance of 2.059 Å). The inhibitor also possessed a conformation in which the hydrogen atom (7) of the hydroxyl group interacted with GLY 48 (a distance of 1.851 Å) in the substrate catalytic core (B). On the other hand, the second ester group (C_2) was inserted deeply into the S_1' hydrophobic pocket (C) and the aromatic ring fitted effectively into the S_1 hydrophobic pocket of the active site of the HIV 1 protease enzyme (D).

When the hydrogen atom at C-4 of ligand **147a** was substituted with a chlorine (compound **147b**), hydrogen bonds were only apparent where the hydroxyl group of the chlorinated analog was involved. In fact, a hydrogen bond was created between the oxygen atom (7) and ASP 29 (a decreased distance of 1.97 Å) and the hydrogen atom (7) and GLY 27 (a distance of 2.98 Å). However, the same hydrophobic interactions of compound **147a** were still apparent (A, B, C). In this particular case, the substitution resulted in a gratifying increase predicted *in silico* inhibition potency (from 45.91 µM to 29.82 µM).

4.2.2.1.4. Modelling studies of benzotriazole analogs

Benzotriazoles present an appealing structural motif in peptidomimetics research because their structural and electronic characteristics resemble those of a peptide bond.¹⁷² Consequently, their usefulness as potential HIV-1 inhibitors was also examined.



111f

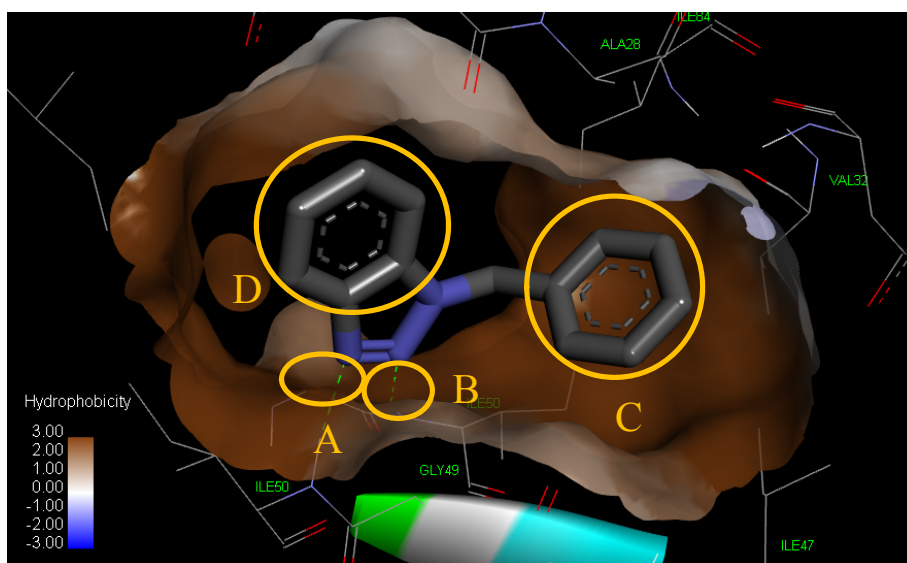


Figure 4.12. Three dimensional representation of ligand **111f** AA in the active site of the HIV-1 protease enzyme (1HXW). Nitrogen atoms are blue, carbon atoms of the protein and the ligand are grey, hydrogen bonds appear as green dots. (Predicted inhibitory concentration: **24.18 µM**)

As illustrated in Figure 4.12, ligand **111f** showed several binding interactions in the active site of 1HXW. The nitrogen atom N-9 of the azo group showed hydrogen bonding (A in Figure 4.12) to ILE (50) amino acid residue (a distance of 1.92 Å), while the second nitrogen atom N-8 interacted with the other ILE (50) dimer at a distance of 2.20 Å (B). The benzyl ring of the inhibitor fitted into the S₁' hydrophobic pocket of the enzyme (C) and the fused aromatic ring in the S₂' pocket (D).

We also looked at the 2D diagram of conjugate **111f** in 1HXW in order to clearly view the distances between the atoms of the ligand and the amino acid residues present at close proximity. The 2D diagram of the conformation adopted by ligand **111f** in 1HXW indicated positions where there was enough space (A, B and C) for specific substitutions around the carbon atoms of the benzyl group (D) and those of the fused heterocyclic ring (Figure 4.13).

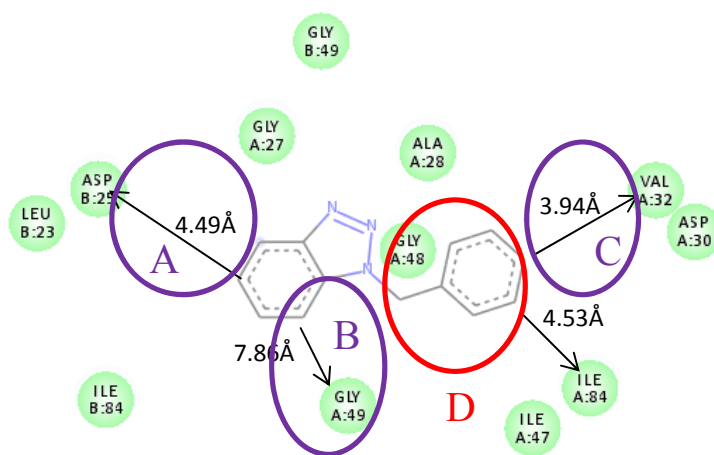


Figure 4.13. 2D diagram of ligand **111f** in the active site of the HIV-1 protease enzyme (1HXW). Amino acid residues are represented by green balls, the distances between the inhibitor carbon atoms and the neighboring amino acids are represented by black arrows

With this observation in mind, conjugates having electronegative substituents such as I, Cl, Br, the strongly electron-withdrawing CF₃ group and electron donating OCH₃ group on the fused aryl moiety were prepared. A comparison was also made between

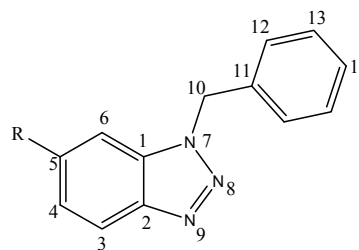
compounds whose aromatic ring (derived from the aniline derivatives) bore electron-releasing groups such as CH₃ or OCH₃ and the un-substituted system. The hydrophilicity as well as the lipophilicity of the electron withdrawing methyl ester group COOCH₃ was of particular interest and its consequent influence on inhibition when attached to the aromatic template was therefore also evaluated *in silico*. Thus, the structural features offered by these scaffolds guided the examination of their predicted structure-activity relationship.

The docking studies performed on these analogs revealed that the substituted benzotriazole scaffolds presented the same binding mode as compound **111f**, particularly the hydrogen bonds of the azo group with ILE 50 and reasonable hydrophobic interactions dominating the remainder of the binding.

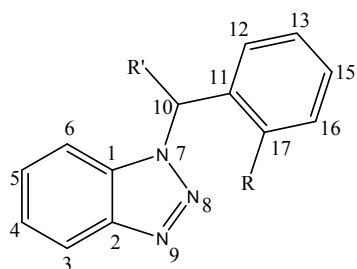
As depicted in Table 4.2, the docking studies indicated that, as far as the electronegativity of substituents at position 5 is concerned, harder/less polarisable electron donating/withdrawing substituents appear to decrease inhibition, while the softer, bulkier electron withdrawing substituents (such as I and Br) appear to fit well in the docking pocket.

Table 4.2. Influence of substituents on the inhibition constant IC₅₀ of benzotriazoles inhibitors.

R	5-I	5-Br	5-Cl	3-CF ₃	5-H	5-MeO
Predicted	7.82	10.98	14.78	23.41	24.18	24.45
IC₅₀ (μM)						



Electron donating groups (Me and MeO) at C-10 and C-12 respectively were introduced so as to study their effect on the conformation of the docked ligand in the 1HXW protease enzyme and (more interestingly) their influence on the binding.



R = MeO

R' = Me

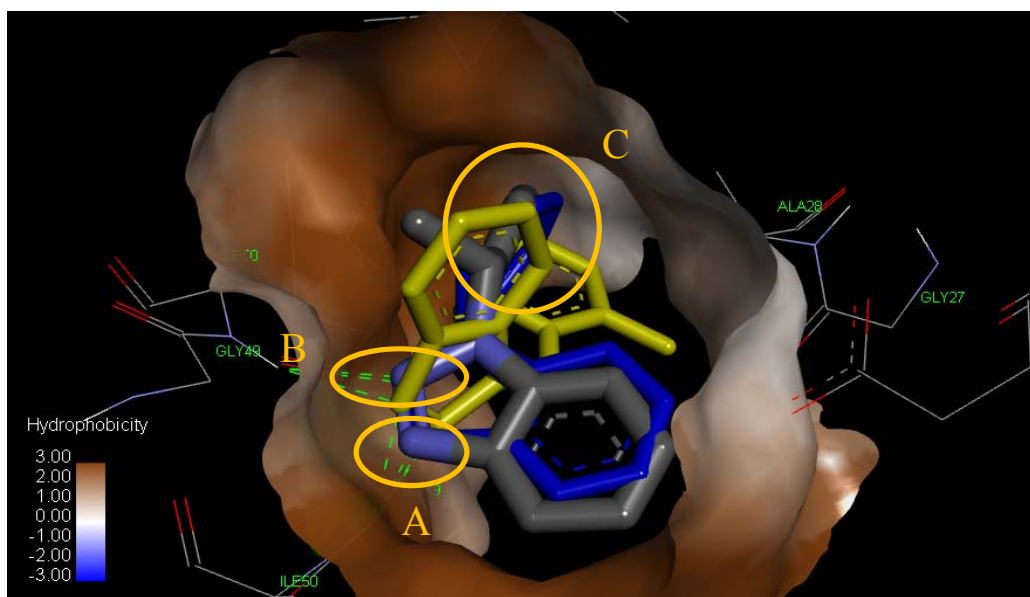


Figure 4.14. Superimposed three dimensional representation of ligands **111h**, **111f** and **111g** in the active site of the HIV-1 protease enzyme (1HXW). The oxygen atom is red, nitrogen atoms are blue, carbon atoms of the protein and the ligand are grey, hydrogen bonds appear as green dots, the protein backbone is drawn as a grey tube, compound **111f** is blue and compound **111g** is yellow

Table 4.3. Interactions between HIV-1 PR and benzotriazole derivatives

		111f	111g	111h
R'		H	H	Me
R		H	MeO	H
Interactions	Hydrogen bonds with Amino acid residues	ILE 50	ILE 50, ASP 29	ILE 50
	Hydrophobic pocket	S ₁ '	S ₁	S ₁ , S ₂ '
Predicted IC₅₀ (μM)		24.18	16.31	19.97

Docking of **111g** with 1HXW (Figure 4.14) revealed a set of three hydrogen-bonding interactions of the azo group with both ILE 50 amino acid residues (a distance of 2.35 Å) (A in Figure 4.14). Only one hydrophobic interaction of the benzyl ring was apparent in the S₁ pocket. As expected, an additional ligand-protein interaction was realized as the OMe group interacted with ASP 29 (a distance of 2.11 Å) (C). Compound **111g** was predicted to be more active than ligand **111f** (lower IC₅₀) owing to the presence of the OMe group. This was a pleasing result.

For comparison, a methyl group was introduced at C-10 of compound **111f** (**111h**) and this was docked to the protease as before. Two hydrogen-bonding interactions of the azo group with both ILE 50 (a distance of 2.33 Å) (A) and two hydrophobic interactions of compound (**111h**) in the S₁ and S₂' pockets (B and C) were observed and are illustrated in Figure 4.14. The value of the inhibitory concentration of this ligand indicated that the methyl group allowed an improvement in the activity of analog **111h** compared to compound **111f**.

As a variation on the benzene ring, 1-aminonaphthalene was used. A naphthalene moiety is very rich in electrons and therefore favors π - π stacking interactions. The binding activity of the resulting compound **121h** in the catalytic region of 1HXW was explored.

An ester group at position 12 of the benzotriazole skeleton was also of particular interest in this study owing to the potential for further hydrogen bonds.

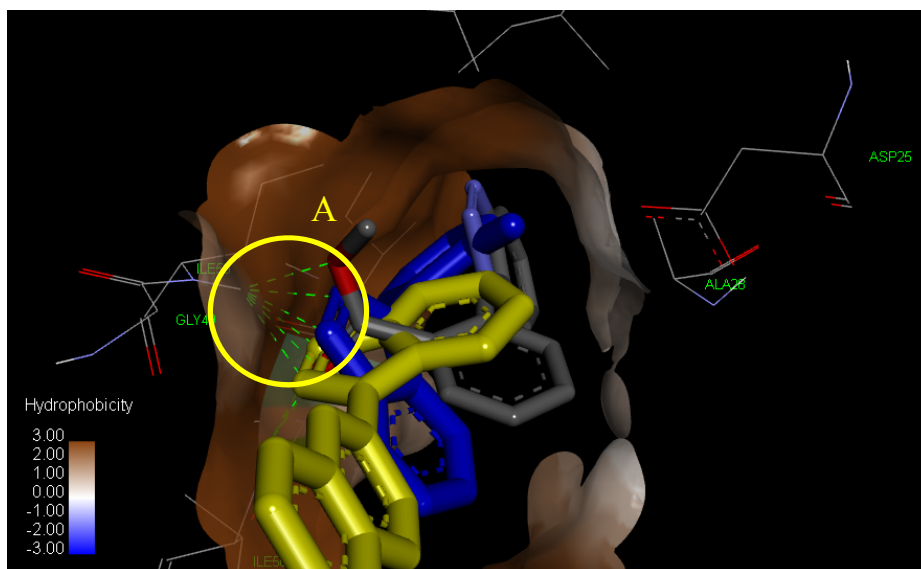


Figure 4.15. Superimposed three dimensional representation of compounds **121b**, **121i** and **121h** in the active site of the HIV-1 protease enzyme (1HXW). Oxygen atoms are red, nitrogen atoms are blue, carbon atoms of the protein and the ligand are grey, hydrogen bonds appear as green dots, the protein backbone is drawn as a cyan tube, compound **121b** is blue and compound **121h** is yellow

Table 3.4. Interactions between HIV-1 PR and substituted benzotriazole derivatives

		121b	121i	121h
Interactions	Hydrogen bonds with Amino acid residues	ILE 50	ILE 50, ASP 29	ILE 50
	Hydrophobic pocket	S ₁ , S ₂ '	S ₁ , S ₂ '	S ₁ '
Predicted IC₅₀ (μM)		18.26	9.99	2.21

Hydrogen bonding interactions of the ester group COOMe in compound **121i** with ILE 50 were detected. The oxygen atom (16) was interacting with ILE 50 at a distance of 2.26 Å and the oxygen atom (17) at a distance of 1.98 Å from the same amino acid (A in Figure 4.15). Surprisingly, the proximity of the ester group did not facilitate any

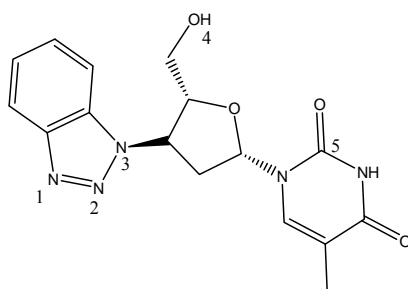
hydrogen-bonding interactions of the azo group (N₈-N₉). Instead, the molecule was stabilized by hydrophobic interactions of the entire fused heterocyclic ring in the S₂' and the aromatic ring in the S₁ pocket of the 1HXW enzyme. These three interactions worked together to effect a better activity of ligand **121i** compared to ligand **121b**.

In silico docking of compound **121h** in the protease active site (Figure 4.15), revealed that the azo group (N₈-N₉) of ligand **121h** showed a set of four non-specific hydrogen-bonding type interactions (N-H bonds) connecting the inhibitor to both ILE 50 amino acid residues (a distance of 2.22 Å). No hydrophobic interactions of the azo group were detected. The naphthalene backbone was inserted deep into the S₁' hydrophobic pocket of the enzyme, a position favoring a greater hydrophobic interaction which could account for an improvement in its activity.³⁷⁵ In addition, the fused ring was stabilized by the S₂ hydrophobic envelope. π Stacking interactions of all the three aromatic rings with various amino acid residues were also observed. As expected, the aromaticity of the naphthalene ring coupled to the fused ring system of ligand **121h** led to the formation of synergistic π stack modes of binding that contributed to the increased activity of compound **121h** (2.21 μ M).

These observed interactions could account for the higher predicted activity of **121h** (2.21 μ M) than other studied benzotriazole analogs in this investigation.

4.2.2.1.5. Modelling studies of benzotriazole-AZT conjugate

The dual action inhibitors developed by conjugation of AZT with benzotriazole derivatives also warranted *in silico* assessment. Particular attention was paid to the effect of the benzotriazole moiety on the binding of AZT to the reverse transcriptase enzyme. The X-ray crystal structure of the reverse transcriptase enzyme (1IKW) is available in the PDB database. The docking framework described in section 6.2.15 was followed.



112a

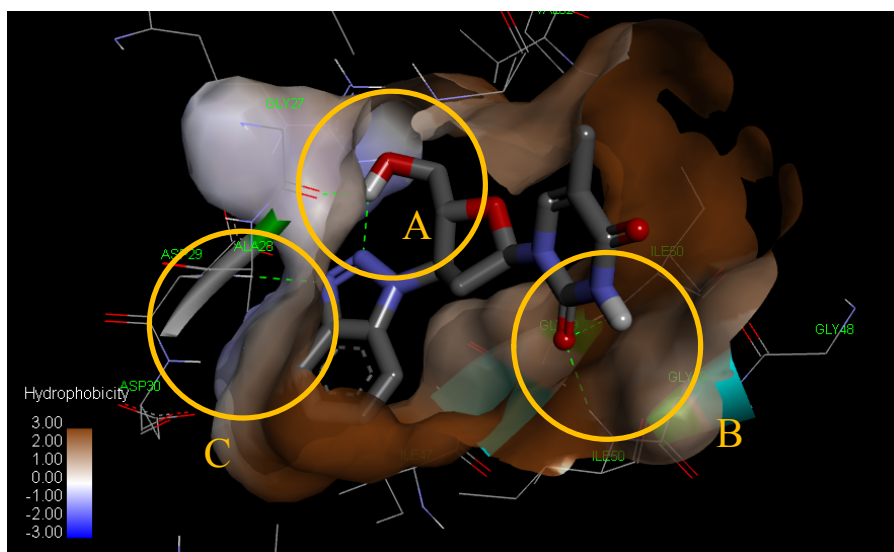


Figure 4.16. Three dimensional representation of conjugate **112a** in the active site of the HIV-1 protease enzyme (1HXW). Oxygen atoms are red, nitrogen atoms are blue, carbon atoms of the protein and the ligand are grey, hydrogen bonds appear as green dots, the protein backbone is drawn as a cyan tube (Predicted inhibitory concentration: **2.14 μM**)

An overview of the docking of **112a** with protease 1HXW (Figure 4.16) revealed both intramolecular hydrogen-bonding interactions (A in Figure 4.16) within conjugate **112a** and intermolecular interactions with atoms in the amino acid residues present in the active site of 1HXW (PR). A closer examination indicated that they appeared between C=O (5) and ILE 50 (a distance of 2.85 Å) (B), N (1) atom (azo group) and ASP 29 (a distance of 2.07 Å) (C), N (2) atom (azo group) and H (4) atom of hydroxyl group (a distance of 1.96 Å) (A), H(4) atom of the hydroxyl group and GLY 27 (a distance of 2.21 Å) (A). Compound **112a** also showed hydrophobic interactions with the S₁ and S₂' hydrophobic pockets of the active site of the HIV-1 protease enzyme as well as π stacking interactions with ILE 47 in this enzyme.

4.2.2.2. Biological studies of heterocycles for inhibition of HIV-1 PR (1HXW)

In order to confirm the predictions from molecular modelling, biological assays were carried out. Since we had a very limited amount of PR enzyme, we were obliged to be selective of which compounds to test *in vitro*. Qualitative fluorometric assays (described in Section 6.2.17.1) of compounds **137**, **134c**, **134b** and **111j** were performed. Kinetics of the cleavage of the PR enzyme were studied as a function of increase in fluorescence against time. Three controls were used during this experiment: the substrate control (the substrate alone), the vehicle control (HIV-1 PR diluent, the substrate and DMSO), the positive control (HIV-1 PR diluent and the substrate). The test compounds were then assayed with the protease diluent and the substrate. The plot of the normalized fluorescence against time gave the curves displayed in Figure 4.17. The data were fitted to logarithmic curves having coefficients as tabulated in Table 4.5.

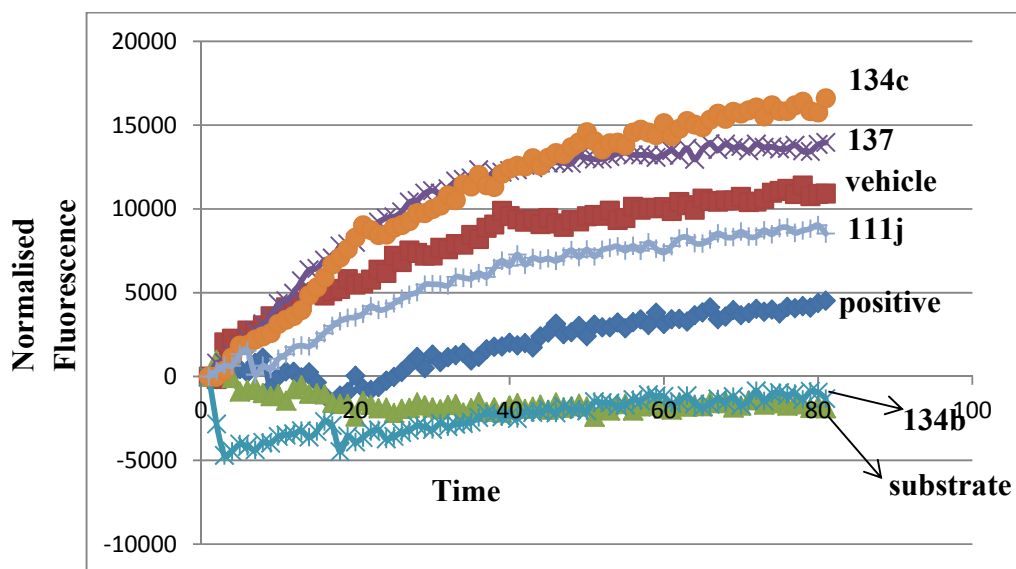


Figure 4.17. Inhibition kinetics of potential PR inhibitors

Table 4.5. Inhibition coefficients

Compounds	substrate	positive	vehicle	134c	137	111j	134b
Gradient	-12.59	67.24	116.05	195.74	148.82	111.28	38.64

According to Figure 4.17 and Table 4.5, HIV-1 PR substrate control has the lowest rate of increase in fluorescence compared to the other controls. This means that the substrate on its own remains completely inactive during the reaction. The rate of increase of fluorescence is higher for the sample which only contained the vehicle compared to the positive control where no inhibitor was used. Out of the four ligands tested, compound **134b** appeared to be the more active since its gradient is the lowest while compound **134c** is the least active and appeared to activate the PR enzyme instead. This result did not correlate with the molecular modelling predictions where the coumarin analogs were reported active against the PR enzyme (Table 4.1). The high dilution of the PR enzyme in the *in vitro* assay due to its limited amount could account for the anomalous results.

4.2.2.3. *In silico* and *in vitro* assays of heterocycles for inhibition of HIV-1 RT (1IKW)

4.2.2.3.1. *Docking studies of heterocycles for inhibition of HIV-1 RT (1IKW)*

- **Docking studies of compound 112a for inhibition of HIV-1 RT (1IKW)**

In order to assess our dual action inhibitor requirement, conjugate **112a** was also docked into the active site of the HIV-1 reverse transcriptase enzyme (1IKW) by following the procedure described in Section 6.2.15 (Figure 4.18).

As depicted in Figure 4.18, in the lowest energy conformation of **112a** in the active site of 1IKW, C=O (5) showed potential hydrogen-bonding with LEU 100 (a distance of 3.13 Å) (A in Figure 4.18). Also, the H (4) atom of the hydroxyl group of the ligand showed an interaction with the carbonyl of LYS 101 (a distance of 2.01 Å) (B in Figure 4.18). Hydrophobic interactions of the AZT moiety with the hydrophobic pocket next to VAL 179 and GLU 138 were observed while a π stacking interaction with TYR 188 was detected as well.

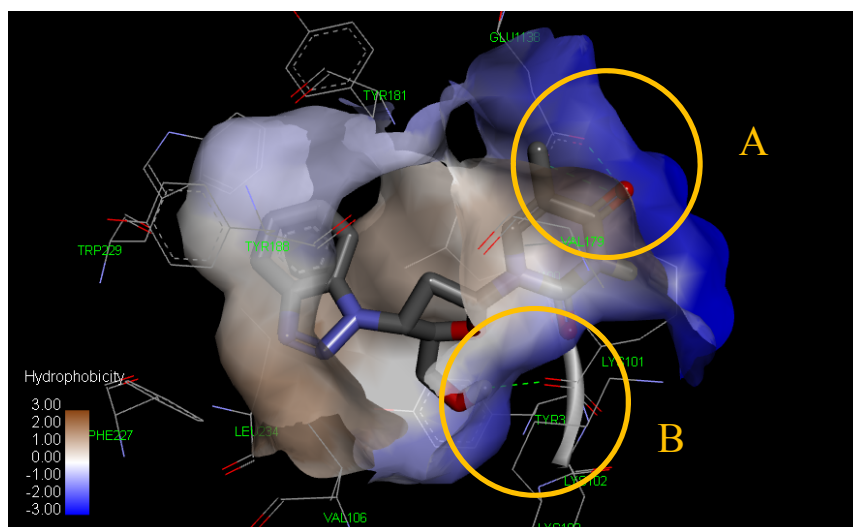


Figure 4.18. Three dimensional representation of ligand **112a** in the active site of the HIV-1 reverse transcriptase enzyme (1IKW). Oxygen atoms are red, nitrogen atoms are blue, carbon atoms of the protein and the ligand are grey, hydrogen bonds appear as green dots.(Predicted inhibitory concentration: **0.56 μ M**)

A comparison of the predicted inhibitory concentration of ligand **112a** in both 1IKW and 1HXW active sites revealed that ligand **112a** is potentially more active against the reverse transcriptase enzyme (0.56 μ M) than the protease enzyme (2.14 μ M). The reported IC_{50} of AZT against the HIV-1 RT enzyme is 4.54 μ M⁸¹ and it appeared that the benzotriazole ring improved the activity of AZT by binding in the hydrophobic pocket next to TRP 229 and TYR 188.

A comparison of the docking modes of conjugate **112a** with Efavirenz, a commercially available reverse transcriptase inhibitor, in the catalytic core of the reverse transcriptase enzyme was also performed.

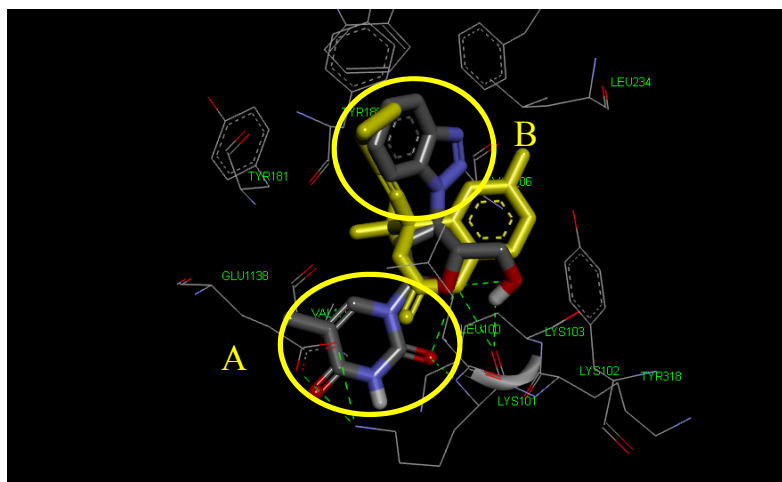


Figure 4.19. Superimposition of conjugate **112a** and Efavirenz ($0.3 \mu\text{M}$)³⁷⁶ (in yellow) in the active site of HIV-1 reverse transcriptase enzyme (1IKW). Oxygen atoms are red, nitrogen atoms are blue, carbon atoms of the protein and the ligand are grey, hydrogen bonds appear as green dots, the protein backbone is materialized as a grey tube

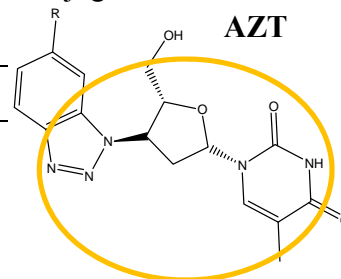
A quick glance at Figure 4.19 indicated that the methylpyrimidine-2,4-dione ring of the AZT moiety of **112a** extended beyond the active site of the RT (A in Figure 4.19). This observation could account for low inhibition of HIV-1 reverse transcriptase of conjugate **112a** compared to Efavirenz. The benzotriazole ring system of ligand **112a** overlapped with the cyclopropylethynyl moiety of Efavirenz (B), indicating the possibility of a similar mode of binding. Beside the fact that cyclising anthranilic acid **82** to AZT **1** improved its activity, the potential dual inhibitor complex **112a** was found to be more active in 1IKW (RT) catalytic core than in 1HXW (PR) binding site. Ligand **112a** exhibited a lower activity than Efavirenz. The simulations indicated that their improper overlap in the active site of the RT enzyme could justify its lower activity compared to Efavirenz.

4.2.2.3.2. Biological studies of heterocycles for inhibition of HIV-1 RT (1IKW)

To conclude the RT inhibition study, *in vitro* colorimetric RT assays (described in Section 6.2.17.3) were carried out on compounds **112a**, **112b**, **112c** and **1**. Their percentage RT inhibition at $50 \mu\text{M}$ are reported in Table 4.6.

Table 4.6. Percentage inhibition of benzotriazole-AZT conjugates in 1IKW

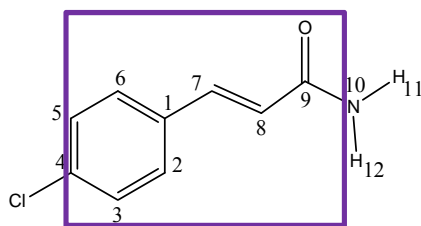
Compounds	112a	112b	112c	1
R	H	I	Br	
Inhibition at 50 μ M (%)	100	77	63	67



As predicted from molecular modelling studies, the 1,3-DC cycloaddition of AZT **1** with anthranilic acid seems to improve the activity of AZT **1**. 100% RT inhibition was observed at 50 μ M with compound **112a** as the inhibitor while compound **112c** and compound **112b** inhibited RT enzyme at 63% and 77% respectively. These results also imply that substituents with higher polarisability on the aromatic ring of the anthranilic acid-AZT conjugate tend to decrease the activity of benzotriazole-AZT conjugates.

4.2.2.4. Molecular modelling of cinnamoyl derivatives for the inhibition of HIV-1 IN (1QS4)

The docking process described in section 6.2.15 was applied to this system, with the notable difference that, before performing Autogrid, electronic charges of +2 were assigned manually to each of the three magnesium atoms present in the catalytic core of the integrase enzyme (1QS4). These changes were made on the PDBQT file of the macromolecule generated in the docking procedure. The grid box with dimensions of - 17.46 Å \times 30.18 Å \times 66.60 Å was centered in the integrase enzyme active site and incorporated the neighboring amino acid residues. The main structural requirement for HIV-1 integrase inhibition activity in the present study was the presence of the cinnamoyl moiety, as highlighted below in compound **166b**. In each case in the discussion which follows, the effect on integrase inhibition of substituents added to this skeleton will be highlighted.



166b

4.2.2.4.1. Acrylamide and protected amino acid analogs

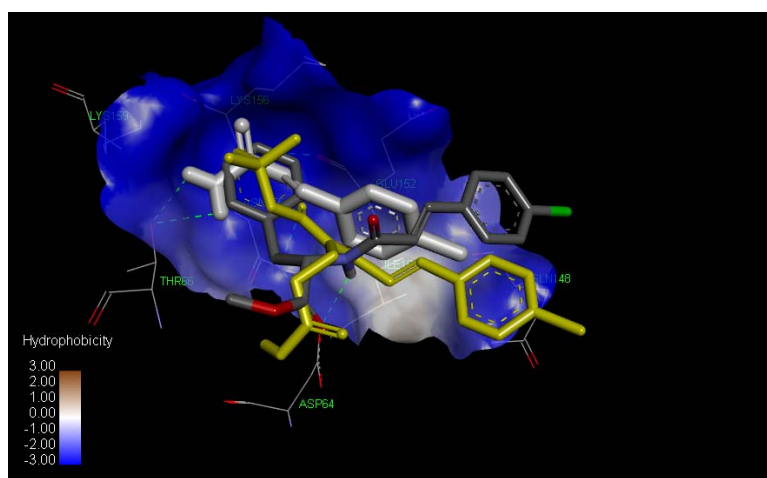
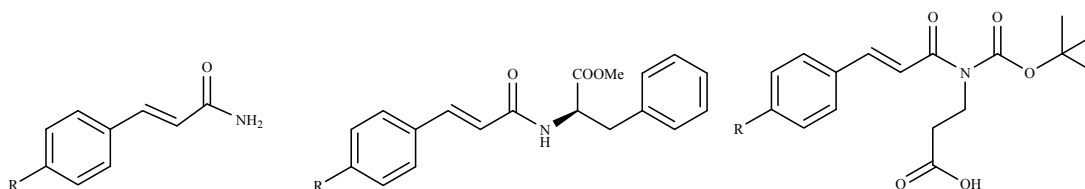


Figure 4.20. Superimposed three dimensional representation of compounds **175b**, **166b** and **171b** in the active site of the HIV-1 integrase enzyme (1QS4). Oxygen atom is red, chlorine atom is green, nitrogen atom is blue, hydrogen atoms are white, carbon atoms of the protein and the ligand are grey, hydrogen bonds appear as green dots, compound **166b** is white, compound **171b** is yellow

As indicated in Figure 4.20, primary, secondary and tertiary amides were docked in 1QS4. In general, the primary amides were hydrogen bonded to THR 66, while the secondary amides were bonded to ASP 64 and the tertiary amides to CYS 65.



R = Cl (**166b**), Br (**166c**)

R = H (**175a**), Cl (**175b**)

R = H, (**171a**), Cl (**171b**)

Table 4.7. Interactions between HIV-1 IN with primary, secondary and tertiary cinnamic acid amide derivatives

		166b	166c	175a	175b	171a	171b
Interactions	Hydrogen bonds	THR 66	THR 66	ASP 64	ASP 64	THR 66, CYS 65	ASN 155, CYS 65
	Hydrophobic interactions of the coumarin ring	ILE 151, GLN 148	THR 66, ASN 155	LYS 156, LYS 159, ASN 155	GLU 152, GLY 149	CYS 65, GLU 152, ASP 64	CYS 65, ASP 64, ILE 151
	Hydrophobic interactions of the R group	ASN 155, LYS 159, LYS 156	ASN 155, GLU 152, ASP 64	GLU 152, ASP 64	GLU 152, ASP 64	HIS 67, THR 66	LYS 156, LYS 159
Predicted IC₅₀ (μM)		996.13	803.76	903.53	593.46	0.258	0.195

Inspired by a study based on Monte Carlo simulations of HIV-1 reverse transcriptase inhibitors carried out by Razzo *et al.*,³⁷⁷ we explored the activity of primary, secondary and tertiary amides in 1QS4 (IN). Secondary amide **175b** was found more active than the primary amides. It appeared that the tertiary amides adopted a conformation favoring more than one hydrogen bond interaction with 1QS4 and this resulted in an enhancement in activity of approximately three orders of magnitude. Comparing the activities of the acrylamide analogs to peptide analogs suggested that primary amide groups on the cinnamoyl fragment were not tolerated since the most significant interactions involved primary amide protons, resulting in unfavorable conformations of the rest of the molecule. The slight enhancing effect of the chlorine atom on the activity of compound **171b** (from 258.4 nM to 195.64 nM, see Table 4.7) could be attributed to a favorable steric arrangement in the pocket of 1QS4 (Figure 4.20).

4.2.2.4.2. Acrylic acid derivatives

Burke *et al.* reported that the number and the nature of ring substituents significantly affect the activity of HIV drug candidates.²⁷⁴ We thus emphasized this feature to monitor the activity of acrylic acid conjugates in 1QS4 (Figure 4.21).

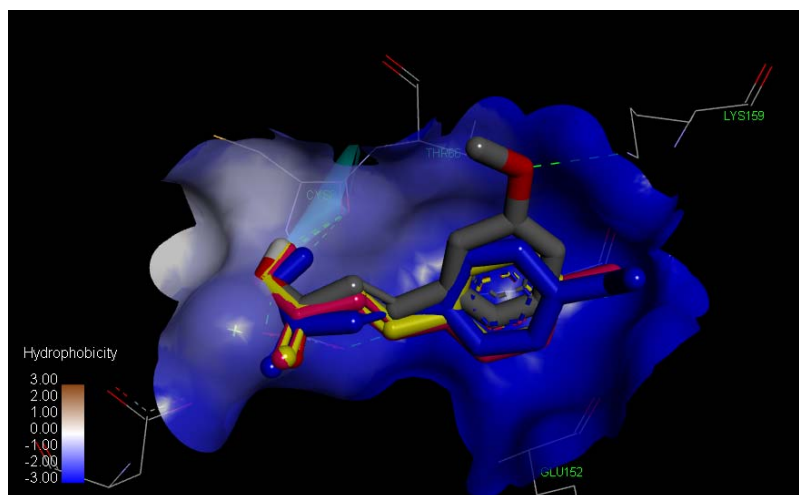
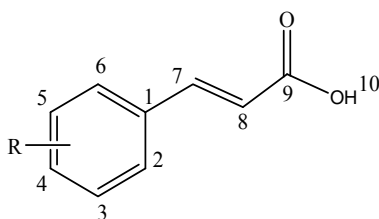


Figure 4.21. Superimposed three dimensional representation of compounds **169a**, **169h**, **169g**, **169i** in the active site of the HIV-1 integrase enzyme (1QS4). Oxygen and bromine atoms are red, nitrogen atom is blue, hydrogen atoms are white, carbon atoms of the protein and the ligand are grey, hydrogen bonds appear as green dots, compound **169h** is blue, compound **169i** is pink, compound **169a** is yellow

Although all four substrates (**169a**, **169h**, **169g** and **169i**) illustrated in Scheme 4.22 occupied the same pocket with the same general orientation, changes in the substituents resulted in significant additional interactions.



	R
169a	H
169b	4-Cl
169g	3-MeO
169h	4-MeO
169i	4-Me

Figure 4.22. Cinnamic acid derivatives

Table 4.8. Interactions of HIV-1 IN with cinnamic acid derivatives

		169a	169b	169i	169g	169h
R		4-H	4-Cl	4-Me	3-MeO	4-MeO
Interactions	Hydrogen bonds (distance Å)	CYS 65 (2.01)	THR 66 (2.00)	CYS 65 (1.98)	CYS 65 (2.06)	THR 66 (1.85)
	Hydrophilic interactions	THR 66, ASN 155, GLU 152	LYS 156, GLU 152, ASN 155, LYS 159, HIS 67	LYS 156, ASN 155, GLU 152, LYS 159	THR 66, LYS 159, ASN 155	THR 66, ASN 155, LYS 159
	Hydrophobic interactions	GLN 148, ILE 151, GLU 152	ASP 116, ASP 64	ILE 151, GLU 152, THR 66, LYS 159	ASP 116, ASP 64, CYS 65	ILE 151, GLU 152, THR 66, LYS 159
Predicted IC₅₀ (nM)		361.26	230.66	230.19	208.51	142.24

A. Influence of electron withdrawing and electron donating group

The effect of electron donating groups and electron withdrawing groups on the aromatic ring was examined. Compound **169h** appeared to be more active than compound **169a**, compound **169i** and compound **169b** (see Table 4.8). Beside the electron donating effect of the methyl group, this observation suggested that a closer hydrogen bond interaction of the acidic hydrogen of the cinnamic acid conjugate with a carbonyl oxygen on 1QS4 (IN) (when only that one hydrogen bonding interaction occurred) might lead to a crucial improvement in the efficacy of the ligand. The change in position of the OMe group on the aromatic ring from position 4 to 3 resulted in an additional hydrogen bond interaction of the OMe group with the hydroxyl oxygen of LYS 159 at a distance of 2.83 Å.

B. Influence of the benzyl group

Since benzyl groups were reported to enhance binding to other HIV-1 enzymes,³⁷⁸ we decided to study their effect as substituents on the aromatic ring of acrylic acid

skeleton.⁸¹ Four benzylated cinnamate ester derivatives were docked in 1QS4 (IN) and, as indicated in Table 4.9, important interactions were observed.

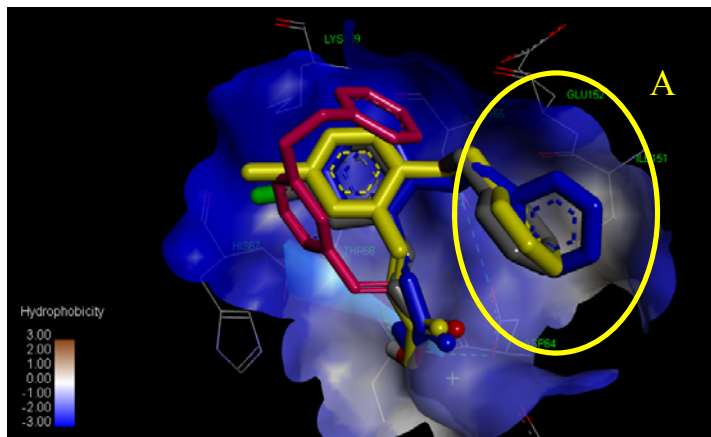
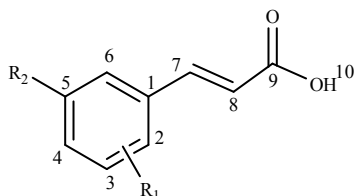


Figure 4.23. Superimposed three dimensional representation of compounds **169f**, **169d**, **169e** and **169c** in the active site of the HIV-1 integrase enzyme (1QS4). Oxygen atoms are red, nitrogen atom is blue, hydrogen atoms are white, chlorine atom is green, carbon atoms of the protein and the ligand are grey, hydrogen bonds appear as green dots, compound **169d** is blue, compound **169e** is pink, compound **169c** is yellow

An overview of the docking of compounds **169d**, **169f** and **169c** (Figure 4.24) in 1QS4 (Figure 4.23) indicated that these ligands interacted with the DDE motif of the catalytic core domain of the HIV-1 IN enzyme (Section 1.1.1.2.). These ligands were inserted in the hydrophilic pocket delimited by LYS 159 and the hydrophobic pocket surrounded by ILE 151 and GLU 152 (A in Figure 4.23). However, compound **169e** adopted a different conformation from the three other ligands by having mostly hydrophilic interactions with LYS 156, GLU 152, ASN 155 and HIS 67. Beside also having hydrophilic interactions with LYS 159, π stacking interactions between the benzyl ring of compound **169e** and the same amino-acid residue were also observed.



	R₁	R₂
169c	2-OBn	5-Br
169d	2-OBn	H
169e	3-OBn	H
169f	2-OBn	5-Cl

Figure 4.24. Benzylated cinnamic acid derivatives

Table 4.9. Interactions between HIV-1 IN and benzylated cinnamate ester derivatives

		169c	169d	169e	169f
R		Br	H	H	Cl
Interactions	Hydrogen bonds	ASP 155, THR 66	CYS 65, ASN 155	THR 66	CYS 65, ASN 155
	Hydrophilic interactions	LYS 159	THR 66, ASN 155, LYS 159	LYS 156, GLU 152, ASN 155, LYS 159, HIS 67	GLU 152, LYS 159
	Hydrophobic interactions	ILE 151, GLU 152, THR 66, LYS 159	GLN 148, ILE 151, GLU 152	ASP 116, ASP 64	ILE 151, GLU 152, THR 66, LYS 159
Predicted IC₅₀ (nM)		46.34	54.45	493.52	26.91

Close contacts between organic chlorine or bromine atoms and aromatic rings were reported to enhance protein-ligand binding affinity. An elegant study in this respect was published by Matter *et al.* in 2009.³⁷⁹ In our case study, this property was confirmed by the predicted good activity of compound **169c** and compound **169f** compared to compound **169d** and compound **169e** (see Table 4.9). As anticipated, benzylated cinnamic acids (Table 4.9) appear to be more active than non-benzylated cinnamic acid (Table 4.8). However, the position of the benzyl group on the aromatic appeared to be very crucial upon the activity of cinnamic acid derivatives. This could explain why compound **169d** was predicted highly active if compared to compound **169e** (54.45 nM to 493.52 nM). The surprisingly good activity of compound **169f** encouraged us to study its docking mode in the active site of 1QS4 compared to **5 CITEP**, a well-known integrase inhibitor.

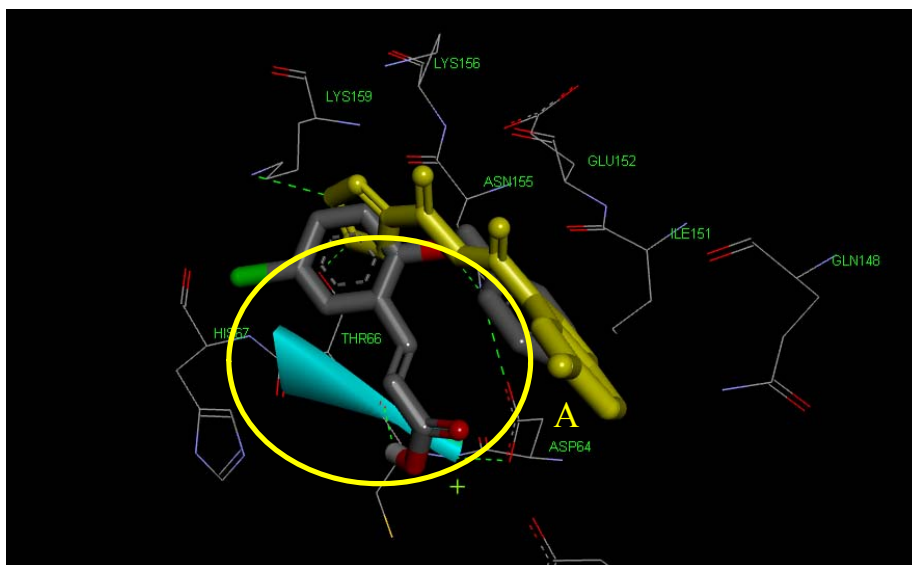


Figure 4.25. Superimposition of conjugate **169f** on **5 CITEP** ($0.65 \mu\text{M}$)³⁸⁰ (in yellow) in the active site of the HIV-1 integrase enzyme (1QS4). Oxygen and bromine atoms are red, chlorine atom is green, hydrogen atoms are white, carbon atoms of the protein and the ligand are grey, hydrogen bonds appear as green dots

Figure 4.25 revealed that the benzyl ring and, to a certain extent, the phenyl ring of compound **169f** appeared to be well aligned with the superimposed structure of **5 CITEP** in 1QS4 (A in Figure 4.25). However, the cinnamic acid moiety did not match the conformation adopted by **5 CITEP** and was bound in the active site in a different orientation. Also of interest was the very good predicted inhibitory activity of compound **169f** (26.91 nM) compared to **5 CITEP** (650 nM) (See structure in Section 1.2.2.1.3).

4.2.2.4.3. Cinnamate ester derivatives

The influence of methyl, benzyl and AZT groups on the activity of cinnamate esters against the HIV-1 integrase enzyme was studied.

Figure 4.26 shows the *in silico* docking of compounds **174b**, **170b** and **178b** in the integrase active site. It appears that the methylation of cinnamic acid by dimethyl formamide (DMF) contributed to the inactivity of **174b** since no hydrogen bond interaction was observed and a complete loss of potency was predicted compared to compound **169b** (see Table 4.8) ($2.30 \times 10^{-4} \text{ mM}$ to 1.56 mM).

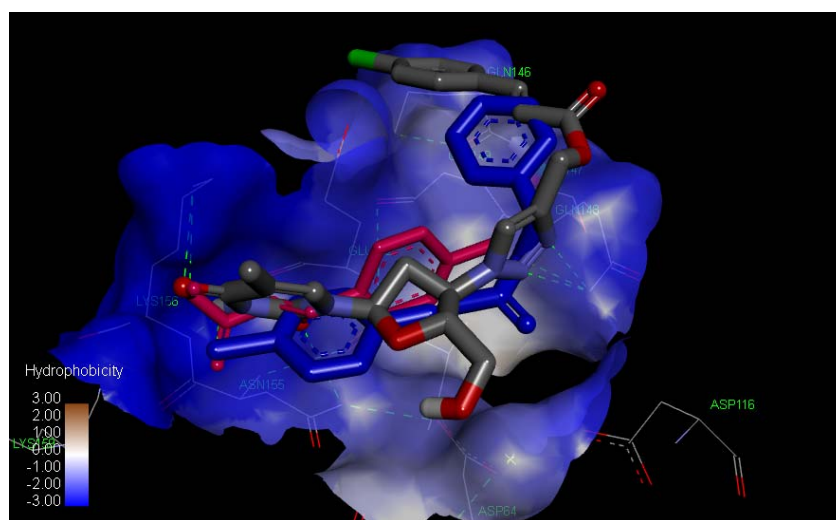


Figure 4.26. Superimposed three dimensional representation of compounds **178b**, **174b** and **170b** in the active site of the HIV-1 integrase enzyme (1QS4). Oxygen and bromine atoms are red, nitrogen atom is blue, hydrogen atoms are white, carbon atoms of the protein and the ligand are grey, hydrogen bonds appear as green dots, compound **174b** is blue, compound **170b** is pink

Table 4.10. Interactions between HIV-1 IN with cinnamate ester derivatives

		174a	174b	170a	170b	178a	178b
Interactions	Hydrogen bonds				GLY 148	ASP 64, GLN 148, LYS 156, ASN 155	GLN 148, ASP 64, LYS 156, ASN 155
	Hydrophilic interactions	LYS 156, GLU 152, ASN 155	LYS 156, ASN 155, GLU 152, LYS 159, THR 66	LYS 156, LYS 159	ASN 155, THR 66, LYS 159	ASN 155, LYS 156	ASN 155, LYS 156
	Hydrophobic interactions	LYS 156, GLU 152, ASN 155	GLN 148, ILE 151, ASP 64	GLN 148, ILE 151	GLY 148, GLY 149	CYS 65, ASP 64	ILE 151, ASP 64, CYS 65
Predicted IC₅₀ (μM)		1.64 × 10 ³	1.56×10 ³	712.17	603.61	22.27	23.66

Replacing the methyl group by a benzyl group provided opportunity for higher binding affinity of the ligands in 1QS4 (IN) and this was confirmed by an enhancement in activity. Cinnamate ester AZT conjugates appeared to be very active compared to the other cinnamate ester analogs probably owing to the increase in hydrogen bonds with 1QS4.

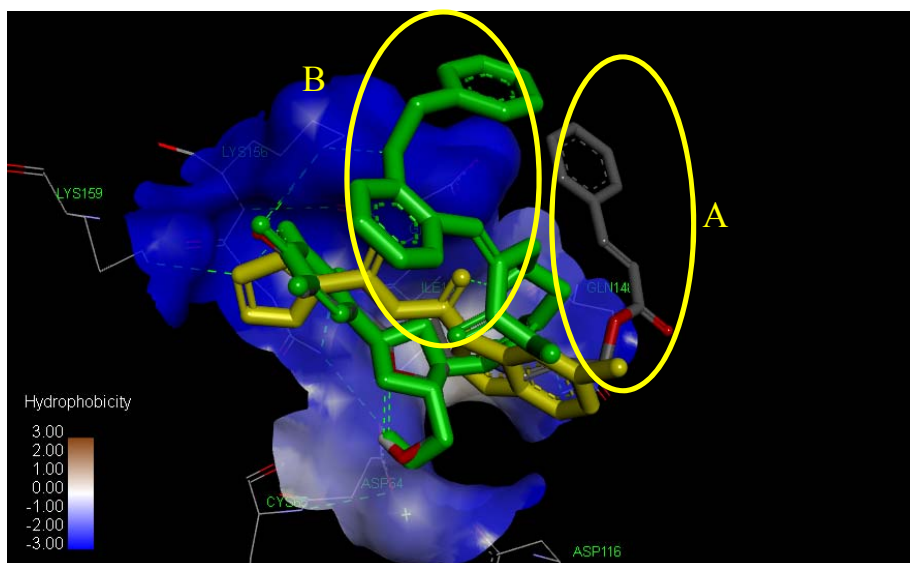


Figure 4.27. Superimposed three dimensional representation of conjugates **178a**, **17** and **5 CITEP** ($0.65 \mu\text{M}$)³⁸⁰ (in yellow) in the active site of the HIV-1 integrase enzyme (1QS4). Oxygen atoms are red, hydrogen atoms are white, carbon atoms of the protein and the ligand are grey, hydrogen bonds appear as green dots, **5 CITEP** is yellow and compound **17** is green

Figure 4.27 illustrates the superimposition of compounds **178a**, **17** (see structure in section 1.3) and **5 CITEP**. It emerged that the cinnamoyl fragments of compounds **178a** and **17** were not aligned with **5 CITEP** in the active site of 1QS4 (A and B in Figure 4.27) while the **AZT** moiety of both **AZT** conjugates matched well with **5 CITEP**.

Table 4.11. Binding energy and IC_{50} of **AZT** conjugates in 1QS4

Compounds	178a	178b	17
Binding energy (kcal/mol)	-6.35	-6.31	-4.71
Predicted IC_{50} (μM)	22.27	23.66	354.19

The docking results revealed that among the three **AZT** conjugates (**178a**, **178b** and **17**), compound **178a** has the lowest binding energy and consequently appeared more active than compound **17** according to its predicted inhibitory concentration. However, it was

predicted by the docking study that compound **178a** and compound **17** were both less active than **5 CITEP** in binding to 1QS4 (IN).

Formyl cinnamate ester **141a** was also docked in 1QS4 and the carbonyl of the formyl group was found to be hydrogen bonded to HIS 67, THR 66 and LYS 159. The aromatic ring was buried in the hydrophilic pocket framed by LYS 159, LYS 156 and GLU 152 while the alkene moiety was accommodated by the hydrophobic pocket delimited by CYS 65 and ASP 64. Compound **141a** was predicted to have a high inhibitory concentration of 388.94 μM and this was the reason why further docking studies on this class of compounds were not carried out.

4.2.2.5. *In vitro* assays of cinnamoyl derivatives for the inhibition of HIV-1 IN

In order to validate the computational studies on this class of compounds, a colorimetric HIV-1 IN assay (described in Section 6.2.17.2) was carried out. The percentage activity of the different classes of cinnamoyl derivatives inhibiting the IN enzyme are indicated in Table 4.12.

Table 4.12. *In vitro* inhibitory activity of different classes of potential IN inhibitors (most promising candidates in each class are highlighted in bold)

Class of compounds	Benzylated acrylic acids			Acrylic acids				
Compounds	169f	169c	169d	169g	169i	169h		
Inhibition at 50 μ M (%)	87	65	50	83	65	58		
Class of compounds	Coumarins			peptides				
Compounds	134b	134c	137	134a	175b	171a	175a	
Inhibition at 50 μ M (%)	66	29	26	5	88	87	41	
Class of compounds	Heck adducts			Acrylamide		Other cinnamoyl derivatives		
Compounds	141d	141g	141a	166c	166b	177b	170b	170a
Inhibition at 50 μ M (%)	29	25	0	76	26	79	66	25

The data contained in Table 4.12 suggested that acrylic acids were the most active IN inhibitors among the classes of cinnamoyl compounds tested, followed by peptide

analogs. We hypothesized that these small acids get into the active site of the enzyme as deep as possible and thus have more efficient interactions. In addition, these acids form very strong hydrogen bonds through the acidic hydroxyl group to a cysteine present in the pocket of the IN enzyme. Among the coumarin analogs, compound **134b** showed a good inhibition while the Heck adducts appeared to be poorly active as forecast by molecular modelling studies.

The free binding energy of these compounds calculated in AUTODOCK 4.0 were compared to their IN percentage inhibition activity (Table 4.13 and Figure 4.28).

Table 4.13. *In-vitro* IN inhibition activities and in-silico 3D molecular modelling calculations (free energy of binding) of cinnamoyl derivatives

Compounds	169f	169g	169i	134a	17	175a	166b	176
Binding energy (kcal/mol)	-10.3	-9.1	-9.0	-5.8	-4.7	-4.3	-4.1	-3.9
IN inhibition activity (%) at 50 μ M	87	83	75	69	58	41	26	25

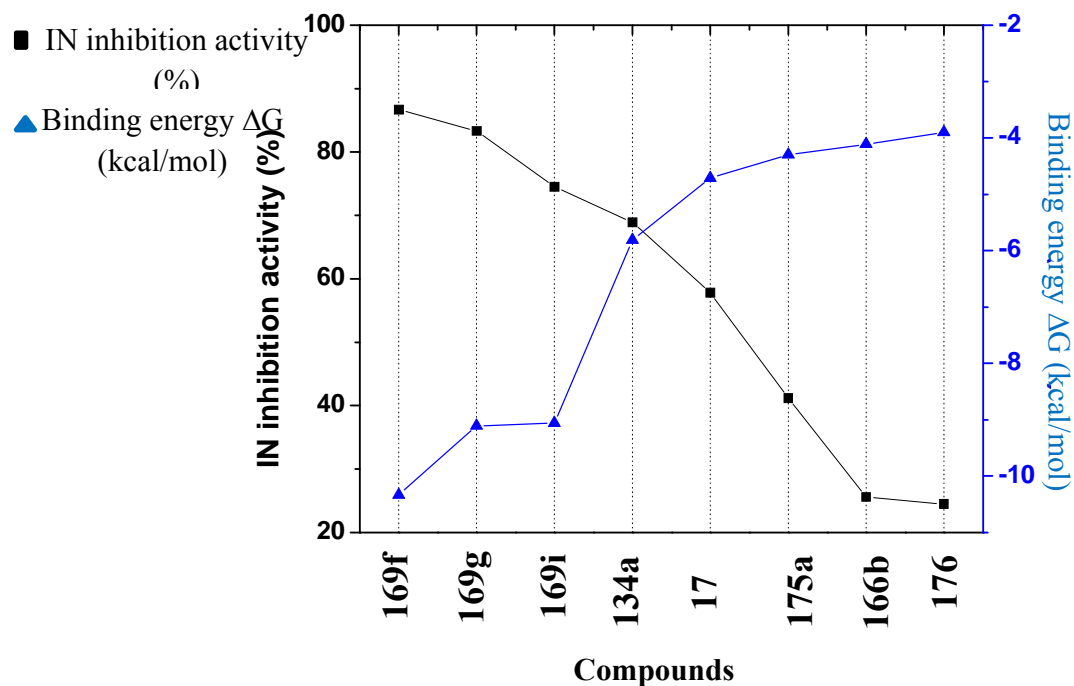


Figure 4.28. IN inhibition potencies of cinnamoyl compounds according to *in vitro* (black curve) and *in silico* (blue curve) analyses ¹⁸⁴

Figure 4.28 shows that the more active compounds have the lowest free binding energy. As indicated in Equation 1, a low free binding energy implies a stronger binding between the ligand and the IN enzyme resulting in a more negative enthalpy and a decrease in entropy leading to the formation of a tight complex.³⁸¹ In other words, ligands showing good HIV-1 IN inhibition activity form a very tight complex with the IN enzyme.

$$\Delta G_{\text{bind}} = \Delta H - T\Delta S \quad (1)$$

In order to improve experimental data, we selected four active IN inhibitors (compounds **175b**, **166c**, **169f** and **171a**) showing at least 60% inhibition against the untreated enzyme (0%) for dose response experiments (Figure 4.29) which were carried out by the candidate. Their EC₅₀ (Effective concentration for 50% inhibition of the enzyme) values are reported in Table 4.14.

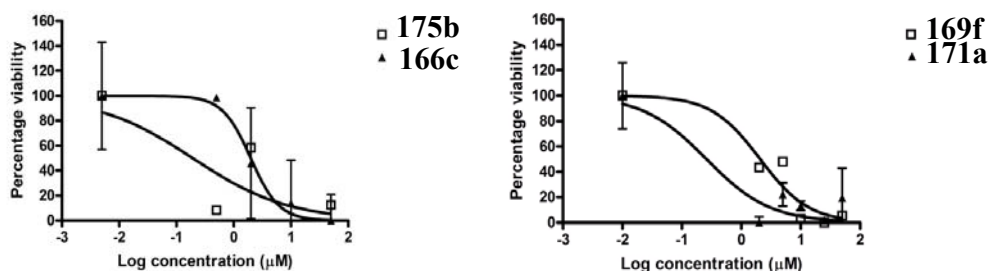


Figure 4.29. Half maximum HIV-IN inhibition by compounds **175b**, **166c**, **169f** and **171**

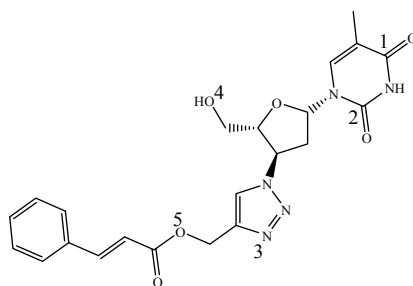
Table 4.14. EC₅₀ values of IN inhibitors

Compounds	171a	175b	166c	169f
EC ₅₀ (μM) from <i>in vitro</i> assays	0.26	0.19	1.98	2.08
EC ₅₀ (μM) predicted from molecular modelling	0.26	593	803	0.026
ΔG(kcal/mol) predicted from molecular modelling	-8.9	-4.4	-4.2	-10.3

The molecular modelling data compared to *in vitro* assays suggested that compound **175b** and compound **166c** are more active than predicted while compound **169f** is less active and compound **171a** has the same activity in both cases. Some of the approximations and assumptions taken into consideration during docking calculations, depend primarily on the strength of binding, while biological experiments are also concerned with kinetic parameters and the solubility of the tested compounds. This could explain why the EC₅₀ values obtained in biological assays were quite different from AUTODOCK predictions (see Table 4.14). However, except for compound **169f**, as far as the *in vitro* activity of the compounds is concerned, the same trend in IN inhibitory activity was observed in molecular modelling predictions. In the case of **169f** and **175b** the thousand fold difference in activity may be due to inadequate accommodation of the various binding factors and bioavailability in the predictive models. Consequently, the predicted values should be viewed with caution.

4.2.2.6. Molecular modelling of cinnamoyl derivatives for the inhibition of HIV-1 RT (1IKW)

Since between the two cinnamate-AZT analogs, compound **178a** showed the best activity against HIV-1 IN, in line with our dual action drug strategy, compound **178a** was also docked into the active site of the reverse transcriptase enzyme.



178a

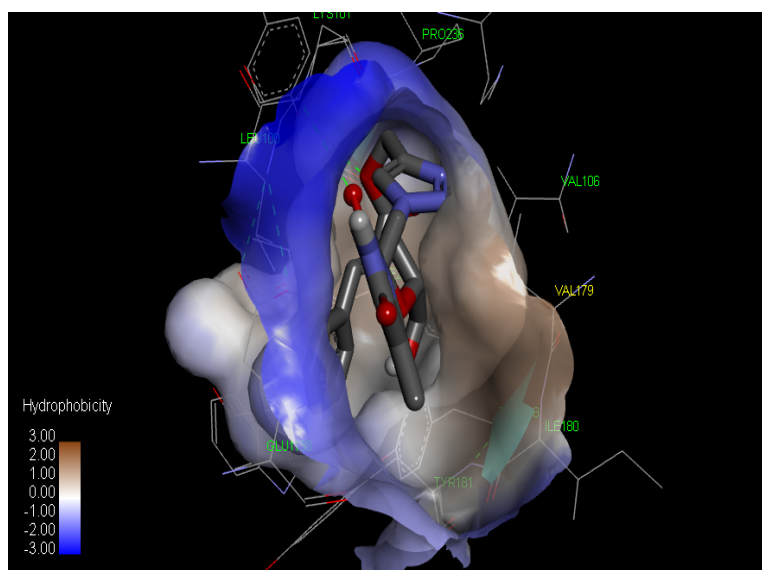


Figure 4.30. Three dimensional representation of compound **178a** in the active site of the HIV-1 reverse transcriptase enzyme (1IKW). Oxygen atoms are red, nitrogen atoms are blue, hydrogen atoms are white, carbon atoms of the protein and the ligand are grey, hydrogen bonds appear as green dots. (Predicted inhibitory concentration: **51.85 nM**)

As depicted in Figure 4.30, compound **178a** occupied a wide hydrophobic cavity surrounded by amino acid residues LEU 100, GLU 1138, TRP 229, LYS 103, LYS 101, VAL 106 and VAL 179. The carbonyl oxygen C-2 appeared hydrogen bonded to the nitrogen atom of LEU 100 (3.13 Å) while the oxygen atom O-5 was bonded to the hydrogen of TYR 318 (2.76 Å). Furthermore, π stacking interactions appeared between LYS 103 and the methylpyrimidine-2,4-dione ring of **AZT 1**.

The docked conformation of compound **178a** and compound **17** in 1IKW was superimposed with Efavirenz, a commercially available reverse transcriptase inhibitor (Figure 4.31).

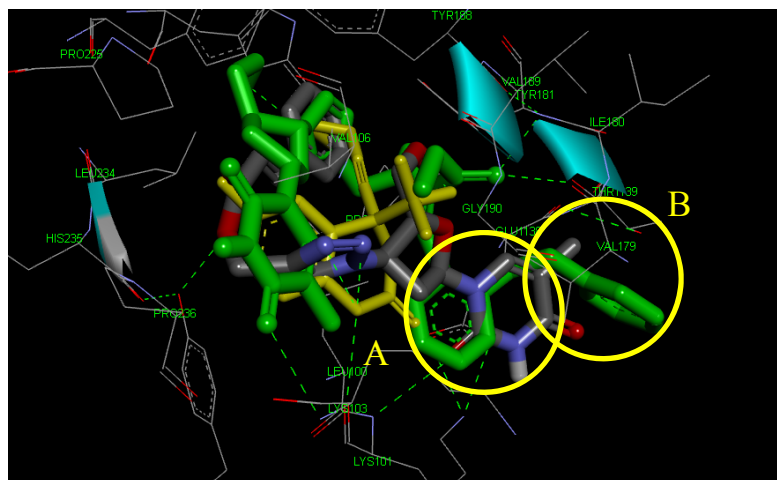


Figure 4.31. Superimposition of conjugate **178a**, **17** and **Efavirenz** ($0.3 \mu\text{M}$)³⁷⁶ (in yellow) in the active site of the HIV-1 reverse transcriptase enzyme (1IKW). Oxygen and bromine atoms are red, hydrogen atoms are white, carbon atoms of the protein and the ligand are grey, compound **17** is green and **Efavirenz** is yellow, hydrogen bonds appear as green dots

It appeared that the cinnamoyl fragment of compound **178a** is in the same pocket of 1IKW as Efavirenz although the methylpyrimidine-2,4-dione of the AZT moiety was directed away from the active site (A in Figure 4.31) and therefore its binding was compromised. Efavirenz therefore has more points of interactions with the enzyme. This could explain why compound **178a** ($22.27 \mu\text{M}$) was predicted less active than Efavirenz ($0.3 \mu\text{M}$). The benzyl group of compound **17** (B) was also outside of the active site and this could justify its lower activity compared to compound **178a** according to both *in vitro* and *in silico* data.

4.2.2.7. *In vitro* assays of cinnamoyl derivatives for the inhibition of HIV-1 RT (1IKW)

Colorimetric bio-assays (described in Section 6.2.17.3) were conducted on compounds **178a**, **17** and **AZT 1** to determine their activity against HIV-1 RT. Percentage *in vitro* RT inhibition, the IC_{50} predict and the binding energy of **AZT 1**, compound **178a** and compound **17** were compared in Table 4.15.

Table 4.15. Comparison of cinnamate ester-AZT conjugates in 1IKW (RT)

Compounds	178a	17	1
Binding energy (kcal/mol)	-9.94	-6.31	-7.39
IC ₅₀ predicted (μM)	5.18×10^{-2}	23.86	3.82
% activity at 50 μM	88	59	67

According to *in vitro* experimental results and docking results, compound **178a** had the highest HIV-1 RT inhibition with the lowest binding energy and predicted inhibition concentration. As predicted, the linearity of compound **178a** has an enhancing effect on its activity compared to compound **17**. The activity of **1** appeared to be improved in 1IKW for compound **178a** owing to the nature of the cinnamoyl fragment attached to it (from 67 to 88% RT inhibition).

4.3. SUMMARY

According to the results obtained for the coumarin derivatives we were able to observe:

- Coumarin-acrylate analogs (**134b**, **134e**, **134d**, **134c**) are more active against HIV-1 PR than our coumarin-acrylonitrile conjugate (**134a**) owing to the interaction of the exocyclic carbonyl (C-3') with the backbone of 1HXW (Table 4.1).
- Coumarin-acrylate (ester) analog **134d** was predicted to be more active than its corresponding coumarin-acrylate (ketone) analog **134e** thanks to the interaction of its exocyclic acyl oxygen O-4'.
- The substitution of three protons on C-5' (see structure of compound **134d**) of the ester group by three methyl groups (**134c**) enhanced its activity if compared to the case where only one proton is substituted (**134b**).
- Coumarin-acrylate analogs (**134b**, **134e**, **134d**, **134c**) were predicted to be more active than the coumarin-alkyne conjugate (**137**).

- Coumarin derivatives appeared to be active only in the HIV-1 PR enzyme *in silico* and inactive in the HIV-1 IN enzyme *in silico* and *in vitro* (Table 4.1 and Table 4.12).

According to the results obtained for the benzotriazole derivatives we were able to observe:

- Benzotriazole derivatives were found to be more active in the active site of 1 HXW enzyme than the indenol analogs. The reason being that geometry of benzotriazole compounds favored more interactions with the binding site of the enzyme than that of the indenol analogs.
- Strongly electron donating/withdrawing substituents at position 5 of benzotriazole analogs hindered the activity of these compounds, while the softer bulkier electron withdrawing substituents appeared to enhance their activity (Table 4.2).
- The nature of the aryl ring in benzotriazole derivatives was somewhat important, since replacement of the phenyl ring by a naphthyl group resulted in a better activity of the corresponding benzotriazole conjugate [Table 4.4, compound **121i** ($IC_{50} = 9.99 \mu M$) and **121h** ($IC_{50} = 2.21 \mu M$)].

According to the docking and *in vitro* results obtained for the cinnamoyl derivatives we were able to conclude that:

- Acrylic acid analogs and, more specifically compound **169f**, showed very good *in silico* and *in vitro* activity against 1QS4 and were also highly active when compared to **5 CITEP** (Figure 4.25, Table 4.14).
- The esterification of cinnamic acid derivatives was deleterious to their inhibitory activity in 1QS4 (Table 4.10).
- Formyl substituted cinnamate esters appeared to be completely inactive against the IN enzyme *in silico* and *in vitro* (Table 4.12).
- The interpretation of trends in the binding affinity of cinnamic acid derivatives revealed that electron donating groups at the *para* position of the aromatic ring

improved their activity if compared to the presence of electron withdrawing groups at the same position (Table 4.8).

- Benzyl group appeared to activate cinnamic acid analogs at the ortho position of the aromatic ring (Table 4.8, Table 4.9).
- Tertiary amides (compound **171b**) appeared to be more active in 1QS4 if compared to secondary (compound **175b**) and primary amides (compound **166b**)(Table 4.7).
- Compound **178a** demonstrated potential activity against both 1QS4 (IN) and 1IKW (RT) even though its predicted inhibition constants appeared to be low if compared to commercially available anti-HIV drugs in both cases. The attachment of a cinnamoyl fragment to **AZT 1** seemed to enhance the activity of **1** significantly *in silico* and *in vitro* against the HIV-1 RT enzyme (Table 4.15) due to an extended capacity for hydrogen bonding and hydrophobic interactions.

CHAPTER FIVE

SUMMARY AND GENERAL CONCLUSIONS

The present study has focussed on the syntheses of novel organic compounds and the study of their inhibitory activity against HIV-1 enzymes.

Having in mind the structure of HIV-1 inhibitor pharmacophores [cinnamoyl skeleton (against IN), coumarin, indenol and benzotriazole skeletons (against PR)], novel potential HIV-1 inhibitors were synthesized *via* green chemistry methods [(microwave assisted synthesis, click chemistry, palladium catalyzed reactions (Heck and Sonogashira coupling)], Baylis Hillman reactions and aldol condensation. These compounds were fully characterized by spectroscopy (IR, 1D and 2D NMR), elemental analysis, melting point and/or HRMS.

Aryne rings generated *in situ* from anthranilic acid derivatives were coupled with a wide range of azides including the well-known RT inhibitor azidothymidine (AZT) using 1,3-dipolar cycloadditions. Twenty-two benzotriazole derivatives (among which were six novel analogs) were generated in good yields (ranging from 46 to 71%).

By using aldol condensation, esterification and peptide chemistry, two acrylamides, eight cinnamic acid derivatives, six cinnamate esters, two novel cinnamate ester-AZT conjugates and four cinnamic acid-peptide analogs (among which two novel peptides) were synthesized. Furthermore, optimisation of the Heck reaction conditions on five novel nonafllyl benzaldehyde coupled with activated alkenes afforded eight novel formyl substituted cinnamate esters (yields ranging from 5 to 47%).

Through Baylis Hillman methodology, chromone and chloromethyl coumarin compounds were prepared. Commercially available coumarin was derivatized by performing palladium catalyzed reactions (the Heck and the Sonogashira coupling) to afford six novel coumarin-alkene and coumarin-alkyne conjugates in decent yields (42 to 62%).

Because of problems related to the rapid decomposition of indenol compounds, they qualify as poor drug candidates. This is the reason why only two novel indenols were

generated by catalytic cyclic vinyl palladation of iodobenzaldehyde derivatives with an internal alkyne. Molecular modelling was performed on the synthesized compounds in order to examine their binding mode in the crystal structure of the three different HIV-1 enzymes, and also for screening purposes since a trend in their potential anti HIV-1 efficiency could be anticipated from their predicted inhibitory concentration and free binding energy.

From docking studies, different types of interactions (hydrophobic, hydrophilic and hydrogen bond) provided valuable information with regards to the binding affinity of the ligands to the targeted enzyme. *In silico* docking of cinnamoyl analogs in 1QS4 showed inhibitory concentration ranging from 904.53 μM to 0.05 μM . In line with our dual action strategy, cinnamate-AZT conjugates bound and showed good activity in both 1QS4 and 1IKW active sites. Furthermore, these compounds also tend to improve the activity of **AZT 1** in 1IKW. Compound **178a** appeared to have a better activity than compound **17** and this implies that our strategy in improving on the linearity of these cinnamate ester-AZT conjugates was successful. Finally, benzotriazole-AZT analogs were also active in both 1HXW and 1IKW active sites.

Saturation Transfer Difference (STD) NMR was employed to determine the binding and the interaction of cinnamoyl derivatives to the IN enzyme. It appeared that compound **178a**, compound **170b**, compound **169e** and compound **169d** showed some binding to the IN enzyme. To conclude this study, *in vitro* biological assays against HIV-1 PR, RT and IN enzymes were conducted.

The biological assay data revealed that, in most cases, there was a correlation with the trend of the inhibitory activity of the compounds from molecular modelling results (binding energy and predicted IC_{50}). Acrylic acid derivatives and benzotriazole-AZT conjugates showed very good IN and RT inhibitory activity respectively. Compound **175b** ($\text{EC}_{50} = 0.19 \mu\text{M}$) and compound **171a** ($\text{EC}_{50} = 0.26 \mu\text{M}$) appeared to be more active than the commercially available IN inhibitor **5 CITEP** ($\text{EC}_{50} = 0.65 \mu\text{M}$). As anticipated by molecular modelling studies, attaching a cinnamoyl fragment to AZT and cyclising AZT with anthranilic acid tend to improve the inhibitory activity of AZT against the RT enzyme. Our IN and PR dual action strategy was not achieved with

coumarin analogs. They appeared to be poor drug candidates as PR inhibitors while compound **134b** showed a good activity as an IN inhibitor.

A combination of molecular modelling (binding modes and interactions strength), STD NMR and *in vitro* assays provided an efficient platform for the discovery of potential HIV-1 enzymes inhibitors. While all the objectives of this investigation have been addressed, future reasearch in this area could include:

- i) Investigate the consistency between molecular modelling and *in vitro* assay by focussing on the approximations accounted for in molecular modelling calculations (for instance predicted inhibitory concentration and free binding energy).
- ii) Optimise the structure of coumarin-alkene derivatives to improve HIV-1 PR and IN inhibitory activity.
- iii) Prevent the decomposition of indenols for further derivatization.
- iv) Investigate a novel procedure for the cyclisation of formyl substituted cinnamate esters to afford five membered heterocyclic ring systems.

CHAPTER SIX

EXPERIMENTAL

6.1. GENERAL

Unless otherwise stated, all procedures were conducted under nitrogen in oven-dried glassware with addition of liquid components by syringe. All solvents were dried by standard procedures outlined in Vogel.³⁸² AZT was obtained from Aspen Pharmacare, courtesy of Dr C. Stubbs. All other chemicals were purchased from Sigma Aldrich®, and unless otherwise stated, were used as received.

Thin layer chromatography (TLC) was carried out on pre-coated Merck® Kieselgel 60 silica gel and basic alumina plastic sheets viewed under UV light (254/365 nm). Preparative plates were prepared using Merck® Kieselgel P/UV₂₅₄ silica gel with fluorescence indicator. Column chromatography was carried out with Merck® silica gel 60 [230-400 mesh (particle size 0.020-0.063 nm)] and aluminum oxide activated basic Brockmann I (standard grade 150 mesh).

The structures of compounds were deduced from ¹H, ¹³C, DEPT-135, COSY, HMBC and HSQC NMR spectroscopic data recorded on a Bruker® AMX 400 MHz or a Bruker® Biospin 600 MHz instrument at 303 K unless otherwise stated. ¹H chemical shifts are given in ppm relative to the residual solvent peak, and ¹³C chemical shifts (ppm) are relative to the central peak of the solvent signal. Calibration of deuterated solvents (CDCl₃, DMSO-*d*₆, MeOH-*d*₄ and D₂O) signals were performed. Coupling constants are given in Hertz (Hz). IR spectra were recorded on a Perkin Elmer Spectrum 400 FT-IR spectrometer. High resolution mass spectra (HRMS) were recorded on a Waters Synapt G2 spectrometer (University of Stellenbosch, Stellenbosch, South Africa). Fluorometric and colorimetric assays were carried out using a Synergy Mx multi-mode microplate reader. Microwave syntheses were performed on a CEM Discover single-mode

microwave apparatus. Melting points were determined using a Reichert (Austria) hot stage apparatus, and are uncorrected.

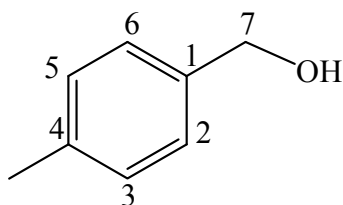
Molecular modelling was performed using AUTODOCK 4.2,³¹⁹ the minimized and docked structures of the ligands viewed in DSV.³³⁰

The numbers used for the characterization of structures do not necessarily comply with the IUPAC rules.

6.2. PROCEDURES

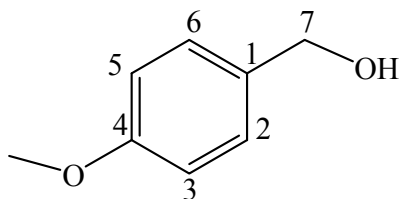
6.2.1. Preparation of benzylalcohol derivatives

p-Tolylmethanol **106a**



p-Methylbenzaldehyde (0.20 mL, 1.7 mmol) was dissolved in MeOH (10 mL) and aqueous solution of NaOH (7.0 mL, 10 M) was added. The mixture was heated at 85 °C. After two hours, the solution was allowed to cool down and extracted into EtOAc (3×15 mL). The combined organic layers were dried over MgSO₄ (anhydrous). The solvent was removed *in vacuo* and pure *p*-tolylmethanol **106a** was obtained as a yellowish solid (0.20 g, 98%); m.p. 52-54 °C (lit.³⁸³ 50-52 °C); ν_{\max} (cm⁻¹) 3344.04 (OH); ¹H NMR (600 MHz, CDCl₃) 1.96 (1H, s, OH), 2.39 (3H, s, CH₃), 4.65 (2H, s, 7-H), 7.20 (2H, d, *J* = 7.91 Hz, 3-H, 5-H, Ar-H), 7.28 (2H, d, *J* = 7.81 Hz, 2-H, 6-H, Ar-H); ¹³C NMR (150 MHz, CDCl₃) 20.8 (CH₃), 64.8 (7-C), 126.7 (2-C, 6-C), 128.9 (3-C, 5-C), 137.0 (4-C), 137.6 (1-C).

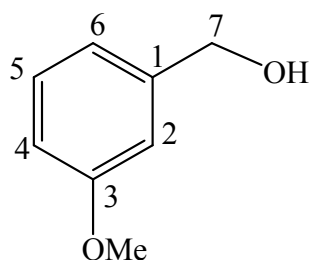
(4-Methoxyphenyl)methanol **106b**



The procedure described for the synthesis of *p*-tolylmethanol **106a** was followed, using *p*-

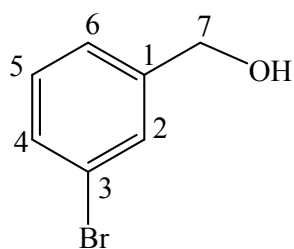
methoxybenzaldehyde (0.21 mL, 1.7 mmol) and NaOH (7.0 mL, 10 M) in MeOH (10mL). Work-up afforded *(4-methoxyphenyl)methanol* as a yellow oil **106b** (0.21 g, 88%); ν_{\max} (cm^{-1}) 3328.88 (OH); ^1H NMR (600 MHz, CDCl_3) 3.81 (3H, s, OCH_3), 4.58 (2H, s, 7-H), 6.89 (2H, d, $J = 8.70$ Hz, 2-H, 6-H, Ar-H), 7.28 (2H, s, $J = 8.62$ Hz, 3-H, 5-H, Ar-H); ^{13}C NMR (150 MHz, CDCl_3) 55.2 (OCH_3), 64.7 (7-C), 113.8 (2-C, 6-C), 128.5 (3-C, 5-C), 133.1 (1-C), 159.0 (4-C).

(3-Methoxyphenyl) methanol **106c**



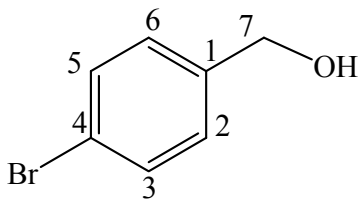
The procedure described for the synthesis of *p*-tolylmethanol **106a** was followed, using *m*-methoxybenzaldehyde (0.21 mL, 1.7 mmol) and aqueous NaOH (7.0 mL, 10 M) in MeOH (10mL). Work-up afforded *(3-methoxyphenyl)methanol* **106c** as a yellow oil (0.23 g, 98%); ν_{\max} (cm^{-1}) 3340.90 (OH); ^1H NMR (600 MHz, CDCl_3) 3.83 (3H, s, OCH_3), 4.67 (2H, s, 7-H), 6.85 (1H, d, $J = 9.39$ Hz, 6-H, Ar-H), 6.94 (1H, s, 2-H, Ar-H), 6.95 (1H, s, 4-H, Ar-H), 7.29 (1H, t, $J = 7.98$ Hz, 5-H, Ar-H); ^{13}C NMR (150 MHz, CDCl_3) 54.9 (OCH_3), 64.9 (7-C), 112.0 (2-C), 113.0 (4-C), 112.0 (6-C), 129.3 (5-C), 142.3 (1-C), 159.5 (3-C).

(3-Bromophenyl)methanol **106d**



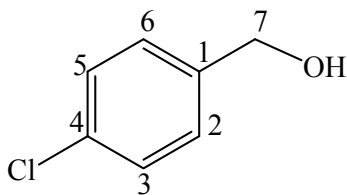
The procedure described for the synthesis of *p*-tolylmethanol **106a** was followed, using *m*-bromobenzaldehyde (0.20 mL, 1.7 mmol) and aqueous NaOH (7.0 mL, 10 M) in MeOH (10 mL). Work-up afforded *(3-bromophenyl)methanol* **106d** as a colorless oil (0.31 g, 96%); ν_{\max} (cm^{-1}) 3299.12 (OH); ^1H NMR (600 MHz, CDCl_3) 2.03 (1H, s, OH), 4.62 (2H, s, 7-H), 7.21-7.28 (2H, m, $J = 8.17$ Hz, 4-H, 5-H, Ar-H), 7.42 (1H, d, $J = 7.55$ Hz, 6-H, Ar-H), 7.51 (1H, s, 2-H, Ar-H); ^{13}C NMR (150 MHz, CDCl_3) 64.2 (7-C), 122.5 (3-C), 125.2 (6-C), 129.8 (4-C), 130.0 (5-C), 130.5 (2-C), 143.0 (1-C).

(4-Bromophenyl)methanol **106e**



The procedure described for the synthesis of *p*-tolylmethanol **106a** was followed, using *p*-bromobenzaldehyde (0.20 mL, 1.7 mmol) and aqueous NaOH (7.0 mL, 10 M) in MeOH (10 mL). Work-up afforded (4-bromophenyl)methanol **106e** as a white solid (0.23 g, 71%); m.p. 78-80 °C (lit. 76-78 °C); ν_{\max} (cm⁻¹) 3377.96 (OH); ¹H NMR (600 MHz, CDCl₃) 2.03 (1H, s, OH), 4.62 (2H, s, 7-H), 7.21 (2H, d, *J* = 8.17 Hz, 2-H, 6-H, Ar-H), 7.47 (2H, d, *J* = 8.26 Hz, 3-H, 5-H, Ar-H); ¹³C NMR (150 MHz, CDCl₃) 64.6 (7-C), 121.4 (4-C), 128.6 (2-C, 6-C), 131.6 (3-C, 5-C), 139.7 (1-C).

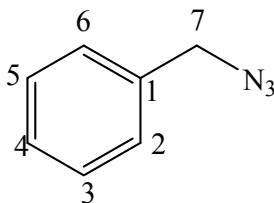
(4-Chlorophenyl)methanol **106f**



The procedure described for the synthesis of *p*-tolylmethanol **106a** was followed, using *p*-chlorobenzaldehyde (0.20 mL, 1.7 mmol) and aqueous NaOH (7.0 mL, 10 M) in MeOH (10 mL). Work-up afforded (4-chlorophenyl)methanol **106f** as a lilac solid (0.23 g, 96%); m.p. 70-72 °C (lit.³⁸³ 68-70 °C); ν_{\max} (cm⁻¹) 2097.16 (OH); ¹H NMR (600 MHz, CDCl₃) 2.32 (1H, s, OH), 4.63 (2H, s, 7-H), 7.28 (2H, d, *J* = 8.54 Hz, 2-H, 6-H, Ar-H), 7.33 (2H, d, *J* = 8.43 Hz, 3-H, 5-H, Ar-H); ¹³C NMR (150 MHz, CDCl₃) 64.2 (7-C), 128.0 (2-C, 6-C), 128.4 (3-C, 5-C), 133.0 (4-C), 139.0 (1-C).

6.2.2. Preparation of benzylazide

1-(Azidomethyl)benzene **109**



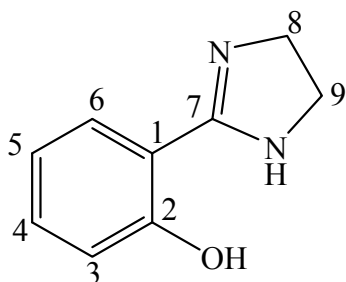
To a solution of benzylbromide (0.49 mL, 4.2 mmol) in 4.8 mL of DMF was added sodium azide (0.29 g, 4.6 mmol). The flask was equipped with a condenser and subjected to microwave irradiation for one hour at 80 °C and 150 W. The reaction mixture was cooled to room temperature and unreacted sodium azide was filtered off and the filtrate extracted with Et₂O (3×10 mL). The combined ether

layers were dried over MgSO_4 (anhydrous) and the solvent was allowed to evaporate to give *1-(azidomethyl)benzene* **109** as a yellow oil (0.48 g, 85%); ν_{max} (cm^{-1}) 2093.15 (N_3); ^1H NMR (600 MHz, CDCl_3) 4.35 (2H, s, 7-H), 7.38 (5H, m, 2-H, 6-H, 3-H, 5-H, 4-H, Ar-H); ^{13}C NMR (100 MHz, CDCl_3) 54.7 (7-C), 128.1 (3-C, 5-C), 128.2 (4-C), 128.7 (2-C, 6-C), 135.3 (1-C).

6.2.3. Iodination/bromination of anthranilic acid

Preparation of the vanadium catalyst

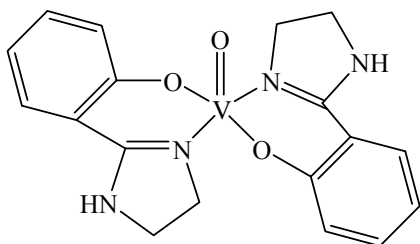
2-(4,5-Dihydro-1H-imidazol-2-yl)phenol **115**



Methylsalicylate (1.6 mL, 12 mmol) was added to an excess of ethylene diamine (3.6 mL, 53 mmol) in a vial and sealed. This vial was subjected to microwave irradiation for 7 minutes at 100 W. The solid material obtained was dissolved in CHCl_3 (3 mL) and purified by preparative thin layer chromatography with hexane:EtOAc (1:1) to afford 2-

(4,5-dihydro-1H-imidazol-2-yl)phenol **115** as a cream solid (1.4 g, 70%); m.p. 200-202 °C (lit.³⁸⁴ 200-203 °C); ν_{max} (cm^{-1}) 3146.86 (NH), 3261.08 (OH), 1591.21 ($\text{C}=\text{N}$); ^1H NMR (600 MHz, MeOD) 3.63 (2H, s, 8-H, 9-H), 6.85-6.88 (2H, m, 6-H, 3-H, Ar-H), 7.35 (1H, m, 5-H, Ar-H), 7.73 (1H, dd, $J = 1.53$ Hz and $J = 6.39$ Hz, 4-H, Ar-H); ^{13}C NMR (150 MHz, MeOD) 40.3 (8-C), 116.9 (1-C), 118.5 (3-C), 120.1 (5-C), 128.88 (6-C), 134.8 (4-C), 161.3 (2-C), 171.6 (7-C).

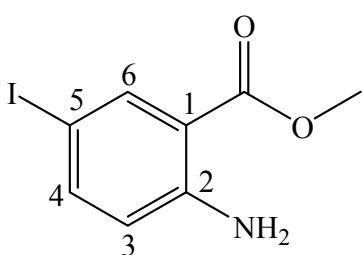
Vanadium catalyst **116**²⁴⁵



A solution of 2-(4,5-dihydro-1H-imidazol-2-yl)phenol (0.25 g, 15 mmol) in MeOH (5 mL) was added to vanadyl sulfate (0.15 g, 0.7 mmol) in water (5 mL). A green precipitate was formed immediately.

The reaction was allowed to proceed for a further 2 hours. The green precipitate was filtered off to afford pure vanadium catalyst **116** (0.13 g, 46%); m.p. 110-112 °C, ν (cm⁻¹) 3248.82 (NH), 1575.62 (C=N), 929.56 (V=O).

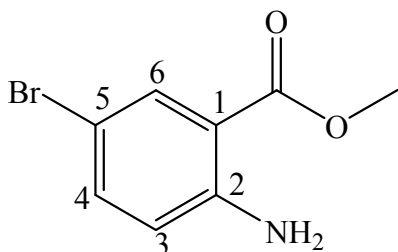
Methyl 2-amino-5-iodobenzoate **117a**



Anthranilic acid (1.0 g, 7.3 mmol) was dissolved in MeOH (15 mL) and heated at 60 °C. Subsequently KI (1.2 g, 7.4 mmol) was added to the warmed solution followed by H₂SO₄ (0.58 mL) and H₂O₂ (0.345 mL, 14.7 mmol). Finally 10 mol% of the vanadium catalyst was added and the solution was left heating overnight under reflux. The

mixture was cooled to room temperature and a saturated solution of Na₂S₂O₃ was added. The catalyst was filtered off and the organic layer was extracted with EtOAc and washed with brine. The combined organic layers were dried over MgSO₄ (anhydrous) and concentrated under vacuum. The residue was purified by preparative thin layer chromatography with hexane:EtOAc (9:1) to afford *methyl 2-amino-5-iodobenzoate* **117a** as a beige solid (1.4 g, 70%); m.p. 84-86 °C (lit.³⁸⁵ 83-84 °C); ν_{max} (cm⁻¹) 3330.1015 (NH₂), 1679.50 (C=O); ¹H NMR (600 MHz, CDCl₃) 3.91(s, 3H, OCH₃), 6.74 (1H, d, *J*= 8.88 Hz, 3-H, Ar-H), 7.55 (1H, d, *J*= 8.86 Hz, 4-H, Ar-H), 8.22 (1H, s, 6-H, Ar-H); ¹³C NMR (150 MHz, CDCl₃) 52.1 (OCH₃), 78.1 (5-C), 112.8 (1-C), 114.5 (3-C), 139.7 (6-C), 143.1 (4-C), 150.9 (2-C), 167.3 (C=O).

Methyl 2-amino-5-bromobenzoate **117b**

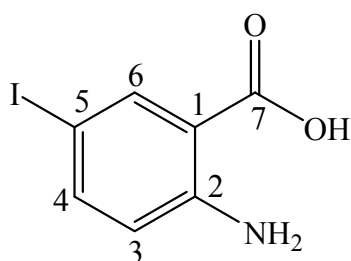


The procedure described for the synthesis of methyl 2-amino-5-iodobenzoate **117a** was followed, using anthranilic acid (1.0 g, 7.3 mmol), MeOH (15 mL), KBr (0.87 g, 7.3 mmol), H₂SO₄ (0.58 mL), H₂O₂ (0.345 mL, 14.7 mmol) and vanadium catalyst (10 mol%). Work-up

and purification by preparative thin layer chromatography [on silica gel and elution with

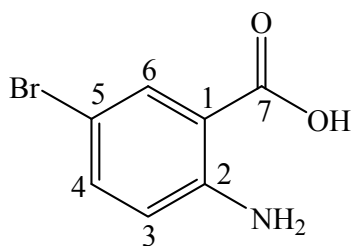
hexane:EtOAc (9:1)] afforded *methyl 2-amino-5-bromobenzoate* as a maroon solid (0.83 g, 49%); m.p. 72-74 °C (lit.³⁸⁶ 74 °C); [HRMS: m/z calculated for $C_8H_8BrNO_2$ (MH^+) 229.9817. Found 229.9808]; ν_{\max} (cm^{-1}) 2948.43 (NH_2), 1685.59 ($C=O$); 1H NMR (600 MHz, $CDCl_3$) 3.85 (3H, s, OCH_3), 5.73 (2H, s, NH_2), 6.54 (1H, d, $J = 8.78$ Hz, 3-H, Ar-H), 7.30 (1H, dd, $J = 2.22$ Hz and $J = 6.55$ Hz, 4-H, Ar-H), 7.95 (1H, d, $J = 8.44$ Hz, 6-H, Ar-H); ^{13}C NMR (150 MHz, $CDCl_3$) 51.8 (OCH_3), 107.3 (1-C), 112.1 (5-C), 118.3 (3-C), 133.1 (6-C), 136.7 (4-C), 149.3 (2-C), 167.5 ($C=O$).

2-Amino-5-iodobenzoic acid **118a**



The procedure described for the synthesis of methyl 2-amino-5-iodobenzoate **117a** was followed, using anthranilic acid (1.0 g, 7.3 mmol), CH_3CN (15 mL), KI (1.22 g, 7.35 mmol), H_2SO_4 (0.58 mL), H_2O_2 (0.345 mL, 14.7 mmol), vanadium catalyst (10 mol%). Work-up and purification by preparative thin layer chromatography [on silica gel and elution with hexane:EtOAc (9:1)] afforded 2-amino-5-iodobenzoic acid **118a** as a maroon solid (1.4 g, 75%); m.p. 222-224 °C (lit.³⁸⁷ 220-225 °C); [HRMS: m/z calculated for $C_7H_6INO_2$ (MH^+) 263.9521. Found 263.9519]; ν_{\max} (cm^{-1}) 3325.20 (OH), 2947.47 (NH_2), 1660.15 ($C=O$); 1H NMR (600 MHz, $CDCl_3$) 6.80 (1H, d, $J = 8.76$ Hz, 3-H, Ar-H), 7.76 (1H, dd, $J = 1.98$ Hz and $J = 6.79$ Hz, 4-H, Ar-H), 7.84 (1H, d, $J = 8.36$ Hz, 6-H, Ar-H); ^{13}C NMR (150 MHz, $CDCl_3$) 80.3 (5-C), 120.2 (1-C), 122.6 (3-C), 141.8 (6-C), 145.3 (4-C), 161.2 (2-C), 195.3 (7- $C=O$).

2-Amino-5-bromobenzoic acid **118b**



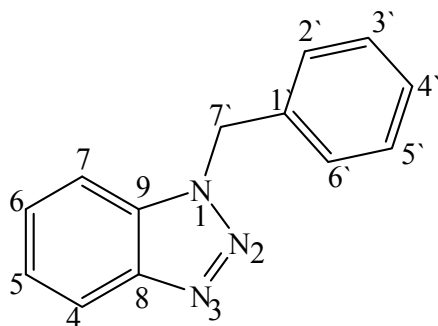
Method 1. The procedure described for the synthesis of methyl 2-amino-5-iodobenzoate **117a** was followed, using anthranilic acid (1.0 g, 7.3 mmol), CH_3CN (15 mL), KBr (0.87 g, 7.3 mmol), H_2SO_4 (0.58 mL), H_2O_2 (0.345 mL, 14.7 mmol) and vanadium catalyst (10 mol%). Work-up

and purification by preparative thin layer chromatography [on silica gel and elution with hexane:EtOAc (9:1)] afforded *2-amino-5-bromobenzoic acid* **118b** as a brown solid (0.21 g, 13%); m.p. 210-212 °C (lit.³⁸⁸ 218-220 °C); [HRMS: m/z calculated for $C_7H_6BrNO_2$ (MH^+) 215.9660. Found 215.9654]; ν_{max} (cm^{-1}) 3354.08 (OH), 3354.45 (NH_2), 1684.39 (C=O); 1H NMR (600 MHz, MeOD) 6.67 (1H, d, J = 8.84 Hz, 3-H, Ar-H), 7.29 (1H, dd, J = 2.39 Hz and J = 6.48 Hz, 4-H, Ar-H), 7.74 (1H, d, J = 8.22 Hz, 6-H, Ar-H); ^{13}C NMR (150 MHz, MeOD) 107.0 (1-C), 113.0 (5-C), 119.6 (3-C), 134.7 (6-C), 137.5 (4-C), 152.0 (2-C), 170.3 (7-C=O).

Method 2. Anthranilic acid (0.7 g, 5 mmol) was added to a reaction flask containing 5 mL of H_2O and KBr (0.6 g, 5 mmol). After the mixture was stirred for one minute at room temperature, 30% H_2O_2 (0.70 mL, 30 mmol) was added dropwise. Vanadium oxide (10 mol%) followed by 70% $HClO_4$ (0.1 mL, 2 mmol) was added to the above mixture. The catalyst was filtered off and the reaction mixture subjected to three ether extractions. The combined filtrates were washed with saturated sodium bicarbonate solution. The organic extract was dried over anhydrous sodium sulfate and the solvent evaporated under reduced pressure to afford pure *2-amino-5-bromobenzoic acid* **118b** as a brown solid (1.1 g, 71%).

6.2.4. Preparation of benzotriazole derivatives

1-Benzyl-1*H*-benzo[1,2,3]triazole **111f**



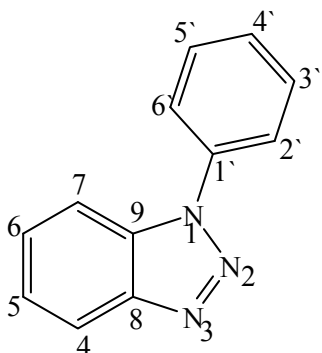
Method 1. 1-(Azidomethyl)benzene (1.5 mL, 12 mmol) and 10 mL of DME (Dimethoxyethane) were mixed in a 100 mL round bottom flask fitted with a reflux condenser and the solution was heated at 70-80 °C. Meanwhile, two solutions were prepared in two 25 mL Erlenmeyer flasks, the first

one containing anthranilic acid (**82**) (0.39 g, 2.9 mmol) with 12 mL of DME and the

second solution containing iso-amyl nitrite (*t*-BuONO 0.60 mL, 4.5 mmol) in 10 mL DME. A 2.0 mL aliquot of each solution was added through the condenser to the refluxing solution, by using two separate Pasteur pipettes at 8-10 minute intervals. The solution turned to a brown color after the reagent solutions were fully added. Then the mixture was refluxed overnight. The mixture was extracted with EtOAc and dried over MgSO₄ (anhydrous). Finally the isolated crude solid was recrystallized in MeOH to give pure *l*-benzyl-1H-benzo[1,2,3]triazole **111f** as yellow crystals (0.43 g, 71%); m.p. 112-114 °C (lit.³⁸⁹ 113-115 °C); [HRMS: *m/z* calculated for C₁₃H₁₁N₃ (MH⁺) 210.1031. Found 210.1029]; ν_{\max} (cm⁻¹) 3067.39, 3031.13, 1224.19, 744.08; ¹H NMR (600 MHz, CDCl₃) 5.87 (2H, s, 7'-H), 7.31-7.39 (8H, m, 5-H, 6-H, 7-H, 3'-H, 4'-H, 5'-H, 2'-H, 6'-H, Ar-H), 8.09 (1H, d, *J* = 8.27 Hz, 4-H, Ar-H); ¹³C NMR (150 MHz, CDCl₃) 52.3 (7'-C), 109.8 (4-C), 120.1 (7-C), 123.9 (5-C), 127.4 (3'-C, 5'-C), 127.6 (4'-C), 128.5 (1'-C), 129.1 (2'-C, 6'-C), 132.8 (9-C), 134.8 (6-C), 146.4 (8-C).

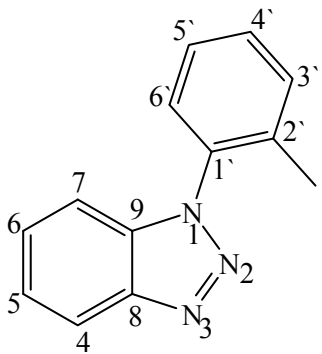
Method 2. Benzylamine (1.1 mL, 10 mmol) was dissolved in DME (12 mL). To the stirring mixture was added *t*-BuONO (0.96 mL, 7.1 mmol) followed by trimethylsilyl azide TMSN₃ (0.56 mL, 4.3 mmol) added dropwise. The resulting solution was stirred at room temperature for one hour. Two solutions, *t*-BuONO (0.56 mL, 4.2 mmol) in DME (10 mL) and the benzyne precursor anthranilic acid (**82**) (0.57 g, 4.2 mmol) in DME (10 mL) were prepared. Over a period of 25 minutes, these two solutions were simultaneously added dropwise to the refluxing reaction. When the addition was complete, the mixture was stirred under reflux overnight. The reaction mixture was allowed to cool to room temperature. Saturated NaHCO₃ solution (10 mL) was added and the mixture was extracted with EtOAc (2×50 mL). The combined organic layers were washed with water (20 mL) and brine (20 mL), and finally dried over anhydrous sodium sulfate. The solvent was removed *in vacuo* and the crude residue purified by silica gel chromatography and elution with hexane:EtOAc (6:1) to afford *l*-benzyl-1H-benzo[1,2,3]triazole **111f** as a brown oil (0.46 g, 53%).

1-Phenyl-1*H*-benzo[1,2,3]triazole **121a**



The procedure described for the synthesis of 1-benzyl-1*H*-benzo[1,2,3]triazole **111f** (Method 2) was followed, using aniline (0.45 mL, 5.0 mmol), *t*-BuONO (0.76 mL, 5.7 mmol) in two portions), TMSN₃ (0.28 mL, 2.1 mmol) and anthranilic acid (**82**) (0.28 g, 2.1 mmol). Work-up and purification by preparative thin layer chromatography [on silica gel and elution with hexane:EtOAc (6:1)] afforded *l*-phenyl-1*H*-benzo[1,2,3]triazole **121a** as a dark solid (0.18 g, 44%); m.p. 80-82 °C (lit.³⁹⁰ 84 °C); ν_{\max} (cm⁻¹) 3057.32, 2923.92, 1499.13, 763.45; ¹H NMR (600 MHz, CDCl₃) 7.44 (1H, t, *J* = 7.61 Hz, 6-H, Ar-H), 7.51 (1H, t, *J* = 7.61 Hz, 5-H, Ar-H), 7.55-7.62 (3H, m, 4'-H, 3'-H, 5'-H, Ar-H), 7.75 (1H, d, *J* = 8.36 Hz, 7-H, Ar-H), 7.77 (2H, d, *J* = 7.97 Hz, 2'-H, 6'-H, Ar-H), 8.15 (1H, d, *J* = 8.38 Hz, 4-H, Ar-H); ¹³C NMR (150 MHz, CDCl₃) 110.3 (4-C), 120.3 (7-C), 122.9 (5-C), 124.4 (6-C), 128.2 (4'-C), 128.7 (3'-C, 5'-C), 129.8 (2'-C, 6'-C), 132.3 (1'-C), 137.0 (9-C), 146.5 (8-C).

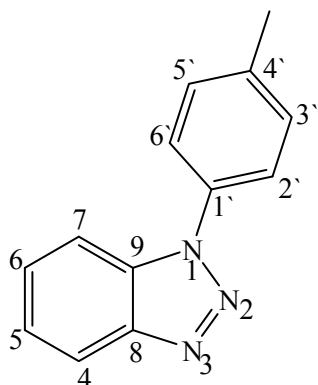
1-*o*-Tolyl-1*H*-benzo[1,2,3]triazole **121b**



The procedure described for the synthesis of 1-benzyl-1*H*-benzo[1,2,3]triazole **111f** (Method 2) was followed, using *o*-toluidine (0.54 mL, 5.0 mmol), *t*-BuONO (0.76 mL, 5.7 mmol), TMSN₃ (0.28 mL, 2.1 mmol) and anthranilic acid (**82**) (0.28 g, 2.1 mmol). Work-up and purification by preparative thin layer chromatography [on silica gel and elution with hexane:EtOAc (6:1)] afforded *l*-*o*-tolyl-1*H*-benzo[1,2,3]triazole **121b** as a reddish oil (0.23 g, 52%); ν_{\max} (cm⁻¹) 3324.61, 2924.52, 1682.33, 745.02; ¹H NMR (600 MHz, CDCl₃) 2.16 (3H, s, CH₃), 7.37 (1H, t, *J* = 8.27 Hz, 3'-H, Ar-H), 7.45-7.52 (6H, m, 4'-H, 5'-H, 6'-H, 4-H, 5-H, 6-H, Ar-H), 8.18 (1H, t, *J* = 8.40 Hz, 7-H, Ar-H); ¹³C NMR (150 MHz, CDCl₃) 17.8 (CH₃), 110.1 (7-C), 120.1 (4-C), 124.1 (5'-C), 125.3 (1'-C),

127.0 (6-C), 127.0 (5-C), 128.0 (4'-C), 130.0 (3'-C), 131.7 (6'-C), 133.9 (9-C), 135.3 (2'-C), 145.6 (8-C).

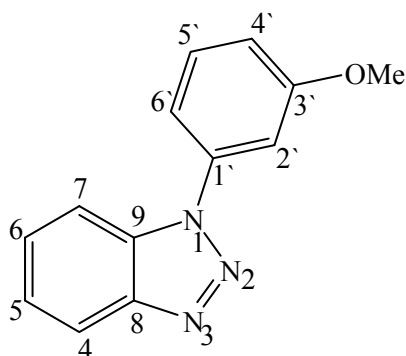
1-*p*-Tolyl-1*H*-benzo[1,2,3]triazole **121c**



The procedure described for the synthesis of 1-benzyl-1*H*-benzo[1,2,3]triazole **111f** (Method 2) was followed, using *p*-toluidine (1.0 mL, 10 mmol), *t*-BuONO (1.5 mL, 11 mmol), TMSN₃ (0.56 mL, 4.3 mmol) and anthranilic acid (**82**) (0.57 g, 4.2 mmol). Work-up and purification by preparative thin layer chromatography [on silica gel and elution with hexane:EtOAc (6:1)] afforded 1-*p*-tolyl-1*H*-benzo[1,2,3]triazole **121c** as a black oil (0.44 g, 50%); ν_{\max}

(cm⁻¹) 2924.36, 1721.11, 1064.80, 818.76; ¹H NMR (600 MHz, CDCl₃) 2.46 (3H, s, CH₃), 7.39-7.41 (3H, m, 5-H, 6'-H, 2'-H, Ar-H), 7.52 (1H, t, *J* = 7.62 Hz, 6-H, Ar-H), 7.64 (2H, d, *J* = 8.29 Hz, 3'-H, 5'-H, Ar-H), 7.71 (1H, d, *J* = 8.33 Hz, 4-H, Ar-H), 8.13 (1H, d, *J* = 8.37 Hz, 7-H, Ar-H); ¹³C NMR (150 MHz, CDCl₃) 21.2 (CH₃), 110.3 (4-C), 120.2 (7-C), 122.8 (3'-C, 5'-C), 124.2 (5-C), 128.0 (6-C), 130.3 (6'-C, 2'-C), 132.5 (1'-C), 134.5 (4'-C), 138.8 (9-C), 146.4 (8-C).

1-(3-Methoxyphenyl)-1*H*-benzo[1,2,3]triazole **121d**

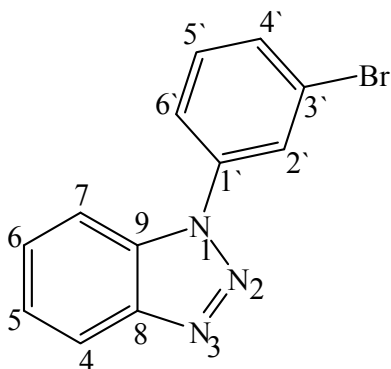


The procedure described for the synthesis of 1-benzyl-1*H*-benzo[1,2,3]triazole **111f** (Method 2) was followed, using *m*-anisidine (1.1 mL, 10 mmol), *t*-BuONO (1.5 mL, 11 mmol) and TMSN₃ (0.56 mL, 4.3 mmol) and anthranilic acid (**82**) (0.57 g, 4.2 mmol). Work-up and purification by preparative thin layer chromatography [on silica gel and elution with

hexane:EtOAc (6:1)] afforded 1-(3-methoxyphenyl)-1*H*-benzo[1,2,3]triazole **121d** as a black oil (0.36 g, 38%); [HRMS: *m/z* calculated for C₁₃H₁₁N₃O (MH⁺) 226.0980. Found 226.0974]; ν_{\max} (cm⁻¹) 3461.36, 2936.68, 1594.05, 743.67; ¹H NMR (600 MHz, CDCl₃)

3.91 (3H, s, OCH₃), 7.04 (1H, d, J = 8.31 Hz, 4-H, Ar-H), 7.36 (2H, m, 2'-H, 4'-H, Ar-H), 7.44 (1H, t, J = 7.61 Hz, 6'-H, Ar-H), 7.51 (1H, d, J = 16.00 Hz, 5-H, Ar-H), 7.55 (1H, t, J = 7.61 Hz, 6-H, Ar-H), 7.77 (1H, d, J = 8.38 Hz, 5'-H, Ar-H), 8.15 (1H, d, J = 8.36 Hz, 7-H, Ar-H); ¹³C NMR (150 MHz, CDCl₃) 55.6 (OCH₃), 109.7 (2'-C), 110.5 (4'-C), 114.5 (7-C), 114.7 (4-C), 120.3 (6'-C), 124.4 (5-C), 128.2 (6-C), 130.6 (5'-C), 132.3 (1'-C), 138.0 (9-C), 146.5 (8-C), 160.7 (3'-C).

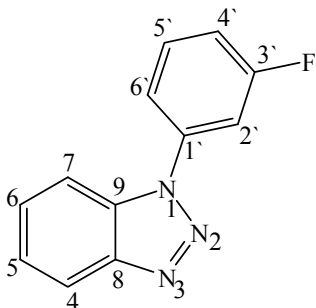
1-(3-Bromophenyl)-1*H*-benzo[1,2,3]triazole **121e**



The procedure described for the synthesis of 1-benzyl-1*H*-benzo[1,2,3]triazole **111f** (Method 2) was followed, using *m*-bromoaniline (0.54 mL, 5.0 mmol), *t*-BuONO (0.76 mL, 5.7 mmol), TMSN₃ (0.56 mL, 4.3 mmol) and anthranilic acid (**82**) (0.28 g, 2.1 mmol). Work-up and purification by preparative thin layer chromatography [on silica gel and elution with hexane:EtOAc (6:1)] afforded 1-(3-bromophenyl)-1*H*-benzo[1,2,3]triazole

121e as yellow crystals (0.32 g, 57%); m.p. 68-70 °C; [HRMS: m/z calculated for C₁₂H₈BrN₃ (MH⁺) 273.9979. Found 273.9977]; ν_{max} (cm⁻¹) 3075.16, 2562.01, 1061.42, 735.07; ¹H NMR (600 MHz, CDCl₃) 7.52 (m, 2H, 7-H, 4-H, Ar-H), 7.61 (1H, t, J = 8.16 Hz, 5'-H, Ar-H), 7.66 (1H, d, J = 9.73 Hz, 6'-H, Ar-H), 7.78 (2H, m, 5-H, 6-H, Ar-H), 8.02 (1H, d, J = 3.83 Hz, 2'-H, Ar-H), 8.18 (1H, d, J = 8.38 Hz, 4'-H, Ar-H); ¹³C NMR (150 MHz, CDCl₃) 110.2 (5'-C), 120.6 (4'-C), 121.2 (2'-C), 123.4 (7-C), 124.7 (4-C), 125.8 (6'-C), 128.7 (6-C), 131.2 (5-C), 131.7 (1'-C), 132.1 (9-C), 138.1 (8-C), 146.6 (3'-C).

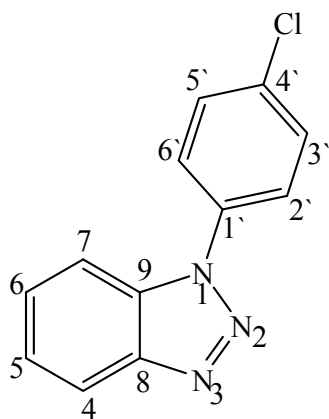
1-(3-Fluorophenyl)-1*H*-benzo[1,2,3]triazole **121f**



The procedure described for the synthesis of 1-benzyl-1*H*-benzo[1,2,3]triazole **111f** (Method 2) was followed, using *m*-fluoroaniline (0.97 mL, 10 mmol), *t*-BuONO (0.76 mL, 5.7

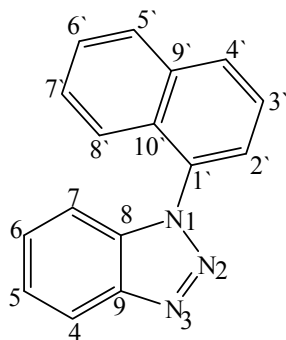
mmol), TMSN₃ (0.28 mL, 2.1 mmol) and anthranilic acid (**82**) (0.28 g, 2.1 mmol). Work-up and purification by preparative thin layer chromatography [on silica gel and elution with hexane:EtOAc (6:1)] afforded *1-(3-fluorophenyl)-1H-benzo[1,2,3]triazole 121f* as a brown solid (0.28 g, 64%); m.p. 110-112 °C; ν_{\max} (cm⁻¹) 3074.62, 2160.09, 1600.55, 1489.39; ¹H NMR (600 MHz, CDCl₃) 7.21 (1H, m, 6'-H, Ar-H), 7.46 (1H, t, *J* = 8.04 Hz, 4'-H, Ar-H), 7.56-7.63 (4H, m, 6-H, 7-H, 2'-H, 5'-H, Ar-H), 7.77 (1H, d, *J* = 8.38 Hz, 4-H, Ar-H), 8.16 (1H, d, *J* = 8.38 Hz, 5-H, Ar-H); ¹³C NMR (150 MHz, CDCl₃) 110.2 (5'-C), 115.1 (4'-C), 118.1 (2'-C), 120.5 (7-C), 124.6 (4-C), 128.1 (6'-C), 131.2 (6-C), 131.3 (5-C), 138.3 (1'-C), 146.6 (9-C), 162.3 (8-C), 163.9 (3'-C).

1-(4-Chlorophenyl)-1H-benzo[1,2,3]triazole 121g



The procedure described for the synthesis of 1-benzyl-1*H*-benzo[1,2,3]triazole **111f** (Method 2) was followed, using *p*-chloroaniline (0.45 mL, 5.0 mmol), *t*-BuONO (0.76 mL, 5.7 mmol), TMSN₃ (0.28 mL, 2.1 mmol) and anthranilic acid (**82**) (0.28 g, 2.1 mmol). Work-up and purification by preparative thin layer chromatography [on silica gel and elution with hexane:EtOAc (6:1)] afforded *1-(4-chlorophenyl)-1H-benzo[1,2,3]triazole 121g* as a yellow oil (0.26 g, 55%); ν_{\max} (cm⁻¹) 3061.65, 3195.33, 2131.64, 2096.92, 1492.74, 736.27; ¹H NMR (600 MHz, CDCl₃) 7.46 (1H, t, *J* = 7.60 Hz, 6-H, Ar-H), 7.58-7.76 (6H, m, 4-H, 5-H, 2'-H, 3'-H, 5'-H, 6'-H, Ar-H), 8.16 (1H, d, *J* = 8.37 Hz, 7-H, Ar-H); ¹³C NMR (150 MHz, CDCl₃) 110.1 (4-C), 120.5 (7-C), 124.0 (3'-C, 5'-C), 124.6 (1'-C), 128.6 (6-C), 130.1 (2'-C, 6'-C), 132.2 (5-C), 134.5 (9-C), 135.6 (4'-C), 146.6 (8-C).

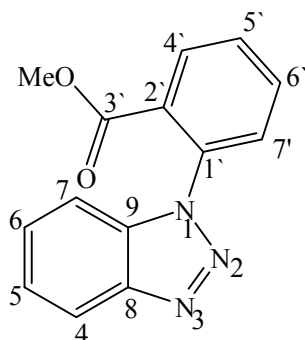
1-(Naphthalen-1-yl)-1H-benzo[1,2,3]triazole 121h



The procedure described for the synthesis of 1-benzyl-1*H*-benzo[1,2,3]triazole **111f** (Method 2) was followed, using 1-naphthylamine (0.65 mL, 5.0 mmol), *t*-BuONO (0.76 mL, 5.7

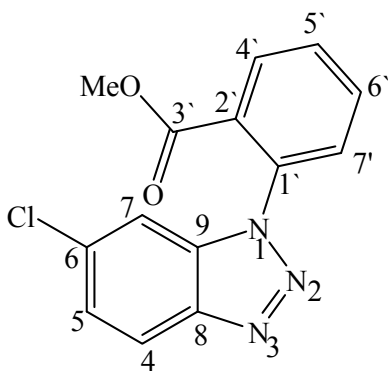
mmol), TMSN₃ (0.28 mL, 2.1 mmol) and anthranilic acid (**82**) (0.28 g, 2.1 mmol). Work-up and purification by preparative layer chromatography [on silica gel and elution with hexane:EtOAc (6:1)] afforded *1-(naphthalen-1-yl)-1H-benzo[1,2,3]triazole* **121h** as a reddish solid (0.28 g, 56%); m.p. 112-114 °C (lit.³⁹¹ 114-115 °C); ν_{\max} (cm⁻¹) 3059.98, 2923.34, 1076.02, 738.66, ¹H NMR (600 MHz, CDCl₃) 7.37 (1H, d, *J* = 7.56 Hz, 2'-H, Ar-H), 7.43-7.49 (3H, m, 5'-H, 8'-H, 7-H, Ar-H), 7.59 (1H, t, *J* = 7.42 Hz, 3'-H, Ar-H), 7.67 (2H, m, 7'-H, 6'-H, Ar-H), 8.01 (1H, d, *J* = 8.27 Hz, 4-H, Ar-H), 8.09 (2H, m, 5-H, 6-H, Ar-H), 8.22 (1H, d, *J* = 7.56 Hz, 4'-H, Ar-H); ¹³C NMR (150 MHz, CDCl₃) 110.4 (7-C), 120.1 (4-C), 122.7 (1'-C), 124.3 (3'-C), 124.6 (6'-C), 125.2 (7'-C), 127.0 (5-C), 127.6 (6-C), 128.1 (8'-C), 128.4 (5'-C), 129.2 (4'-C), 130.4 (2'-C), 132.6 (8-C), 134.4 (9'-C), 134.7 (10'-C), 145.7 (9-C).

Methyl 2-(1H-benzo[1,2,3]triazol-1-yl)benzoate **121i**



The procedure described for the synthesis of 1-benzyl-1H-benzo[1,2,3]triazole **111f** (Method 2) was followed, using anthranilic acid (**82**) (1.3 g, 2×5.0 mmol), *t*-BuONO (0.76 mL, 5.7 mmol) and TMSN₃ (0.28 mL, 2.1 mmol). Work-up and purification by preparative thin layer chromatography [on silica gel and elution with hexane:EtOAc (6:1)] afforded *methyl 2-(1H-benzo[1,2,3]triazol-1-yl)benzoate* **121i** as a yellow oil (0.77 g, 61%); [HRMS: *m/z* calculated for C₁₃H₁₁N₃ (MH⁺) 254.0930. Found 254.0928]; ν_{\max} (cm⁻¹) 3080.13, 2923.69, 1724.54, 1683.68, 746.23; ¹H NMR (600 MHz, CDCl₃) 3.48 (3H, s, OCH₃), 7.39-7.43 (2H, m, 5-H, 7-H, Ar-H), 7.51 (1H, t, *J* = 7.61 Hz, 6-H, Ar-H), 7.61 (1H, d, *J* = 7.83 Hz, 4-H, Ar-H), 7.66 (1H, t, *J* = 7.64 Hz, 4'-H, Ar-H), 7.76 (1H, t, *J* = 7.63 Hz, 5'-H, Ar-H), 8.11-8.15 (2H, m, 6'-H, 7'-H, Ar-H); ¹³C NMR (150 MHz, CDCl₃) 52.3 (OCH₃), 109.8 (4-C), 120.1 (7-C), 123.9 (6'-C), 127.4 (5-C), 127.6 (5'-C), 128.5 (6-C), 129.1 (4'-C), 132.8 (9-C), 134.8 (2'-C), 146.4 (8-C), 165.6 (3'-C=O).

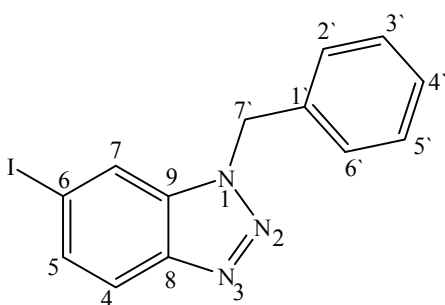
Methyl 2-(6-chloro-1*H*-benzo[1,2,3]triazol-1-yl)benzoate **121j**



The procedure described for the synthesis of 1-benzyl-1*H*-benzo[1,2,3]triazole **111f** (Method 2) was followed, using 5-chloroanthranilic acid (0.85 g, 5.0 mmol), *t*-BuONO (0.76 mL, 5.7 mmol) and TMSN₃ (0.28 mL, 2.1 mmol) and anthranilic acid (**82**) (0.28 g, 2.1 mmol). Work-up and purification by preparative thin layer chromatography [on silica gel and elution with hexane:EtOAc (6:1)] afforded *methyl 2-(6-chloro-1H*-

benzo[1,2,3]triazol-1-yl)benzoate **121j** as a yellow solid (0.37 g; 63%); m.p. 110-112 °C; ν_{\max} (cm⁻¹) 3042.92, 2951.13, 1726.97, 746.14; ¹H NMR (600 MHz, CDCl₃) 3.50 (s, 3H, OCH₃), 7.36-7.47 (4H, m, 5-H, 7-H, 6'-H, 7'-H, Ar-H), 7.73 (1H, dd, *J* = 2.44 Hz and *J* = 5.96 Hz, 6-H, Ar-H), 8.09 (1H, d, *J* = 2.41 Hz, 4-H, Ar-H), 8.15 (1H, d, *J* = 8.37 Hz, 4'-H, Ar-H); ¹³C NMR (150 MHz, CDCl₃) 52.7 (OCH₃), 109.4 (4-C), 120.3 (7-C), 124.3 (6-C), 128.4 (5-C), 128.7 (4'-C), 129.5 (1'-C), 131.8 (7'-C), 133.0 (6'-C), 133.8 (2'-C), 133.9 (5'-C), 136.0 (9-C), 145.7 (8-C), 164.4 (3'-C=O).

1-Benzyl-6-iodo-1*H*-benzo[1,2,3]triazole **111a**

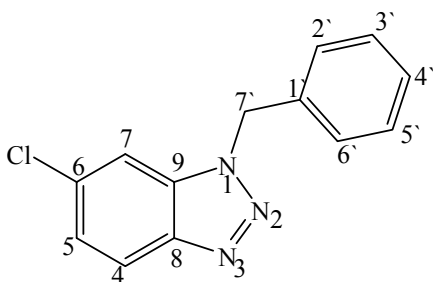


The procedure described for the synthesis of 1-benzyl-1*H*-benzo[1,2,3]triazole **111f** (Method 2) was followed, using benzylamine (0.55 mL, 5.0 mmol), *t*-BuONO (0.76 mL, 5.7 mmol), TMSN₃ (0.28 mL, 2.1 mmol) and 5-iodoanthranilic acid (**118a**) (0.55 g, 2.1 mmol). Work-up and

purification by preparative thin layer chromatography [on silica gel and elution with hexane:EtOAc (6:1)] afforded *1-benzyl-6-iodo-1H-benzo[1,2,3]triazole* **111a** as a yellow solid (0.44 g, 63%); m.p. 106-108 °C; [HRMS: *m/z* calculated for C₁₃H₁₀IN₃ (MH⁺) 335.9998. Found 335.9998]; ν_{\max} (cm⁻¹) 3059.48, 2928.97, 1205.39, 794.97; ¹H NMR (600 MHz, CDCl₃) 5.82 (2H, s, 7'-H), 7.13 (1H, d, *J* = 8.66 Hz, 2'-H, Ar-H), 7.26-7.28

(m, 4H, 3'-H, 4'-H, 5'-H, 6'-H, Ar-H), 7.65 (1H, t, J = 9.57 Hz, 5-H, Ar-H), 7.83 (1H, d, J = 8.69 Hz, 4-H, Ar-H), 8.47 (1H, s, 7-H, Ar-H); ^{13}C NMR (150 MHz, CDCl_3) 52.3 (7'-C), 93.1 (6-C), 111.4 (4'-C), 118.8 (3'-C), 121.4 (5'-C), 127.5 (2'-C), 127.6 (6'-C), 128.7 (4-C), 129.1 (9-C), 129.2 (1'-C), 133.1 (7-C), 134.3 (5-C), 136.0 (8-C).

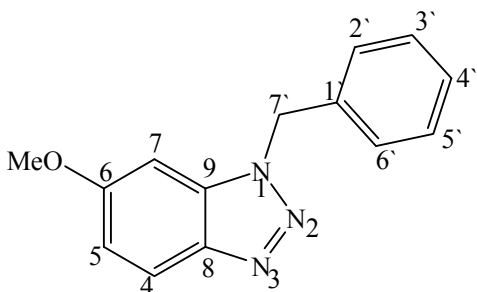
1-Benzyl-6-chloro-1*H*-benzo[1,2,3]triazole **111c**



The procedure described for the synthesis of 1-benzyl-1*H*-benzo[1,2,3]triazole **111f** (Method 2) was followed, using benzylamine (0.55 mL, 5.0 mmol), *t*-BuONO (0.76 mL, 5.7 mmol), TMSN_3 (0.28 mL, 2.1 mmol) and 5-chloroanthranilic acid (**118c**) (0.36 g, 2.1 mmol). Work-up and purification

by preparative thin layer chromatography [on silica gel and elution with hexane:EtOAc (6:1)] afforded 1-benzyl-6-chloro-1*H*-benzo[1,2,3]triazole **111c** as a brownish solid (0.23 g, 45%); m.p. 112-114 °C; ν_{max} (cm^{-1}) 3485.63, 3321.54, 1689.61, 695.08; ^1H NMR (600 MHz, CDCl_3) 5.34 (s, 2H, 7'-H), 6.23 (1H, d, J = 8.81 Hz, 4'-H), 7.20 (1H, dd, J = 2.58 Hz and J = 6.23 Hz, 5-H, Ar-H), 7.37-7.47 (5H, m, 4-H, 2'-H, 3'-H, 6'-H, 5'-H, Ar-H), 7.90 (1H, d, J = 7.82 Hz, 7-H, Ar-H); ^{13}C NMR (150 MHz, CDCl_3) 66.2 (7'-C), 117.9 (7-C), 120.4 (5-C), 128.0 (3'-C, 5'-C), 128.2 (4'-C), 128.5 (2'-C, 6'-C), 130.2 (4-C), 134.0 (9-C), 135.6 (2-C), 149.0 (6-C), 166.7 (8-C).

1-Benzyl-6-methoxy-1*H*-benzo[1,2,3]triazole **111d**

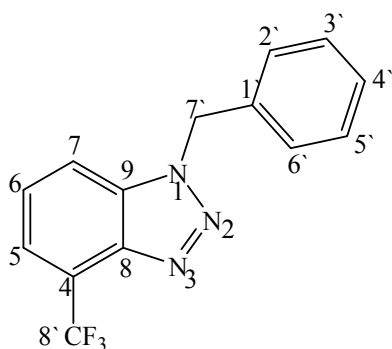


The procedure described for the synthesis of 1-benzyl-1*H*-benzo[1,2,3]triazole **111f** (Method 2) was followed, using benzylamine (0.36 mL, 3.3 mmol), *t*-BuONO (0.51 mL, 3.8 mmol), TMSN_3 (0.19 mL, 1.4 mmol) and 5-methoxyanthranilic acid (**118d**) (0.23 g, 1.4 mmol). Work-up and

purification by preparative thin layer chromatography [on silica gel and elution with

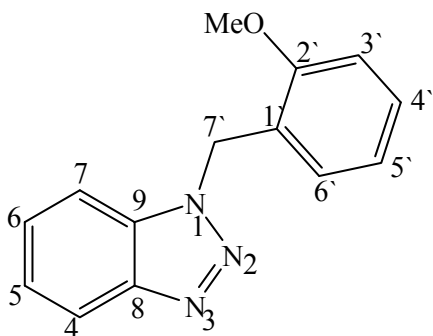
hexane:EtOAc (6:1)] afforded *1-benzyl-6-methoxy-1H-benzo[1,2,3]triazole 111d* as a yellow solid (0.29 g, 87%); m.p. 66-68 °C; [HRMS: m/z calculated for $C_{14}H_{13}N_3O$ (MH^+) 240.1137. Found 240.1019]; ν_{\max} (cm^{-1}) 3474.90, 3365.15, 1673.31, 1233.56, 695.47, 1H NMR (600 MHz, $CDCl_3$) 3.78 (s, 3H, OCH_3), 5.30 (s, 2H, 7'-H), 6.10 (1H, d, $J = 8.29$ Hz, 5-H, Ar-H), 6.23 (1H, dd, $J = 2.44$ Hz and $J = 6.52$ Hz, 2'-H, Ar-H), 7.37-7.43 (5H, m, 7-H, 3'-H, 4'-H, 5'-H, 6'-H, Ar-H), 7.85 (1H, d, $J = 8.96$ Hz, 4-H, Ar-H); ^{13}C NMR (150 MHz, $CDCl_3$) 55.1 (OCH_3), 65.7 (7'-C), 99.3 (7-C), 104.6 (5-C), 127.9 (3'-C, 5'-C), 128.0 (4'-C), 128.5 (2'-C, 6'-C), 133.2 (4-C), 136.5 (9-C), 152.6 (1'-C), 164.3 (8-C), 167.6 (6-C).

1-Benzyl-4-(trifluoromethyl)-1H-benzo[1,2,3]triazole 111e



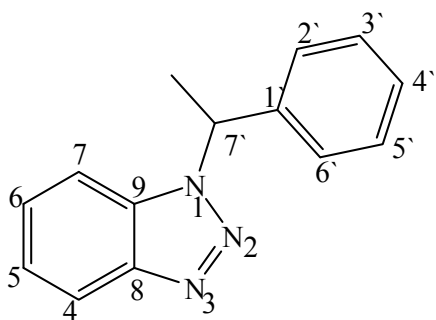
The procedure described for the synthesis of 1-benzyl-1H-benzo[1,2,3]triazole **111f** (Method 2) was followed, using benzylamine (3.3 mmol, 0.36 mL), *t*-BuONO (0.51 mL, 3.8 mmol), TMSN₃ (0.19 mL, 1.4 mmol) and 3-trifluoromethylantranilic acid (**118e**) (0.28 g, 1.39 mmol). Work-up and purification by preparative thin layer chromatography [on silica gel and elution with hexane:EtOAc (6:1)] afforded *1-benzyl-4-(trifluoromethyl)-1H-benzo[1,2,3]triazole 111e* as a yellow oil (0.15 g, 40%); ν_{\max} (cm^{-1}) 3519.87, 3361.37, 1618.34, 752.82, 1H NMR (600 MHz, $CDCl_3$) 5.34 (2H, s, 7'-H), 6.66 (1H, t, $J = 7.82$ Hz, 6-H, Ar-H), 7.35-7.44 (5H, m, 2'-H, 3'-H, 4'-H, 5'-H, 6'-H, Ar-H), 7.60 (1H, d, $J = 7.67$ Hz, 7-H, Ar-H), 8.12 (1H, d, $J = 7.97$ Hz, 5-H, Ar-H); ^{13}C NMR (150 MHz, $CDCl_3$) 66.5 (7'-C), 114.7 (6-C), 123.7 (8'-C), 128.1 (3'-C, 5'-C), 128.3 (4'-C), 128.6 (2'-C, 6'-C), 131.9 (7-C), 132.0 (1'-C), 135.6 (5-C), 135.8 (4-C), 148.2 (9-C), 167.3 (8-C).

1-(2-Methoxybenzyl)-1*H*-benzo[1,2,3]triazole **111g**



The procedure described for the synthesis of 1-benzyl-1*H*-benzo[1,2,3]triazole **111f** (Method 2) was followed, using 2-methoxybenzylamine (0.65 mL, 5.0 mmol), *t*-BuONO (0.76 mL, 5.7 mmol), TMSN₃ (0.28 mL, 2.1 mmol) and anthranilic acid (**82**) (0.28 g, 2.1 mmol). Work-up and purification by preparative thin layer chromatography [on silica gel and elution with hexane:EtOAc (6:1)] afforded 1-(2-methoxybenzyl)-1*H*-benzo[1,2,3]triazole **111g** as a yellowish solid (0.35 g, 71%); m.p. 56-58 °C; ν_{\max} (cm⁻¹) 3483.21, 3381.69, 1675.81, 748.33, ¹H NMR (600 MHz, CDCl₃) 3.90 (s, 3H, OCH₃), 5.44 (s, 2H, 7'-H), 6.67-6.70 (2H, m, 3'-H, 4'-H, Ar-H), 6.95 (1H, d, *J* = 8.25 Hz, 6'-H, Ar-H), 7.02 (1H, t, *J* = 7.44 Hz, 5'-H, Ar-H), 7.30 (1H, t, *J* = 7.75 Hz, 6-H, Ar-H), 7.36 (1H, t, *J* = 7.79 Hz, 5-H, Ar-H), 7.47 (1H, d, *J* = 7.39 Hz, 4-H, Ar-H), 7.99 (1H, d, *J* = 7.98 Hz, 7-H, Ar-H); ¹³C NMR (150 MHz, CDCl₃) 55.3 (OCH₃), 61.5 (7'-C), 99.3 (7-C), 110.4 (3'-C), 111.0 (5-C), 116.1 (5'-C), 116.6 (1'-C), 120.4 (6'-C), 129.1 (2'-C), 129.3 (4-C), 131.3 (6-C), 134.0 (9-C), 150.4 (8-C), 157.3 (4'-C).

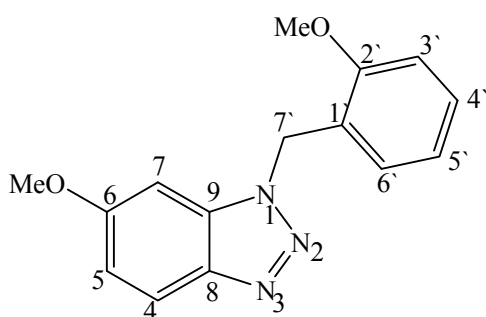
1-(1-Phenylethyl)-1*H*-benzo[1,2,3]triazole **111h**



The procedure described for the synthesis of 1-benzyl-1*H*-benzo[1,2,3]triazole **111f** (Method 2) was followed, using 1-phenylethylamine (0.65 mL, 5.0 mmol), *t*-BuONO (0.76 mL, 5.7 mmol), TMSN₃ (0.28 mL, 2.1 mmol) and anthranilic acid (**82**) (0.28 g, 2.1 mmol). Work-up and purification by preparative thin layer chromatography [on silica gel and elution with hexane:EtOAc (6:1)] afforded 1-(1-phenylethyl)-1*H*-benzo[1,2,3]triazole **111h** as a yellow oil (0.20 g, 44%); ν_{\max} (cm⁻¹) 3484.75, 3373.48,

1683.41, 1240.55, 748.93; ^1H NMR (600 MHz, CDCl_3) 1.70 (3H, d, $J = 6.74$ Hz, CH_3), 6.12 (1H, q, $J = 6.61$ Hz, 7'-H), 6.65 (2H, m, 5-H, 2'-H, Ar-H), 7.28-7.46 (6H, m, 6-H, 7-H, 3'-H, 4'-H, 5'-H, 6'-H, Ar-H), 8.01 (1H, d, $J = 7.97$ Hz, 4-H, Ar-H); ^{13}C NMR (150 MHz, CDCl_3) 22.5 (CH_3), 72.1 (7'-C), 116.1 (7-C), 116.6 (5-C), 125.8 (3'-C, 5'-C), 127.7 (4'-C), 128.5 (2'-C, 6'-C), 131.2 (4-C), 134.0 (9-C), 142.1 (1'-C), 150.6 (8-C), 167.2 (6-C).

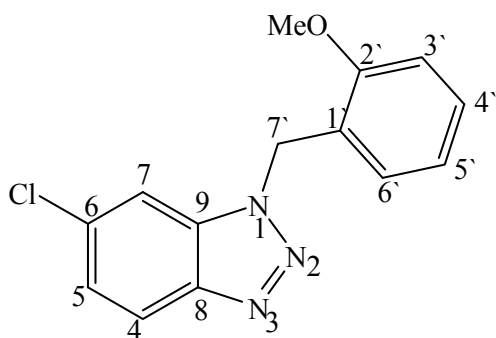
1-(2-Methoxybenzyl)-6-methoxy-1*H*-benzo[1,2,3]triazole **111i**



The procedure described for the synthesis of 1-benzyl-1*H*-benzo[1,2,3]triazole **111f** (Method 2) was followed, using 2-methoxybenzylamine (0.44 mL, 3.3 mmol), *t*-BuONO (0.51 mL, 3.8 mmol), TMSN_3 (0.19 mL, 1.4 mmol) and 5-methoxyanthranilic acid (**118d**) (0.23 g, 1.4 mmol). Work-up and purification by preparative

thin layer chromatography [on silica gel and elution with hexane:EtOAc (6:1)] afforded 1-(2-methoxybenzyl)-6-methoxy-1*H*-benzo[1,2,3]triazole **111i** as a yellow oil (0.24 g, 65%); ν_{max} (cm^{-1}) 3474.38, 3365.14, 2939.77, 1679.54, 751.15; [HRMS: m/z calculated for $\text{C}_{15}\text{H}_{15}\text{N}_3\text{O}_2$ (MH^+) 270.1243. Found 270.1133]; ^1H NMR (600 MHz, CDCl_3) 3.78 (3H, s, OCH_3), 3.88 (3H, s, OCH_3), 5.30 (s, 2H, 7'-H), 6.10 (1H, d, $J = 7.23$ Hz, 5-H, Ar-H), 6.23 (1H, dd, $J = 2.42$ Hz and $J = 6.53$ Hz, 6'-H, Ar-H), 7.37-7.43 (4H, m, 7-H, 5'-H, 4'-H, 3'-H, Ar-H), 7.85 (1H, d, $J = 8.96$ Hz, 4-H, Ar-H); ^{13}C NMR (150 MHz, CDCl_3) 55.1 (OCH_3), 55.4 (OCH_3), 61.2 (7'-C), 99.3 (7-C), 104.4 (3'-C), 110.4 (5-C), 120.4 (5'-C), 124.9 (1'-C), 129.0 (4'-C), 129.2 (6'-C), 133.2 (4-C), 152.5 (9-C), 157.3 (8-C), 164.2 (2'-C), 167.7 (6-C).

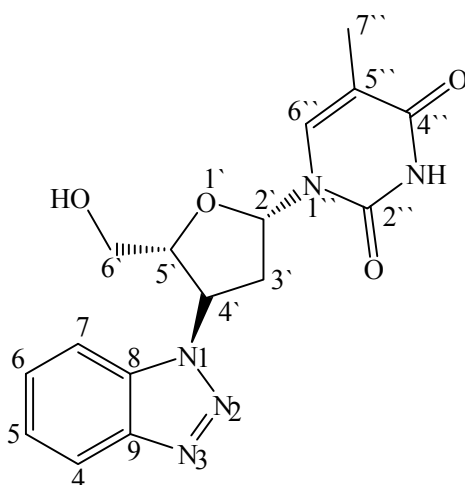
1-(2-Methoxybenzyl)-6-chloro-1*H*-benzo[1,2,3]triazole **111j**



The procedure described for the synthesis of 1-benzyl-1*H*-benzo[1,2,3]triazole **111f** (Method 2) was followed, using 2-methoxybenzylamine (0.65 mL, 5.0 mmol), *t*-BuONO (0.76 mL, 5.7 mmol), TMSN₃ (0.28 mL, 2.1 mmol) and 5-chloroanthranilic acid (**118c**) (0.36 g, 2.1 mmol).

Work-up and purification by preparative thin layer chromatography [on silica gel and elution with hexane:EtOAc (6:1)] afforded 1-(2-methoxybenzyl)-6-chloro-1*H*-benzo[1,2,3]triazole **111j** as a yellowish solid (0.34 g, 60%); m.p. 58-60 °C; ν_{max} (cm⁻¹) 3492.91, 3369.31, 1687.81, 755.06; ¹H NMR (600 MHz, CDCl₃) 3.86 (s, 3H, OCH₃), 5.37 (s, 2H, 7'-H), 6.60 (1H, d, *J* = 8.78 Hz, 3'-H, Ar-H), 6.91-7.39 (5H, m, 5-H, 4'-H, 5'-H, 6'-H, 4-H, Ar-H), 7.86 (1H, d, *J* = 7.44 Hz, 7-H, Ar-H); ¹³C NMR (150 MHz, CDCl₃) 55.4 (7'-C), 61.9 (OCH₃), 110.4 (3'-C), 118.0 (7-C), 120.4 (5'-C), 120.6 (1'-C), 124.1 (4'-C), 129.5 (5-C), 129.6 (6'-C), 130.5 (4-C), 134.0 (8-C), 149.0 (6-C), 157.5 (9-C), 167.0 (2'-C).

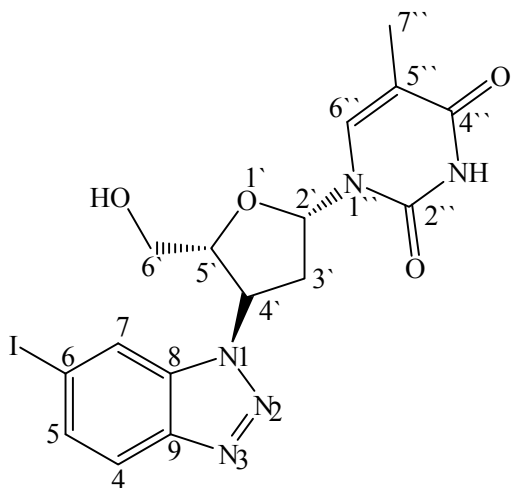
1-(4'-(1*H*-Benzo[1,2,3]-triazol-1-yl)-tetrahydro-5'-(hydroxymethyl)furan-2'-yl)-5''-methylpyrimidine-2'',-4''(1*H*,3*H*)-dione **112a**



The procedure described for the synthesis of 1-benzyl-1*H*-benzo[1,2,3]triazole **111f** (Method 2) was followed, using zidovudine (AZT, 0.89 g, 3.3 mmol), *t*-BuONO (0.51 mL, 3.8 mmol), TMSN₃ (0.19 mL, 1.4 mmol) and anthranilic acid (**82**) (0.19 g, 1.4 mmol). Work-up and purification by preparative thin layer chromatography (on silica gel and elution with EtOAc) afforded 1-(4'-(1*H*-benzo[1,2,3]triazol-1-yl)-tetrahydro-5'-

(hydroxymethyl)furan-2'-yl)-5''-methylpyrimidine-2'',-4''(1H,3H)-dione **112a** as yellow crystals (0.29 g, 63%) m.p. 206-208 °C (lit.²⁴⁴ 205-207 °C); [HRMS: m/z calculated for $C_{16}H_{17}N_5O_4$ (MH^+) 344.1359. Found 344.1359]; ν_{\max} (cm^{-1}) 3460.81, 3004.95, 2817.03, 1662.51, 747.71; 1H NMR (600 MHz, $CDCl_3$) 1.93 (3H, s, CH_3), 2.85 (1H, m, 3'-H), 3.11 (1H, m, 3'-H), 3.76 (1H, dd, $J = 3.15$ Hz and $J = 9.07$ Hz, 6'-H), 3.93 (1H, dd, $J = 3.28$ Hz and $J = 8.94$ Hz, 6'-H), 4.50 (1H, dd, $J = 3.22$ Hz and $J = 5.23$ Hz, 5'-H), 5.76 (1H, q, $J = 8.63$ Hz, 4'-H), 6.62 (1H, t, $J = 6.58$ Hz, 2'-H), 7.47 (1H, t, $J = 7.98$ Hz, 6-H, Ar-H), 7.60 (1H, t, $J = 7.45$ Hz, 5-H, Ar-H), 7.86 (1H, d, $J = 8.43$ Hz, 4-H, Ar-H), 7.97 (1H, s, 6''-H), 8.01 (1H, d, $J = 8.41$ Hz, 7-H, Ar-H); ^{13}C NMR (150 MHz, $CDCl_3$) 12.5 (CH_3), 38.5 (3'-C), 59.0 (4'-C), 62.4 (6'-C), 86.3 (5'-C), 87.1 (2'-C), 111.3 (5''-C), 111.8 (4-C), 120.3 (7-C), 126.1 (6-C), 129.2 (5-C), 134.5 (8-C), 138.4 (6''-C), 146.9 (9-C), 152.41(2''-C=O), 166.5 (4''-C=O).

1-(Tetrahydro-5'-(hydroxymethyl)-4'-(6-iodo-1H-benzo[1,2,3]-triazol-1-yl)furan-2'-yl)-5''-methylpyrimidine-2'',-4''(1H,3H)-dione 112b

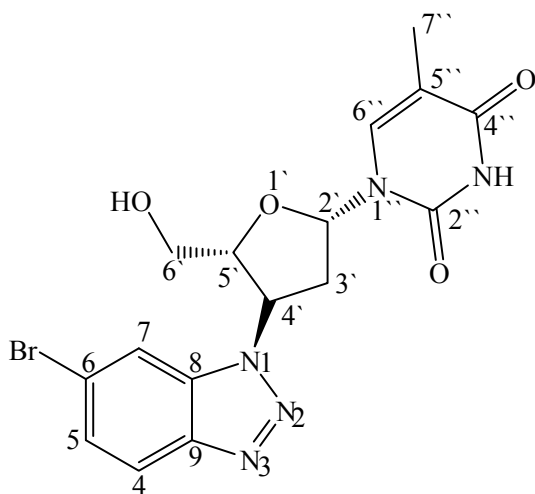


The procedure described for the synthesis of 1-benzyl-1H-benzo[1,2,3]triazole **111f** (Method 2) was followed, using zidovudine (AZT, 0.89 g, 3.3 mmol), *t*-BuONO (0.51 mL, 3.8 mmol), $TMSN_3$ (0.19 mL, 1.4 mmol) and 5-iodoanthranilic acid (**118a**) (0.36 g, 1.4 mmol). Work-up and purification by column chromatography (on basic alumina and elution with EtOAc) afforded 1-(tetrahydro-5'-

(hydroxymethyl)-4'-(6-iodo-1H-benzo[1,2,3]-triazol-1-yl)furan-2'-yl)-5''-methylpyrimidine-2'',-4''(1H,3H)-dione **112b** as a brown oil (0.52 g, 80%); [HRMS: m/z calculated for $C_{16}H_{16}IN_4O_5$ (MH^+) 470.0325. Found 470.0316]; ν_{\max} (cm^{-1}) 2927.88, 2101.77, 1674.60, 1262.81, 745.96; 1H NMR (600 MHz, MeOD) 1.87 (3H, s, CH_3), 2.38 (2H, m, 3'-H), 3.72-3.90 (3H, m, 6'-H, 5'-H), 4.34 (1H, q, $J = 8.59$ Hz, 4'-H), 7.23 (1H, t, $J = 7.81$ Hz, 2'-H), 7.78 (1H, s, 6''-H), 7.91-8.00 (2H, m, 5-H, 4-H, Ar-H), 8.32 (1H, s,

7-H, Ar-H); ^{13}C NMR (150 MHz, MeOD) 12.5 (CH₃), 38.3 (3'-C), 61.7 (4'-C), 62.5 (6'-C), 86.1 (2'-C, 5'-C), 94.4 (6-C), 111.7 (5''-C), 130.0 (4-C), 131.4 (7-C), 138.1 (8-C, 6''-C), 139.7 (5-C), 142.8 (9-C), 152.3 (2''-C=O), 166.4 (4''-C=O).

1-(4'-(6-Bromo-1*H*-benzo[1,2,3]-triazol-1-yl)-tetrahydro-5'-(hydroxymethyl)furan-2'-yl)-5''-methylpyrimidine-2'',-4''(1*H*,3*H*)-dione **112c**

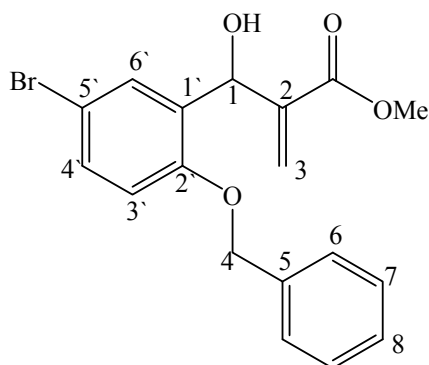


The procedure described for the synthesis of 1-benzyl-1*H*-benzo[1,2,3]triazole **111f** (Method 2) was followed, using zidovudine (AZT, 0.89 g, 3.3 mmol), *t*-BuONO (0.51 mL, 3.8 mmol), TMSN₃ (0.19 mL, 1.4 mmol) and 5-bromoanthranilic acid (**118b**) (0.30 g, 1.4 mmol). Work-up and purification by column chromatography (on basic alumina and elution with EtOAc) afforded 1-(4'-(6-bromo-1*H*-benzo[1,2,3]-

triazol-1-yl)-tetrahydro-5'-(hydroxymethyl)furan-2'-yl)-5''-methylpyrimidine-2'',-4''(1*H*,3*H*)-dione **112c** as a brown oil (0.46 g, 79%); ν_{max} (cm⁻¹) 3186.06, 2929.54, 1667.67, 748.56; ^1H NMR (600 MHz, MeOD) 1.86 (3H, s, CH₃), 2.38 (2H, m, 3'-H), 3.74-3.90 (3H, m, 6'-H, 5'-H), 4.35 (1H, q, J = 8.46 Hz, 4'-H), 7.38 (1H, t, J = 7.84 Hz, 2'-H), 7.72 (1H, d, J = 7.85 Hz, 5-H, Ar-H), 7.78 (1H, s, 6''-H), 7.96 (1H, d, J = 7.73 Hz, 4-H, Ar-H), 8.11 (1H, s, 7-H, Ar-H); ^{13}C NMR (150 MHz, MeOD) 12.5 (CH₃), 38.3 (3'-C), 61.7 (4'-C), 62.4 (6'-C), 86.1 (2'-C, 5'-C), 111.6 (5'-C), 123.3 (6-C), 129.4 (4-C), 131.3 (7-C), 133.6 (5-C), 136.8 (9-C), 138.0 (6''-C, 8-C), 152.3 (2'-C=O), 166.3 (4''-C=O).

6.2.5. Preparation of coumarin analogs

Methyl 2-((2'-(benzyloxy)-5'-bromophenyl)(hydroxy)methyl)acrylate **124**

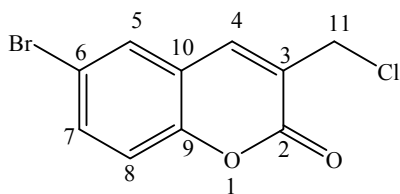


A mixture of 2-(benzyloxy)-5-bromobenzaldehyde (0.63 g, 2.2 mmol), methyl acrylate (0.29 mL, 3.2 mmol) and DABCO (0.06 g, 0.56 mmol) was sealed in a glass tube and irradiated under microwave conditions for 12 hours. The excess of methylacrylate was removed under vacuum and the crude mixture was purified by flash chromatography [on silica gel; elution with hexane:EtOAc (9:1)] to afford *methyl 2-[(2'-(benzyloxy)-5'-bromophenyl)(hydroxy)methyl]acrylate* **124** as a yellow oil (0.64 g, 79%); ν_{\max} (cm⁻¹) 3441.03 (OH), 1714.22 (C=O); ¹H NMR (600 MHz, CDCl₃) 3.32 (1H, s, OH), 3.74 (3H, s, OCH₃), 5.05 (2H, s, 4-H), 5.66 (1H, s, 1-H), 5.89 and 6.29 (2H, 2 × s, C=CH₂), 6.79 (1H, d, *J* = 8.66 Hz, 3'-H, Ar-H), 7.33-7.37 (6H, 4'-H, 6-H × 2, 7-H × 2, 8-H, Ar-H), 7.54 (1H, d, *J* = 8.80 Hz, 6'-H, Ar-H); ¹³C NMR (150 MHz, CDCl₃) 52.0 (OCH₃), 67.7 (1-C), 70.5 (4-C), 113.5 (5'-C), 113.6 (3'-C), 126.4 (1'-C), 127.3 (6-C × 2), 128.1 (8-C), 128.6 (7-C × 2), 130.6 (4'-C), 131.5 (6'-C), 131.9 (3-C), 136.2 (5-C), 140.7 (2-C=CH₂), 154.7 (2'-C), 166.9 (C=O).

General procedure for the synthesis of compounds **126**, **127** and **128**

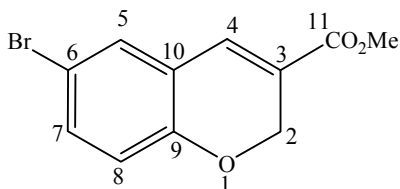
Concentrated HCl (6.5 mL) was added to a solution of 2-[(2-(benzyloxy)-5-bromophenyl)(hydroxy)methyl]acrylate (0.60 g, 1.6 mmol) in AcOH (6.5 mL). The mixture was refluxed for 2 hours and allowed to cool to room temperature and then poured into ice-cooled H₂O (15 mL). Stirring for 30 minutes gave a precipitate which was filtered off, dried and purified by column chromatography [on silica gel; elution with hexane:EtOAc (1:1)] to afford three products: *Dimethyl (2-acetoxy-5-bromophenyl)methylenepentanedioate* **128** (31%), *6-bromo-3-(chloromethyl)-2H-chromen-2-one* **126** (40%) and *methyl 6-bromo-2H-chromene-3-carboxylate* **127** (15%).

6-Bromo-3-(chloromethyl)-2H-chromen-2-one **126**



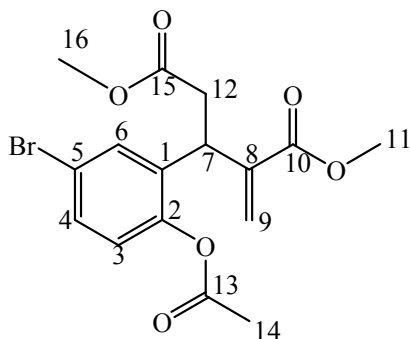
6-Bromo-3-(chloromethyl)-2H-chromen-2-one **126** as a yellow solid (0.17 g, 40%); m.p. 118-120 (lit.²⁵² 116-118 °C); ν_{\max} (cm⁻¹) 1671.67 (C=O); ¹H NMR (600 MHz, CDCl₃) 4.57 (2H, s, 11-H), 7.27 (1H, d, J = 9.19 Hz, 8-H, Ar-H), 7.66 (1H, d, J = 8.93 Hz, 7-H, Ar-H), 7.69 (1H, s, 4-H), 7.84 (1H, s, 5-H, Ar-H); ¹³C NMR (150 MHz, CDCl₃) 41.3 (11-C), 117.3 (6-C), 118.4 (8-C), 120.3 (10-C), 126.2 (3-C), 130.3 (5-C), 134.7 (7-C), 139.6 (4-C), 152.2 (3-C), 159.8 (2-C=O).

Methyl 6-bromo-2H-chromene-3-carboxylate **127**



Methyl 6-bromo-2H-chromene-3-carboxylate **127** as a white crystal (0.07 g, 15%); m.p. 106-108 °C; ν_{\max} (cm⁻¹) 1715.84 (C=O); ¹H NMR (600 MHz, CDCl₃) 3.82 (3H, s, OCH₃), 4.99 (2H, s, 2-H), 6.72 (1H, d, J = 8.59 Hz, 4-H), 7.23 (1H, d, J = 8.40 Hz, 8-H, Ar-H), 7.30 (1H, dd, J = 2.23 Hz and J = 6.37 Hz, 7-H), 7.34 (1H, s, 5-H, Ar-H). ¹³C NMR (150 MHz, CDCl₃) 52.5 (OCH₃), 66.1 (2-C), 114.1 (6-C), 118.4 (8-C), 123.1 (10-C), 124.1 (5-C), 131.5 (7-C), 132.7 (3-C), 134.8 (4-C), 154.5 (9-C), 165.1 (11-C=O).

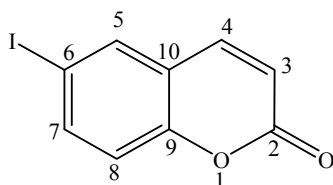
Dimethyl (2-acetoxy-5-bromophenyl)methylenepentanedioate **128**



Dimethyl(2-acetoxy-5-bromophenyl)methylenepentanedioate **128** as a white solid (0.19 g, 31%), m.p. 126-128 °C; ν_{\max} (cm⁻¹) 1741.56, 1708.21, 1741.56 (3 × C=O); ¹H NMR (600 MHz, CDCl₃) 2.14 (3H, s, 16-H), 2.12 and 3.40 (2H, 2 × m, 12-H), 3.68 (3H, s, 14-H), 3.73 (3H, s, 11-H), 4.48 (1H, t, J = 7.26 Hz, 7-H), 5.45 and 6.08 (2H, 2 × s, C=CH₂), 7.19 (1H, d, J = 8.44 Hz, 3-H, Ar-H), 7.53 (1H, d, J = 8.65 Hz, 4-H, Ar-H), 7.68 (1H, s,

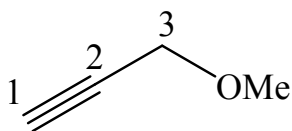
6-H, Ar-H); ^{13}C NMR (150 MHz, CDCl_3) 13.9 (14-C), 33.1 (12-C), 44.2 (7-C), 52.2 (16-C), 52.8 (11-C), 117.0 (5-C), 119.0 (3-C), 126.8 (6-C), 129.3 (9-C=CH₂), 133.4 (4-C), 135.8 (2-C), 144.7 (8-C), 151.0 (1-C), 161.1 (13-C=O), 166.8 (10-C=O), 171.8 (15-C=O).

6-Iodo-2H-chromen-2-one **133**



Finely powdered I₂ (1.12 g, 176 mmol) and NaIO₃ (0.44 g, 88 mmol) were suspended in concentrated sulfuric acid (7.5 mL). The mixture was stirred for 30 minutes at 30 °C to give a dark brown iodinating solution. Coumarin (1.5 g, 10 mmol) was added to the solution containing the I⁺ intermediate and the stirring was continued overnight. The final reaction mixture was poured with stirring into ice-water solution (75 g). The crude product was collected by filtration, washed with cold water until the filtrates were neutral, then recrystallized in CHCl_3 and air dried in the dark to give *6-iodo-2H-chromen-2-one* **133** as a brown solid (2.0 g, 72%); m.p. 162-164 °C (lit.³⁹² 165 °C); [HRMS: m/z calculated for $\text{C}_9\text{H}_5\text{IO}_2$ (MH^+) 272.9412. Found 272.9409]; ν_{max} (cm^{-1}) 1720.38 (C=O), ^1H NMR (600 MHz, CDCl_3) 6.44 (1H, d, J = 9.56 Hz, 3-H), 7.09 (1H, d, J = 8.65 Hz, 8-H, Ar-H), 7.62 (1H, d, J = 9.58 Hz, 4-H), 7.79 (1H, dd, J = 1.96 Hz and J = 6.70 Hz, 7-H, Ar-H), 7.81 (1H, d, J = 7.56 Hz, 5-H, Ar-H); ^{13}C NMR (150 MHz, CDCl_3) 87.3 (6-C), 117.8 (3-C), 119.0 (8-C), 120.9 (10-C), 136.3 (5-C), 140.4 (7-C), 142.1 (4-C), 153.7 (9-C), 160.0 (2-C=O).

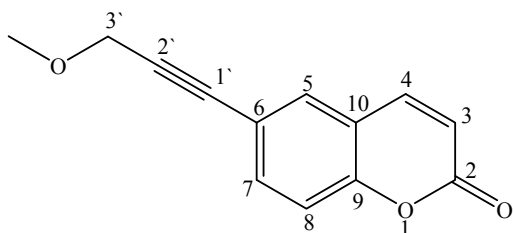
3-Methoxyprop-1-yne **136**



Propargyl alcohol (6.9 mL, 0.12 mol) was introduced slowly into a stirred solution of potassium hydroxide (4.3 g, 77 mmol) in water (5.0 mL). Dimethyl sulfate was added dropwise *via* a dropping funnel and the reaction mixture was stirred at ambient temperature for 12 hours. A colorless oil identified as *3-methoxyprop-1-yne* **136** was collected by distillation at 63 °C in a yield of 67%; ^1H NMR (400 MHz, CDCl_3) 2.41 (1H, s, 1-H), 3.35 (3H, s, OCH₃),

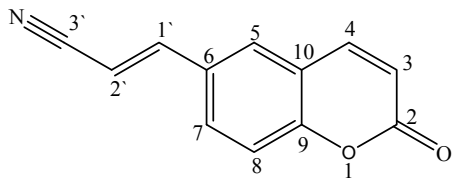
4.06 (2H, s, 3-H); ^{13}C NMR (100 MHz, CDCl_3) 57.3 (OCH_3), 59.4 (3-C), 74.3 (1-C), 79.3 (2-C).

6-(3-Methoxyprop-1-ynyl)-2H-chromen-2-one **137**



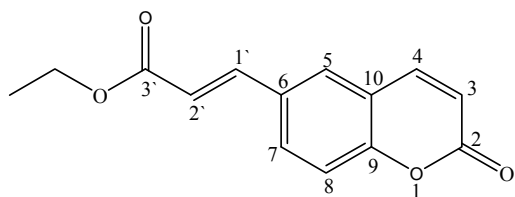
6-Iodocoumarin (**133**) (2.7 g, 10 mmol), $\text{PdCl}_2(\text{PPh}_3)_2$ (0.21 g, 3.0 mol%), and CuI (0.08 g, 4.0 mol%) were placed in a two neck flask under Ar. Et_3N (5.5 mL, 40 mmol) and dry DMF (1 mL) were added and the mixture was heated to 65 °C. 3-Methoxyprop-1-yne (**155**) (1.01 mL, 12.0 mmol) in 5 mL of dry DMF was added dropwise over 15 minutes. After complete addition, the temperature was increased to 80 °C and the reaction mixture was stirred for 4 hours at room temperature under an argon atmosphere. The resulting dark solution was allowed to cool down and filtered through a thin pad of Celite®. The filtrate was diluted with water and extracted with EtOAc (3×10 mL). The organic layers were combined, dried over Na_2SO_4 (anhydrous), and evaporated to dryness. Purification by silica gel column chromatography (hexane: EtOAc 4:1) gave 4-chloro-2-(3-methoxyprop-1-ynyl)benzaldehyde **137** as a pale yellow solid (1.1 g, 53%); m.p. 88-90 °C; [HRMS: m/z calculated for $\text{C}_{13}\text{H}_{10}\text{O}_3$ (MH^+) 215.0708. Found 215.0707]; ν_{max} (cm^{-1}) 1715.01 ($\text{C}=\text{O}$); ^1H NMR (600 MHz, CDCl_3) 3.36 (3H, s, OCH_3), 4.22 (2H, s, 3'-H), 6.35 (1H, d, $J=9.57$ Hz, 3-H), 7.17-7.48 (3H, m, 8-H, 5-H, 7-H, Ar-H), 7.55 (1H, d, $J=9.55$ Hz, 4-H); ^{13}C NMR (150 MHz, CDCl_3) 57.9 (OCH_3), 60.3 (3'-C), 84.6 (1'-C), 85.8 (2'-C), 117.2 (3-C), 117.5 (8-C), 118.8 (6-C), 119.2 (10-C), 131.1 (5-C), 135.0 (7-C), 142.7 (4-C), 153.7 (9-C), 160.1 (2-C=O).

(Coumarin-6-yl)acrylonitrile **134a**



6-Iodocoumarin (**133**) (0.07 g, 0.25 mmol), acrylonitrile (0.13 mL, 2.0 mmol), $\text{PdCl}_2(\text{PPh}_3)_2$ (7.0 mg, 0.01 mmol), and Et_3N (0.14 mL, 1.0 mmol) were dissolved in 20 mL of dry DMF and stirred for 24 hours at 40 °C. The reaction mixture was allowed to cool down and the resulting dark solution was filtered through a thin pad of Celite®. The filtrate was diluted with water and extracted with EtOAc (3×10 mL). The organic layers were combined, dried over MgSO_4 (anhydrous) and concentrated under vacuum. Purification of the crude product by preparative thin layer chromatography (hexane:EtOAc 1:1) afforded (coumarin-6-yl)acrylonitrile **134a** as a grey solid (0.02 g; 42%); m.p. 176-178 °C; ν_{max} (cm^{-1}) 1718.17 (C=O); ^1H NMR (600 MHz, CDCl_3) 5.90 (1H, d, $J = 16.61$ Hz, 2'-H), 6.49 (1H, d, $J = 9.58$ Hz, 3-H), 7.38-7.44 (2H, m, 1'-H, 8-H), 7.55 (1H, d, $J = 7.04$ Hz, 7-H, Ar-H), 7.63 (1H, dd, $J = 1.94$ Hz and $J = 6.71$ Hz, 5-H, Ar-H), 7.71 (1H, d, $J = 9.59$ Hz, 4-H); ^{13}C NMR (150 MHz, CDCl_3) 97.4 (2'-C), 117.9 (3-C), 118.0 (3'-C), 119.3 (8-C), 127.2 (10-C), 130.0 (5-C), 132.3 (7-C), 134.8 (6-C), 142.6 (4-C), 148.4 (1'-C), 155.6 (9-C), 159.7 (2-C=O).

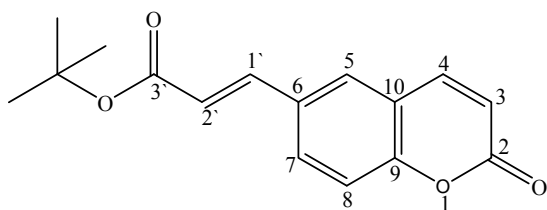
Ethyl (coumarin-6-yl)acrylate **134b**



The procedure described for the synthesis of 3-(2-oxo-2H-chromen-7-yl)acrylonitrile **134a** was followed, using 6-iodocoumarin (**133**) (0.07 g, 0.25 mmol), ethylacrylate (0.21 mL, 2.0 mmol), $\text{PdCl}_2(\text{PPh}_3)_2$ (7.0 mg, 0.01 mmol), and Et_3N (0.14 mL, 1.0 mmol) in 20 mL of dry DMF. Work-up and purification by preparative thin layer chromatography [on silica gel; elution with CHCl_3 :MeOH (200:1)] afforded ethyl (coumarin-6-yl)acrylate **134b** as a yellowish solid (0.04 g, 62%); m.p. 138-140 °C; ν_{max} (cm^{-1}) 1699.21 and 1634.81 ($2 \times \text{C=O}$); ^1H NMR (600 MHz, CDCl_3) 1.30 (3H, t, $J = 7.13$ Hz, CH_3), 4.23 (2H, q, $J = 7.12$ Hz, OCH_2), 6.42 (2H, m, 3-H, 2'-H), 7.30 (1H, d, $J = 8.63$

Hz, 8-H, Ar-H), 7.59-7.65 (3H, m, 7-H, 5-H, 4-H), 7.70 (1H, d, $J = 9.58$ Hz, 1'-H); ^{13}C NMR (150 MHz, CDCl_3) 14.2 (CH_3), 60.6 (OCH_2), 117.3 (8-C), 117.5 (6-C), 119.0 (3-C, 2'-C), 127.6 (4-C), 130.7 (5-C), 130.9 (7-C), 142.3 (10-C), 143.0 (1'-C), 154.8 (9-C), 160.0 (2-C=O), 166.4 (3'-C=O).

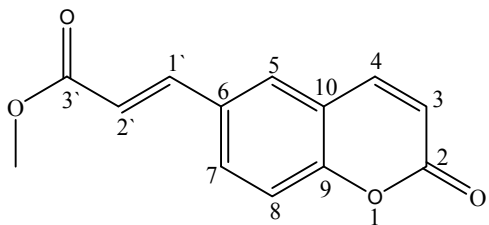
tert*-Butyl (coumarin-6-yl)acrylate **134c*



The procedure described for the synthesis of 3-(2-oxo-2*H*-chromen-7-yl)acrylonitrile **134a** was followed, using 6-iodocoumarin (**133**) (0.07 g, 0.25 mmol), *tert*-butylacrylate (0.29 mL, 2.0 mmol),

$\text{PdCl}_2(\text{PPh}_3)_2$ (7.0 mg, 0.01 mmol), and Et_3N (0.14 mL, 1.0 mmol) in 20 mL of dry DMF. Work-up and purification by preparative thin layer chromatography [on silica gel; elution with $\text{CHCl}_3:\text{MeOH}$ (200:1)] afforded *tert*-butyl (coumarin-6-yl)acrylate **134c** as a brown solid (0.03 g, 45%); m.p. 154-158 °C; [HRMS: m/z calculated for $\text{C}_{16}\text{H}_{16}\text{O}_4$ (MH^+) 273.1127. Found 273.1131]; ν_{max} (cm^{-1}) 1696.83 and 1719.01 ($2 \times \text{C}=\text{O}$); ^1H NMR (600 MHz, CDCl_3) 1.55 (9H, s, $\text{OC}(\text{CH}_3)_3$), 6.39 (1H, d, $J = 15.97$ Hz, 3-H), 6.48 (1H, d, $J = 9.55$ Hz, 2'-H), 7.35 (1H, d, $J = 8.61$ Hz, 8-H, Ar-H), 7.61-7.72 (3H, m, 7-H, 5-H, 4-H), 7.72 (1H, d, $J = 9.58$ Hz, 1'-H); ^{13}C NMR (150 MHz, CDCl_3) 28.2 [$\text{OC}(\text{CH}_3)_3$], 80.9 [$\text{CO}(\text{CH}_3)_3$], 117.4 (8-C), 117.6 (6-C), 119.1 (3-C), 121.2 (2'-C), 127.5 (4-C), 130.8 (5-C), 131.3 (7-C), 141.4 (10-C), 143.0 (1'-C), 154.8 (9-C), 160.2 (2-C=O), 165.9 (3'-C=O).

Methyl (coumarin-6-yl)acrylate **134d**

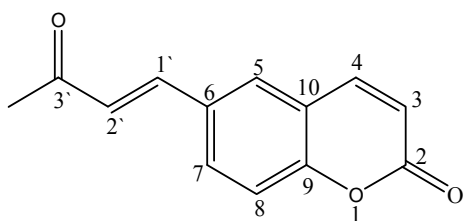


The procedure described for the synthesis of 3-(2-oxo-2*H*-chromen-7-yl)acrylonitrile **134a**

was followed, using 6-iodocoumarin (**133**) (0.07 g, 0.25 mmol), methylacrylate (0.18 mL, 2.0 mmol), $\text{PdCl}_2(\text{PPh}_3)_2$ (7.0 mg, 0.01 mmol), and Et_3N (0.14 mL, 1.0 mmol) in 20 mL of dry DMF. Work-up and purification by preparative thin layer chromatography [on silica

gel; elution with CHCl₃:MeOH (200:1)] afforded *methyl (coumarin-6-yl)acrylate* **134d** as a brownish solid (0.04 g, 53%); m.p. 158-160 °C; ν_{\max} (cm⁻¹) 1710.45 and 1637.04 (2 × C=O); ¹H NMR (600 MHz, CDCl₃) 3.81 (3H, s, OCH₃), 6.45 (2H, m, 2'-H, 3-H), 7.34 (1H, d, *J* = 8.63 Hz, 8-H, Ar-H), 7.60 (1H, d, *J* = 9.69 Hz, 4-H), 7.67-7.71 (3H, m, 5-H, 7-H, 1'-H); ¹³C NMR (150 MHz, CDCl₃) 51.8 (OCH₃), 117.5 (8-C), 117.6 (6-C), 118.7 (4-C), 119.1 (3-C, 2'-C), 127.7 (5-C), 130.8 (7-C), 142.7 (10-C), 142.9 (1'-C), 155.0 (9-C), 160.0 (2-C=O), 167.0 (3'-C=O).

Methyl (coumarin-6-yl)venylketone **134e**

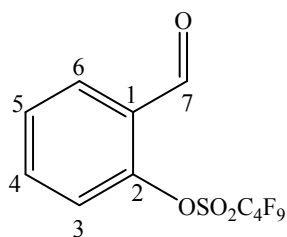


The procedure described for the synthesis of 3-(2-oxo-2*H*-chromen-7-yl)acrylonitrile **134a**

was followed, using 6-iodocoumarin (**133**) (0.07 g, 0.25 mmol), methyl vinyl ketone (0.17 mL, 2.0 mmol), PdCl₂(PPh₃)₂ (7.0 mg, 0.01 mmol), and Et₃N (0.14 mL, 1.0 mmol) in 20 mL of dry DMF. Work-up and purification by preparative thin layer chromatography [on silica gel; elution with hexane:EtOAc (1:1)] afforded *methyl (coumarin-6-yl)venylketone* **134e** as a brown solid (0.03 g, 51%); m.p. 110-112 °C; [HRMS: *m/z* calculated for C₁₃H₁₀O₃ (MH⁺) 215.0708. Found 215.0708]; ν_{\max} (cm⁻¹) 1710.05 and 1665.16 (2 × C=O); ¹H NMR (600 MHz, CDCl₃) 2.38 (3H, s, CH₃), 6.46 (1H, d, *J* = 9.56 Hz, 3-H), 6.71 (1H, d, *J* = 16.23 Hz, 2'-H), 7.34 (1H, d, *J* = 8.61 Hz, 8-H, Ar-H), 7.50 (1H, d, *J* = 16.12 Hz, 1'-H), 7.63 (1H, d, *J* = 8.64 Hz, 7-H, Ar-H), 7.70-7.72 (2H, m, 5-H, 4-H); ¹³C NMR (150 MHz, CDCl₃) 27.9 (CH₃), 117.6 (8-C), 117.7 (6-C), 119.2 (3-C, 2'-C), 127.7 (4-C), 127.9 (5-C), 131.0 (7-C), 141.1 (10-C), 142.9 (1'-C), 155.1 (9-C), 160.0 (2-C=O), 197.8 (3'-C=O).

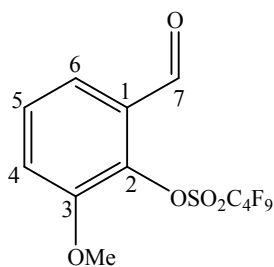
6.2.6. Nonaflation of salicylaldehyde derivatives

Nonafllyl salicylaldehyde **139a**



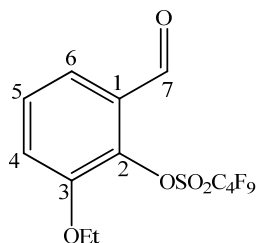
To a stirring solution of Et₃N (0.34 mL, 2.5 mmol) in dry CH₃CN on ice was added salicylaldehyde (0.18 mL, 1.7 mmol) followed by the gradual addition of perfluoro 1-butane sulfonyl fluoride (N_F-F) (0.45 mL, 2.5 mmol). The mixture was stirred for 12 hours under argon and after extraction with H₂O and EtOAc, the crude product was purified by preparative thin layer chromatography [on silica gel; elution with hexane:EtOAc (2:1)] to afford *nonafllyl salicylaldehyde* **139a** as a yellow oil (0.66 g, 99%); ν_{\max} (cm⁻¹) 1704.83 (C=O); ¹H NMR (400 MHz, CDCl₃) 7.39 (1H, d, *J* = 8.29 Hz, 3-H, Ar-H), 7.53 (1H, t, *J* = 7.52 Hz, 5-H, Ar-H), 7.69 (1H, t, *J* = 7.86 Hz, 4-H, Ar-H), 7.96 (1H, d, *J* = 7.65 Hz, 6-H, Ar-H), 10.24 (1H, s, CHO); ¹³C NMR (100 MHz, CDCl₃) 122.4 (3-C), 128.5 (1-C), 128.9 (5-C), 130.9 (6-C), 135.9 (4-C), 149.9 (2-C), 186.6 (CHO).

Nonafllyl 3-methoxysalicylaldehyde **139b**



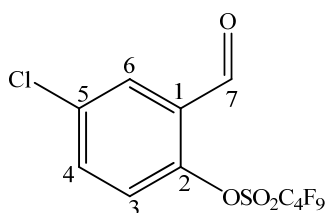
The procedure described for the synthesis of nonaflated salicylaldehyde was followed, using Et₃N (0.34 mL, 2.5 mmol), 3-methoxysalicylaldehyde (0.25 g, 1.7 mmol) and (N_F-F) (0.45 mL, 2.5 mmol) in dry CH₃CN. Work-up and purification by preparative thin layer chromatography [on silica gel; elution with hexane:EtOAc (2:1)] afforded *nonafllyl 3-methoxysalicylaldehyde* **139b** as a colorless oil (0.69 g, 96%); [HRMS: *m/z* calculated for C₁₂H₇O₅F₉S (MH⁺) 434.9949. Found 434.9958]; ν_{\max} (cm⁻¹) 1694.02 (C=O); ¹H NMR (400 MHz, CDCl₃) 3.94 (3H, s, OMe), 7.32-7.48 (3H, m, 4-H, 5-H, 6-H, Ar-H), 10.24 (1H, s, CHO); ¹³C NMR (100 MHz, CDCl₃) 56.7 (OMe), 119.1 (4-C), 121.4 (5-C), 129.5 (6-C), 130.0 (1-C), 139.7 (2-C), 152.1 (3-C), 187.0 (CHO).

Nonaflyl 3-ethoxysalicylaldehyde **139c**



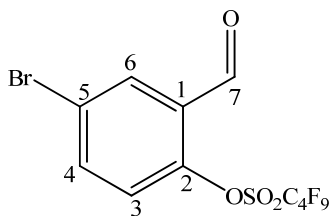
The procedure described for the synthesis of nonaflated salicylaldehyde was followed, using Et₃N (0.34 mL, 2.5 mmol), 3-ethoxysalicylaldehyde (0.28 g, 1.7 mmol) and N_F-F (0.45 mL, 2.5 mmol) in dry CH₃CN. Work-up and purification by preparative thin layer chromatography [on silica gel; elution with hexane:EtOAc (2:1)] afforded *nonaflyl 3-ethoxysalicylaldehyde* **139c** as a yellow oil (0.73 g, 98%); [HRMS: *m/z* calculated for C₁₃H₉O₅F₉S (MH⁺) 449.0105. Found 449.0092]; ν_{\max} (cm⁻¹) 1700.61 (C=O); ¹H NMR (600 MHz, CDCl₃) 1.47 (3H, t, *J* = 7.00 Hz, CH₃), 4.17 (2H, q, *J* = 6.98 Hz, OCH₂), 7.27 (1H, dd, *J* = 1.49 Hz and *J* = 6.72 Hz, 4-H, Ar-H), 7.42 (1H, t, *J* = 7.98 Hz, 5-H, Ar-H), 7.49 (1H, dd, *J* = 1.52 Hz and *J* = 6.26 Hz, 6-H, Ar-H), 10.26 (1H, s, CHO); ¹³C NMR (150 MHz, CDCl₃) 14.1 (CH₃), 65.6 (OCH₂), 119.3 (4-C), 120.6 (5-C), 130.0 (6-C), 129.5 (1-C), 139.6 (2-C), 151.2 (3-C), 186.8 (CHO).

Nonaflyl 5-chlorosalicylaldehyde **139d**



The procedure described for the synthesis of nonaflated salicylaldehyde was followed, using Et₃N (0.34 mL, 2.5 mmol), 5-chlorosalicylaldehyde (0.24 g, 1.7 mmol) and N_F-F (0.45 mL, 2.5 mmol) in dry CH₃CN. Work-up and purification by preparative thin layer chromatography [on silica gel; elution with hexane:EtOAc (2:1)] afforded *nonaflyl 5-chlorosalicylaldehyde* **139d** as a colorless oil (0.55 g, 76%); [HRMS: *m/z* calculated for C₁₁H₄ClO₄F₉S (MH⁺) 438.9453. Found 438.9405]; ν_{\max} (cm⁻¹) 1706.60 (C=O); ¹H NMR (400 MHz, CDCl₃) 7.38 (1H, d, *J* = 8.80 Hz, 3-H, Ar-H), 7.66 (1H, dd, *J* = 2.59 Hz and *J* = 6.21 Hz, 4-H, Ar-H), 7.94 (1H, d, *J* = 7.53 Hz, 6-H, Ar-H), 10.22 (1H, s, CHO); ¹³C NMR (100 MHz, CDCl₃) 123.9 (4-C), 129.5 (5-C), 130.2 (6-C), 135.2 (1-C), 135.6 (3-C), 148.3 (2-C), 185.1 (CHO).

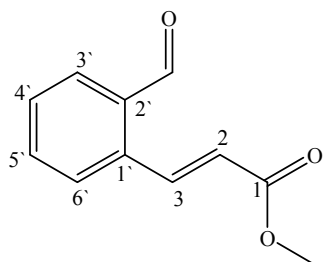
Nonaflyl 5-bromosalicylaldehyde **139e**



The procedure described for the synthesis of nonaflated salicylaldehyde was followed, using Et₃N (0.34 mL, 2.5 mmol), 5-bromosalicylaldehyde (0.34 g, 1.7 mmol) and N_T-F (0.45 mL, 2.5 mmol) in dry CH₃CN. Work-up and purification by preparative thin layer chromatography [on silica gel; elution with hexane:EtOAc (2:1)] afforded *nonaflyl 5-bromosalicylaldehyde* **139e** as a colorless oil (0.52 g, 65%); [HRMS: *m/z* calculated for C₁₁H₄BrF₉O₄S (MH⁺) 484.8928. Found 484.8911]; ν_{\max} (cm⁻¹) 1704.75 (C=O); ¹H NMR (400 MHz, CDCl₃) 7.30 (1H, d, *J* = 8.73 Hz, 3-H, Ar-H), 7.79 (1H, dd, *J* = 1.94 Hz and *J* = 6.54 Hz, 4-H, Ar-H), 8.06 (1H, d, *J* = 8.12 Hz, 6-H, Ar-H), 10.18 (1H, s, CHO); ¹³C NMR (100 MHz, CDCl₃) 123.2 (4-C), 124.5 (5-C), 130.2 (6-C), 133.7 (1-C), 138.9 (3-C), 149.3 (2-C), 185.4 (CHO).

6.2.7. Preparation of Heck adducts

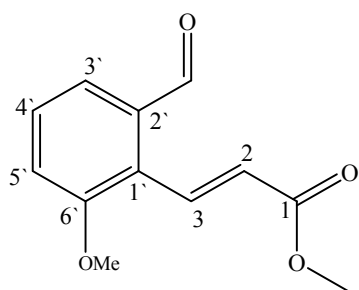
Methyl 3-(2'-formylphenyl)acrylate **141a**



Tetrabutyl-ammonium bromide (0.14 g, 0.42 mmol), Et₃N (0.52 g, 3.8 mmol), Pd(OAc)₂ (16 mg, 0.07 mmol), P(*o*-tolyl)₃ (0.07 g, 0.24 mmol) and methyl acrylate (0.68 mL, 7.5 mmol) were stirred for 5 minutes under nitrogen. To the brown solution obtained was added the nonaflyl salicylaldehyde (**139a**) (0.60 g, 1.5 mmol) in dry CH₃CN (0.75 mL) and the mixture was stirred at 80 °C for 72 hours. The reaction mixture was allowed to cool down and diluted with EtOAc (20 mL). The resulting dark solution was filtered through a thin pad of Celite® and the filtrate was diluted with water and extracted with EtOAc (3×10 mL). The organic layers were combined, dried over MgSO₄ (anhydrous), and concentrated under vacuum. The dark thick oil obtained was chromatographed on thin layer preparative plates [elution with hexane:EtOAc (6:1)] to obtain *methyl 3-(2'-formylphenyl)acrylate*

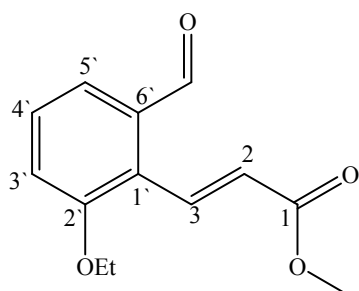
141a as a yellow solid (0.06 g, 24%); m.p. 42-44 °C (lit.³⁹³ 43-44 °C); [HRMS: m/z calculated for $C_{11}H_{10}O_3$ (MH^+) 191.0708. Found 191.0708]; ν_{\max} (cm^{-1}) 1700.32 and 1623.49 ($2 \times C=O$); 1H NMR (400 MHz, $CDCl_3$) 3.78 (3H, s, OCH_3), 6.33 (1H, d, $J=15.89$ Hz, 2-H), 7.52-7.61 (4H, m, 3'-H, 4'-H, 5'-H, 6'-H, Ar-H), 8.48 (1H, d, $J=15.91$ Hz, 3-H), 10.23 (1H, s, CHO); ^{13}C NMR (100 MHz, $CDCl_3$) 51.7 (OCH_3), 122.5 (2-C), 127.8 (3'-C), 129.8 (4'-C), 132.3 (5'-C), 133.7 (6'-C), 136.3 (1'-C, 2'-C), 141.1 (3-C), 166, 4 (1-C=O), 191.6 (CHO).

Methyl 3-(2'-formyl-6'-methoxyphenyl)acrylate **141b**



The procedure described for the synthesis of methyl 3-(2'-formylphenyl)acrylate **141a** (Method 1) was followed, using tetrabutyl-ammonium bromide (0.14 g, 0.42 mmol), Et_3N (0.52 g, 3.8 mmol), $Pd(OAc)_2$ (16 mg, 0.07 mmol), $P(o\text{-tolyl})_3$ (0.07 g, 0.24 mmol), methyl acrylate (0.68 mL, 7.5 mmol) and nonaflyl 3-methoxysalicylaldehyde (**139b**) (0.65 g, 1.5 mmol) in dry CH_3CN . Work-up and purification by preparative thin layer chromatography [on silica gel; elution with hexane:EtOAc (6:1)] afforded *methyl 3-(2'-formyl-6'-methoxyphenyl)acrylate* **141b** as a black solid (0.04 g, 12%); m.p. 62-64 °C; [HRMS: m/z calculated for $C_{12}H_{12}O_4$ (MH^+) 221.0814. Found 221.0813]; ν_{\max} (cm^{-1}) 1713.24 and 1692.80 ($2 \times C=O$); 1H NMR (400 MHz, $CDCl_3$) 3.81 (3H, s, OCH_3), 3.89 (3H, s, OCH_3), 6.30 (1H, d, $J=16.15$ Hz, 2-H), 7.13-7.48 (3H, m, 3'-H, 4'-H, 5'-H, Ar-H), 8.17 (1H, d, $J=16.13$ Hz, 3-H), 10.19 (1H, s, CHO); ^{13}C NMR (100 MHz, $CDCl_3$) 51.8 (OCH_3), 55.9 (OCH_3), 115.5 (2-C), 121.8 (1'-C), 126.3 (5'-C), 126.5 (3'-C), 130.2 (4'-C), 135.8 (2'-C), 136.5 (3-C), 158.3 (6'-C), 166.7 (1-C=O), 191.6 (CHO).

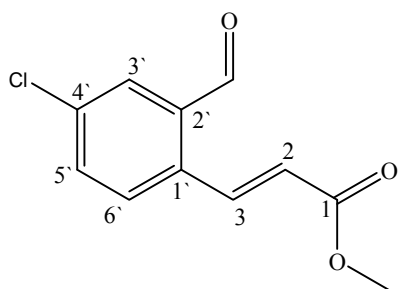
Methyl 3-(2'-ethoxy-6'-formylphenyl)acrylate **141c**



The procedure described for the synthesis of methyl 3-(2'-formylphenyl)acrylate **141a** (Method 1) was followed, using tetrabutyl-ammonium bromide (0.14 g, 0.42 mmol),

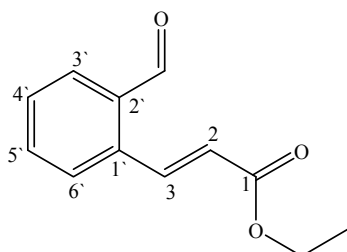
Et₃N (0.52 g, 3.8 mmol), Pd(OAc)₂ (16 mg, 0.07 mmol), P(*o*-tolyl)₃ (0.07 g, 0.24 mmol), methyl acrylate (0.68 mL, 7.5 mmol) and nonafllyl 3-ethoxysalicylaldehyde (**139c**) (0.67 g, 1.5 mmol) in dry CH₃CN. Work-up and purification by preparative thin layer chromatography [on silica gel; elution with hexane:EtOAc (6:1)] afforded *methyl 3-(2'-ethoxy-6'-formylphenyl)acrylate* **141c** as a dark oil (0.06 g, 18%); ν_{\max} (cm⁻¹) 1712.66, 1684.05 (2 × C=O); ¹H NMR (600 MHz, CDCl₃) 1.46 (3H, t, *J* = 6.96 Hz, CH₃), 3.81 (3H, s, OCH₃), 4.12 (2H, q, *J* = 6.98 Hz, OCH₂), 6.34 (1H, d, *J* = 16.12 Hz, 2-H), 7.12 (1H, d, *J* = 8.19 Hz, 5'-H, Ar-H), 7.43 (1H, t, *J* = 7.92 Hz, 4'-H, Ar-H), 7.49 (1H, d, *J* = 8.76 Hz, 3'-H, Ar-H), 8.20 (1H, d, *J* = 16.12 Hz, 3-H), 10.21 (1H, s, CHO); ¹³C NMR (150 MHz, CDCl₃) 14.7 (CH₃), 51.8 (OCH₂), 64.6 (OCH₃), 116.5 (2-C), 121.8 (1'-C), 126.4 (3'-C), 130.1 (4'-C, 5'-C), 137.0 (6'-C), 135.6 (3-C), 157.8 (2'-C), 166.8 (1-C=O), 191.6 (CHO).

Methyl 3-(4'-chloro-2'-formylphenyl)acrylate **141d**



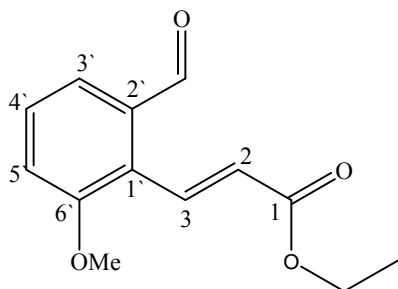
The procedure described for the synthesis of methyl 3-(2'-formylphenyl)acrylate **141a** (Method 1) was followed, using tetrabutyl-ammonium bromide (0.14 g, 0.42 mmol), Et₃N (0.52 g, 3.8 mmol), Pd(OAc)₂ (16 mg, 0.07 mmol), P(*o*-tolyl)₃ (0.07 g, 0.24 mmol), methyl acrylate (0.68 mL, 7.5 mmol) and nonafllyl 5-chlorosalicylaldehyde (**139d**) (0.66 g, 1.5 mmol) in dry CH₃CN. Work-up and purification by preparative thin layer chromatography [on silica gel; elution with hexane:EtOAc (6:1)] afforded *methyl 3-(4'-chloro-2'-formylphenyl)acrylate* **141d** as a brown solid (0.02 g, 4.6%); m.p. 108-110 °C; [HRMS: *m/z* calculated for C₁₁H₉ClO₃ (MH⁺) 225.0318. Found 225.0316]; ν_{\max} (cm⁻¹) 1724.87 and 1678.16 (2 × C=O); ¹H NMR (400 MHz, CDCl₃) 3.83 (3H, s, OCH₃), 6.38 (1H, d, *J* = 15.89 Hz, 2-H), 7.58 (2H, m, 5'-H, 6'-H, Ar-H), 7.85 (1H, s, 3'-H, Ar-H), 8.43 (1H, d, *J* = 15.89 Hz, 3-H), 10.26 (1H, s, CHO); ¹³C NMR (100 MHz, CDCl₃) 52.0 (OCH₃), 123.3 (2-C), 129.4 (6'-C), 131.6 (3'-C), 133.9 (5'-C), 134.8 (1'-C), 134.8 (4'-C), 136.4 (2'-C), 139.7 (3-C), 166.4 (1-C=O), 190.2 (CHO).

Ethyl 3-(2'-formylphenyl)but-2-enoate **141e**



The procedure described for the synthesis of methyl 3-(2'-formylphenyl)acrylate **141a** (Method 1) was followed, using tetrabutyl-ammonium bromide (0.14 g, 0.42 mmol), Et₃N (0.52 g, 3.8 mmol), Pd(OAc)₂ (16 mg, 0.07 mmol), P(*o*-tolyl)₃ (0.07 g, 0.24 mmol), ethyl acrylate (0.80 mL, 7.5 mmol) and nonaflyl salicylaldehyde (**139a**) (0.60 g, 1.5 mmol) in dry CH₃CN. Work-up and purification by preparative thin layer chromatography [on silica gel; elution with hexane:EtOAc (6:1)] afforded *ethyl 4-(2'-formylphenyl)but-2-enoate* **141e** as a yellowish solid (0.15 g, 47%); m.p. 116-118 °C; lit.³⁹⁴ 120 °C; ν_{\max} (cm⁻¹) 1702.15 and 1640.03 (2 × C=O); ¹H NMR (600 MHz, CDCl₃) 1.33 (3H, t, *J* = 7.12 Hz, CH₃), 4.27 (2H, q, *J* = 6.97 Hz, OCH₂), 6.36 (1H, d, *J* = 15.89 Hz, 2-H), 7.52-7.61 (3H, m, 4'-H, 5'-H, 6'-H, Ar-H), 7.86 (1H, d, *J* = 7.83 Hz, 3'-H, Ar-H), 8.49 (1H, d, *J* = 15.89 Hz, 3-H), 10.28 (1H, s, CHO); ¹³C NMR (100 MHz, CDCl₃) 14.2 (CH₃), 60.7 (OCH₂), 123.2 (2-C), 127.9 (3'-C), 129.8 (4'-C), 132.1 (5'-C), 133.8 (6'-C), 136.6 (1'-C, 2'-C), 140.9 (3-C), 166.2 (1-C=O), 191.7 (CHO).

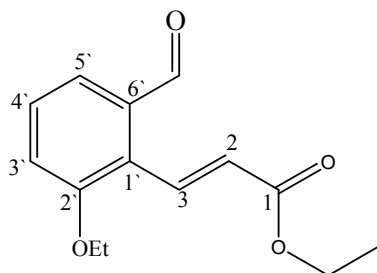
Ethyl 3-(2'-formyl-6'-methoxyphenyl)acrylate **141f**



The procedure described for the synthesis of methyl 3-(2'-formylphenyl)acrylate **141a** (Method 1) was followed, using tetrabutyl-ammonium bromide (0.14 g, 0.42 mmol), Et₃N (0.52 g, 3.8 mmol), Pd(OAc)₂ (16 mg, 0.07 mmol), P(*o*-tolyl)₃ (0.07 g, 0.24 mmol), ethyl acrylate (0.80 mL, 7.5 mmol) and nonaflyl 3-methoxysalicylaldehyde (**139b**) (0.65 g, 1.5 mmol) in dry CH₃CN. Work-up and purification by preparative thin layer chromatography [on silica gel; elution with hexane:EtOAc (6:1)] afforded *ethyl 3-(2'-formyl-6'-methoxyphenyl)acrylate* **141f** as a brownish solid (0.08 g, 22%); ν_{\max} (cm⁻¹) 1695.11 and 1633.65 (2 × C=O); ¹H NMR (400 MHz, CDCl₃) 1.33 (3H, t, *J* = 6.92 Hz, CH₃), 3.90 (3H, s, OCH₃), 4.27 (2H, q, *J* = 6.98

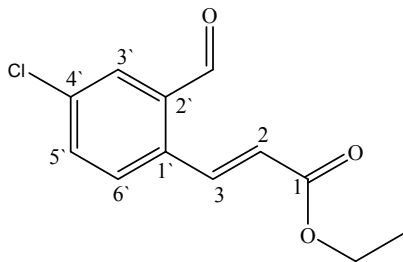
Hz, OCH₂), 6.28 (1H, d, J = 16.09 Hz, 2-H), 7.14 (1H, d, J = 8.06 Hz, 3'-H, Ar-H), 7.44-7.51 (2H, m, 4'-H, 5'-H, Ar-H), 8.16 (1H, d, J = 16.13 Hz, 3-H), 10.22 (1H, s, CHO); ¹³C NMR (100 MHz, CDCl₃) 14.2 (CH₃), 56.0 (OCH₃), 60.7 (OCH₂), 115.6 (5'-C), 126.6 (3'-C), 127.1 (2-C), 130.1 (4'-C), 135.2 (1'-C), 135.9 (2'-C), 136.2 (3-C), 158.4 (6'-C), 166.3 (1-C=O), 191.5 (CHO).

Ethyl 3-(2'-ethoxy-6'-formylphenyl)acrylate **141g**



The procedure described for the synthesis of methyl 3-(2'-formylphenyl)acrylate **141a** (Method 1) was followed, using tetrabutyl-ammonium bromide (0.14 g, 0.42 mmol), Et₃N (0.52 g, 3.8 mmol), Pd(OAc)₂ (16 mg, 0.07 mmol), P(*o*-tolyl)₃ (0.07 g, 0.24 mmol), ethyl acrylate (0.80 mL, 7.5 mmol) and nonaflyl 3-ethoxysalicylaldehyde (**139c**) (0.67 g, 1.5 mmol) in dry CH₃CN. Work-up and purification by preparative thin layer chromatography [on silica gel; elution with hexane:EtOAc (6:1)] afforded *ethyl 3-(2'-ethoxy-6'-formylphenyl)acrylate* **141g** as a yellow oil (0.02 g, 4.9%); ν_{\max} (cm⁻¹) 1711.33, 1692.15 (2 × C=O); ¹H NMR (600 MHz, CDCl₃) 1.34 and 1.47 (6H, 2 × t, J = 6.97 Hz and J = 7.14 Hz, 2 × CH₃), 4.13 and 4.28 (4H, 2 × q, J = 6.97 Hz and J = 6.98 Hz, 2 × OCH₂), 6.31 (1H, d, J = 16.10 Hz, 2-H), 7.13 (1H, d, J = 9.01 Hz, 5'-H, Ar-H), 7.43 (1H, d, J = 7.96 Hz, 4'-H, Ar-H), 7.50 (1H, d, J = 7.72 Hz, 3'-H, Ar-H), 8.19 (1H, d, J = 16.10 Hz, 3-H), 10.23 (1H, s, CHO); ¹³C NMR (150 MHz, CDCl₃) 14.3 and 14.7 (2 × CH₃), 60.7 and 64.6 (2 × OCH₂), 116.5 (2-C), 121.6 (1'-C), 126.7 (3'-C), 127.0 (5'-C), 130.1 (4'-C), 136.0 (6'-C), 136.3 (3-C), 157.8 (2'-C), 166.4 (1-C=O), 191.7 (CHO).

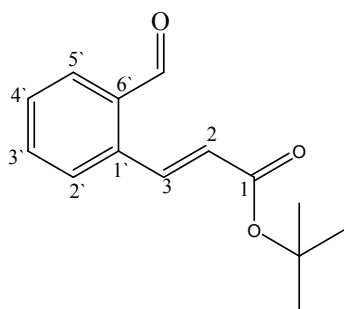
Ethyl 3-(4'-chloro-2'-formylphenyl)acrylate **141h**



The procedure described for the synthesis of methyl 3-(2'-formylphenyl)acrylate **141a** (Method 1) was followed, using tetrabutyl-ammonium bromide (0.14 g, 0.42 mmol), Et₃N (0.52 g, 3.8 mmol), Pd(OAc)₂ (16

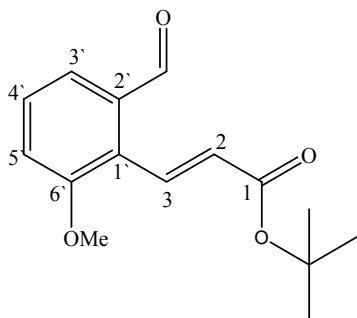
mg, 0.07 mmol), $P(o\text{-tolyl})_3$ (0.07 g, 0.24 mmol), ethyl acrylate (0.80 mL, 7.5 mmol) and nonaflyl 5-chlorosalicylaldehyde (**139d**) (0.66 g, 1.5 mmol) in dry CH_3CN . Work-up and purification by preparative thin layer chromatography [on silica gel; elution with hexane:EtOAc (6:1)] afforded *ethyl 3-(4'-chloro-2'-formylphenyl)acrylate* **141h** as a yellowish solid (0.04 g, 11%); m.p. 90-92 °C; ν_{max} (cm^{-1}) 1710.45 and 1687.51 ($2 \times \text{C=O}$); ^1H NMR (400 MHz, CDCl_3) 1.34 (3H, t, $J = 7.11$ Hz, CH_3), 4.28 (2H, q, $J = 6.95$ Hz, OCH_2), 6.37 (1H, d, $J = 15.86$ Hz, 2-H), 7.58 (2H, m, 5'-H, 6'-H, Ar-H), 7.85 (1H, s, 3'-H, Ar-H), 8.41 (1H, d, $J = 15.87$ Hz, 3-H), 10.27 (1H, s, CHO); ^{13}C NMR (100 MHz, CDCl_3) 14.3 (CH_3), 60.9 (OCH_2), 123.8 (2-C), 129.4 (3'-C), 131.4 (6'-C), 133.9 (5'-C), 134.8 (1'-C), 135.0 (4'-C), 136.3 (2'-C), 139.3 (3-C), 165.9 (1-C=O), 190.1 (CHO).

tert*-Butyl 3-(2'-formylphenyl)acrylate **141i*



The procedure described for the synthesis of methyl 3-(2'-formylphenyl)acrylate **141a** (Method 1) was followed, using tetrabutyl-ammonium bromide (0.14 g, 0.42 mmol), Et_3N (0.52 g, 3.8 mmol), $\text{Pd}(\text{OAc})_2$ (16 mg, 0.07 mmol), $P(o\text{-tolyl})_3$ (0.07 g, 0.24 mmol), *tert*-butylacrylate (1.1 mL, 7.5 mmol) and nonaflyl salicylaldehyde (**139a**) (0.60 g, 1.5 mmol) in dry CH_3CN . Work-up and purification by preparative thin layer chromatography [on silica gel; elution with hexane:EtOAc (6:1)] afforded *tert*-butyl 3-(2'-formylphenyl)acrylate **141i** as a yellow oil (0.04 g, 11%); ^1H NMR (400 MHz, CDCl_3) 1.54 (9H, s, $(\text{CH}_3)_3$), 6.30 (1H, d, $J = 15.84$ Hz, 2-H), 7.51-7.61 (3H, m, 2'-H, 3'-H, 4'-H, Ar-H), 7.87 (1H, d, $J = 7.38$ Hz, 5'-H, Ar-H), 8.41 (1H, d, $J = 15.83$ Hz, 3-H), 10.31 (1H, s, CHO); ^{13}C NMR (100 MHz, CDCl_3) 29.7 [$(\text{CH}_3)_3$], 82.0 [$\text{C}(\text{CH}_3)_3$], 125.7 (2-C), 128.1 (3'-C), 130.1 (4'-C), 132.6 (5'-C), 133.9 (2'-C), 136.4 (1'-C), 142.7 (6'-C), 142.8 (3-C), 168.7 (1-C=O), 191.9 (CHO).

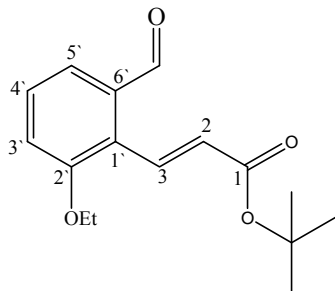
tert*-Butyl 3-(2'-formyl-6'-methoxyphenyl)acrylate **141j*



The procedure described for the synthesis of methyl 3-(2'-formylphenyl)acrylate **141a** (Method 1) was followed, using tetrabutyl-ammonium bromide (0.14 g, 0.42 mmol), Et₃N (0.52 g, 3.8 mmol), Pd(OAc)₂ (16 mg, 0.07 mmol), P(*o*-tolyl)₃ (0.07 g, 0.24 mmol), *tert*-butylacrylate (1.1 mL, 7.5 mmol) and nonaflyl 3-methoxysalicylaldehyde (**139b**)

(0.65 g, 1.5 mmol) in dry CH₃CN. Work-up and purification by preparative thin layer chromatography [on silica gel; elution with hexane:EtOAc (6:1)] afforded *tert*-butyl 3-(2'-formyl-6'-methoxyphenyl)acrylate **141j** as a brown oil (0.02 g, 6.3%); ¹H NMR (400 MHz, CDCl₃) 1.43 (9H, s, (CH₃)₃), 3.93 (3H, s, OCH₃), 6.40 (1H, d, *J* = 16.10 Hz, 2-H), 7.17 (1H, d, *J* = 7.73 Hz, 3'-H, Ar-H), 7.51 (2H, m, 4'-H, 5'-H, Ar-H), 8.32 (1H, d, *J* = 16.12 Hz, 3-H), 10.24 (1H, s, CHO); ¹³C NMR (100 MHz, CDCl₃) 28.1 [(CH₃)₃], 56.0 (OCH₃), 77.2 [C(CH₃)₃], 115.7 (2-C), 122.4 (3'-C), 125.7 (4'-C), 126.0 (5'-C), 130.5 (2'-C), 135.9 (1'-C), 138.5 (3-C), 158.6 (6'-C), 171.1 (1-C=O), 191.6 (CHO).

tert*-Butyl 3-(2'-ethoxy-6'-formylphenyl)acrylate **141k*

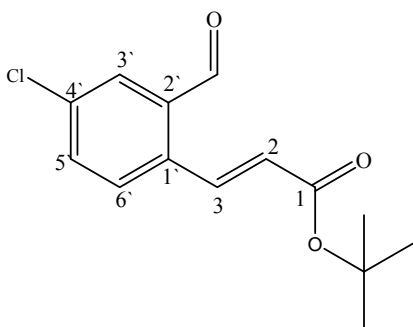


The procedure described for the synthesis of methyl 3-(2'-formylphenyl)acrylate **141a** (Method 1) was followed, using tetrabutyl-ammonium bromide (0.14 g, 0.42 mmol), Et₃N (0.52 g, 3.8 mmol), Pd(OAc)₂ (16 mg, 0.07 mmol), P(*o*-tolyl)₃ (0.07 g, 0.24 mmol), *tert*-butyl acrylate (1.1 mL, 7.5

mmol) and nonaflyl 3-ethoxysalicylaldehyde (**139c**) (0.67 g, 1.5 mmol) in dry CH₃CN. Work-up and purification by preparative thin layer chromatography [on silica gel; elution with hexane:EtOAc (6:1)] afforded *tert*-butyl 3-(2'-ethoxy-6'-formylphenyl)acrylate **141k** as a yellow oil (0.04 g, 10%); ν_{\max} (cm⁻¹) 1691.11, 1658.05 (2 × C=O); ¹H NMR (600 MHz, CDCl₃) 1.47 (3H, t, *J* = 5.97 Hz, CH₃), 1.53 (9H, s, (CH₃)₃), 4.12 (2H, q, *J* = 6.98 Hz, OCH₂), 6.16 (1H, d, *J* = 16.08 Hz, 2-H), 7.11 (1H, d, *J* = 8.23 Hz, 5'-H, Ar-H), 7.41 (1H, t, *J* = 7.96 Hz, 4'-H, Ar-H), 7.49 (1H, d, *J* = 7.69 Hz, 3'-H, Ar-H), 8.08 (1H, d, *J* =

16.06 Hz, 3-H), 10.21 (1H, s, CHO); ^{13}C NMR (150 MHz, CDCl_3) 14.7 (CH_3), 28.1 [$(\text{CH}_3)_3$], 64.5 (OCH_2), 80.8 [$\text{C}(\text{CH}_3)_3$], 116.3 (2-C), 119.5 (1'-C), 121.1 (3'-C), 124.5 (5'-C), 129.1 (4'-C), 135.2 (6'-C), 135.9 (3-C), 157.7 (2'-C), 165.5 (1-C=O), 191.8 (CHO).

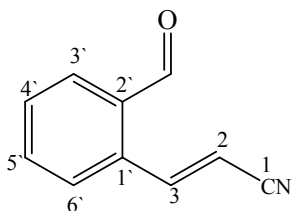
tert*-Butyl 3-(4'-chloro-2'-formylphenyl)acrylate **141l*



The procedure described for the synthesis of methyl 3-(2'-formylphenyl)acrylate **141a** (Method 1) was followed, using tetrabutyl-ammonium bromide (0.14 g, 0.42 mmol), Et_3N (0.52 g, 3.8 mmol), $\text{Pd}(\text{OAc})_2$ (16 mg, 0.07 mmol), $\text{P}(o\text{-tolyl})_3$ (0.07 g, 0.24 mmol), *tert*-butyl acrylate (1.1 mL, 7.5 mmol) and nonafllyl 5-

chlorosalicylaldehyde (**139d**) (0.66 g, 1.5 mmol) in dry CH_3CN . Work-up and purification by preparative thin layer chromatography [on silica gel; elution with hexane:EtOAc (6:1)] afforded *tert*-butyl 3-(4'-chloro-2'-formylphenyl)acrylate **141l** as a yellow oil (0.07 g, 16%); ν_{max} (cm^{-1}) 1698.59 and 1634.79 ($2 \times \text{C}=\text{O}$); ^1H NMR (400 MHz, CDCl_3) 1.54 (9H, s, $(\text{CH}_3)_3$), 6.30 (1H, d, $J = 15.83$ Hz, 2-H), 7.56 (2H, m, 5'-H, 6'-H, Ar-H), 7.85 (1H, s, 3'-H, Ar-H), 8.30 (1H, d, $J = 15.84$ Hz, 3-H), 10.28 (1H, s, CHO); ^{13}C NMR (100 MHz, CDCl_3) 28.1 [$(\text{CH}_3)_3$], 81.2 [$\text{C}(\text{CH}_3)_3$], 125.8 (2-C), 129.3 (1'-C), 131.0 (6'-C), 133.9 (3'-C), 134.7 (5'-C), 135.3 (4'-C), 136.1 (2'-C), 138.1 (3-C), 165.2 (1-C=O), 190.1 (CHO).

3-(2'-Formylphenyl)but-2-enitrile **141m**

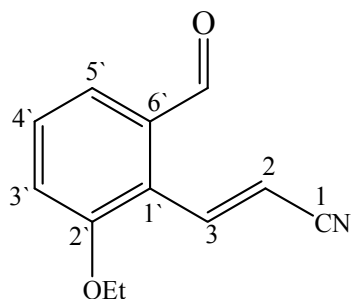


The procedure described for the synthesis of methyl 3-(2'-formylphenyl)acrylate **141a** (Method 1) was followed, using tetrabutyl-ammonium bromide (0.14 g, 0.42 mmol), Et_3N (0.52 g, 3.8 mmol), $\text{Pd}(\text{OAc})_2$ (16 mg, 0.07 mmol), $\text{P}(o\text{-tolyl})_3$ (0.07 g, 0.24 mmol), acrylonitrile (0.49 mL, 7.5 mmol) and nonafllyl

salicylaldehyde (**139a**) (0.60 g, 1.5 mmol) in dry CH_3CN . Work-up and purification by preparative thin layer chromatography [on silica gel; elution with hexane:EtOAc (6:1)] afforded 4-(2'-formylphenyl)but-2-enitrile **141m** as a dark solid (0.04 g, 16%); m.p.

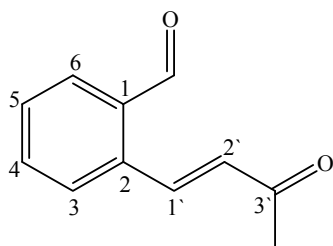
100-102 °C; [HRMS: m/z calculated for $C_{10}H_7NO$ (MH^+) 158.0606. Found 158.0608]; ν_{\max} (cm^{-1}) 1689.25 (C=O); 1H NMR (400 MHz, $CDCl_3$) 5.65 (1H, d, J = 11.87 Hz, 3-H), 7.65-7.91 (4H, m, 3'-H, 4'-H, 5'-H, 6'-H, Ar-H), 8.04 (1H, d, J = 11.88 Hz, 2-H), 10.12 (1H, s, CHO), ^{13}C NMR (100 MHz, $CDCl_3$) 99.75 (2-C), 117.0 (CN), 129.9 (6'-C), 130.9 (4'-C), 134.1 (1'-C, 2'-C), 134.6 (3'-C), 135.0 (5'-C), 148.6 (3-C), 192.8 (CHO).

3-(2'-Ethoxy-6'-formylphenyl)acrylonitrile **141n**



The procedure described for the synthesis of methyl 3-(2'-formylphenyl)acrylate **141a** (Method 1) was followed, using tetrabutyl-ammonium bromide (0.14 g, 0.42 mmol), Et_3N (0.52 g, 3.8 mmol), $Pd(OAc)_2$ (16 mg, 0.07 mmol), $P(o\text{-tolyl})_3$ (0.07 g, 0.24 mmol), acrylonitrile (0.49 mL, 7.5 mmol) and nonaflyl 3-ethoxysalicylaldehyde (**139c**) (0.67 g, 1.5 mmol) in dry CH_3CN . Work-up and purification by preparative thin layer chromatography [on silica gel; elution with hexane:EtOAc (6:1)] afforded 3-(2'-ethoxy-6'-formylphenyl)acrylonitrile **141n** as a dark oil (0.04 g, 12%); m.p. 58-60 °C; [HRMS: m/z calculated for $C_{12}H_{11}NO_2$ (MH^+) 202.0868. Found 202.0869]; ν_{\max} (cm^{-1}) 1693.39 (C=O); 1H NMR (400 MHz, $CDCl_3$) 1.50 (3H, t, J = 6.96 Hz, CH_3), 4.16 (2H, q, J = 6.97 Hz, OCH_2), 6.27 (1H, d, J = 16.75 Hz, 2-H), 7.18 (1H, d, J = 8.01 Hz, 3'-H, Ar-H), 7.45 (1H, d, J = 8.61 Hz, 5'-H, Ar-H), 7.51 (1H, t, J = 7.90 Hz, 4'-H, Ar-H), 8.19 (1H, d, J = 16.76 Hz, 3-H), 10.14 (1H, s, CHO); ^{13}C NMR (100 MHz, $CDCl_3$) 14.8 (CH_3), 65.0 (OCH_2), 104.2 (2-C), 117.1 (CN), 118.5 (3'-C), 123.0 (1'-C), 125.4 (5'-C), 131.1 (4'-C), 135.4 (6'-C), 142.9 (3-C), 158.5 (2'-C), 192.1 (CHO).

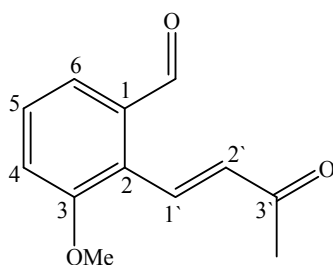
2-(3'-Oxobut-1'-enyl)benzaldehyde **141o**



The procedure described for the synthesis of methyl 3-(2'-formylphenyl)acrylate **141a** (Method 1) was followed, using tetrabutyl-ammonium bromide (0.14 g, 0.42 mmol), Et_3N (0.52 g, 3.8 mmol), $Pd(OAc)_2$ (16 mg, 0.07 mmol), $P(o\text{-$

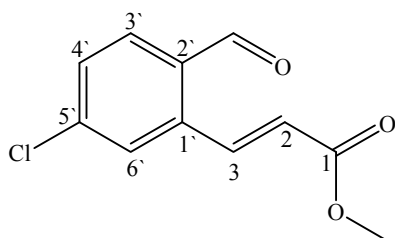
tolyl)₃ (0.07 g, 0.24 mmol), methyl vinyl ketone (0.63 mL, 7.5 mmol) and nonafllyl salicylaldehyde (**139a**) (0.60 g, 1.5 mmol) in dry CH₃CN. Work-up and purification by preparative thin layer chromatography [on silica gel; elution with hexane:EtOAc (6:1)] afforded 2-(3'-oxobut-1'-enyl)benzaldehyde **141o** as a yellow oil (0.06 g, 24%); ¹H NMR (400 MHz, CDCl₃) 2.42 (3H, s, CH₃), 6.57 (1H, d, *J* = 16.33 Hz, 2'-H), 7.57-7.85 (4H, m, 3-H, 4-H, 5-H, 6-H, Ar-H), 8.46 (1H, d, *J* = 16.32 Hz, 1'-H), 10.22 (1H, s, CHO); ¹³C NMR (100 MHz, CDCl₃) 27.4 (CH₃), 128.3 (2'-C), 130.5 (3-C), 132.2 (4-C), 134.3 (5-C), 134.3 (6-C), 136.9 (1-C, 2-C), 140.9 (1'-C), 192.9 (CHO), 199.0 (3'-C=O).

3-Methoxy-2-(3'-oxobut-1'-enyl)benzaldehyde **141p**



The procedure described for the synthesis of methyl 3-(2'-formylphenyl)acrylate **141a** (Method 1) was followed, using tetrabutyl-ammonium bromide (0.14 g, 0.42 mmol), Et₃N (0.52 g, 3.8 mmol), Pd(OAc)₂ (16 mg, 0.07 mmol), P(*o*-tolyl)₃ (0.07 g, 0.24 mmol), methyl vinyl ketone (0.63 mL, 7.5 mmol) and nonafllyl 3-methoxysalicylaldehyde (**139b**) (0.65 g, 1.5 mmol) in dry CH₃CN. Work-up and purification by preparative thin layer chromatography [on silica gel; elution with hexane:EtOAc (6:1)] afforded 3-methoxy-2-(3'-oxobut-1'-enyl)benzaldehyde **141p** as a brown solid (0.04 g, 12%); ¹H NMR (400 MHz, CDCl₃) 2.41 (3H, s, CH₃), 3.91 (3H, s, OCH₃), 6.57 (1H, d, *J* = 16.42 Hz, 1'-H), 7.16 (1H, d, *J* = 7.37 Hz, 6-H, Ar-H), 7.47-7.51 (2H, m, 4-H, 5-H, Ar-H), 8.09 (1H, d, *J* = 16.43 Hz, 2'-H), 10.17 (1H, s, CHO). ¹³C NMR (100 MHz, CDCl₃) 27.34 (CH₃), 56.0 (OCH₃), 115.7 (2'-C), 123.0 (2-C), 126.2 (5-C), 130.3 (4-C), 135.5 (6-C), 135.6 (1-C), 135.9 (1'-C), 158.5 (3-C), 191.8 (3'-C=O), 191.7 (CHO).

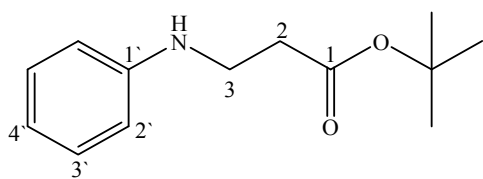
Methyl 3-(5'-chloro-2'-formylphenyl)acrylate **141q**



The procedure described for the synthesis of methyl 3-(2'-formylphenyl)acrylate **141a** (Method 1) was followed, using tetrabutyl-ammonium bromide (0.14 g,

0.42 mmol), Et₃N (0.52 g, 3.8 mmol), Pd(OAc)₂ (16 mg, 0.07 mmol), P(*o*-tolyl)₃ (0.07 g, 0.24 mmol), methylacrylate (0.68 mL, 7.5 mmol) and 4-chloro 2-iodobenzaldehyde (**144b**) (0.40 g, 1.50 mmol) in dry CH₃CN. Work-up and purification by preparative layer chromatography [on silica gel; elution with hexane:EtOAc (6:1)] afforded *methyl 3-(5'-chloro-2-formylphenyl)acrylate* **141q** as a yellow oil (0.28 g, 83%); ¹H NMR (600 MHz, CDCl₃) 3.84 (3H, s, OCH₃), 6.55 (1H, d, *J* = 16.01 Hz, 2-H), 7.60 (1H, t, *J* = 8.23 Hz, 3'-H, Ar-H), 7.82 (1H, d, *J* = 8.16 Hz, 4'-H), 8.08-8.11 (2H, m, 3-H, 6'-H), 10.01 (1H, s, CHO); ¹³C NMR (150 MHz, CDCl₃) 52.1 (OCH₃), 122.3 (2-C), 127.8 (6'-C), 128.8 (3'-C), 131.1 (4'-C), 133.9 (5'-C), 135.2 (2'-C), 139.3 (1'-C), 140.9 (3-C), 166.5 (1-C=O), 190.4 (CHO).

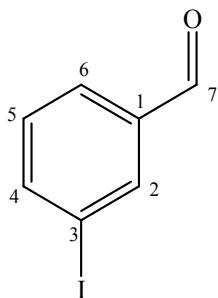
tert*-Butyl 3-(phenylamino)propanoate **145*



The procedure described for the synthesis of methyl 3-(2'-formylphenyl)acrylate **141a** (Method 1) was followed, using tetrabutyl-ammonium bromide (0.14 g, 0.42 mmol), aniline (0.34 mL, 3.8 mmol), Pd(OAc)₂ (16 mg, 0.07 mmol), P(*o*-tolyl)₃ (0.07 g, 0.24 mmol), *tert*-butylacrylate (1.1 mL, 7.5 mmol) and 3-iodobenzaldehyde (**144a**) (0.35 g, 1.5 mmol) in dry CH₃CN. Work-up and purification by column chromatography [on silica gel; elution with hexane:EtOAc (3:1)] afforded *tert-butyl 3-(phenylamino)propanoate* **145** as a yellow oil (0.16 mL, 10%); ¹H NMR (400 MHz, CDCl₃) 1.46 (9H, s, 3 × CH₃), 2.53 and 3.40 (2H, t, *J* = 6.37 Hz, 2 × CH₂), 6.62-7.18 (5H, m, 2'-H × 2, 3'-H × 2, 4'-H, Ar-H); ¹³C NMR (100 MHz, CDCl₃) 28.1 (3 × CH₃), 35.1 [C(CH₃)], 39.6 (2-C), 80.8 (3-C), 133.0 (2'-C × 2), 117.6 (4'-C), 129.2 (3'-C × 2), 147.8 (1'-C), 171.7 (1-C=O).

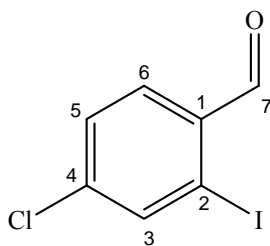
Iodination of benzaldehyde derivatives

3-Iodobenzaldehyde **144a**



The procedure described for the synthesis of 6-iodocoumarin **133** was followed, using finely powdered I_2 (11.2 g, 176 mmol), $NaIO_3$ (4.4 g, 88 mmol) and benzaldehyde (1.1 g, 10 mmol). Work-up afforded pure 3-iodobenzaldehyde **144a** as a beige solid (1.5 g, 63%); m.p. 52-54 °C (lit.³⁹⁵ 55-56 °C); ν_{max} (cm^{-1}) 1677.09 (C=O); 1H NMR (600 MHz, $CDCl_3$) 7.25(1H, m, 4-H, Ar-H), 7.81 (1H, d, J = 7.65 Hz, 5-H, Ar-H), 7.92 (1H, d, J = 7.84 Hz, 6-H, Ar-H), 8.18 (1H, s, 2-H, Ar-H), 9.89 (1H, s, CHO); ^{13}C NMR (150 MHz, $CDCl_3$) 94.6 (2-C), 128.9 (5-C), 130.7 (6-C), 138.0 (1-C), 138.4 (3-C), 143.1 (4-C), 190.6 (CHO).

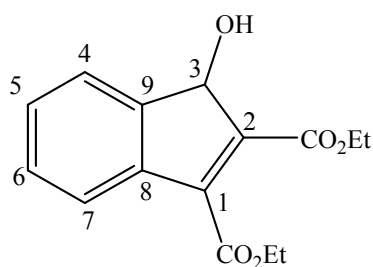
4-Chloro-2-iodobenzaldehyde **144b**



The procedure described for the synthesis of 6-iodocoumarin **133** was followed, using finely powdered I_2 (0.28 g, 4.4 mmol), $NaIO_3$ (0.11 g, 2.2 mmol), concentrated sulfuric acid (7.5 mL) and *p*-chlorobenzaldehyde (0.35 g, 2.5 mmol). Work-up afforded 4-chloro-2-iodobenzaldehyde **144b** as a lilac solid (0.54 g, 81%); m.p. 74-76 °C; ν_{max} (cm^{-1}) 1685.39 (C=O); 1H NMR (600 MHz, $CDCl_3$) 7.59 (1H, d, J = 8.17 Hz, 6-H, Ar-H), 7.78 (1H, dd, J = 1.50 Hz and J = 6.64 Hz, 5-H, Ar-H), 8.33 (1H, d, J = 7.15 Hz, 3-H, Ar-H), 9.90 (1H, s, CHO); ^{13}C NMR (150 MHz, $CDCl_3$) 98.8 (2-C), 129.5 (5-C), 130.0 (6-C), 135.7 (3-C), 141.4 (4-C), 145.1 (1-C), 189.4 (CHO).

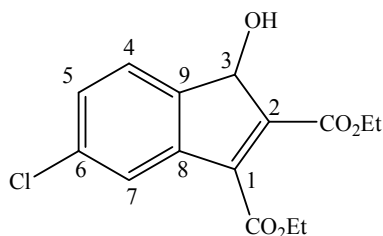
6.2.8. Preparation of indenol derivatives

Diethyl 3-hydroxy-3*H*-indene-1,2-dicarboxylate **147a**



3-Iodobenzaldehyde (**144a**) (0.5 g, 2.15 mmol) was reacted at 60 °C in an oil bath with diethylacetylenedicarboxylate (0.47 mL, 3.2 mmol) in the presence of Pd(OAc)₂ (0.05 g, 10 mol%), potassium acetate KOAc (0.42 g, 4.3 mmol) and dry EtOH (1.3 mL) under argon atmosphere in dry DMF (8 mL). The reaction mixture was allowed to cool down and the resulting dark solution was filtered through a thin pad of Celite®. The filtrate was diluted with water and extracted with EtOAc (3×10 mL). The organic layers were combined, dried over MgSO₄ (anhydrous) and concentrated under vacuum. Work-up and purification by preparative thin layer chromatography [on silica gel and elution with hexane:EtOAc (6:1)] afforded *diethyl 3-hydroxy-3H-indene-1,2-dicarboxylate* **147a** as a yellow oil (0.18 g, 30%); ¹H NMR (600 MHz, CDCl₃) 1.23 (6H, t, *J* = 7.02 Hz, 2 × CH₃), 3.57 (4H, m, 2 × OCH₂), 5.43 (1H, s, 3-H), 7.09–7.83 (4H, m, 5-H, 4-H, 7-H, 6-H, Ar-H); ¹³C NMR (150 MHz, CDCl₃) 14.2 (CH₃), 61.1 (OCH₂), 94.9 (3-C), 100.3 (1-C, 2-C), 125.9 (4-C), 129.9 (5-C), 137.3 (6-C), 138.5 (7-C), 138.9 (8-C, 9-C), 142.4 (2 × C=O).

Diethyl 6-chloro-3-hydroxy-3*H*-indene-1,2-dicarboxylate **147b**

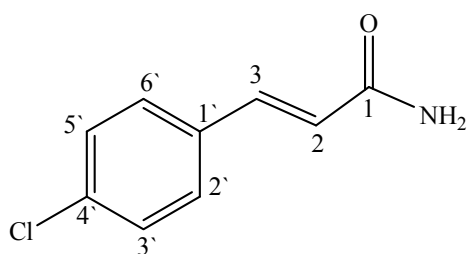


The procedure described for the synthesis of diethyl 3-hydroxy-3*H*-indene-1,2-dicarboxylate **147a** was followed, using 4-chloro-2-iodobenzaldehyde (**144b**) (0.57 g, 2.2 mmol), diethylacetylenedicarboxylate (0.47 mL, 3.2 mmol), Pd(OAc)₂ (0.05 g, 10 mol%) and KOAc (0.42 g, 4.3 mmol) in dry EtOH-DMF. Work-up and purification by preparative thin layer chromatography [on silica gel and elution with hexane:EtOAc (6:1)] afforded *diethyl 6-chloro-3-hydroxy-3H-indene-1,2-dicarboxylate* **147b** as a yellow oil (0.35 g, 53%); ν_{\max}

(cm^{-1}) 2974.53 (OH), 1722.40 (C=O); ^1H NMR (600 MHz, CDCl_3) 1.23 (6H, t, $J = 7.10$ Hz, $2 \times \text{CH}_3$), 3.54 (4H, m, $2 \times \text{OCH}_2$), 5.42 (1H, s, 3-H), 7.41-7.96 (3H, m, 5-H, 4-H, 7-H, Ar-H); ^{13}C NMR (150 MHz, CDCl_3) 15.1 (CH_3), 61.0 (OCH_2), 97.8 (3-C), 99.7 (1-C, 2-C), 127.8 (5-C), 128.9 (4-C), 138.2 (6-C), 138.5 (7-C), 139.3 (8-C, 9-C), 141.2 ($2 \times \text{C}=\text{O}$).

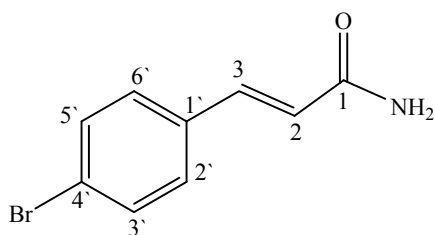
6.2.9. Preparation of acrylamide derivatives

3-(4'-Chlorophenyl)acrylamide **166b**



The dissolution of acetamide (0.10 g, 1.7 mmol) in MeOH (10 mL) was followed by the addition of *p*-chlorobenzaldehyde (0.15 g, 1.1 mmol). The mixture was heated at 85 °C and a hot aqueous solution of NaOH (7 mL, 2 M) was added. After an hour, the solution was allowed to cool down and the yellow precipitate obtained was filtered off and recrystallized in MeOH to afford pure *3-(4'-chlorophenyl)acrylamide* **166b** as yellow crystals (0.14 g, 71%); m.p. 206-208 °C (lit.³⁹⁶ 209-210 °C); ν_{max} (cm^{-1}) 3051.42 (NH_2), 1646.77 (C=O); ^1H NMR (600 MHz, CDCl_3) 7.02 (1H, d, $J = 15.91$ Hz, 2-H), 7.39 (2H, d, $J = 8.43$ Hz, 3'-H, 5'-H, Ar-H), 7.54 (2H, d, $J = 8.42$ Hz, 2'-H, 6'-H, Ar-H), 7.68 (1H, d, $J = 15.91$ Hz, 3-H, Ar-H); ^{13}C NMR (150 MHz, CDCl_3) 125.7 (2-C), 129.3 (2'-C, 6'-C), 129.5 (3'-C, 5'-C), 133.2 (4'-C), 136.5 (1'-C), 142.1 (3-C), 188.2 (1-C=O).

3-(4'-Bromophenyl)acrylamide **166c**

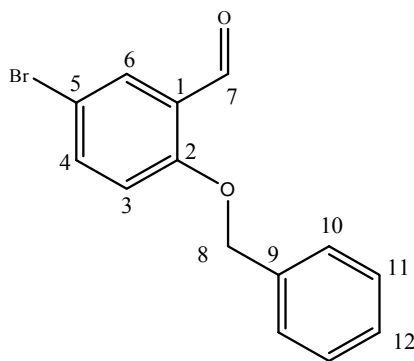


The procedure described for the synthesis of 3-(4'-chlorophenyl)acrylamide **166b** was followed, using acetamide (0.10 g, 1.7 mmol) and *p*-chlorobenzaldehyde (0.27 g, 1.9 mmol) in MeOH. Work-up afforded *3-(4'-bromophenyl)acrylamide* **166c** as yellow crystals (0.23 g, 96%), m.p. 184-186 °C; ν_{max} (cm^{-1}) 3050.93 (NH_2),

1647.01 (C=O); ^1H NMR (600 MHz, CDCl_3) 7.04 (1H, d, $J = 15.91$ Hz, 2-H), 7.47 (1H, d, $J = 15.92$ Hz, 3-H), 7.55 (2H, d, $J = 8.37$ Hz, 3'-H, 5'-H, Ar-H), 7.66 (2H, d, $J = 8.41$ Hz, 2'-H, 6'-H, Ar-H); ^{13}C NMR (150 MHz, CDCl_3) 125.8 (2-C), 129.3 (2'-C, 6'-C), 129.6 (3'-C, 5'-C), 133.3 (4'-C), 136.6 (1'-C), 142.1 (3-C), 188.4 (1-C=O).

6.2.10. Preparation of benzyl ether derivatives

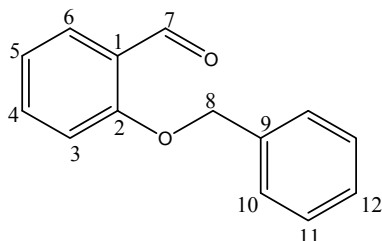
2-(Benzyloxy)-5-bromobenzaldehyde **123d**



Benzylbromide (0.59 mL, 5.0 mmol) and aqueous NaOH (10 mL, 0.1 M) were added to 5-bromosalicylaldehyde (1.0 g, 4.9 mmol) and the mixture was heated under reflux at 80 °C for an hour. The reaction mixture was allowed to cool down and the precipitate formed was filtered off and recrystallized in hexane to afford 2-(benzyloxy)-5-

bromobenzaldehyde **123d** as a yellow solid (1.3 g, 91%); m.p. 74-76 °C (lit.³⁹⁷ 73-74 °C); ν_{max} (cm^{-1}) 1677.06 (C=O); ^1H NMR (600 MHz, CDCl_3) 5.18 (2H, s, 8-H), 6.95 (1H, d, $J = 8.86$ Hz, 3-H, Ar-H), 7.36-7.42 (5H, m, 10-H \times 2, 11-H \times 2, 12-H, Ar-H), 7.60 (1H, d, $J = 8.84$ Hz, 4-H), 7.94 (1H, s, 6-H), 10.47 (1H, s, CHO); ^{13}C NMR (150 MHz, CDCl_3) 70.9 (8-C), 113.8 (5-C), 115.1 (3-C), 126.5 (12-C), 127.3 (10-C \times 2), 128.5 (1-C), 128.8 (11-C \times 2), 131.0 (6-C), 135.5 (4-C), 138.2 (9-C), 159.9 (2-C), 188.2 (CHO).

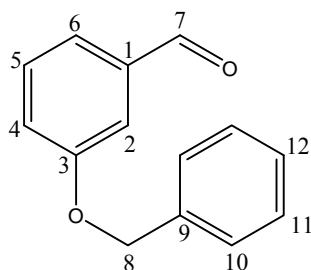
2-(Benzyloxy)benzaldehyde **123f**



The procedure described for the synthesis of 2-(benzyloxy)-5-bromobenzaldehyde **123d** was followed, using benzylbromide (0.59 mL, 5.0 mmol), aqueous NaOH (10 mL, 0.1 M) and 2-hydroxybenzaldehyde (0.61 g, 4.9 mmol). Work-up and purification by preparative thin layer chromatography [on silica gel and elution with hexane:EtOAc

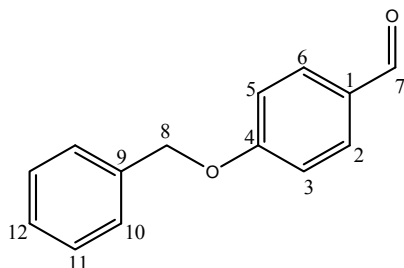
(3:1)] afforded 2-(benzyloxy)benzaldehyde **123f** as a yellow oil (0.91 g, 86%); ν_{\max} (cm^{-1}) 1683.25 (C=O); ^1H NMR (600 MHz, CDCl_3) 5.20 (2H, s, 8-H), 7.05 (2H, m, 3-H, 5-H, Ar-H), 7.36-7.44 (5H, m, 10-H \times 2, 11-H \times 2, 12-H, Ar-H), 7.54 (1H, t, J = 6.97 Hz, 4-H, Ar-H), 7.86 (1H, d, J = 7.77 Hz, 6-H, Ar-H), 10.56 (1H, s, CHO); ^{13}C NMR (150 MHz, CDCl_3) 70.4 (8-C), 113.0 (4-C, 5-C), 121.0 (3-C, 6-C), 127.3 (10-C \times 2), 128.3 (12-C), 128.4 (1-C), 128.7 (11-C \times 2), 135.9 (9-C), 161.0 (2-C), 189.8 (CHO).

3-(Benzyloxy)benzaldehyde **123g**



The procedure described for the synthesis of 2-(benzyloxy)-5-bromobenzaldehyde **123d** was followed, using benzylbromide (0.59 mL, 5.0 mmol), aqueous NaOH (10 mL, 0.1 M) and 3-hydroxybenzaldehyde (0.61 g, 4.9 mmol). Work-up and purification by preparative thin layer chromatography [on silica gel and elution with CHCl_3 :MeOH (200: 1)] afforded 3-(benzyloxy)benzaldehyde **123g** as a yellow oil (0.98 g, 93%); m.p. 58-60 $^{\circ}\text{C}$ (lit.³⁹⁸ 57-58 $^{\circ}\text{C}$); ν_{\max} (cm^{-1}) 1693.73 (C=O); ^1H NMR (600 MHz, CDCl_3) 5.15 (2H, s, 8-H), 7.43-7.52 (9H, m, 2-H, 4-H, 5-H, 6-H, 10-H \times 2, 11-H \times 2, 12-H, Ar-H), 10.00 (1H, s, CHO); ^{13}C NMR (150 MHz, CDCl_3) 70.0 (8-C), 113.1 (5-C), 122.0 (3-C), 123.6 (12-C), 127.4 (10-C \times 2), 128.0 (1-C), 128.5 (11-C \times 2), 130.0 (6-C), 136.1 (4-C), 137.6 (9-C), 159.1 (2-C), 191.9 (CHO).

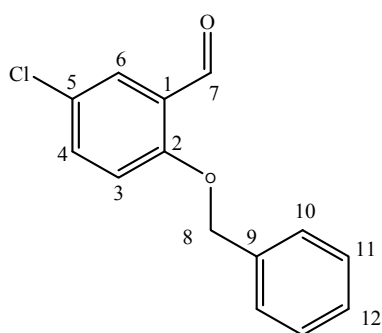
4-(Benzyloxy)benzaldehyde **123h**



The procedure described for the synthesis of 2-(benzyloxy)-5-bromobenzaldehyde **123d** was followed, using benzylbromide (0.59 mL, 5.0 mmol), aqueous NaOH (10 mL, 0.1 M) and 4-hydroxybenzaldehyde (0.60 g, 4.9 mmol). Work-up afforded 4-(benzyloxy)benzaldehyde **123h** as a lilac solid (0.98 g, 93%); m.p. 70-72 $^{\circ}\text{C}$ (lit.³⁹⁹ 71-72 $^{\circ}\text{C}$); ν_{\max} (cm^{-1}) 1685.91 (C=O); ^1H

NMR (600 MHz, CDCl₃) 5.15 (2H, s, 8-H), 7.08 (2H, d, J = 8.60 Hz, 3-H, 5-H, Ar-H), 7.35-7.43 (5H, m, 10-H \times 2, 11-H \times 2, 12-H, Ar-H), 7.84 (2H, d, J = 8.62 Hz, 2-H, 6-H), 9.89 (1H, s, CHO); ¹³C NMR (150 MHz, CDCl₃) 70.2 (8-C), 115.1 (3-C, 5-C), 127.4 (10-C), 128.3 (12-C), 128.7 (11-C), 130.1 (1-C), 131.9 (2-C, 6-C), 135.9 (9-C), 163.7 (4-C), 190.7 (CHO).

2-(Benzyloxy)-5-chlorobenzaldehyde **123i**

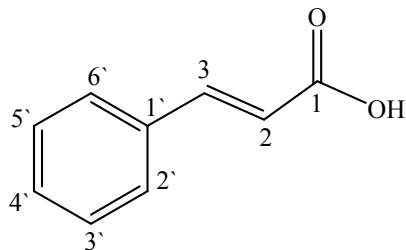


The procedure described for the synthesis of 2-(benzyloxy)-5-bromobenzaldehyde **123d** was followed, using benzylbromide (0.59 mL, 5.0 mmol), aqueous NaOH (10 mL, 0.1 M) and 5-chlorosalicylaldehyde (0.78 g, 4.9 mmol). Work-up afforded 2-(benzyloxy)-5-chlorobenzaldehyde **123i** as a lilac solid (1.2 g, 95%); m.p. 78-80 °C (lit.⁴⁰⁰ 78-79 °C); ν_{\max} (cm⁻¹) 1678.56

(C=O); ¹H NMR (600 MHz, CDCl₃) 5.18 (2H, s, 8-H), 7.00 (1H, d, J = 8.87 Hz, 3-H), 7.36-7.41 (5H, m, 10-H \times 2, 11-H \times 2, 12-H, Ar-H), 7.46 (1H, dd, J = 2.66 Hz and J = 6.20 Hz, 4-H, Ar-H), 7.80 (1H, d, J = 7.98 Hz, 6-H, Ar-H), 10.47 (1H, s, CHO); ¹³C NMR (150 MHz, CDCl₃) 70.9 (8-C), 114.7 (5-C), 126.1 (3-C), 126.7 (12-C), 127.3 (10-C \times 2), 128.0 (1-C), 128.4 (11-C \times 2), 128.7 (6-C), 135.3 (4-C), 135.5 (9-C), 159.4 (2-C), 188.3 (CHO).

6.2.11. Preparation of cinnamic acid derivatives

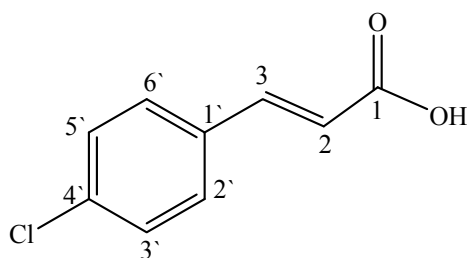
Cinnamic acid **169a**



A mixture of benzaldehyde (1.0 mL, 10 mmol), malonic acid (1.6 g, 15 mmol) and pyridine (20 mL) was heated at 100 °C. After an hour, additional malonic acid (5.0 mmol, 0.52 g) was added to the reaction mixture and heating was continued for a

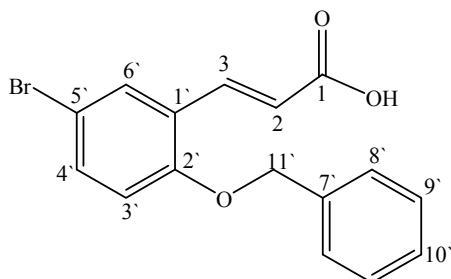
further 30 minutes. After the removal of the solvent *in vacuo*, the crude product mixture was purified by preparative thin layer chromatography [silica gel; elution with hexane:EtOAc:Et₂O (120:20:1)] to afford *cinnamic acid* **169a** as a white solid (0.72 g, 49%); m.p. 134-136 °C (lit.⁴⁰¹ 132-133 °C); ν_{\max} (cm⁻¹) 2830.71 (OH), 1669.24 (C=O); ¹H NMR (600 MHz, CDCl₃) 6.46 (1H, d, *J* = 15.96 Hz, 2-H), 7.41 (3H, m, 3'-H, 4'-H, 5'-H, Ar-H), 7.56 (2H, m, 2'-H, 6'-H, Ar-H), 7.80 (1H, d, *J* = 15.97 Hz, 3-H); ¹³C NMR (150 MHz, CDCl₃) 117.4 (2-C), 128.3 (2'-C, 6'-C), 128.9 (3'-C, 5'-C), 130.7 (1'-C), 134.0 (4'-C), 147.0 (3-C), 172.5 (1-C=O).

3-(4'-Chlorophenyl)acrylic acid **169b**



The procedure described for the synthesis of cinnamic acid **169a** was followed, using malonic acid (0.34 g, 3.4 mmol) and *p*-chlorobenzaldehyde (0.20 mL, 1.7 mmol) in pyridine (10 mL). Work-up and purification by preparative thin layer chromatography [on silica gel; elution with CHCl₃:MeOH (200:1)] afforded 3-(4'-chlorophenyl)acrylic acid **169b** as a white solid (0.16 g, 53%); m.p. 246-248 °C (lit.⁴⁰² 244-248 °C); ¹H NMR (600 MHz, MeOD) 6.46 (1H, d, *J* = 15.99 Hz, 2-H), 7.38 (2H, d, *J* = 8.34 Hz, 2'-H, 6'-H, Ar-H), 7.57 (2H, d, *J* = 8.32 Hz, 3'-H, 5'-H, Ar-H), 7.61 (1H, d, *J* = 16.02 Hz, 3-H); ¹³C NMR (150 MHz, MeOD) 120.3 (2-C), 130.2 (2'-C, 6'-C), 130.7 (3'-C, 5'-C), 134.7 (1'-C), 137.2 (4'-C), 144.7 (3-C), 170.1 (1-C=O).

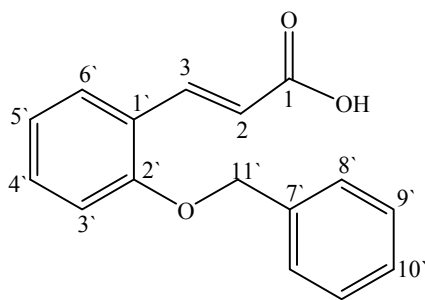
3-[2'-(Benzyloxy)-5'-bromophenyl]acrylic acid **169c**



The procedure described for the synthesis of cinnamic acid **169a** was followed, using malonic acid (0.07 g, 0.63 mmol) and 2-(benzyloxy)-5-bromobenzaldehyde (**123d**) (0.36 g, 1.3 mmol) in pyridine (10 mL). Work-up and purification by preparative thin layer chromatography [on silica gel and elution with CHCl₃:MeOH

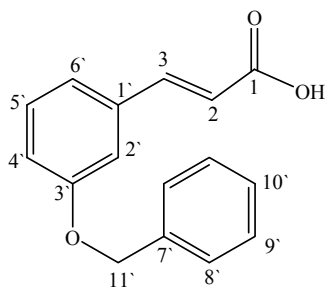
(200:1)] afforded 3-[2'-(benzyloxy)-5'-bromophenyl]acrylic acid **169c** as a white solid (0.34 g, 83%); m.p. 138-140 °C; ν_{\max} (cm^{-1}) 2878.41 (OH), 1691.43 (C=O); ^1H NMR (600 MHz, CDCl_3) 5.16 (2H, s, 11'-H), 6.52 (1H, d, J = 16.11 Hz, 2-H), 6.83 (1H, d, J = 8.82 Hz, 3'-H, Ar-H), 7.35 -7.40 (5H, m, 8'-H \times 2, 9'-H \times 2, 10'-H, Ar-H), 7.66 (1H, s, 6'-H, Ar-H), 8.06 (1H, d, J = 16.11 Hz, 3-H); ^{13}C NMR (150 MHz, CDCl_3) 70.7 (11'-C), 113.4 (5'-C), 114.6 (2-C), 119.1 (3'-C), 125.5 (10'-C), 127.2 (8'-C \times 2), 128.2 (1'-C), 128.8 (9'-C \times 2), 131.4 (6'-C), 134.2 (4'-C), 136.0 (7'-C), 140.6 (3-C), 156.4 (2'-C), 171.8 (1-C=O).

3-[2'-(Benzyloxy)phenyl]acrylic acid **169d**



The procedure described for the synthesis of cinnamic acid **169a** was followed, using malonic acid (0.09 g, 0.83 mmol) and 2-(benzyloxy)benzaldehyde (**123f**) (0.35 g, 1.7 mmol) in pyridine (10 mL). Work-up and purification by preparative thin layer chromatography [on silica gel and elution with CHCl_3 :MeOH (200:1)] afforded 3-[2'-(benzyloxy)phenyl]acrylic acid **169d** as white crystals (0.14 g, 33%); m.p. 132-134 °C (lit.⁴⁰³ 135-145 °C); ν_{\max} (cm^{-1}) 3404.66 (OH), 1678.36 (C=O); ^1H NMR (600 MHz, CDCl_3) 5.18 (2H, s, 11'-H), 6.56 (1H, d, J = 16.11 Hz, 2-H), 6.97-7.57 (9H, m, 3'-H, 4'-H, 5'-H, 6'-H, 8'-H \times 2, 9'-H \times 2, 10'-H, Ar-H), 8.18 (1H, d, J = 16.11 Hz, 3-H); ^{13}C NMR (150 MHz, CDCl_3) 70.5 (11'-C), 112.9 (2-C), 118.0 (1'-C), 121.1 (3'-C), 123.6 (5'-C), 127.2 (8'-C \times 2), 128.1 (10'-C), 128.7 (9'-C \times 2), 129.2 (6'-C), 131.9 (4'-C), 136.5 (7'-C), 142.3 (3-C), 157.6 (2'-C), 172.6 (1-C=O).

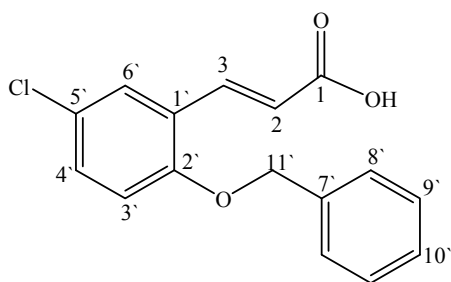
3-[3'-(Benzyloxy)phenyl]acrylic acid **169e**



The procedure described for the synthesis of cinnamic acid **169a** was followed, using malonic acid (0.09 g, 0.83 mmol) and 3-(benzyloxy)benzaldehyde (**123g**) (0.35 g, 1.7 mmol) in

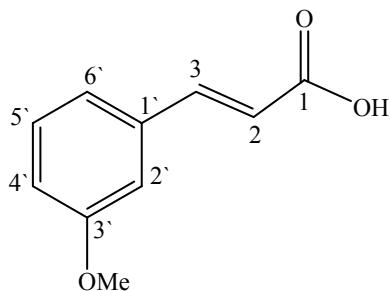
pyridine (10 mL). Work-up and purification by preparative thin layer chromatography [on silica gel; elution with hexane:EtOAc (2:1)] afforded 3-[3'-(benzyloxy)phenyl]acrylic acid **169e** as white crystals (0.13 g, 31%); m.p. 150-152 °C (lit.⁴⁰³ 153-154 °C); ν_{\max} (cm⁻¹) 2924.48 (OH), 1690.55 (C=O); ¹H NMR (600 MHz, CDCl₃) 5.10 (2H, s, 11'-H), 6.42 (1H, d, J = 15.93 Hz, 2-H), 7.03-7.45 (9H, m, 3'-H, 4'-H, 5'-H, 6'-H, 8'-H \times 2, 9'-H \times 2, 10'-H, Ar-H), 7.74 (1H, d, J = 15.94 Hz, 3-H); ¹³C NMR (150 MHz, CDCl₃) 70.1 (11'-C), 114.2 (2'-C), 117.5 (4'-C, 5'-C), 121.3 (2-C), 127.5 (8'-C \times 2), 128.1 (10'-C), 128.7 (9'-C \times 2), 130.0 (6'-C), 135.4 (1'-C), 136.6 (7'-C), 146.9 (3-C), 159.1 (3'-C), 171.3 (1-C=O).

3-[2'-(Benzyloxy)-5'-chlorophenyl]acrylic acid **169f**



The procedure described for the synthesis of cinnamic acid **169a** was followed, using malonic acid (0.04 g, 0.42 mmol) and 2-(benzyloxy)-5-chlorobenzaldehyde (**123i**) (0.21 g, 0.83 mmol) in pyridine (10 mL). Work-up and purification by preparative thin layer chromatography [on silica gel and elution with CHCl₃:MeOH (200:1)] afforded 3-[2'-(benzyloxy)-5'-chlorophenyl]acrylic acid **169f** as a yellow oil (0.13 g; 53%); ν_{\max} (cm⁻¹) 3355.44 (OH), 1686.47 (C=O); ¹H NMR (600 MHz, CDCl₃) 4.85 (2H, s, 11'-H), 6.40 (1H, d, J = 15.18 Hz, 2-H), 6.52 (1H, d, J = 8.57 Hz, 3'-H, Ar-H), 6.92 (1H, d, J = 8.86 Hz, 6'-H, Ar-H), 7.09 (1H, t, J = 6.25 Hz, 4'-H), 7.15-7.20 (5H, m, 8'-H \times 2, 9'-H \times 2, 10'-H, Ar-H), 7.71 (1H, d, J = 15.99 Hz, 3-H); ¹³C NMR (150 MHz, CDCl₃) 70.4 (11'-C), 100.0 (5'-C), 113.7 (2-C), 125.7 (3'-C), 126.3 (10'-C), 126.7 (8'-C \times 2), 127.1 (1'-C), 127.7 (6'-C), 128.0 (4'-C), 128.4 (7'-C), 128.5 (9'-C \times 2), 129.4 (3-C), 136.5 (2'-C), 155.2 (1-C=O).

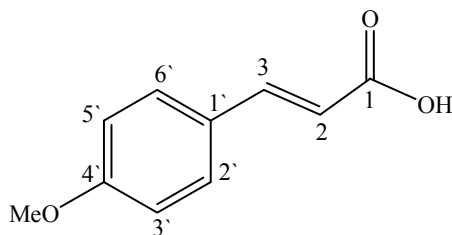
3-(3'-Methoxyphenyl)acrylic acid **169g**



The procedure described for the synthesis of cinnamic acid **169a** was followed, using malonic acid (0.34 g, 3.4 mmol) and *m*-methoxybenzaldehyde (0.20 mL, 1.7 mmol) in pyridine (10 mL). Work-up and purification by preparative thin layer chromatography [on silica gel; elution with CHCl₃:MeOH (200:1)] afforded 3-(3'-methoxyphenyl)acrylic acid **169g** as a yellowish solid

(0.24 g, 82%); m.p. 114-116 °C (lit.⁴⁰⁴ 116-119 °C); ν_{\max} (cm⁻¹) 2959.42 (OH), 1675.04 (C=O); ¹H NMR (600 MHz, CDCl₃) 3.84 (3H, s, OCH₃), 6.45 (1H, d, *J* = 15.94 Hz, 2-H), 6.97 (1H, dd, *J* = 2.51 Hz and *J* = 5.71 Hz, 4'-H, Ar-H), 7.07 (1H, d, *J* = 7.24 Hz, 6'-H, Ar-H), 7.15 (1H, d, *J* = 7.63 Hz, 2'-H, Ar-H), 7.32 (1H, t, *J* = 7.92 Hz, 5'-H, Ar-H), 7.71 (1H, d, *J* = 15.94 Hz, 3-H); ¹³C NMR (150 MHz, CDCl₃) 55.3 (OCH₃), 113.1 (2'-C), 116.7 (4'-C), 117.6 (2-C), 121.1 (6'-C), 129.9 (5'-C), 135.4 (1'-C), 147.0 (3-C), 159.9 (3'-C), 172.4 (1-C=O).

3-(4'-Methoxyphenyl)acrylic acid **169h**

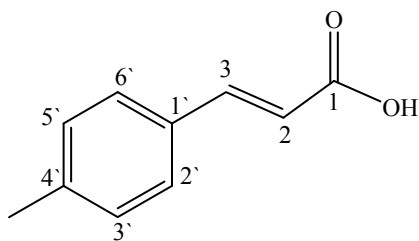


The procedure described for the synthesis of cinnamic acid **169a** was followed, using malonic acid (0.34 g, 3.4 mmol) and *p*-methoxybenzaldehyde (0.21 mL, 1.7 mmol) in pyridine (10 mL). Work-up and purification by

preparative thin layer chromatography [on silica gel and elution with CHCl₃:MeOH (200:1)] afforded 3-(4'-methoxyphenyl)acrylic acid **169h** as a brownish solid (0.25 g, 83%); m.p. 172-174 °C (lit.⁴⁰⁵ 175-180 °C); ν_{\max} (cm⁻¹) 2938.71 (OH), 1674.42 (C=O); ¹H NMR (600 MHz, CDCl₃) 3.85 (3H, s, OCH₃), 6.32 (1H, d, *J* = 15.89 Hz, 2-H), 6.92 (2H, d, *J* = 8.52 Hz, 3'-H, 5'-H, Ar-H), 7.51 (2H, d, *J* = 8.51 Hz, 2'-H, 6'-H, Ar-H), 7.75 (1H, d, *J* = 15.88 Hz, 3-H); ¹³C NMR (150 MHz, CDCl₃) 55.4 (OCH₃), 114.4 (3'-C, 5'-

C), 126.9 (1'-C), 130.1 (2'-C, 6'-C), 132.4 (2-C), 146.8 (3-C), 161.8 (4'-C), 172.5 (1-C=O).

P*-tolylacrylic acid **169i*



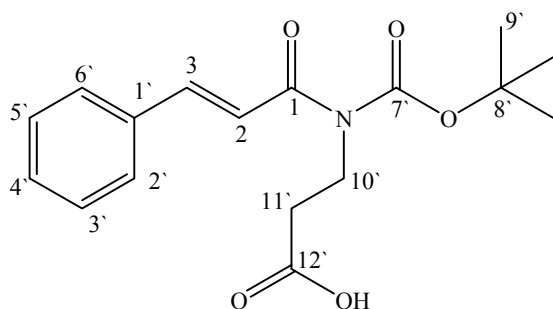
The procedure described for the synthesis of cinnamic acid **169a** was followed, using malonic acid (0.34 g, 3.4 mmol) and *p*-methylbenzaldehyde (1.2 mL, 1.7 mmol) in pyridine (10 mL). Work-up and purification by preparative thin layer chromatography [on silica gel and elution with CHCl₃:MeOH (200:1)] afforded *p*-tolylacrylic acid **169i** as a brownish solid (0.21 g, 75%); m.p. 196-198 °C (lit.⁴⁰¹ 197-198 °C); ν_{\max} (cm⁻¹) 2919.73 (OH), 1670.19 (C=O); ¹H NMR (600 MHz, CDCl₃) 2.38 (3H, s, CH₃), 6.41 (1H, d, *J* = 15.93 Hz, 2-H), 7.21 (2H, d, *J* = 7.82 Hz, 3'-H, 5'-H, Ar-H), 7.45 (2H, d, *J* = 7.84 Hz, 2'-H, 6'-H, Ar-H), 7.77 (1H, d, *J* = 15.93 Hz, 3-H); ¹³C NMR (150 MHz, CDCl₃) 21.5 (CH₃), 116.2 (2-C), 128.4 (2'-C, 6'-C), 129.7 (3'-C, 5'-C), 131.3 (1'-C), 141.3 (4'-C), 147.1 (3-C), 172.5 (1-C=O).

6.2.12. Preparation of protected amino acid cinnamate conjugates

General procedure for the synthesis of compounds **171a, **171b**, **174a** and **174b****

Method 1. A solution of *N*-Boc- β -alanine (0.21 g, 1.1 mmol) in dry DMF (10 mL) was added to a stirred solution of cinnamic acid (0.31 g, 2.1 mmol) and 1,1'-carbonyldiimidazole (CDI, 0.34 g, 2.1 mmol) in dry DMF (2 mL) under argon. The reaction mixture was stirred at room temperature for 48 hours and the reaction was quenched with H₂O (3 mL). The mixture was extracted with EtOAc (3×10 mL) and the combined extracts were washed with 10% citric acid (5 mL). The extracts were dried over anhydrous Na₂SO₄ and the solvent was evaporated *in vacuo*. Purification by preparative thin layer chromatography by eluting with EtOAc afforded conjugate *N*-Boc- β -alanine cinnamide **171a** as a yellow oily residue (0.18 g, 27%) and methyl cinnamate **174a** as a white solid (0.11 g, 32%).

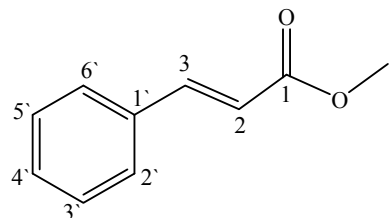
N-Boc- β -alanine cinnamide conjugate **171a**



Compound *N*-Boc- β -alanine cinnamide as a yellow oil (0.18 g, 27%); ν_{\max} (cm^{-1}) 1710.32 and 1637.13 ($2 \times \text{C=O}$); ^1H NMR (600 MHz, CDCl_3) 1.41 (9H, s, 9'-H), 2.50 (2H, t, $J = 8.43$ Hz, 10'-H), 3.37 (2H, q, $J = 8.53$ Hz, 11'-H), 5.05 (1H, s, OH), 6.43 (1H, d, $J = 16.02$ Hz, 2-H), 7.37 (3H, m, 3'-

H, 4'-H, 5'-H, Ar-H), 7.50 (2H, m, 2'-H, 6'-H, Ar-H), 7.68 (1H, d, $J = 16.02$ Hz, 3-H); ^{13}C NMR (150 MHz, CDCl_3) 28.3 (9'-C), 34.3 (11'-C), 36.0 (10'-C), 79.3 (8'-C), 117.7 (2-C), 128.0 (3'-C, 5'-C), 128.8 (2'-C, 6'-C), 130.3 (4'-C), 134.3 (1'-C), 144.8 (3-C), 155.7 (7'-C=O), 167.4 (1-C=O), 172.9 (12'-C=O).

Methyl cinnamate **174a**



Methyl cinnamate **174a** as a white solid (0.11 g, 32%); m.p. 36-38 °C (lit.⁴⁰⁶ 37 °C); ν_{\max} (cm^{-1}) 1713.75 (C=O), ^1H NMR (600 MHz, CDCl_3) 3.80 (3H, s, OCH₃), 6.44 (1H, d, $J = 16.02$ Hz, 2-H), 7.37 (3H, m, 3'-H, 4'-H, 5'-H, Ar-H), 7.52 (2H, m, 2'-H, 6'-H, Ar-H), 7.69 (1H, d, $J = 16.02$ Hz, 3-H); ^{13}C NMR (150

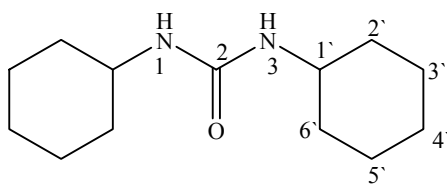
MHz, CDCl_3) 51.7 (OCH₃), 117.8 (2-C), 128.0 (2'-C, 6'-C), 128.9 (3'-C, 5'-C), 130.3 (4'-C), 134.4 (1'-C), 144.8 (3-C), 167.4 (1-C=O).

Method 2. To a 0 °C solution of cinnamic acid (0.09 g, 0.63 mmol) in DCM (5 mL) was added Et₃N (0.09 mL, 0.63 mmol), *N*-hydroxysuccinimide (NHS, 0.07 g, 0.63 mmol) and *N*-Boc- β -alanine (0.12 g, 0.63 mmol) and the mixture was stirred for 10 minutes. *N,N'*-dicyclohexylcarbodiimide (DCC, 0.13 g, 0.63 mmol) was added, stirring was continued at 0 °C for a further 10 minutes and the solution was then left stirring at room temperature

over 18 hours. The mixture was filtered and the precipitate was dried to afford *1,3-dicyclohexylurea* **172** as a white solid in a yield of 80%. The filtrate was evaporated under reduced pressure dissolved in EtOAc (5 mL), washed with aqueous 2M HCl (2.5 mL), aqueous NaHCO₃ (2.5 mL, 0.1 M) and H₂O (2.5 mL). The residue was extracted with EtOAc, dried with MgSO₄ (anhydrous) and evaporated. The crude product was chromatographed on silica gel and eluted with EtOAc to afford conjugate *N-Boc-β-alanine cinnamide* **171a** as a yellow oil in a yield of 9.1%.

Product 1. Compound *N-Boc-β-alanine cinnamide* **171a** as a yellow oil (0.02 g, 9.1%).

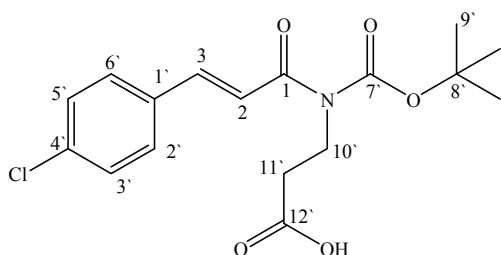
1,3-Dicyclohexylurea **172**



Product 2. Compound *1,3-dicyclohexylurea* **172** as a white solid (0.11 g, 80%); m.p. 236-238 °C (lit.⁴⁰⁷ 235-237.5 °C); ν_{\max} (cm⁻¹) 3244.42 (OH), 1704.62 (C=O); ¹H NMR (600 MHz, CDCl₃) 1.08-1.10 (2H, m, 4'-H), 1.34 (2H, q, J = 12.01 Hz, 3'-H), 1.60 (2H, m, 5'-H), 1.68 (2H, m, 2'-H), 1.93 (2H, m, 6'-H), 3.47 (1H, m, 1'-H), 4.05 (1H, d, J = 7.24 Hz, NH); ¹³C NMR (150 MHz, CDCl₃) 24.9 (4'-C), 25.6 (3'-C), 34.0 (2'-C), 49.2 (1'-C), 156.7 (2-C=O).

The procedure described for the synthesis of *N-Boc-β-alanine cinnamide* conjugate **171a** (method 1) was followed, using *N-Boc-β-alanine* (0.21 g, 1.1 mmol), *p*-chlorocinnamic acid (0.38 g, 2.1 mmol) and 1,1'-carbonyldiimidazole (CDI, 0.34 g, 2.1 mmol) in dry DMF (12 mL). Work-up and purification by preparative thin layer chromatography [on silica gel and elution with EtOAc] afforded *N-Boc-β-alanine-4'-chlorocinnamide* **171b** conjugate as a yellow oil in a yield of 12% and *methyl 3-(4'-chlorophenyl)acrylate* **174b** as colorless needles in a yield of 37%.

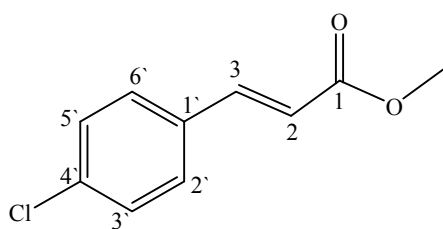
N-Boc-β-alanine-4'-chlorocinnamide **171b**



N-Boc-β-alanine-4'-chlorocinnamide conjugate **171b** (0.09 g, 12%); ν_{\max} (cm⁻¹) 1702.53 and 1633.80 (2 × C=O); ¹H NMR

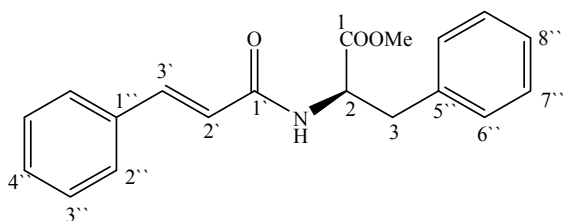
(600 MHz, CDCl₃) 1.42 (9H, s, 9'-H), 2.52 (2H, t, J = 5.89 Hz, 10'-H), 3.39 (2H, q, J = 8.84 Hz, 11'-H), 5.03 (1H, s, OH), 6.42 (1H, d, J = 16.01 Hz, 2-H), 7.35 (2H, d, J = 8.49 Hz, 2'-H, 6'-H, Ar-H), 7.45 (2H, d, J = 8.48 Hz, 3'-H, 5'-H, Ar-H), 7.63 (1H, d, J = 16.01 Hz, 3-H, Ar-H); ¹³C NMR (150 MHz, CDCl₃) 28.4 (9'-C), 34.4 (11'-C), 36.0 (10'-C), 79.4 (8'-C), 118.3 (2-C), 129.2 (3'-C, 5'-C), 129.2 (2'-C, 6'-C), 132.8 (4'-C), 136.2 (1'-C), 143.4 (3-C), 155.8 (7'-C=O), 167.2 (1-C=O), 173.0 (12'-C=O).

Methyl 3-(4'-chlorophenyl)acrylate **174b**



Methyl 3-(4'-chlorophenyl)acrylate **174b** as colorless needles (0.15 g, 37%); m.p. 72-74 °C (lit.³⁹⁶ 76-76.5 °C); ν_{\max} (cm⁻¹) 1702.58 (C=O); ¹H NMR (600 MHz, CDCl₃) 3.80 (3H, s, OCH₃), 6.40 (1H, d, J = 16.01 Hz, 2-H), 7.35 (2H, d, J = 8.44 Hz, 3'-H, 5'-H, Ar-H), 7.45 (2H, d, J = 8.42 Hz, 2'-H, 6'-H, Ar-H), 7.63 (1H, d, J = 16.02 Hz, 3-H); ¹³C NMR (150 MHz, CDCl₃) 51.7 (OCH₃), 118.4 (2-C), 129.2 (2'-C, 6'-C), 129.2 (3'-C, 5'-C), 132.9 (4'-C), 136.2 (1'-C), 143.4 (3-C), 167.1 (1-C=O).

Methyl 2'-(phenylacrylamido)-3-phenylpropanoate **175a**

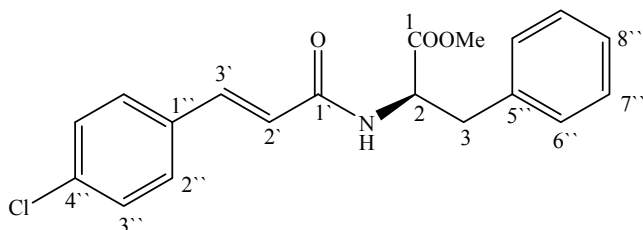


The procedure described for the synthesis of cinnamide *N*-Boc- β -alanine conjugate **171a** (method 1) was followed, using methyl 2-amino-3-phenylpropanoate (0.10 g, 0.55 mmol), *p*-chlorocinnamic acid

(0.19 g, 1.1 mmol) and 1,1'-carbonyldiimidazole (CDI, 0.17 g, 1.1 mmol) in dry DMF (12 mL). Work-up and purification by preparative thin layer chromatography [on silica gel and elution with hexane:EtOAc (6:1)] afforded *methyl 2'-(cinnamamido)-3-phenylpropanoate* **175a** as a yellow solid (0.22 g, 69%); m.p. 94-96 °C; (HRMS: m/z calculated for C₁₉H₁₉NO₃ (MH⁺) 310.1443. Found 310.1450]; ν_{\max} (cm⁻¹) 3271.21 (NH), 1739.65 and 1619.51 (2 \times C=O); ¹H NMR (600 MHz, CDCl₃) 3.25 (2H, m, 3-H), 3.77

(3H, s, OCH₃), 5.07 (1H, q, J = 7.69 Hz, 2-H), 6.30 (1H, s, NH), 6.44 (1H, d, J = 15.63 Hz, 2'-H), 7.14-7.31 (5H, m, 6''-H \times 2, 7''-H \times 2, 8''-H, Ar-H), 7.36-7.51 (5H, 2''-H \times 2, 3''-H \times 2, 4''-H, Ar-H), 7.65 (1H, d, J = 15.63 Hz, 3'-H); ¹³C NMR (150 MHz, CDCl₃) 37.9 (3-C), 52.4 (OCH₃), 53.4 (2-C), 120.0 (2'-C), 127.2 (8''-C), 127.9 (2''-C \times 2), 128.6 (6''-C \times 2), 128.8 (3''-C \times 2), 129.4 (7''-C \times 2), 129.9 (4''-C), 134.7 (1''-C), 135.9 (5''-C), 141.8 (3'-C), 165.4 (1'-C=O), 172.8 (1-C=O).

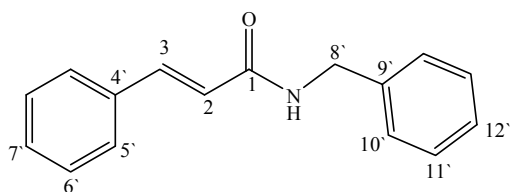
Methyl 2'-[3'-(4''-chlorophenyl)acrylamido]-3-phenylpropanoate **175b**



The procedure described for the synthesis of cinnamide *N*-Boc- β -alanine conjugate **171a** (method 1) was followed, using methyl 2-amino-3-phenylpropanoate (0.10 g,

0.55 mmol), cinnamic acid (0.15 g, 1.1 mmol) and 1,1'-carbonyldiimidazole (CDI, 0.17 g, 1.1 mmol) in dry DMF (12 mL). Work-up and purification by preparative thin layer chromatography [on silica gel and elution with hexane:EtOAc (6:1)] afforded *methyl 2'-[3'-(4''-chlorophenyl)acrylamido]-3-phenylpropanoate 175b* as a white solid (0.23 g, 64%); m.p. 122-124 °C; ν_{max} (cm⁻¹) 3315.12 (NH), 1736.88 and 1616.62 (2 \times C=O); ¹H NMR (600 MHz, CDCl₃) 3.18 (2H, m, 3-H), 3.74 (3H, s, OCH₃), 5.02 (1H, q, J = 7.65 Hz, 2-H), 6.34 (1H, s, NH), 6.37 (1H, d, J = 15.61 Hz, 2'-H), 7.11 (2H, 3''-H \times 2, Ar-H), 7.23-7.31 (5H, 6''-H \times 2, 7''-H \times 2, 8''-H, Ar-H), 7.37 (2H, 2''-H \times 2, Ar-H), 7.55 (1H, d, J = 15.61 Hz, 3'-H); ¹³C NMR (150 MHz, CDCl₃) 37.8 (3-C), 52.3 (OCH₃), 53.3 (2-C), 120.5 (2'-C), 127.1 (8''-C), 128.5 (7''-C \times 2), 128.9 (2''-C \times 2), 129.0 (6''-C \times 2), 129.2 (3''-C \times 2), 133.1 (4''-C), 135.6 (1''-C), 135.8 (5''-C), 140.3 (3'-C), 165.0 (1'-C=O), 172.1 (1-C=O).

N-Benzylcinnamide **176**

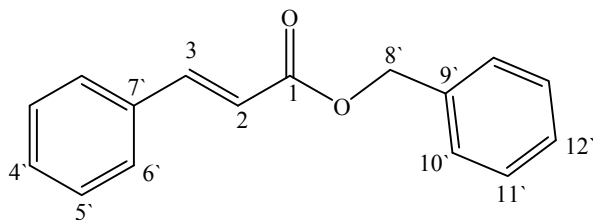


The procedure described for the synthesis of cinnamide *N*-Boc- β -alanine conjugate **171a** (method 1) was followed, using benzylamine

(0.12 mL, 1.1 mmol), *p*-chlorocinnamic acid (0.38 g, 2.1 mmol) and 1, 1'-carbonyldiimidazole (CDI, 0.34 g, 2.1 mmol) in dry DMF (12 mL). Work-up and purification by preparative thin layer chromatography [on silica gel and elution with hexane:EtOAc (2:1)] afforded *N*-benzylcinnamide **176** as a beige solid (0.24 g, 47%); m.p. 98-100 °C (lit.⁴⁰⁸ 98 °C), ν_{\max} (cm⁻¹) 2977.91 (NH), 1693.96 (C=O); ¹H NMR (600 MHz, CDCl₃) 4.57 (2H, d, *J* = 5.74 Hz, 8'-H), 5.99 (1H, s, NH), 6.42 (1H, d, *J* = 15.60 Hz, 2-H), 7.28-7.49 (10H, m, 5'-H × 2, 6'-H × 2, 7'-H, 10'-H × 2, 11'-H × 2, 12'-H, Ar-H), 7.67 (1H, d, *J* = 15.60 Hz, 3-H); ¹³C NMR (150 MHz, CDCl₃) 43.9 (8'-C), 120.5 (2-C), 127.6 (12'-C), 127.8 (5'-C × 2), 128.0 (10'-C × 2), 128.7 (6'-C × 2), 128.8 (11'-C × 2), 129.7 (7'-C), 134.8 (4'-C), 138.2 (9'-C), 141.5 (3-C), 165.8 (1-C=O).

6.2.13. Preparation of cinnamate ester derivatives

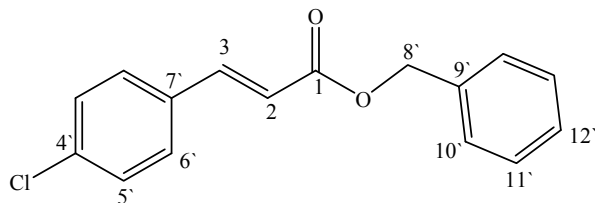
Benzyl cinnamate **170a**



The procedure described for the synthesis of 2-(benzyloxy)-5-bromobenzaldehyde **123d** was followed, using benzylbromide (0.29 mL, 2.5 mmol), aqueous NaOH (10 mL, 0.1 M) and cinnamic acid (0.37 g,

2.5 mmol). Work-up and purification by preparative thin layer chromatography [on silica gel; elution with hexane:EtOAc (2:1)] gave *benzyl cinnamate* **170a** as a yellow solid (0.45 g, 75%); m.p. 34-36 °C (lit.⁴⁰⁹ 33-34 °C); ν_{\max} (cm⁻¹) 1710.13 (C=O); ¹H NMR (600 MHz, CDCl₃) 5.25 (2H, s, 8'-H), 6.49 (1H, d, *J* = 16.00 Hz, 2-H), 7.38-7.53 (10H, m, 6'-H × 2, 5'-H × 2, 4'-H, 10'-H × 2, 11'-H × 2, 12'-H, Ar-H), 7.73 (1H, d, *J* = 16.01 Hz, 3-H); ¹³C NMR (150 MHz, CDCl₃) 66.4 (8'-C), 117.8 (2-C), 128.1 (6'-C × 2), 128.2 (12'-C), 128.3 (10'-C × 2), 128.6 (5'-C × 2), 128.9 (11'-C × 2), 130.3 (4'-C), 134.3 (7'-C), 136.0 (9'-C), 145.2 (3-C), 166.8 (1-C=O).

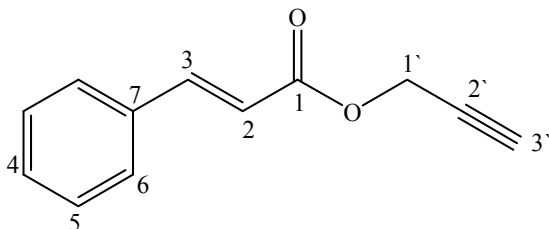
Benzyl 3-(4'-chlorophenyl)acrylate **170b**



Benzyltriethylammonium chloride (0.06 g, 0.3 mmol) was added to a mixture of cinnamic acid (0.37 g, 2.5 mmol), benzylchloride (0.29 mL, 2.5

mmol) and 20 mL of aqueous NaOH (0.5 M). The reaction mixture was heated at 70 °C for 4 hours and *benzyl 3-(4'-chlorophenyl)acrylate* **170b** was recovered by filtration as a yellow solid (0.59 g, 87%); m.p. 68-70 °C (lit.²⁸⁵ 65-68 °C); [HRMS: m/z calculated for $C_{16}H_{13}ClO_2$ (MH^+) 273.0682. Found 273.0675]; ν_{\max} (cm^{-1}) 1688.84 (C=O); 1H NMR (600 MHz, $CDCl_3$) 5.25 (2H, s, 8'-H), 6.45 (1H, d, J = 16.00 Hz, 2-H), 7.35-7.45 (9H, m, 6'-H \times 2, 5'-H \times 2, 10'-H \times 2, 11'-H \times 2, 12'-H, Ar-H), 7.67 (1H, d, J = 16.00 Hz, 3-H); ^{13}C NMR (150 MHz, $CDCl_3$) 66.5 (8'-C), 118.5 (2-C), 128.3 (10'-C \times 2), 128.6 (5'-C \times 2), 129.1 (11'-C \times 2), 129.2 (6'-C \times 2), 132.8 (12'-C), 135.9 (4'-C), 136.3 (9'-C), 143.7 (7'-C, 3-C), 166.5 (1-C=O).

Prop-2'-ynyl cinnamate **177a**

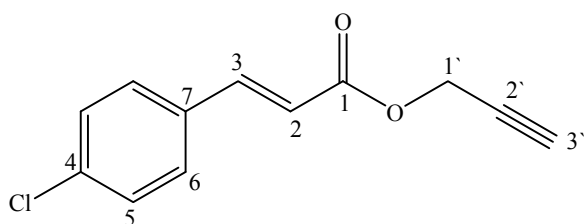


A mixture of cinnamic acid **169a** (0.30 g, 2.1 mmol), thionyl chloride $SOCl_2$ (5.0 mL, 0.07 mmol) and 2 drops of DMF was heated under reflux for 4 hours. The excess of $SOCl_2$ was removed on the rotary

evaporator and the residue was dissolved in 4 mL of dry benzene. To this solution was slowly added 1 mL of pyridine and propargyl alcohol (0.14 mL, 2.4 mmol) and the resulting mixture was stirred overnight at room temperature. After removal of the solvents, the residue was dissolved in DCM (25 mL), the organic extract washed with H_2O (2 \times 20 mL), brine (2 \times 20 mL) and dried over $MgSO_4$ (anhydrous). Purification by preparative thin layer chromatography [on silica gel; elution with hexane:EtOAc (6:1)] afforded *prop-2'-ynyl cinnamate* **177a** as a brown oil (0.25 g, 65%); [HRMS: m/z calculated for $C_{12}H_{10}O_2$ (MH^+) 187.0759. Found 187.0762]; ν_{\max} (cm^{-1}) 1706.92 (C=O);

^1H NMR (600 MHz, CDCl_3) 2.51 (1H, t, $J = 2.04$ Hz, 3'-H), 4.81 (2H, d, $J = 2.18$ Hz, 1'-H), 6.43 (1H, d, $J = 16.01$ Hz, 2-H), 7.36-7.46 (5H, m, 6-H \times 2, 5-H \times 2, 4-H, Ar-H), 7.68 (1H, d, $J = 16.01$ Hz, 3-H); ^{13}C NMR (150 MHz, CDCl_3) 52.0 (1'-C), 74.9 (3'-C), 77.8 (2'-C), 117.0 (2-C), 128.2 (6-C \times 2), 128.9 (5-C \times 2), 130.5 (7-C), 134.1 (4-C), 145.9 (3-C), 165.9 (1-C=O).

Prop-2'-ynyl 3-(4-chlorophenyl)acrylate **177b**

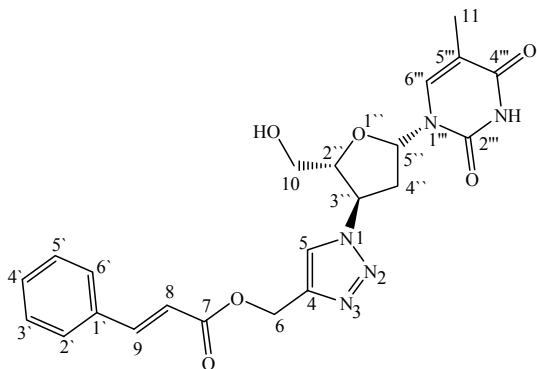


The procedure described for the synthesis of prop-2'-ynyl cinnamate **177a** was followed, using *p*-chlorocinnamic acid **169b** (0.37 g, 2.0 mmol), thionyl chloride SOCl_2 (5.0 mL,

0.07 mmol), pyridine (1.0 mL, 12 mmol) and propargyl alcohol (0.14 mL, 2.4 mmol). Work-up and purification by preparative thin layer chromatography [on silica gel; elution with hexane: EtOAc (6:1)] afforded *prop*-2'-ynyl 3-(4-chlorophenyl)acrylate **177b** as a white solid (0.34 g, 77%); m.p. 56-58 °C (lit.⁴¹⁰ 56-58 °C); [HRMS: m/z calculated for $\text{C}_{12}\text{H}_9\text{ClO}_2$ (MH^+) 221.0369. Found 221.0373]; ν_{max} (cm^{-1}) 1706.26 (C=O); ^1H NMR (600 MHz, CDCl_3) 2.51 (1H, t, $J = 2.42$ Hz, 3'-H), 4.81 (2H, d, $J = 2.43$ Hz, 1'-H), 6.43 (1H, d, $J = 16.01$ Hz, 2-H), 7.36-7.46 (4H, m, 6-H \times 2, 5-H \times 2, Ar-H), 7.68 (1H, d, $J = 16.01$ Hz, 3-H); ^{13}C NMR (150 MHz, CDCl_3) 52.2 (1'-C), 75.0 (3'-C), 77.7 (2'-C), 117.6 (2-C), 129.3 (6-C \times 2), 129.4 (5-C \times 2), 132.6 (7-C), 136.5 (4-C), 144.5 (3-C), 165.8 (1-C=O).

6.2.14. Preparation of cinnamate ester-AZT conjugates

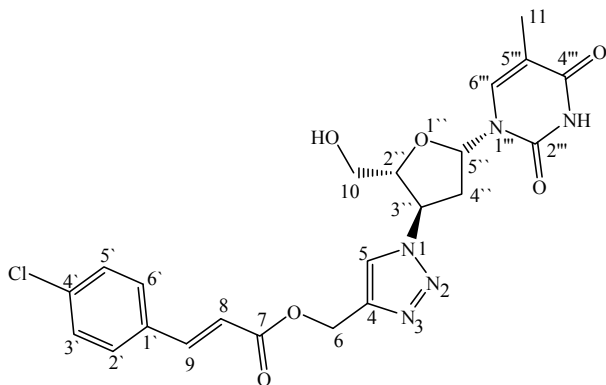
1-{(2''R, 3''R, 5''S)-Tetrahydro-5-[3''', 4'''-dihydro-5'''-methyl-2'', 4'''-dioxypyrimidin-1(2H)-yl]-2''-(hydroxymethyl)fur-3''-yl}-(1H-1,2,3-triazol-4-yl)methyl cinnamate 178a



To a stirred solution of AZT (1.0 mmol, 0.27 g) and prop-2-ynyl cinnamate (0.19 g, 1.0 mmol) dissolved in a 1:1 mixture of H₂O-THF (3 mL) was sequentially added CuSO₄ (0.05 mmol, 0.01 g) and ascorbic acid (0.05 mmol, 0.01 g). The reaction mixture was stirred at room temperature for 24 hours.

Work-up and purification by preparative thin layer chromatography (on silica gel; elution with EtOAc) afforded *1-{(2''R, 3''R, 5''S)-tetrahydro-5-[3''', 4'''-dihydro-5'''-methyl-2'', 4'''-dioxypyrimidin-1(2H)-yl]-2''-(hydroxymethyl)fur-3''-yl}-(1H-1,2,3-triazol-4-yl)methyl cinnamate 178a* as a yellow solid (0.26 g, 57%); m.p. 144-148 °C; [HRMS: *m/z* calculated for C₂₂H₂₃N₅O₆ (MH⁺) 454.1727. Found 454.1721]; ν_{max} (cm⁻¹) 1682.43 (C=O); ¹H NMR (600 MHz, CDCl₃) 3.38 (3H, s, CH₃), 4.22 (1H, m, 4''-H), 4.40 (1H, m, 4''-H), 5.27 (1H, m, 10-H), 5.39 (1H, m, 10-H), 5.86 (1H, q, *J* = 5.46 Hz, 2''-H), 6.82 (2H, s, 6-H), 6.94 (2H, q, *J* = 5.62 Hz, 4''-H), 8.00 (2H, m, 8-H, 5''-H), 8.88 (3H, m, 3'-H, 4'-H, 5'-H, Ar-H), 9.07 (2H, m, 2'-H, 6'-H, Ar-H), 9.20 (1H, d, *J* = 11.15 Hz, 9-H), 9.37 (1H, s, 6'''-H); 9.70 (1H, s, 5-H); ¹³C NMR (150 MHz, CDCl₃) 12.6 (CH₃), 39.1 (4''-C), 58.3 (6-C), 61.2 (3''-C), 62.2 (10-C), 86.4 (2''-C), 86.8 (5''-C), 111.77 (5''-C), 118.4 (8-C), 125.7 (5-C), 129.3 (2'-C, 6'-C), 130.1 (3'-C, 5'-C), 131.7 (4'-C), 135.6 (1'-C), 138.2 (6'''-C), 144.4 (4-C), 146.9 (9-C), 152.8 (2'''-C=O), 167.1 (4'''-C=O), 168.1 (7-C=O).

1-{(2''R, 3''R, 5''S)-Tetrahydro-5''[-3''',4'''-dihydro-5'''-methyl-2''', 4'''-dioxypyrimidin-1(2H)-yl]-2'-(hydroxymethyl)fur-3-yl}-(1H-1,2,3-triazol-4-yl)methyl 3''-(4' chlorophenyl)acrylate **178b**



The procedure described for the synthesis of 1-{(2''R, 3''R, 5''S)-tetrahydro-5''[-3''',4'''-dihydro-5'''-methyl-2''',4'''-dioxypyrimidin-1(2H)-yl]-2'-(hydroxymethyl)fur-3-yl}-(1H-1,2,3-triazol-4-yl)methyl cinnamate **178a** was followed, using AZT (1.0 mmol, 0.27 g), prop-2-ynyl

3-(4-chlorophenyl)acrylate (0.22 g, 1.0 mmol), CuSO₄ (0.05 mmol, 0.01 g), ascorbic acid (0.05 mmol, 0.01 g). Work-up afforded 1-{(2''R, 3''R, 5''S)-tetrahydro-5''[-3''',4'''-dihydro-5'''-methyl-2''',4'''-dioxypyrimidin-1(2H)-yl]-2'-(hydroxymethyl)fur-3-yl}-(1H-1,2,3-triazol-4-yl)methyl 3''-(4'-chlorophenyl)acrylate **178b** as a yellowish solid (0.34 g, 71%); m.p. 152-154 °C; [HRMS: *m/z* calculated for C₂₂H₂₂ClN₅O₆ (MH⁺) 488.1337. Found 488.1333]; ν_{max} (cm⁻¹) 3466.39; 3063.61; 1678.77, 1635.07; ¹H NMR (600 MHz, CDCl₃) 1.91 (3H, s, CH₃), 2.73 (1H, m, 4''-H), 2.90 (1H, m, 4''-H), 3.79-3.90 (2H, m, 10-H), 4.37 (1H, q, *J* = 5.56 Hz, 2''-H), 4.70 and 5.34 (2H, s, 6-H), 5.46 (1H, m, 3''-H), 6.50-9.56 (2H, m, 8-H, 5'-H), 7.42 (2H, d, *J* = 8.53 Hz, 3'-H, 5'-H, Ar-H), 7.61 (1H, d, *J* = 8.55 Hz, 2'-H, 6'-H, Ar-H), 7.71 (1H, d, *J* = 16.02 Hz, 9-H), 7.92 (1H, s, 5-H), 8.07 (1H, s, 6'''-H); ¹³C NMR (150 MHz, CDCl₃) 12.5 (CH₃), 39.1 (4''-C), 56.5 (6-C), 58.4 (3''-C), 61.1 (10-C), 86.4 (2'''-C), 86.8 (5''-C), 111.7 (5'''-C), 119.2 (8-C), 123.9 (5-C), 125.8 (2'-C), 128.8 (6'-C), 130.2 (3'-C), 130.3 (5'-C), 143.3 (2''-C), 131.7 (4'-C), 135.6 (1'-C), 138.2 (6'''-C), 143.2 (4-C), 145.4 (9-C), 148.1 (2'''-C=O), 152.3 (4'''-C=O), 166.4 (7-C=O).

6.2.15. General procedure for docking studies

The simulations were achieved using the X-ray crystal structure of the HIV-1 enzymes (1HXW, 1QS4, 1IKW) retrieved from the PDB. The structures of the heterocycles were constructed and the protein enzymes (1HXW, 1QS4, 1IKW) were prepared for docking using Discovery Studio Visualiser 3.5.⁴¹¹ Water molecules and the original inhibitors (Ritonavir, 5CITEP, Efavirenz) were removed from the protein structures. Non polar hydrogens (C-H) were merged and only polar hydrogens (OH and NH) on the protein were added. Moreover, gasteiger charges were calculated to ensure that the atoms are in conformity with AUTODOCK4 (AD4) atoms type requirements. Next, AD4 atoms were assigned by using Autodock tools (ADT). Torsion trees around the ligand were generated automatically to favor rotation of bonds in the ligand during the docking process. PDBQT files (extended PDB format) were generated to coordinate files containing atomic partial charges. These PDBQT files were created from PDB files by using ADT. Grid boxes with dimensions of 11.14 Å × 23.57 Å × 3.31 Å, -17.46 Å × 30.18 Å × 66.60 Å and -10.86 Å × 143.09 Å × 174.20 Å were centered in the active site of 1HXW, 1QS4 and 1IKW respectively. Autogrid was used to pre-calculate grid maps of the interaction energies of different atom types of the ligand with the macromolecule. Docking proceeded using the Lamarckian Genetic Algorithm, the population size was 150, the maximum number of evaluations was medium and the number of GA runs used to perform the docking was ten. The docking process was completed after a reasonable time frame of 50 minutes. After docking and extraction of the lowest energy bound conformation,⁴¹² DSV 3.5 was used to search and view the docking mode of the inhibitor in the binding site of the enzyme.

6.2.16. Saturation Transfer Difference (STD) Assay

6.2.16.1. Standardisation of the STD experiment

An STD assay using BSA as the protein with L-tryptophan and D-glucose as ligands was carried out to validate and optimize STD parameters. A buffer solution of pH 7.18 was prepared by diluting one buffer tablet of pH 7.18 in 100 mL of distilled water. Solutions of BSA (84 μ M), L-tryptophan (7.75 mM) and D-glucose (53.25 mM) were prepared in 50 mM HCl buffer (pH 7.18). A sample containing BSA (240 μ L), buffer solution (120 μ L), L-tryptophan (130 μ L), glucose (19 μ L) and D₂O (25 μ L) was made up in an NMR tube to give a final assay solution containing 40 μ M BSA, 2 mM L-tryptophan and 2mM D-glucose in a buffer solution (pH 7.18).

6.2.16.2. HIV-1 integrase STD experiment

HIV-1 IN was purchased from Xpress Biotech International. Ligands **178a**, **170b**, **169e**, **169d** (8 nmol) were dissolved in 1 mL of D₂O. To 10 μ L of that sample, was added 5 μ L of HIV-1 IN (0.2 μ M) and 45 μ L of D₂O to make a 50 μ L solution which was inserted in a 1 mm micro NMR tube.

All NMR experiments were performed on Bruker Biospin Avance 600-MHz spectrometer using a 1 mm (¹⁵N/¹³C/¹H) microprobe equipped with triple axis actively shielded gradients (for STD experiments). STD spectra covered a sweep width of 10 ppm with a total saturation time of 2s. Water suppression was achieved using a 3-9-19 water gate sequence and the protein signals were removed using a spin lock sequence. The number of scans was 16 for TOCSY experiments and 512 for STD 19 experiments and the power attenuation was 40 dB. For the STD, the protein was irradiated at 0.8 ppm and the off resonance reference was at 40 ppm.

6.2.17. HIV-1 enzyme inhibition assays

HIV-1 protease subtype B and the Sensolyte® 490 HIV 1 Protease Assay kit *Fluorometric* were purchased from ANASPEC. HIV-1 integrase enzyme and assay kit were purchased from XpressBio while the RT Roche colorimetric assay kit was obtained from Roche Diagnostics. HIV-1 enzyme inhibition assays were carried out on ligands designed as potential PR, IN and RT inhibitors.

6.2.17.1. HIV-1 protease fluorometric experiments

Preliminary fluorescence measurements were carried out on the ligands in order to ensure that the excitation/emission spectra of the ligands were not between 490 nm and 520 nm and thus to avoid interference due to fluorescent compounds giving non-specific responses leading to false interpretation. A vehicle control and a substrate control were prepared as follows. The vehicle control was made up of a mixture of 10 µL of PR diluent (17.4 µg/mL), 10 µL of deionised water containing 0.1% DMSO and 30 µL of assay buffer; 50 µL of assay buffer comprised the substrate control. The test solutions each contained 10 µL of PR diluent (17.4 µg/mL), 10 µL of the ligand (50 µM in deionised water containing 0.1% DMSO) and 30 µL of assay buffer. Finally, (both controls and test solutions) were pre-incubated at 37 °C for 15 minutes and the reaction was initiated by the addition of 50 µL of the HIV-1 fluorescent peptide protease substrate solution in each well. The fluorescence intensities were measured with a Synergy Mx multi-mode microplate reader equipped with a quadruple monochromator system. The experiment was carried out at 37 °C ± 0.5 °C in a 96 well microplate format for 60 minutes with an excitation wavelength of 490 nm and an emission wavelength of 520 nm. Fluorescence data were recorded every minute and all the samples were run in duplicate. Data analysis was performed with Microsoft Excel® and curves of the fluorescence data were plotted as a function of time.

6.2.17.2. HIV-1 integrase colorimetric experiments

Absorbance measurements of each ligand were carried out to make sure the compounds did not absorb at 450 nm. Each well of a streptavidine-coated 96-well plate was loaded with 100 µL of a double stranded donor substrate HIV-1 oligo nucleotide DNA solution

(10 µL of DS DNA diluted in 990 µL of reaction buffer) and incubated at 37 °C for 30 minutes. The plate was then washed five times by adding 300 µL of wash buffer 20 X solution (1 mL of wash buffer concentrate diluted in 19 mL of deionised water) in each well. Subsequently, the plate was blocked by adding 200 µL of blocking solution in each well and placed at 2-8 °C overnight and later incubated at 37 °C for 20 minutes. The plate was washed three times with 200 µL of reaction buffer per wash per well and 100 µL of reaction buffer or HIV-1 IN (0.07 µM) were added according to the test controls and the plate was incubated for 30 minutes at 37 °C. Since NaN₃ is a known inhibitor of HIV-1 IN, NaN₃ (20%) was used as a test control to confirm the activity of the enzyme during the experiment by its inhibition and also to make sure that the procedure followed was effective. After washing the plate three times with 200 µL of reaction buffer per wash, 50 µL of test articles [reaction buffer, NaN₃ (20%), vehicle and inhibitors] were added, one per well, and the plate was incubated for five minutes at room temperature. A volume of 50 µL of TS oligo DNA 100 X solution (10 µL of TS DNA diluted in 990 µL of reaction buffer) was added directly to the 50 µL buffer/test articles present in the wells and incubated for 30 minutes at 37 °C after gentle mixing. The plate was washed five times with 300 µL of wash buffer concentrate per well and 100 µL of Hepatoma related protein (HRP) antibody solution was added per well and the plate was incubated for a further 30 minutes at 37 °C. The plate was washed five times with 300 µL of wash buffer concentrate 20 X and a 100 µL of 3,3',5,5' tetramethylbenzidine (TMB) peroxidase substrate was added and the plate was incubated in the dark where the progress of the reaction was watched. Subsequent to the appearance of a blue color in the wells containing the negative control and the vehicle control, a 100 µL of stop solution was added and a change in color (yellow) was observed in those wells. The absorbances of the components in each well were measured with a Dower Wave_x spectrophotometer Biotek instrument at 450 nm.

6.2.17.3. HIV-1 reverse transcriptase colorimetric experiments

Absorbance measurements of each ligand were carried out to make sure the compounds did not absorb at 405 nm To streptavidine precoated well plates was added 20 µL of buffer mixture working solution containing nucleotides followed by the HIV-1 RT

enzyme (20 μ L, 0.2 ng/ μ L). RT Inhibitors (20 μ L, 50 μ M) were added to each well which were then covered with foil and incubated for one hour at 37 °C. The lysis buffer with no HIV-1 RT added was used as the negative control while HIV-1 RT enzyme with no inhibitor was considered the positive control. The wells were rinsed five times with 250 μ L of washing buffer per well and 200 μ L of anti-DIG-POD working dilution was added per well which were then covered with foil and incubated for one hour at 37 °C. The wells were rinsed five times with washing buffer and 200 μ L of ABTS substrate solution per well was added and incubated at 25 °C until a green color was detected. The absorbances of the samples were measured at 405 nm with Dower Wave_x spectrophotometer Biotek instrument.

REFERENCES

1. UNAIDS. UNAIDS World AIDS Day Report 2012, **2013**,
http://www.unaids.org/en/media/unaids/contentassets/documents/epidemiology/2012/gr2012/jc2434_worldaidsday_results_en.pdf (Accessed February 19, 2013).
2. UNAIDS. UNAIDS report on the global AIDS epidemic, **2012**,
http://www.unaids.org/en/media/unaids/contentassets/documents/epidemiology/2012/gr2012/20121120_unaids_global_report_2012_with_annexes_en.pdf
(Accessed February 19, 2013).
3. M. J. Camarasa, S. Velazquez, A. San-Falix, M. J. Perez-Perez and F. Gago, *Antivir. Res.*, **2006**, 71, 260-267.
4. A. Brik and C. H. Wong, *Org. Biomol. Chem.*, **2003**, 1, 5-14.
5. NIH website, National Institute of Allergy and Infectious Diseases <http://www.niaid.nih.gov/Pages/default.aspx> (Accessed April 19, 2012).
6. G. Maga, M. Radi, M. Gerard, M. Botta and E. Ennifar, *Viruses*, **2010**, 2, 880-899.
7. S. Sierra, B. Kupfer and R. Kaiser, *J. Clin. Virol.*, **2005**, 34, 233-244.
8. D. W. Rodgers, S. J. Gamblin, B. A. Harris, J. S. Culp, B. Hellmig, D. J. Woolf, C. Debouck, S. C. Harrison and S. Ray, *P. Natl. Acad. Sci. U. S. A.*, **1995**, 92, 1222-1226.
9. A. Jacobo-Molina, J. Ding, R. G. Nanni, A. D. Clark Jr, X. Lu, C. Tantillo, R. L. Williams, G. Kamer and A. L. Ferris, *P. Natl. Acad. Sci. U. S. A.*, **1993**, 90, 6320-6324.
10. N. Kaushik, D. Harris, N. Rege, M. J. Modak, N. S. Yadav and V. N. Pandey, *Biochemistry*, **1997**, 36, 14430-14438.
11. M. Gotte, *Viruses*, **2011**, 3, 331-335.
12. A. J. B. Alberts, J. Lewis, M. Raff, K. Roberts and P. Walter, *Molecular Biology of the Cell*, Garland Science, New York, 4th edn., **2002**.
13. A. S. Perelson, A. U. Neumann, M. Markowitz, J. M. Leonard and D. D. Ho, *Science*, **1996**, 271, 1582-1586.
14. L. Ratner, W. Haseltine, R. Patarca, K. J. Livak, B. Starcich, S. F. Josephs, E. R. Doran, J. A. Rafalski and E. A. Whitehorn, *Nature*, **1985**, 313, 277-284.
15. S. R. Di, R. Costi, M. Artico, E. Tramontano, C. P. La and A. Pani, *Pure Appl. Chem.*, **2003**, 75, 195-206.
16. T. K. Chiu and D. R. Davies, *Curr. Top. Med. Chem.*, **2004**, 4, 965-977.
17. R. Zheng, T. M. Jenkins and R. Craigie, *P. Natl. Acad. Sci. U. S. A.*, **1996**, 93, 13659-13664.
18. M. Cai, R. Zheng, M. Caffrey, R. Craigie, G. M. Clore and A. M. Gronenborn, *Nat. Struct. Biol.*, **1997**, 4, 567-577.
19. S. P. Goff, *Annu. Rev. Genet.*, **1992**, 26, 527-544.
20. Z. Chen, Y. Yan, S. Munshi, Y. Li, J. Zugay-Murphy, B. Xu, M. Witmer, P. Felock, A. Wolfe, V. Sardana, E. A. Emimi, D. Hazuda and L. C. Kuo, *J. Mol. Biol.*, **2000**, 296, 521-533.
21. J. F. Mouscadet and D. Desmaele, *Molecules*, **2010**, 15, 3048-3078.
22. M. Artico, S. R. Di, R. Costi, E. Novellino, G. Greco, S. Massa, E. Tramontano, M. E. Marongiu, M. A. De and C. P. La, *J. Med. Chem.*, **1998**, 41, 3948-3960.

23. A. S. Espeseth, P. Felock, A. Wolfe, M. Witmer, J. Grobler, N. Anthony, M. Egbertson, J. Y. Melamed, S. Young, T. Hamill, J. L. Cole and D. J. Hazuda, *P. Natl. Acad. Sci. U. S. A.*, **2000**, 97, 11244-11249.
24. H. Chen and A. Engelman, *J. Virol.*, **2000**, 74, 8188-8193.
25. H. Saibil, *Structure*, **1996**, 4, 1-4.
26. R. Craigie, *J. Biol. Chem.*, **2001**, 276, 23213-23216.
27. M. K. Holloway, J. M. Wai, T. A. Halgren, P. M. D. Fitzgerald, J. P. Vacca, B. D. Dorsey, R. B. Levin, W. J. Thompson and L. J. Chen, *J. Med. Chem.*, **1995**, 38, 305-317.
28. O. Aruksankunwong, S. Hannongbua and P. Wolschann, *J. Mol. Struct.*, **2006**, 790, 174-182.
29. T. Oyoshi and R. Kurokawa, *Cell Biosci.*, **2012**, 2, 1-8.
30. A. L. Perryman, J. H. Lin and J. A. McCammon, *Protein Sci.*, **2004**, 13, 1108-1123.
31. J. L. Martinez-Cajas and M. A. Wainberg, *Antiviral Res.*, **2007**, 76, 203-221.
32. A. L. Jayewardene, F. Zhu, F. T. Aweeka and J. G. Gambertoglio, *J. Chromatogr. B: Biomed. Sci. Appl.*, **1998**, 707, 203-211.
33. L. M. Mansky, *J. Gen. Virol.*, **1998**, 79, 1337-1345.
34. L. M. Mansky and H. M. Temin, *J. Virol.*, **1995**, 69, 5087-5094.
35. J. G. Julias, T. Kim, G. Arnold and V. K. Pathak, *J. Virol.*, **1997**, 71, 4254-4263.
36. Merriam-webster website, <http://www.merriam-webster.com/dictionary/drug>. (Accessed June 14, 2013).
37. Top 200 Pharmaceutical Products by Worldwide Sales in 2009, **2009**, <http://cbc.arizona.edu/njardarson/group/sites/default/files/Top200PharmaceuticalProductsByWorldwideSalesin2009.pdf> (Accessed March 02, 2013).
38. F. Esposito, A. Corona and E. Tramontano, *Mol. Biol. Int.*, **2012**, 2012, 1-23.
39. M. W. Hoetelmans, D. M. Burger, P. L. Meenhorst and J. H. Beijnen, *Clin. Pharmacokinet.*, **1996**, 30, 314-327.
40. M. A. Fischl, D. D. Richman, M. H. Grieco, M. S. Gottlieb, P. A. Volberding, O. L. Laskin, J. M. Leedom, J. E. Groopman, D. Mildvan and R. T. Schooley, *N. Engl. J. Med.*, **1987**, 317, 185-191.
41. F. T. Papadopoulos-Eleopoulos, J. M. Papadimitriou, H. Alfonso, B. A. P. Page, D. Causer, S. Mhlongo, C. Fiala, T. Miller, A. Brink and N. Hodgkinson, *Mother to child transmission of HIV and its prevention with AZT and Nevirapine, a critical analysis of evidence.*, The Perth Group, Perth, western australia, **2001**.
42. T. Cihlar and A. S. Ray, *Antiviral Res.*, **2010**, 85, 39-58.
43. NIH website, Guidelines for the Use of Antiretroviral Agents in HIV-1-Infected Adults and Adolescents, <http://aidsinfo.nih.gov/contentfiles/lvguidelines/AdultandAdolescentGL.pdf>.
44. J. J. Kessl, C. J. McKee, J. O. Eidahl, N. Shkriabai, A. Katz and M. Kvaratskhelia, *Viruses*, **2009**, 1, 713-736.
45. C. R. Allen, *Drug Discov. Today*, **2005**, 10, 237-239.
46. X. Chen, D. J. Kempf, L. Li, H. L. Sham, S. Vasavanonda, N. E. Wideburg, A. Saldivar, K. C. Marsh, E. McDonald and D. W. Norbeck, *Bioorg. Med. Chem. Lett.*, **2003**, 13, 3657-3660.
47. M. Tukulula, MSc thesis, Rhodes University, **2009**.

48. M. Whiting, J. C. Tripp, Y. C. Lin, W. Lindstrom, A. J. Olson, J. H. Elder, K. B. Sharpless and V. V. Fokin, *J. Med. Chem.*, **2006**, 49, 7697-7710.
49. FDA website, Overview FDA, **2011**, <http://www.fda.gov/downloads/Training/ClinicalInvestigatorTrainingCourse/UCM283299.pdf> (Accessed March 03, 2013).
50. E. F. Healy, J. Sanders, P. J. King and W. E. Robinson, *J. Mol. Graphics Model.*, **2009**, 27, 584-589.
51. R. Pauwels, *Curr. Opin. Pharmacol.*, **2004**, 4, 437-446.
52. J. C. Tilton and R. W. Doms, *Antiviral Res.*, **2010**, 85, 91-100.
53. G. H. Wynn, M. J. Zapor, B. H. Smith, G. Wortmann, J. R. Oesterheld, S. C. Armstrong and K. L. Cozza, *Psychosomatics*, **2004**, 45, 262-270.
54. J. A. H. Droste, Verweij-van, C. P. W. G. M. Wissen and D. M. Burger, *Ther. Drug Monit.*, **2003**, 25, 393-399.
55. P. G. Hoggard, V. Manion, M. G. Barry and D. J. Back, *Br. J. Clin. Pharmacol.*, **1998**, 45, 164-167.
56. P. A. J. Janssen, P. J. Lewi, E. Arnold, F. Daeyaert, J. M. de, J. Heeres, L. Koymans, M. Vinkers, J. Guillemont, E. Pasquier, M. Kukla, D. Ludovici, K. Andries, B. M. P. de, R. Pauwels, K. Das, A. D. Clark Jr, Y. V. Frenkel, S. H. Hughes, B. Medaer, K. F. De, H. Bohets, C. F. De, A. Lampo, P. Williams and P. Stoffels, *J. Med. Chem.*, **2005**, 48, 1901-1909.
57. C. E. De, *Med. Res. Rev.*, **1996**, 16, 125-157.
58. C. E. De, *Antiviral Res.*, **2005**, 67, 56-75.
59. C. E. De, *Int. J. Antimicrob. Agents*, **2009**, 33, 307-320.
60. D. Faulds and R. N. Brogden, *Drugs*, **1992**, 44, 94-116.
61. W. Manosuthi, W. Mankatitham, A. Lueangniyomkul, W. Prasithsirikul, P. Tantanathip, B. Suntisuklappon, A. Narkksoksung, S. Nilkamhang and S. Sungkanuparph, *AIDS Res. Ther.*, **2010**, 7, 1-8.
62. J. W. Beach, *Clin. Ther.*, **1998**, 20, 2-25.
63. Y. Alfonso and L. Monzote, *Open Med. Chem. J.*, **2011**, 5, 40-50.
64. T. Ikezoe, Y. Hisatake, T. Takeuchi, Y. Ohtsuki, Y. Yang, J. W. Said, H. Taguchi and H. P. Koeffler, *Cancer Res.*, **2004**, 64, 7426-7431.
65. M. Jayakanthan, S. Chandrasekar, J. Muthukumaran and P. P. Mathur, *J. Mol. Graphics Model.*, **2010**, 28, 455-463.
66. L. Xu and M. C. Desai, *Curr. Opin. Invest. Drugs*, **2009**, 10, 775-786.
67. J. A. Grobler, K. Stillmock, B. Hu, M. Witmer, P. Felock, A. S. Espeseth, A. Wolfe, M. Egbertson, M. Bourgeois, J. Melamed, J. S. Wai, S. Young, J. Vacca and D. J. Hazuda, *P. Natl. Acad. Sci. U. S. A.*, **2002**, 99, 6661-6666.
68. V. Summa, A. Petrocchi, V. G. Matassa, C. Gardelli, E. Muraglia, M. Rowley, O. G. Paz, R. Laufer, E. Monteagudo and P. Pace, *J. Med. Chem.*, **2006**, 49, 6646-6649.
69. E. Serrao, S. Odde, K. Ramkumar and N. Neamati, *Retrovirology*, **2009**, 6, 1-2.
70. S. G. Deeks, S. Kar, S. I. Gubernick and P. Kirkpatrick, *Nat. Rev. Drug Discovery*, **2008**, 7, 117-118.
71. Z. Temesgen and D. S. Siraj, *Ther. Clin. Risk Manag.*, **2008**, 4, 493-500.
72. M. D. Evering and H. Teresa, *The PRN notebook*, **2008**, 13, 1-9.

73. C. Laurent, C. Kouanfack, S. Koulla-Shiro, N. Nkoue, A. Bourgeois, A. Calmy, B. Lactuock, V. Nzeusseu, R. Mognutou, G. Peytavin, F. Liegeois, E. Nerrienet, M. Tardy, M. Peeters, I. Andrieux-Meyer, L. Zekeng, M. Kazatchkine, E. Mpoudi-Ngole and E. Delaporte, *Lancet*, **2004**, 364, 29-34.
74. S. N. Pujari, A. K. Patel, E. Naik, K. K. Patel, A. Dravid, J. K. Patel, A. A. Mane and S. Bhagat, *J. Acquired Immune Defic. Syndr.*, **2004**, 37, 1566-1569.
75. J. E. Gallant, *Drug Resistance after Failure of Initial Antiretroviral Therapy in Resource-Limited Countries in HIV/AIDS*, Baltimore, Maryland, 44, **2007**.
76. V. Simon, D. D. Ho and K. Q. Abdool, *Lancet*, **2006**, 368, 489-504.
77. G. L. Amidon and H. J. Lee, *Annu. Rev. Pharmacol. Toxicol.*, **1994**, 34, 321-341.
78. J. G. Bartlett and R. D. Moore, *Sci. Am.*, **1998**, 279, 84-87.
79. WHO website, WHO, Coverage of selected health services for HIV/AIDS prevention and care in less developed countries in 2001, **2001**, <http://whqlibdoc.who.int/publications/9241590319.pdf> (Accessed June 28, 2012).
80. W. A. Chow, C. Jiang and M. Guan, *Lancet Oncol.*, **2009**, 10, 61-71.
81. T. O. Olomola, PhD thesis, Rhodes University, **2011**.
82. Y. C. Lee, MSc thesis, Rhodes University, **2008**.
83. K. C. Idahosa, PhD thesis, Rhodes University, **2012**.
84. G. Singh, S. S. Bhella and M. P. S. Ishar, *Int. J. Nat. Prod. Sci.*, **2012**, 101-116.
85. Y. Che, B. R. Brooks and G. R. Marshall, *Biopolymers*, **2007**, 86, 288-297.
86. S. Moradi, S. Soltani, A. M. Ansari and S. Sardari, *Anti-Infect. Agents Med. Chem.*, **2009**, 8, 327-344.
87. P. V. Murphy, J. L. O'Brien, L. J. Gorey-Feret and A. B. Smith, *Bioorg. Med. Chem. Lett.*, **2002**, 12, 1763-1766.
88. P. V. Murphy, J. L. O'Brien, L. J. Gorey-Feret and A. B. Smith, *Tetrahedron*, **2003**, 59, 2259-2271.
89. I. Cerminara, L. Chiumminto, M. Funicello, A. Guarnaccio and P. Lupattelli, *Pharmaceuticals*, **2012**, 5, 297-316.
90. F. Airaghi, A. Fiorati, G. Lesma, M. Musolino, A. Sacchetti and A. Silvani, *Beilstein J. Org. Chem.*, **2013**, 9, 147-154.
91. M. G. Bursavich, C. W. West and D. H. Rich, *Org. Lett.*, **2001**, 3, 2317-2320.
92. D. Yadav, S. Paliwal, R. Yadav, M. Pal and A. Pandey, *PLoS One*, **2012**, 7, 48942-48960.
93. P. B. Reddy, S. D. Sawant, S. Koul, S. C. Taneja and H. M. S. Kumar, *ARKIVOC*, **2006**, 8, 142-146.
94. K. Muralirajan, K. Parthasarathy and C. H. Cheng, *Angew. Chem. Int. Ed.*, **2011**, 50, 4169-4172.
95. J. Vicente, J. A. Abad and J. Gil-Rubio, *Organometallics*, **1996**, 15, 3509-3519.
96. P. P. Singh, P. B. Reddy, S. D. Sawant, S. Koul, S. C. Taneja and H. M. S. Kumar, *Tetrahedron Lett.*, **2006**, 47, 7241-7243.
97. F. J. S. Duarte, E. J. Cabrita, G. Frenking and A. G. Santos, *Chem. Eur. J.*, **2009**, 15, 1734-1746.
98. S. Rodriguez-Esrich, D. Popa, C. Jimeno, A. Vidal-Ferran and M. A. Pericas, *Org. Lett.*, **2005**, 7, 3829-3832.
99. V. Singh and S. Batra, *Tetrahedron*, **2008**, 64, 4511-4574.

100. G. P. Black, F. Dinon, S. Fratucello, P. J. Murphy, M. Nidelsen, H. L. Williams and N. D. A. Waishe, *Tetrahedron Lett.*, **1997**, 38, 8561-8564.
101. R. F. Heck, *Organotransition metal chemistry, a mechanistic approach*, New York and London, **1974**.
102. V. Gevorgyan, L. G. Quan and Y. Yamamoto, *Tetrahedron Lett.*, **1999**, 40, 4089-4092.
103. A. V. Ghazaryan, A. S. Khatchadourian, M. K. Karagyozyan, A. R. Kachatryan, E. S. Sekoyan, H. K. Bdoyan, H. V. Melkumyan and K. G. Karageuzyan, *Cardiovasc. Hematol. Disord.: Drug Targets*, **2007**, 7, 170-173.
104. R. M. Patel and N. J. Patel, *J. Adv. Pharm. Ed. Res.*, **2011**, 1, 52-68.
105. S. S. Mousavi, H. Bokharaie, S. Rahimi, S. A. Soror and M. Hamidi, *Adv. Appl. Bioinf. Chem.*, **2010**, 3, 59-66.
106. T. Taechowisan, C. Lu, Y. Shen and S. Lumyong, *J. Cancer Res. Ther.*, **2007**, 3, 86-91.
107. T. Ojala, S. Remes, P. Haansuu, H. Vuorela, R. Hiltunen, K. Haahtela and P. Vuorela, *J. Ethnopharmacol.*, **2000**, 73, 299-305.
108. R. Argotte-Ramos, G. Ramirez-Avila, M. C. Rodriguez-Gutierrez, M. Ovilla-Munoz, H. Lanz-Mendoza, M. H. Rodriguez, M. Gonzalez-Cortazar and L. Alvarez, *J. Nat. Prod.*, **2006**, 69, 1442-1444.
109. R. Ahmad, M. Asad, Z. N. Siddiqui and A. Kumar, *J. Pharm. Res. Health Care*, **2009**, 1, 46-62.
110. M. Tasior, R. Voloshchuk, Y. M. Poronik, T. Rowicki and D. T. Gryko, *J. Porphyrins Phthalocyanines*, **2011**, 15, 1011-1023.
111. B. C. Ranu and R. Jana, *Eur. J. Org. Chem.*, **2006**, 3767-3770.
112. H. S. P. Rao and S. Sivakumar, *J. Org. Chem.*, **2006**, 71, 8715-8723.
113. A. V. Kalinin, A. J. M. Da Silva, C. C. Lopes, R. S. C. Lopes and V. Snieckus, *Tetrahedron Lett.*, **1998**, 39, 4995-4998.
114. D. V. Kadnikov and R. C. Larock, *Org. Lett.*, **2000**, 2, 3643-3646.
115. B. Rajitha, P. Someshwar, J. V. Madhav, P. N. Reddy and Y. T. Reddy, *ARKIVOC* **2006**, 7, 23-27.
116. A. H. Neilson and A. Allard, *Chemistry of organic pollutants*, Stockholm, IVL Swedish Environmental Research Institute., **2008**, 1, 1-11.
117. P. Anastas and N. Eghbali, *Chem. Soc. Rev.*, **2010**, 39, 301-312.
118. P. T. Anastas, L. B. Bartlett, M. M. Kirchhoff and T. C. Williamson, *Catal. Today*, **2000**, 55, 11-22.
119. G. Centi and S. Perathoner, *Catal. Today*, **2003**, 77, 287-297.
120. P. Tundo, P. Anastas, D. S. Black, J. Breen, T. Collins, S. Memoli, J. Miyamoto, M. Polyakoff and W. Tumas, *Pure Appl. Chem.*, **2000**, 72, 1207-1228.
121. P. T. Anastas and M. M. Kirchhoff, *Acc. Chem. Res.*, **2002**, 35, 686-694.
122. K. Cavell, S. Golunski, D. Miller, *Platinum Metals Rev.*, **2010**, 54, 233-238.
123. F. M. Kerton, *Alternative solvents for green chemistry*, the Royal Society of Chemistry Cambridge, **2009**.
124. V. R. Batchu, V. Subramanian, K. Parasuraman, N. K. Swamy, S. Kumar and M. Pal, *Tetrahedron*, **2005**, 61, 9869-9877.
125. B. Zeynizadeh and D. Setamdideh, *J. Chin. Chem. Soc.*, **2005**, 52, 1179-1184.

126. Pennakem website, 2-MeTHF for greener processes, <http://www.pennakem.com/pdfs/methfpenngreenchemistry.pdf> (Accessed January 30, 2014).
127. P. E. Rakita, *Challenges to the Commercial Production of Ionic Liquids* in "Ionic Liquids as Green Solvents: Progress and Prospects, ACS Symposium Series, 856, **2003**.
128. M. Charde, A. Shukla, V. Bukhariya, J. Mehta and R. Chakole, *Int. J. Phytopharm.*, **2012**, 2, 39-50.
129. P. Lidstrom, J. Tierney, B. Wathey and J. Westman, *Tetrahedron*, **2001**, 57, 9225-9283.
130. G. W. Kabalka, L. Wang, V. Namboodiri and R. M. Pagni, *Tetrahedron Lett.*, **2000**, 41, 5151-5154.
131. S. C. O. Sousa, C. G. L. Junior, F. P. L. Silva, N. G. Andrade, T. P. Barbosa and M. L. A. A. Vasconcellos, *J. Braz. Chem. Soc.*, **2011**, 22, 1634-1643.
132. M. A. Surati, S. Jauhari and K. R. Desai, *Arch. Appl. Sci. Res.*, **2012**, 4, 645-661.
133. A. R. Katritzky, M. S. Kim and K. Widyana, *ARKIVOC*, **2008**, 3, 91-101.
134. S. G. Hansen and H. H. Jensen, *Synlett.*, **2009**, 20, 3275-3278.
135. H. C. Kolb, M. G. Finn and K. B. Sharpless, *Angew. Chem., Int. Ed.*, **2001**, 40, 2004-2021.
136. M. G. Finn and V. V. Fokin, *Chem. Soc. Rev.*, **2010**, 39, 1231-1232.
137. C. D. Hein, X. M. Liu and D. Wang, *Pharm. Res.*, **2008**, 25, 2216-2230.
138. K. Nwe and M. W. Brechbiel, *Cancer Biother. Radiopharm.*, **2009**, 24, 289-302.
139. C. R. Becer, R. Hoogenboom and U. S. Schubert, *Angew. Chem. Int. Ed.*, **2009**, 48, 4900-4908.
140. H. C. Kolb and K. B. Sharpless, *Drug Discovery Today*, **2003**, 8, 1128-1137.
141. J. E. Moses and A. D. Moorhouse, *Chem. Soc. Rev.*, **2007**, 36, 1249-1262.
142. P. Thirumurugan, D. Matosiuk and K. Jozwiak, *Chem. Rev.*, **2011**, 113, 4905-4979.
143. V. D. Bock, H. Hiemstra and J. H. Maarseveen, *Eur. J. Org. Chem.*, **2006**, 1, 51-68.
144. H. A. Orgueira, D. Fokas, Y. Isome, P. C. M. Chan and C. M. Baldino, *Tetrahedron Lett.*, **2005**, 46, 2911-2914.
145. C. W. Tornøe, C. Christensen and M. Meldal, *J. Org. Chem.*, **2002**, 67, 3057-3064.
146. B. C. Boren, S. Narayan, L. K. Rasmussen, L. Zhang, H. Zhao, Z. Lin, G. Jia and V. V. Fokin, *J. Am. Chem. Soc.*, **2008**, 130, 8923-8930.
147. R. Huisgen, *Angew. Chem. Int. Ed. Engl.*, **1963**, 2, 565-632.
148. K. V. Gothelf and K. A. Jorgensen, *Chem. Rev.*, **1998**, 98, 863-909.
149. W. Carruthers, *Cycloaddition Reactions in Organic Synthesis*, Tetrahedon Organic Chemistry Series, 8, **1990**.
150. F. A. Carey and R. J. Sundberg, *Advanced Organic Chemistry*, Pergamon press, Springer, 5th edn., **2007**.
151. J. McMurry, *Organic chemistry*, Carey and Sundberg, Cornell University, International Student, New York, 6th edn.
152. R. Huisgen, *J. Org. Chem.*, **1976**, 41, 403-419.

153. P. G. Wenthold, M. L. Polak and W. C. Lineberger, *J. Phys. Chem.*, **1996**, 100, 6920-6926.
154. A. Lopusinski and J. Michalski, *Angew. Chem. Int. Ed. Engl.*, **1972**, 11, 838-843.
155. R. Sustmann, *Pure Appl. Chem.*, **1974**, 40, 569-593.
156. H. W. Fruhauf, *Coord. Chem. Rev.*, **2002**, 230, 79-96.
157. L. Zhang, X. Chen, P. Xue, H. H. Y. Sun, I. D. Williams, K. B. Sharpless, V. V. Fokin and G. Jia, *J. Am. Chem. Soc.*, **2005**, 127, 15998-15999.
158. V. V. Rostovtsev, L. G. Green, V. V. Fokin and K. B. Sharpless, *Angew. Chem. Int. Ed.*, **2002**, 41, 2596-2599.
159. F. Amblard, J. H. Cho and R. F. Schinazi, *Chem. Rev.*, **2009**, 109, 4207-4220.
160. W. J. Choi, Z. D. Shi, K. M. Worthy, L. Bindu, R. G. Karki, M. C. Nicklaus, R. J. Fisher and T. R. Burke, *Bioorg. Med. Chem. Lett.*, **2006**, 16, 5265-5269.
161. J. Szychowski, A. Mahdavi, J. J. L. Hodas, J. D. Bagert, J. T. Ngo, P. Landgraf, D. C. Dieterich, E. M. Schuman and D. A. Tirrell, *J. Am. Chem. Soc.*, **2010**, 132, 18351-18360.
162. S. Brase, C. Gil, K. Knepper and V. Zimmermann, *Angew. Chem. Int. Ed.*, **2005**, 44, 5188-5240.
163. P. Ji, J. H. Atherton and M. I. Page, *Org. Biomol. Chem.*, **2012**, 10, 7965-7969.
164. M. M. Majireck and S. M. Weinreb, *J. Org. Chem.*, **2006**, 71, 8680-8683.
165. S. T. Abu-Orabi, *Molecules*, **2002**, 7, 302-314.
166. S. B. Otvos, A. Georgiades, I. M. Mandity, L. Kiss and F. Fulop, *Beilstein J. Org. Chem.*, **2013**, 9, 1508-1516.
167. J. D. Roberts, H. E. Simmons Jr, L. A. Carlsmith and W. C. Vaughan, *J. Am. Chem. Soc.*, **1953**, 75, 3290-3291.
168. R. T. Morrison and R. N. Boyd, *Organic Chemistry*, Allyn and Bacon Inc, 4th edn., 1008, **1983**.
169. L. Campbell-Verduyn, P. H. Elsinga, L. Mirfeizi, R. A. Dierckx and B. L. Feringa, *Org. Biomol. Chem.*, **2008**, 6, 3461-3463.
170. C. Spiteri, C. Mason, F. Zhang, D. J. Ritson, P. Sharma, S. Keeling and J. E. Moses, *Org. Biomol. Chem.*, **2010**, 8, 2537-2542.
171. B. V. Suma, N. N. Natesh and V. Madhavan, *J. Chem. Pharm. Res.*, **2011**, 3, 375-381.
172. D. S. Pedersen and A. Abell, *Eur. J. Org. Chem.*, **2011**, 2399-2411.
173. K. Matsui, S. Takizawa and H. Sasai, *J. Am. Chem. Soc.*, **2005**, 127, 3680-3681.
174. M. Shi, G. N. Ma and J. Gao, *J. Org. Chem.*, **2007**, 72, 9779-9781.
175. W. P. Hong, H. N. Lim, H. W. Park and K. J. Lee, *Bull. Korean Chem. Soc.*, **2005**, 26, 655-657.
176. J. N. Kim, Y. J. Im, G. J. Hyeon and K. Y. Lee, *Tetrahedron Lett.*, **2001**, 42, 4195-4197.
177. M. Shi, C. Q. Li and J. K. Jiang, *Molecules*, **2002**, 7, 721-733.
178. J. B. Park, S. H. Ko, B. G. Kim, W. P. Hong and K. J. Lee, *Bull. Korean Chem. Soc.*, **2004**, 25, 27-28.
179. D. Basavaiah, K. V. Rao and R. J. Reddy, *Chem. Soc. Rev.*, **2007**, 36, 1581-1588.
180. J. N. Kim, Y. M. Chung and Y. J. Im, *Tetrahedron Lett.*, **2002**, 43, 6209-6211.
181. Y. J. Im, K. Y. Lee, T. H. Kim and J. N. Kim, *Tetrahedron Lett.*, **2002**, 43, 4675-4678.

182. P. Ribiere, N. Yadav-Bhatnagar, J. Martinez and F. Lamaty, *QSAR Comb. Sci.*, **2004**, 23, 911-914.
183. D. Basavaiah, A. J. Rao and T. Satyanarayana, *Chem. Rev.*, **2003**, 103, 811-891.
184. P. T. Kaye and X. W. Nocanda, *J. Chem. Soc., Perkin Trans.*, **2000**, 1, 1331-1332.
185. P. T. Kaye and X. W. Nocanda, *J. Chem. Soc., Perkin Trans. 1*, **2002**, 1, 44-47.
186. P. T. Kaye, *S. Afr. J. Sci.*, **2004**, 100, 545-548.
187. F. Ameer, S. E. Drewes, S. Freese and P. T. Kaye, *Synth. Commun.*, **1988**, 18, 495-500.
188. O. B. Familoni, P. J. Klaas, K. A. Lobb, V. E. Pakade and P. T. Kaye, *Org. Biomol. Chem.*, **2006**, 4, 3960-3965.
189. Y. Fort, M. C. Berthe and P. Caubere, *Tetrahedron*, **1992**, 48, 6371-6384.
190. K. E. Price, S. J. Broadwater, H. M. Jung and D. T. McQuade, *Org. Lett.*, **2005**, 7, 147-150.
191. L. S. Hegedus, *Tetrahedron*, **1984**, 40, 2415-2434.
192. M. Sahu and P. Sapkale, *Int. J. Pharm. Chem. Sci.*, **2013**, 2, 1159-1170.
193. I. P. Beletskaya and A. V. Cheprakov, *Chem. Rev.*, **2000**, 100, 3009-3066.
194. S. Cacchi, *Pure Appl. Chem.*, **1996**, 68, 45-52.
195. A. C. Hillier, G. A. Grasa, M. S. Viciu, H. M. Lee, C. Yang and S. P. Nolan, *J. Organomet. Chem.*, **2002**, 653, 69-82.
196. A. Czech, T. Ganicz, M. Noskowska, W. A. Stanczyk and A. Szelag, *J. Organomet. Chem.*, **2009**, 694, 3386-3389.
197. H. U. Blaser and A. Spencer, *J. Organomet. Chem.*, **1982**, 233, 267-274.
198. J. M. Gaudin, *Tetrahedron Lett.*, **1991**, 32, 6113-6116.
199. R. G. Heidenreich, J. G. E. Krauter, J. Pietsch and K. Kohler, *J. Mol. Catal. A: Chem.*, **2002**, 182-183, 499-509.
200. J. G. Taylor, A. V. Moro and C. R. D. Correia, *Eur. J. Org. Chem.*, **2011**, 1403-1428.
201. H. A. Dieck and R. F. Heck, *J. Am. Chem. Soc.*, **1974**, 96, 1133-1136.
202. Y. S. Hon, Y. C. Hsu and C. Y. Cheng, *J. Chin. Chem. Soc.*, **2006**, 53, 1447-1462.
203. S. Caddick and W. Kofie, *Tetrahedron Lett.*, **2002**, 43, 9347-9350.
204. M. Mori, K. Chiba and Y. Ban, *Tetrahedron Lett.*, **1977**, 18, 1037-1040.
205. A. R. Hajipour and G. Azizi, *Green Chem.*, **2013**, 15, 1030-1034.
206. T. Jeffery, *Tetrahedron*, **1996**, 52, 10113-10130.
207. A. J. Carmichael, M. J. Earle, J. D. Holbrey, P. B. McCormac and K. R. Seddon, *Org. Lett.*, **1999**, 1, 997-1000.
208. J. A. Marshall and G. M. Schaaf, *J. Org. Chem.*, **2003**, 68, 7428-7432.
209. R. F. Heck, *Pure Appl. Chem.*, **1978**, 50, 691-701.
210. R. Sheldon, *Chem. Commun.*, **2001**, 2399-2407.
211. W. Cabri and I. Candiani, *Acc. Chem. Res.*, **1995**, 28, 2-7.
212. K. Kohler, R. G. Heidenreich, J. G. E. Krauter and J. Pietsch, *Chem. Eur. J.*, **2002**, 8, 622-631.
213. A. Biffis, M. Zecca and M. Basato, *J. Mol. Catal. A: Chem.*, **2001**, 173, 249-274.
214. S. Thorand and N. Krause, *J. Org. Chem.*, **1998**, 63, 8551-8553.
215. E. Shirakawa, T. Kitabata, H. Otsuka and T. Tsuchimoto, *Tetrahedron*, **2005**, 61, 9878-9885.

216. A. Soheili, J. Albaneze-Walker, J. A. Murry, P. G. Dormer and D. L. Hughes, *Org. Lett.*, **2003**, 5, 4191-4194.
217. Y. Tohda, N. Hagihara and K. Sonogashira, *Tetrahedron Lett.*, **1975**, 16, 4467-4470.
218. W. M. Dai, D. S. Guo and L. P. Sun, *Tetrahedron Lett.*, **2001**, 42, 5275-5278.
219. Y. He and C. Cai, *J. Organomet. Chem.*, **2011**, 696, 2689-2692.
220. Z. Novak, A. Szabo, J. Repasi and A. Kotschy, *J. Org. Chem.*, **2003**, 68, 3327-3329.
221. L. Yin and J. Liebscher, *Chem. Rev.*, **2007**, 107, 133-173.
222. K. Wikander, K. Holmberg and P. Handa, *Micropor. Mesopor. Mat.*, **2009**, 117, 126-135.
223. J. T. Guan, G. A. Yu, L. Chen, T. Q. Weng, J. J. Yuan and S. H. Liu, *Appl. Organomet. Chem.*, **2009**, 23, 75-77.
224. S. Mehta and R. C. Larock, *J. Org. Chem.*, **2010**, 75, 1652-1658.
225. B. H. Lipshutz, D. W. Chung and B. Rich, *Org. Lett.*, **2008**, 10, 3793-3796.
226. J. Clayden, N. Greeves, S. Warren and P. Wothers, *Organic Chemistry*, Oxford University press, 1330, **1967**.
227. K. C. Nicolaou and W. M. Dai, *Angew. Chem. Int. Ed. Engl.*, 1991, 1387-1416.
228. M. E. Maier, *Synlett.*, **1995**, 13-26.
229. J. W. Grissom, G. U. Gunawardena, D. Klingberg and D. Huang, *Tetrahedron*, **1996**, 52, 6453-6518.
230. R. C. Larock, M. J. Doty and S. Cacchi, *J. Org. Chem.*, **1993**, 58, 4579-4583.
231. K. R. Roesch and R. C. Larock, *J. Org. Chem.*, **1998**, 63, 5306-5307.
232. R. Thorwirth, A. Stolle and B. Ondruschka, *Green Chem.*, **2010**, 12, 985-991.
233. F. Yang, X. Cui, Y. Li, J. Zhang, G. Ren and Y. Wu, *Tetrahedron*, **2007**, 63, 1963-1969.
234. J. H. Li, Y. Liang and Y. X. Xie, *J. Org. Chem.*, **2005**, 70, 4393-4396.
235. C. Yang and S. P. Nolan, *Organometallics*, **2002**, 21, 1020-1022.
236. Y. Lin, Y. Chen, X. Ma, D. Xu, W. Cao and J. Chen, *Tetrahedron*, **2011**, 67, 856-859.
237. F. Zhang and J. E. Moses, *Org. Lett.*, **2009**, 11, 1587-1590.
238. J. H. Boyer and F. C. Canter, *Chem. Rev.*, **1954**, 54, 1-57.
239. W. Zhu and D. Ma, *Chem. Commun.*, **2004**, 888-889.
240. P. Pawaiya, A. Sharma, W. A. Khanday and R. Tomar, *J. Chem. Pharm. Res.*, **2012**, 4, 3089-3099.
241. L. Rokhum and G. Bez, *J. Chem. Sci.*, **2012**, 124, 687-691.
242. K. Kim and Y. H. Kim, *Arch. Pharmacol. Res.*, **1993**, 16, 94-98.
243. S. G. Hansen and H. H. Jensen, *Synlett.*, **2009**, 3275-3278.
244. S. Chandrasekhar, M. Seenaiiah, C. L. Rao and C. R. Reddy, *Tetrahedron*, **2008**, 64, 11325-11327.
245. R. S. Walmsley, Z. R. Tshentu, M. A. Fernandes and C. L. Frost, *Inorg. Chim. Acta*, **2010**, 363, 2215-2221.
246. T. G. Bora, T. D. Tokluman, K. Yelekci and H. Yurter, *Turk. J. Chem.*, **2011**, 35, 861-870.
247. S. V. Khansole, S. S. Mokle, M. A. Sayyed and Y. B. Vibhute, *J. Chin. Chem. Soc.*, **2008**, 55, 871-874.

248. S. Bhunia, D. Saha and S. Koner, *Langmuir*, **2011**, 27, 15322-15329.
249. P. Zhou, Y. Takaishi, H. Duan, B. Chen, G. Honda, M. Itoh, Y. Takeda, O. K. Kodzhimatov and K. H. Lee, *Phytochemistry*, **2000**, 53, 689-697.
250. D. Yu, M. Suzuki, L. Xie, S. L. Morris-Natschke and K. H. Lee, *Med. Res. Rev.*, **2003**, 23, 322-345.
251. C. Spino, M. Dodier and S. Sotheeswaran, *Bioorg. Med. Chem. Lett.*, **1998**, 8, 3475-3478.
252. P. T. Kaye and M. A. Musa, *Synthesis*, **2002**, 2701-2706.
253. P. T. Kaye, M. A. Musa and X. W. Nocanda, *Synthesis*, **2003**, 531-534.
254. S. Fletcher and P. T. Gunning, *Tetrahedron Lett.*, **2008**, 49, 4817-4819.
255. P. T. Kaye, M. A. Musa, X. W. Nocanda and R. S. Robinson, *Org. Biomol. Chem.*, **2003**, 1, 1133-1138.
256. L. Kraszkiewicz, M. Sosnowski and L. Skulski, *Tetrahedron*, **2004**, 60, 9113-9119.
257. M. Y. Jiang, J. Y. Shin, B. O. Patrick and D. Dolphin, *Dalton Trans.*, **2008**, 2598-2602.
258. Y. Fall, G. Gomez and C. Fernandez, *Tetrahedron Lett.*, **1999**, 40, 8307-8308.
259. D. K. Rayabarapu, C. H. Yang and C. H. Cheng, *J. Org. Chem.*, **2003**, 68, 6726-6731.
260. G. Quan Chang, C. Tu-Lin, Z. Jian-She and Z. Gai, *Chinese J. Chem.*, **2008**, 26, 1079-1084.
261. B. Bennua-Skalmowski and H. Vorbrueggen, *Tetrahedron Lett.*, **1995**, 36, 2611-2614.
262. M. Rottlaender and P. Knochel, *J. Org. Chem.*, **1998**, 63, 203-208.
263. S. E. Denmark and W. J. Chung, *J. Org. Chem.*, **2006**, 71, 4002-4005.
264. A. F. Littke and G. C. Fu, *J. Org. Chem.*, **1999**, 64, 10-11.
265. J. H. Clark, D. J. Macquarrie and E. B. Mubofu, *Green Chem.*, **2000**, 2, 53-56.
266. B. M. Choudary, S. Madhi, N. S. Chowdari, M. L. Kantam and B. Sreedhar, *J. Am. Chem. Soc.*, **2002**, 124, 14127-14136.
267. A. Zapf and M. Beller, *Chem. Eur. J.*, **2001**, 7, 2908-2915.
268. A. Jutand, *Pure Appl. Chem.*, **2004**, 76, 565-576.
269. V. M. Wall, A. Eisenstadt, D. J. Ager and S. A. Laneman, *Platinum Met. Rev.*, **1999**, 43, 138-145.
270. C. Yang, H. M. Lee and S. P. Nolan, *Org. Lett.*, **2001**, 3, 1511-1514.
271. G. T. Crisp, *Chem. Soc. Rev.*, **1998**, 27, 427-436.
272. Fischer scientific website, Palladium-Catalysed Coupling Chemistry. <http://www.acros.com/mybrochure/aowhpapdbrochuslow.pdf> (Accessed January 30, 2014).
273. P. G. Kislitsin, S. G. Zlotin and O. A. Luk'yanov, *Russ. Chem. Bull.*, **1998**, 47, 3, 517-519.
274. T. R. Burke Jr, M. Fesen, A. Mazumder, J. Yung, J. Wang, A. M. Carothers, D. Grunberger, J. Driscoll, Y. Pommier and K. Kohn, *J. Med. Chem.*, **1995**, 38, 4171-4178.
275. B. Ason, D. J. Knauss, A. M. Balke, G. Merkel, A. M. Skalka and W. S. Reznikoff, *Antimicrob. Agents Chemother.*, **2005**, 49, 2035-2043.

276. H. S. Bodiwala, S. Sabde, P. Gupta, R. Mukherjee, R. Kumar, P. Garg, K. K. Bhutani, D. Mitra and I. P. Singh, *Bioorg. Med. Chem.*, **2011**, 19, 1256-1263.
277. S. U. Lee, C. Shin, C. Lee and Y. S. Lee, *Eur. J. Med. Chem.*, **2007**, 42, 1309-1315.
278. K. Wadhwa and J. G. Verkade, *J. Org. Chem.*, **2009**, 74, 4368-4371.
279. K. Voigtritter, S. Ghorai and B. H. Lipshutz, *J. Org. Chem.*, **2011**, 76, 4697-4702.
280. J. Lu and P. H. Toy, *Synlett.*, **2007**, 1723-1726.
281. J. Kim, D. H. Kang and D. O. Jang, *Synlett.*, **2008**, 443-447.
282. J. M. Concellon, C. Concellon and C. Mejica, *J. Org. Chem.*, **2005**, 70, 6111-6113.
283. L. Fernandes, A. J. Bortoluzzi and M. M. Sa, *Tetrahedron*, **2004**, 60, 9983-9989.
284. C. G. Frost, S. D. Penrose and R. Gleave, *Synthesis*, **2009**, 627-635.
285. A. El-Batta, C. Jiang, W. Zhao, R. Anness, A. L. Cooksy and M. Bergdahl, *J. Org. Chem.*, **2007**, 72, 5244-5259.
286. P. R. Blakemore, D. K. H. Ho and W. M. Nap, *Org. Biomol. Chem.*, **2005**, 3, 1365-1368.
287. J. Tijani, R. Suleiman and A. B. El, *Appl. Organomet. Chem.*, **2008**, 22, 553-559.
288. Y. Liao, C. Xing, M. Israel and Q. S. Hu, *Org. Lett.*, **2011**, 13, 2058-2061.
289. R. T. Morrison and R. N. Boyd, *Organic Chemistry*, Allyn and Bacon Inc, 593, **1983**.
290. Y. Zhao, D. Zhou, Q. Chen, X. Zhang, N. Bian, A. Qi and B. Han, *Macromolecules*, **2008**, 44, 6382-6388.
291. D. R. Roque, J. L. Neill, J. W. Antoon and E. P. Stevens, *Synthesis*, **2005**, 2497-2502.
292. M. Iwata, R. Yazaki, Y. Suzuki, N. Kumagai and M. Shibasaki, *J. Am. Chem. Soc.*, **2009**, 131, 18244-18245.
293. T. Misaki, G. Takimoto and T. Sugimura, *J. Am. Chem. Soc.*, **2010**, 132, 6286-6287.
294. R. D. Roque, J. L. Neill, J. W. Antoon and S. P. Erland, *Synthesis*, **2005**, 15, 2497-2502.
295. A. Nohara, H. Kuriki, T. Saijo, K. Ukawa, T. Murata, M. Kanno and Y. Sanno, *J. Med. Chem.*, **1975**, 18, 34-37.
296. A. Breitenbach, C. Meese, H. M. Wolff and R. Drews, *Highly pure bases of 3,3-diphenyl propylamine monoesters*, Patent, EP1613584A1, Germany, **2003**.
297. X. Chen, M. Tsiang, F. Yu, M. Hung, G. S. Jones, A. Zeynalzadegan, X. Qi, H. Jin, C. U. Kim, S. Swaminathan and J. M. Chen, *J. Mol. Biol.*, **2008**, 380, 504-519.
298. T. T. Wang, T. C. Huang and M. Y. Yeh, *J. Mol. Catal.*, **1990**, 57, 271-289.
299. N. Kaushik-Basu, A. Basu and D. Harris, *BioDrugs*, **2008**, 22, 161-175.
300. H. Li, Z. Zawahir, L. Song, Y. Long and N. Neamati, *J. Med. Chem.*, **2006**, 49, 4477-4486.
301. R. G. Maroun, S. Gayet, M. S. Benleulmi, H. Porumb, L. Zargarian, H. Merad, H. Leh, J. F. Mouscadet, F. Troalen and S. Femandjian, *Biochemistry*, **2001**, 40, 13840-13848.
302. S. Raju, O. Tšubrik and U. Mäeorg, *ARKIVOC*, **2009**, 6, 291-297.

303. R. K. Pandey, P. Dagade, M. K. Dongare and P. Kumara, *ARKIVOC*, **2002**, 7, 28-33.
304. M. M. Joullié and K. M. Lassen, *ARKIVOC*, **2010**, 8, 189-250.
305. A. T. Nchinda, PhD thesis, Rhodes University, **2001**.
306. L. F. Bornaghi, S. A. Poulsen, P. C. Healy and A. R. White, *Acta Crystallogr. Sect. E*, **2008**, 64, 139-149.
307. L. H. Boudreau, N. Picot, J. Doiron, B. Villebonnet, M. E. Surette, G. A. Robichaud and M. Touaibia, *New J. Chem.*, **2009**, 33, 1932-1940.
308. D. B. Marron, Research and Development in the Pharmaceutical Industry, *The Congress of the United States-Congressional Budget Office*, United States, **2006**.
309. J. A. DiMasi, R. W. Hansen and H. G. Grabowski, *J. Health Econ.*, **2003**, 22, 151-185.
310. CBRA website, California Biomedical Research Association. Fate sheet: New drug development process. <http://ca-biomed.org/pdf/media-kit/fact-sheets/cbradrugdevelop.pdf> (Accessed April 25, 2013).
311. M. J. R. Yunta, *Computer and Information Science, Numerical Analysis and Scientific Computing*, Horacio Pérez-Sánchez, **2012**.
312. D. B. Kitchen, H. Decornez, J. R. Furr and J. Bajorath, *Nat. Rev. Drug Discovery*, **2004**, 3, 935-949.
313. U. M. M. Arumugam, A. Kuppusamy, S. Thirumalaisamy, S. Varadharajan and J. Puliyath, *Der Pharma Chemica*, **2011**, 3, 240-247.
314. D. Plewczynski, M. Lazniewski, R. Augustyniak and K. Ginalski, *J. Comput. Chem.*, **2011**, 32, 742-755.
315. P. Cos, B. T. De, N. Hermans, S. Apers, B. D. Vanden and A. J. Vlietinck, *Curr. Med. Chem.*, **2004**, 11, 1345-1359.
316. J. M. Goodman, *Chemical Applications of Molecular Modelling*, **1998**.
317. G. P. Miller and J. Mack, *Org. Lett.*, **2000**, 2, 3979-3982.
318. M. Totrov and R. Abagyan, *PROTEINS: Structure, Function and Genetics Suppl.*, **1997**, 215-220.
319. G. M. Morris, R. Huey, W. Lindstrom, M. F. Sanner, R. K. Belew, D. S. Goodsell and A. J. Olson, *J. Comput. Chem.*, **2009**, 30, 2785-2791.
320. S. F. Sousa, P. A. Fernandes and M. J. Ramos, *Proteins: Structure, Function and Bioinformatics*, **2006**, 65, 15-26.
321. A. Y. Tenoro-Barajas, A. Hernández-Santoyo, V. Altuzar, H. Vivanco-Cid and C. Mendoza-Barrera, *Protein-Protein and Protein-Ligand Docking, Protein Engineering - Technology and Application*, InTech., **2013**.
322. R. D. Taylor, P. J. Jewsbury and J. W. Essex, *J. Comput. Aided Mol. Des.*, **2002**, 16, 151-166.
323. S. Olgen, E. Akaho and D. Nebioglu, *Eur. J. Med. Chem.*, **2001**, 36, 747-770.
324. J. Westbrook, H. M. Berman, Z. Feng, G. Gilliland, T. N. Bhat, H. Weissig, I. N. Shindyalov and P. E. Bourne, *Nucleic Acid Research*, **2000**, 28, 235-242.
325. R. J. Meshram and S. N. Jangle, *International Journal of Drug Discovery*, **2009**, 1, 34-39.
326. J. J. Irwin and B. K. Shoichet, *J. Chem. Inf. Model.*, **2005**, 45, 177-182.
327. ChemsSketch, http://www.acdlabs.com/products/draw_nom/draw/chemsketch/ (Accessed February 03, 2014).

328. Chemdraw, https://www.cambridgesoft.com/Ensemble_for_Chemistry/ChemDraw/ (Accessed February 03, 2014).
329. Vega ZZ, http://www.msg.ucsf.edu/local/programs/Vega/pages/gl_index.htm (Accessed February 03, 2014).
330. NIH website, Discovery Studio Visualizer, <http://pubchem.ncbi.nlm.nih.gov/summary/summary.cgi?cid=5287411#x299> (Accessed January 15, 2012).
331. M. L. Verdonk, M. J. Hartshorn, C. W. Murray and R. D. Taylor, *Proteins: Structure, Function and Genetics*, **2005**, 177-182.
332. B. D. Bursulaya, M. Totrov, R. Abagyan and C. L. Brooks, *J. Comput. Aided Mol. Des.*, **2003**, 17, 755-763.
333. G. M. Morris, D. S. Goodsell, R. S. Halliday, R. Huey, W. E. Hart, R. K. Belew and A. J. Olson, *J. Comput. Chem.*, **1998**, 19, 1639-1662.
334. R. Tiwari, K. Mahasenan, R. Pavlovicz, C. Li and W. Tjarks, *J. Chem. Inf. Model.*, **2009**, 49, 1581-1589.
335. R. Kiralj and M. M. C. Ferreira, *J. Mol. Graphics Model.*, **2003**, 21, 499-515.
336. Y. C. Cheng and W. H. Prusoff, *Biochem. Pharmacol.*, **1973**, 22, 3099-3108.
337. R. Garcia-Domenech, D. N. Mahmoudi, J. Galvez, K. Farhati, J. F. Franetich, R. Sauerwein, L. Hannoun, F. Derouin, M. Danis and D. Mazier, *J. Antimicrob. Chemother.*, **2008**, 52, 1215-1220.
338. J. V. Julian-Ortiz, N. Mahmoudi, L. Ciceron, J. Gálvez, D. Mazier, M. Danis, F. Derouin and R. García-Domenech, *J. Antimicrob. Chemother.*, **2006**, 57, 489-497.
339. G. R. Marshall, *J. Comput. Aided Mol. Des.*, **2013**, 27, 107-114.
340. L. Muley, B. Baum, M. Smolinski, M. Freindorf, A. Heine, G. Klebe and D. G. Hangauer, *J. Med. Chem.*, **2010**, 53, 2126-2135.
341. R. Kaźmierkiewicz, *Introduction to molecular modeling*, Intercollegiate Faculty of Biotechnology UG-MUG, Gdańsk, **2011**.
342. M. Balakrishnan, R. C. Srivastava and M. Pokhriyal, *Indian J. Biotechnol.*, **2010**, 9, 96-100.
343. M. Ramalingam, S. Karthikeyan and S. D. Kumar, *Int. J. Comput. Appl.*, **2012**, 43, 16-22.
344. M. L. Doss and K. G. Lalitha, *J. Curr. Chem. Pharm. Sci.*, **2011**, 1, 52-58.
345. Z. Yu, T. Kabashima, C. Tang, T. Shibata, K. Kitazato, N. Kobayashi, M. K. Lee and M. Kai, *Anal. Biochem.*, **2010**, 397, 197-201.
346. P. Bagossi, J. Kadas, G. Miklossy, P. Boross, I. T. Weber and J. Tozser, *J. Virol. Methods*, **2004**, 119, 87-93.
347. V. Looock, V. Schoubroeck, T. Ivens, P. Dehertogh, D. Jochmans and G. Dams, *Methods Mol. Biol.*, **2013**, 1030, 19-24.
348. S. Yamazaki and M. M. Famulok, *Methods Mol. Biol.*, **2009**, 535, 187-199.
349. I. Al-Masri, Y. Bustanji, A. Qasem, A. Al-Bakri and M. Taha, *Chem. Biol. Drug Des.*, **2009**, 74, 258-265.
350. F. P. Feorino, C. Schable and D. Warfield, *J. Clin. Microbiol.*, **1987**, 25, 2344-2346.
351. Y. Han, W. Xiao, P. K. Quashie, T. Mesplede, H. Xu, E. Deprez, O. Delelis, J. Pu, H. Sun and M. A. Wainberg, *Antiviral Res.*, **2013**, 98, 441-448.

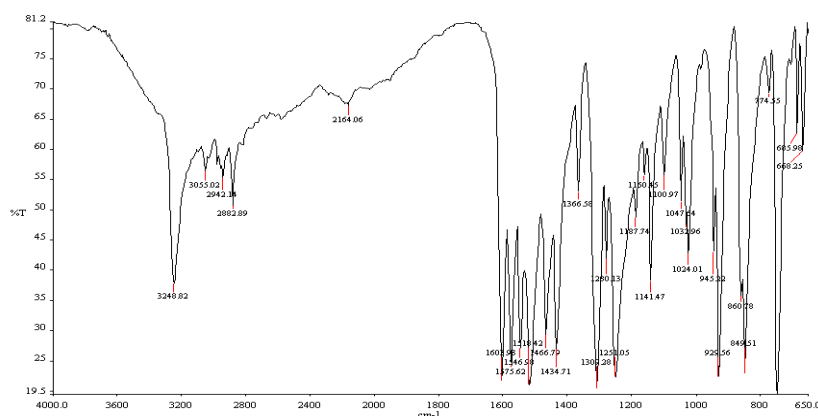
352. C. M. Farnet, B. Wang, J. R. Lipford and F. D. Bushman, *P. Natl. Acad. Sci. U. S. A.*, **1996**, 93, 9742-9747.
353. T. K. Au, R. A. Collins, T. L. Lam, T. B. Ng, W. P. Fong and D. C. C. Wan, *FEBS Lett.*, **2000**, 471, 169-172.
354. R. Pauwels, J. Balzarini, M. Baba, R. Snoeck, D. Schols, P. Herdewijn, J. Desmyter and C. E. De, *J. Virol. Methods*, **1988**, 20, 309-321.
355. K. Zhu, M. L. Cordeiro, J. Atienza, W. E. Robinson Jr and S. A. Chow, *J. Virol.*, **1999**, 73, 3309-3316.
356. M. Mayer and T. L. James, *J. Am. Chem. Soc.*, **2002**, 124, 13376-13377.
357. V. Jayalakshmi and N. R. Krishna, *J. Am. Chem. Soc.*, **2005**, 127, 14080-14084.
358. Z. Ji, Z. Yao and M. Liu, *Anal. Biochem.*, **2009**, 385, 380-382.
359. J. Klein, R. Meinecke, M. Mayer and B. Meyer, *J. Am. Chem. Soc.*, **1999**, 121, 5336-5337.
360. X. Wen, Y. Yuan, D. A. Kuntz, D. R. Rose and B. M. Pinto, *Biochemistry*, **2005**, 44, 6729-6737.
361. V. Jayalakshmi and N. R. Krishna, *J. Magn. Reson.*, **2002**, 155, 106-118.
362. Y. S. Wang, D. Liu and D. F. Wyss, *Magn. Reson. Chem.*, **2004**, 42, 485-489.
363. J. Yan, A. D. Kline, H. Mo, M. J. Shapiro and E. R. Zartler, *J. Magn. Reson.*, **2003**, 163, 270-276.
364. L. Fielding, S. Rutherford and D. Fletcher, *Magn. Reson. Chem.*, **2005**, 43, 463-470.
365. University of Luebeck, Chemistry Department unpublished work, Luebeck, **2010**.
366. H. J. Schraml, A. De Bruyn, R. Contreras, M. Maras and P. Herdewijn, *Magn. Res. Chem.*, **1997**, 35, 883-888.
367. G. A. Morris and A. Gibbs, *Magn. Reson. Chem.*, **1991**, 29, 83-87.
368. D. D. Traficante, *Concepts Magnetic Res.*, **1998**, 10, 59-62.
369. S. J. Cho, G. M. L. Serrano, J. Bier and A. Tropsha, *J. Med. Chem.*, **1996**, 39, 5064-5071.
370. M. Vieth and D. J. Cummins, *J. Med. Chem.*, **2000**, 43, 3020-3032.
371. C. Perez, M. Pastor, A. R. Ortiz and F. Gago, *J. Med. Chem.*, **1998**, 41, 836-852.
372. M. K. Parai, D. J. Huggins, H. Cao, M. N. L. Nalam, A. Ali, C. A. Schiffer, B. Tidor and T. M. Rana, *J. Med. Chem.*, **2012**, 55, 6328-6341.
373. J. A. Meredith, PhD thesis, Stockholm University, **2009**.
374. O. Vajragupta, P. Boonchoong, G. M. Morris and A. J. Olson, *Bioorg. Med. Chem. Lett.*, **2005**, 15, 3364-3368.
375. S. Marchais-Oberwinkler, P. Kruchten, M. Frotscher, E. Ziegler, A. Neugebauer, U. Bhoga, E. Bey, U. Mueller-Vieira, J. Messinger, H. Thole and R. W. Hartmann, *J. Med. Chem.*, **2008**, 51, 4685-4698.
376. NIH website, Efavirenz, http://pubchem.ncbi.nlm.nih.gov/summary/summary.cgi?cid=64139&loc=ec_rcs#x299, (consulted in November 24, 2013).
377. R. C. Rizzo, J. Tirado-Rives and W. L. Jorgensen, *J. Med. Chem.*, **2001**, 44, 145-154.
378. T. O. Olomola, R. Klein, K. A. Lobb, Y. Sayed and P. T. Kaye, *Tetrahedron Lett.*, **2010**, 51, 6325-6328.

379. N. H. Matter, S. Gssregen, D. W. Will, H. Schreuder, A. Bauer, K. R. M. Urmann, M. Wagner and V. Wehner, *Angew. Chem.*, **2009**, 121, 2955-2960.
380. NIH website, 5CITEP, <http://pubchem.ncbi.nlm.nih.gov/summary/summary.cgi?cid=5287411#x29> (Accessed November 24, 2013).
381. M. Fornabaio, P. Cozzini, A. Marabotti, D. J. Abraham, G. E. Kellogg and A. Mozzarelli, *Curr. Med. Chem.*, **2004**, 11, 1345-1359.
382. A. J. Hannaford, B. S. Furniss, P. G. W. Smith and A. R. Tatchell, *Vogel's textbook of practical organic chemistry*, Longman Scientific and Technical, New York, 5th edn., **1989**.
383. M. R. Naimi-Jamal, M. G. Dekamin and G. Kaupp, *Eur. J. Org. Chem.*, **2009**, 3567-3572.
384. Z. Gan, K. Kawamura, K. Eda and M. Hayashi, *J. Organomet. Chem.*, **2010**, 695, 2022-2029.
385. M. C. Venuti, R. A. Stephenson, R. Alvarez, J. J. Bruno and A. M. Strosberg, *J. Med. Chem.*, **1988**, 31, 2136-2145.
386. M. Parthasarathy and R. Gopalakrishnan, *Spectrochim. Acta Part A*, **2012**, 97, 1152-1158.
387. A. T. Shinde, S. B. Zangade, S. B. Chavan, A. Y. Vibhute, Y. S. Nalwar and Y. B. Vibhute, *Synth. Commun.*, **2010**, 40, 3506-3513.
388. G. R. Srunivas, D. Channe and K. Abiraj, *Synth. Commun.*, **2005**, 35,2, 223-230.
389. E. Biehl and H. Ankati, *Tetrahedron Lett.*, **2009**, 50, 4677-4682.
390. R. R. Kale, V. Prasad, H. A. Hussain and V. K. Tiwari, *Tetrahedron Lett.*, **2010**, 51, 5740-5743.
391. A. C. Tome, *Sci. Synth.*, **2004**, 13, 415-601.
392. B. B. Dey and K. K. Row, *Action of sodium sulfite on coumarins*, Presidency college, Madras, **1923**.
393. S. K. Meegalla and R. Rodrigo, *J. Org. Chem.*, **1991**, 56, 1882-1888.
394. D. P. Munro and J. T. Sharp, *J. Chem. Soc. Perkin Trans. 1*, **1984**, 849-858.
395. J. Arotzky, R. Butler and A. C. Darby, *Chem. Commun.*, **1966**, 650-655.
396. C. S. Roxdestvedt and C. D. Nooy, *Diels-Alder Reaction of Cinnamic Acid Derivatives with Cyclopentadiene*, Michigan, 77, **1955**.
397. L. C. Raiford and L. K. Tanzer, *J. Org. Chem.*, **1941**, 6, 722-731.
398. M. D. Armstrong and K. N. F. Shaw, *J. Biol. Chem.*, **1957**, 225, 269-278.
399. T. Shintou and T. Mukaiyama, *J. Am. Chem. Soc.*, **2004**, 126, 7359-7367.
400. C. Lin, J. Yang, C. Chang, S. Kuo, M. Lee and L. Huang, *Bioorg. Med. Chem.*, **2005**, 13, 1537-1544.
401. I. Wang, Y. Hu, B. Wei and L. Bai, *Synth. Commun.*, **2002**, 32, 1607-1614.
402. H. Khabazzadeh, R. M. Nejad, H. Sheibani and K. Saidi, *Catal. Commun.*, **2007**, 8, 1411-1413.
403. A. V. Lebedev, A. B. Lebedeva, V. D. Sheludyakov, E. A. Kovaleva, O. L. Ustinova and I. B. Kozhevnikov, *Russ. J. Gen. Chem.*, **2005**, 75, 1113-1124.
404. P. M. Pawar, K. J. Jarag and G. S. Shankarling, *Green Chem.*, **2011**, 13, 2130-2134.
405. V. N. Britsun, A. N. Chernega and M. O. Lozinskii, *Russ. J. Org. Chem.*, **2005**, 41, 108-113.

406. T. P. T. Tran, V. A. Nguyen, N. A. Ho, D. Q. Tran, T. V. Sung and Z. Naturforsch., *J. Chem. Sci.*, **2009**, 64, 323-327.
407. F. Bigi, B. Frullanti, R. Maggi, G. Sartori and E. Zambonin, *J. Org. Chem.*, **1999**, 64, 1004-1006.
408. X. Cui, Y. Zhang, F. Shi and Y. Deng, *Chem. Eur. J.*, **2011**, 17, 1021-1028.
409. E. B. Vliet and E. H. Volwiler, *J. Am. Chem. Soc.*, **1992**, 43, 1672-1676.
410. H. Adolphister, H. J. Neubauer, W. Seppelt and P. Hofmei, *Propargyl cinnamates, their preparation and their use for controlling pests*, patent, US4767782, USA, **1988**.
411. 374. NIH website, Discovery Studio Visualizer, <http://pubchem.ncbi.nlm.nih.gov/summary/summary.cgi?cid=5287411#x299> (Accessed January 15, 2012).
412. S. Y. Huang and X. Zou, *Int. J. Mol. Sci.*, **2010**, 11, 3016-3034.
413. T. J. A. Ewing and I. D. Kuntz, *J. Comput. Chem.*, **1997**, 18, 1175-1189.
414. R. T. Kroemer, *Curr. Protein Pept. Sci.*, **2007**, 8, 312-328.
415. M. Kharb, R. K. Jat, G. Parjapati and A. Gupta, *Int. J. Drug Res. Tech*, **2012**, 2, 189-197.
416. G. Jones, P. Willett, R. C. Glen, A. R. Leach and R. Taylor, *J. Mol. Biol.*, **1997**, 267, 727-748.
417. G. M. Verkhivker, D. Bouzida, D. K. Gehlhaar, P. A. Rejto, S. Arthurs, A. B. Colson, S. T. Freer, V. Larson, B. A. Luty, T. Marrone and P. W. Rose, *J. Comput. Aided Mol. Des.*, **2000**, 14, 731-751.
418. E. Perola, W. P. Walters and P. S. Charifson, *Proteins: Struct. Funct. Bioinformatics*, **2004**, 56, 235-249.
419. T. D. W. Claridge, *High Resolution NMR Techniques in Organic Chemistry*, Tetrahedron Organic Chemistry Series, 19, J. E. Baldwin and R. M. Williams, p 142.

APPENDIX

A.1. IR OF VANADIUM CATALYST



A.2. CHARACTERISTICS OF COMMON DOCKING PROGRAMS

DOCK

DOCK employs an incremental reconstruction algorithm which attempts to reconstruct the bound ligand by first placing a rigid anchor in the binding site and later using an algorithm to add fragments and complete the ligand structure.³³² The core of the DOCK search algorithm is the superimposition of ligand atoms onto predefined site points that map out the negative image of the binding site. A matching process is used to determine which ligand atoms and site points are to be superimposed.⁴¹³ Matches can be scored in this program by the quality of the geometric fit as well as by the molecular mechanics interaction energy.³¹¹ The energy scoring function includes van der Waals and electrostatic components.³³²

FlexX

FlexX is another fragment based method where fragments are generated by severing all noncyclic bonds in a given ligand. All the base fragments identified are used as starting points for docking.⁴¹⁴ Therefore, the choice of the ligand base fragment is the key step since it makes the ligand core responsible for principal interactions with a target protein. MIMUMBA is an interaction geometry database used to exactly describe intermolecular interaction pattern. FlexX uses the MIMUMBA torsion angle database for the creation of conformers.⁴¹⁵ The torsion angle database is used to generate different poses of a fragment that are then considered rigid in further steps. Subsequently, the selected fragment is placed in the active site of the protein and alignment procedures are carried out to establish favorable interactions. Once a single fragment is docked and all steric distortions are removed, the interaction energy is estimated by a docking score using the model of molecular interactions developed by Böhm and Klebe.³¹⁴ This score function takes into account the loss of ligand entropy upon binding (counting the number of rotatable bonds in the ligand), hydrogen bonds, ionic interactions accounting for electrostatic interactions, aromatic interactions, and lipophilic contacts accounting for hydrophobic interactions.^{332, 414}

GOLD

GOLD was developed by Jones *et al.* in 1997 and is distributed by the Cambridge Crystallographic Data Centre (CCDC). Similarly to AUTODOCK, GOLD employs a Genetic Algorithm (GA) with an island model which explores the full range of conformational flexibility of the ligand and the rotational flexibility of selected receptor hydroxyl groups to sample intermolecular hydrogen bond networks and ligand conformations.⁴¹⁶ However, the lack of a desolvation component renders it more susceptible to failures in predicting hydrophobic interactions.⁴¹⁷

The mechanism for ligand placement is based on fitting points. Fitting points are added to hydrogen-bonding groups on the protein and the ligand while the program maps acceptor points in the ligand on donor points in the protein and inversely. Four scoring functions are implemented in this software. They include force field-based GoldScore, Piecewise Linear Potential (PLP), empirically based ChemScore and knowledge-based

Astex Statistical Potential (ASP).³¹⁴ The development of GOLD is currently focussed on improving the computational algorithm and adding a support for parallel processing.⁴¹⁵

ICM

ICM program is based on a stochastic algorithm that relies on global optimization of the entire flexible ligand in the receptor field (flexible ligand/grid receptor approach).⁴¹⁸ To optimize the energy function, a Monte-Carlo Minimization (MCM) procedure in the internal coordinate space is employed to find the global minimum of the energy function. The performance of ICM and GOLD is more binding site-dependent and it is significantly poorer when binding is predominantly driven by hydrophobic interactions.⁴¹⁸

In 2003, Bursulaya *et al.* carried out a speed comparison study of the five above mentioned docking programs and found that FlexX was the fastest while AUTODOCK was the slowest among them.³³² Still according to the comparative study of Bursulaya *et al.*, ICM provides the highest accuracy in ligand docking.³³²